Imperial College London

Department of Life Sciences

Investigation of neuronal pathways underlying sleep regulation

A thesis submitted in fulfilment of the requirements for the degree of

Doctor of Philosophy

By

Giulia Miracca

October 2019

Abstract

Sleep is a fundamental physiological function and regulates many complex physiological aspects, such as mental health, metabolism, cognition and memory. Despite numerous efforts to understand the function of sleep, we still do not know why we spend a third of our life asleep. One way to tackle this mystery is the investigation of processes regulating sleep time and need, such as sleep homeostasis. Synaptic plasticity has been proposed as a mechanism capable of explaining sleep homeostasis, as synapse structure could change with fluctuations in sleep pressure. To understand whether plasticity mechanisms regulate sleep patterns, I deleted from lateral preoptic (LPO) hypothalamic neurons, key sleep regulators, the NR1 gene encoding a NMDA receptor subunit, fundamental for synaptic potentiation. Using floxed-NR1 animals and injections of Cre recombinase, I deleted the NMDAr from LPO neurons and observed sleep behaviours. ΔNR1-LPO animals were constantly hyperactive and showed dramatic sleep fragmentation and continuous sleep loss. Although sleepy, these animals were incapable of recuperating lost sleep after sleep deprivation, despite showing a delta power rebound- an indicator of sleep homeostasis. This phenotype was not present when the NR1 gene was deleted from other hypothalamic nuclei, suggesting that the NMDAr in LPO is a specific mechanism capable of coupling phenotypic sleep rebound to cortical delta power activity.

To better understand LPO functions during behavioural states, I analysed the *in vivo* calcium activity of subsets of LPO neurons and successfully dissected sleep and wake active circuits, to find that most of LPO neurons are REM sleep active but fire under Dexmedetomidine sedation.

Additionally, I studied Grm2 expressing neurons of the lateral habenula. Using a Grm2-cre mouse line, I performed *in vivo* calcium imaging and optogenetic stimulation showing how these neurons might be a connecting hub for the regulation of both NREM sleep and propofol-induced sedation.

Acknowledgements

I would like to thank Prof Nick Franks and Prof William Wisden for giving me the opportunity to carry out my research without restrictions and hesitations. Their trust in my abilities has been motivating and inspirational during these years.

Thank you to all the members of our lab: Bryan, David, Ed, Lily, Mathieu, Wei, Xiao and Ying for their presence during these last 4 years. A special thanks goes to Raquel Yustos, for her kindness and great patience in dealing with my extravagant experiments and long list of orders. Above all, I would like to thank my two dear friends and extraordinary researchers, Dr Kyoko Tossell and Dr Berta Anuncibay-Soto. In the last year, they gave me the strength, the encouragement, and a solid scientific rigor to develop my project beyond what I could have expected. Thanks also to Leda, the third *mousquetaire*, whose strong character and determination set an example for me in difficult situations.

A big thank you to everybody on our 4th floor: Esteban, Hazel, Lukas, Marta, Patricia, Quentin, Rita, and Saffi, for making our work environment friendly and fun.

I would also like to thank my friend and collaborator from The Crick Institute, Dr Julia Harris, for her scientific and career advice, and my two undergraduate students, Fergus and Catalina, for their contribution to my project.

During these years, my friends and mentors from all over the world have made this journey a little easier. A special thanks goes to Prof Bruce and Dr Sally Zetter for making me a part of their wonderful family, and for setting the example for what I want to be in the future. I am also deeply grateful to Dr Chloe Alexandre and Dr Alban Latremoliere who, since my time at Harvard Medical School, have taught me with patience and care how to be the scientist I am today. Thanks also to some very important people in my life, including Michio and Patrick, my long-time friends Francesco, Laura and Michela, whose friendship and support have been precious gifts for almost 10 years now, and my dear friends Juan and Minos, for our wonderful trips to come.

My family has always been present for encouragement and support, starting with my mom Antonella, my aunt Barbara, my grandmothers Luisa and Elsa, and my two brothers, Alessandro and Filippo. Thanks to Noémie who stepped into my world half way through

the PhD and, somehow, is still around. With her love and infectious smile, she has made me feel supported and valued, even during the most stressful times. Thanks also to her family for welcoming me with open arms.

Finally, none of this would have been possible without my Dad. He is my number one supporter, mentor and advisor. He sacrificed everything to help me fulfil my dreams and aspirations and gave me the strength to always strive for more and better for myself. I am so grateful to him, above anyone else.

All this work is for you, thanks Dad.

Declaration of originality and copyright

I declare that the contents of this thesis are my own work and have not been submitted in any form for another degree. All information derived from the work of others has been acknowledged in the text and a list of references given. Figures that rely on published material are attributed in the figures' legends.

This work was funded by the Imperial College Schrödinger Scholarship and the Wellcome Trust.

Table of content

Table of figures

Acronyms and abbreviations

5HT	Serotonin/serotoninergic
AAV	Adeno-Associate virus
AMPA	α-amino-3-hydroxy-5-methyl-4-isoxazolepropionic acid
ArchT	Archaerhodopsin T
BL	Baseline
Ca^{2+}	Calcium
CaMKII	Ca^{2+}/calmodulin-dependent protein kinase II
CDS	Coding sequence
CeA	Central nucleus of the amygdala
ChAT	Acetylcholine/ cholinergic
ChR2	Channelrhodopsin 2
CNO	Clozapine-N-oxide
CNS	Central nervous system
Cre	Cre recombinase
Ctr	Control
Cx/Ctx	Cortex
DA	Dopamine/dopaminergic
DAPI	4′,6-diamidino-2-phenylindole
Dex	Dexmedetomidine
DMH	Dorsomedial hypothalamic nucleus
DNA	Deoxyribonucleic acid
DP	Dark period
DRN	Dorsal raphe nucleus
DREADD	Designer receptor exclusively activated by designer drugs
EEG	Electroencephalogram
EMG	Electromyogram
Ephys	Electrophysiology/electrophysiological
fNR1	Floxed NR1

FR	Firing rate
GABA	Gamma-Aminobutyric acid
GAD1	Glutamate decarboxylase 1
Gal	Galanin
GFAP	Glial fibrillary acidic protein
GFP	Green fluorescent protein
Grm2	Glutamate metabotropic receptor 2
His	Histamine
Hsyn	Human synapsin
IBA1	Ionized calcium binding adaptor molecule 1
IHC	Immunohistochemistry
iGluRs	Ionotropic glutamate receptors
IEI	Inter event interval
KO	Knockout
LC	Locus coeruleus
LDT	Laterodorsal tegmental area
LH	Lateral hypothalamus
LHb	Lateral Habenula
LP	Light period
LPGi	lateral paragigantocellular nuclei
LPO	Lateral preoptic of the hypothalamus
LPT	Lateral pontine tegmentum
MCH	Melanin-concentrating hormone
MHb	Medial habenula
MnPO	Median preoptic
MPO/MPA	Medial preoptic
NMDA	N-methyl-D-aspartate
Nos1	Nitric oxide synthase
NR1	NR1 subunit of the N-methyl-D-aspartate receptor
NREM	Non rapid eye movement
NTS	Neurotensin
Orx	Orexin
PFC	Prefrontal cortex

PBS	Phosphate buffer saline
PO/POA	Preoptic area
pPRIME	Potent RNA interference using microRNA expression
PPT	Peduncolopontine nucleus
PV	Parvalbumin
PZ	Parafacial zone
REM	Rapid eye movement
RNA	Ribonucleic acid
SCN	Suprachiasmatic nucleus
shRNA	Short interfering RNA
SLD	Sublaterodorsal nucleus
SOM	Somatostatin
SWA	Slow wave activity
SWS	Slow wave sleep
TeLC	Tetanus toxin light-chain
TMN	Tuberomammilary nucleus
V1	Primary visual cortex
Vgat	Vesicular GABA Transporter
Vglut	Vesicular glutamate transporter
VLPO	Ventrolateral preoptic of the hypothalamus
VMM	Ventromedial medulla
VTA	Ventral tegmental area
vPAG	Ventral periaqueductal grey area
ZI	Zona incerta

1 Introduction

1.1 Why sleep?

Sleep is a fundamental component of our lives. Not only does it make us feel more rested, but it also affects and determines our emotional, psychological and physical health. Decades of studies have proven how good quality sleep is fundamental for memory and learning consolidation [1, 2], cognition and alertness [3, 4], mental health and stress [5] and so on. As well as regulating higher cognitive functions, it has an effect in maintaining a healthy molecular and cellular environment in the brain, removing metabolic waste [6] and possibly regulating synaptic homeostasis and plasticity [7, 8]. In the rest of the body, sleep affects metabolism [9] immune response [10] and the heart [11].

On the other hand, research shows that reduced sleep is a cause of altered mood and depression, lack of concentration [12-14], and is linked to higher risks of developing diabetes [15], obesity [16], cancer [17], cardiovascular diseases [18] and even early onset of neurodegenerative diseases like Alzheimer's [19, 20].

Sleep actively participates in a healthy maintenance of most of our cognitive and physiological functions, explaining why it has been conserved through evolution [21]. However, at least in mammals, we are still far away from understanding sleep itself and how to manipulate it in order to improve general human health. One way to better understand sleep and its functions is to investigate its neuronal and cellular circuits, and possibly to dissect the sleep network into defined and restricted circuits. Separating these sub-networks could allow us to understand whether they all work cooperatively to maintain a healthy body and brain, or whether each of these circuits is independent in regulating specific body functions. To study these circuits, researchers have developed new advanced techniques, including specific transgenic animal models, virus-based neuronal tracers [22, 23] and high definition calcium and voltage sensors [24, 25]. These allow tracing, tracking, and recording, both off and on-line, of specific cellular subtypes and circuits related to behaviour.

Thanks to these techniques, many research laboratories have been able to interrogate and identify a great number of neuronal circuits that actively participate in sleep and wake promotion. However more ought to be discovered regarding molecular mechanisms underlying neuronal activation and functioning during sleep and wake, as well as different brain areas and neuronal populations regulating sleep and behaviours. These results could help us better understand how sleep participates in higher cognitive functions and in brain restorative processes, and ultimately why we sleep. For these reasons, I decided to focus my research on dissecting both neuronal networks and specific molecular and cellular pathways involved in sleep regulation. To do so, my work combines molecular biology, transgenic mouse models, behavioural analysis and novel neuronal imagining and manipulation in freely behaving animals.

1.2 Definition of behavioural states

In mammals, sleep is characterized by two distinct states defined as Rapid Eye Movement sleep (REM) and Non-Rapid Eye Movement sleep (NREM). These states are distinguished from each other and from wakefulness using recordings of the cortical neuronal electrical activity and the muscles electrical activity, defined as electroencephalogram (EEG) and electromyogram (EMG), respectively.

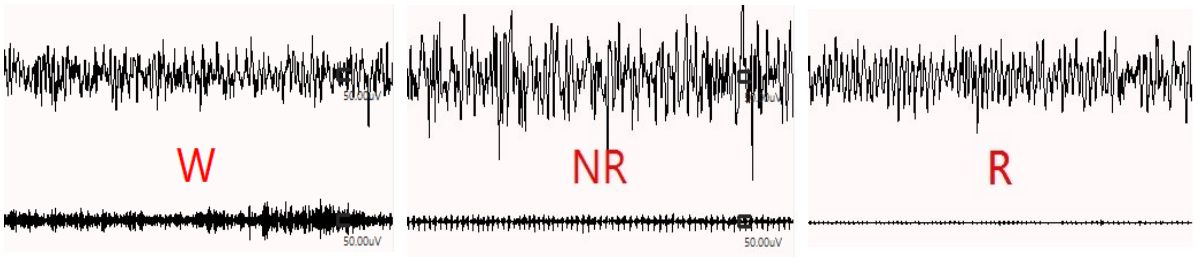

Figure 1.2.1 Examples of wake, NREM, and REM in mice.
Representative 10-sec EEG (up) and EMG (bottom) epochs of Wake (A), NREM sleep (B) and REM sleep (C) of a wild-type mouse. Figure from personal EEG/EMG recordings.

Wakefulness, or wake, is characterized by high-frequency, low-amplitude waves in the EEG (cortical desynchronization), and high muscle tone in the EMG (Figure 1.2.1, A). NREM sleep is defined by high-amplitude low-frequency EEG activity (cortical synchronization), and decreased muscle tone (Figure 1.2.1, B). In humans, NREM sleep is

divided in 3 different states, going from lighter to deeper sleep, while in experimental animals like mice, NREM sleep is considered as one stage only. Lastly, REM sleep is defined by a low-amplitude high frequencies waves in the EEG, similar to wakefulness, and a complete loss of muscle tone, or atonia, in the EMG (Figure 1.2.1, C). Since during REM sleep the brain cortical activity is high while the body is paralyzed, this state is also referred as paradoxical sleep.

Each vigilance state is characterized by the prevalence of a specific range of frequencies in the EEG. In mice, during wake the theta (6-10 Hz), beta (15-30 Hz) and gamma waves (30- 200 Hz) are associated with active exploratory behaviour and attentive wakefulness. During quiet wakefulness, slower EEG frequencies become more prevalent. Slow oscillations (0.5-1 Hz) and delta waves (1-4 Hz) are typical prominent features of NREM sleep, explaining why NREM sleep is also referred as Slow Wave Sleep (SWS). During REM sleep in mice, theta waves originating from the hippocampus dominate the EEG (Figure 1.2.2).

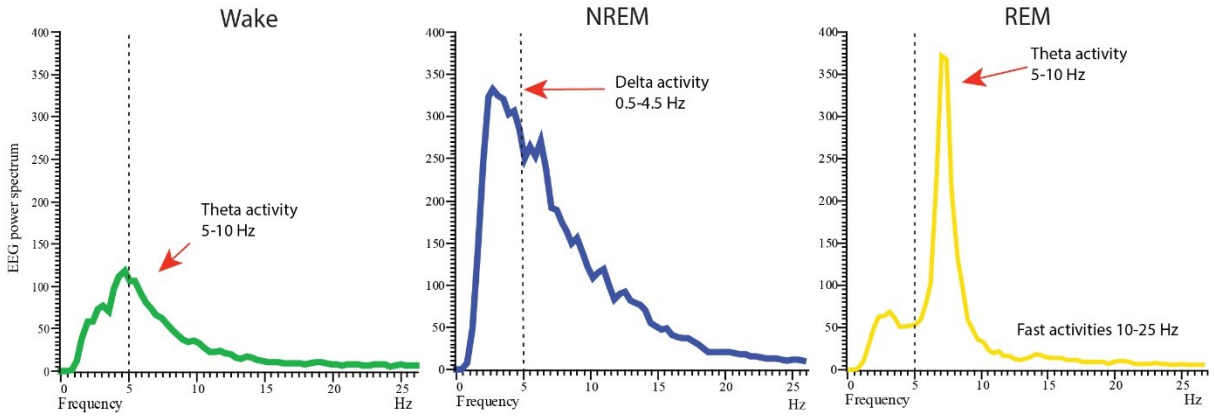

Figure 1.2.2 EEG power spectra of the three major behavioural states.
Three characteristic power spectra of Wake, NREM and REM sleep. Wake shows peak activity in the theta range, and lower power in the fast (10-25 Hz) frequency range. During NREM sleep, delta waves are the predominant frequency band, and most of the power in this state is concentrated in the delta band. REM sleep, instead, presents a marked peak in the theta activity, and power in faster frequency ranges (> 10 Hz). Overall, the EEG power is maximal during NREM sleep. Figure from personal EEG/EMG recordings.

1.3 The timing of sleep

One prominent theory that guided research in mammals for decades explains how timing and intensity of sleep are dictated by the interaction of two major biological factors: process S, or homeostatic process, and process C, or circadian process [26]. The former refers to sleep pressure, or sleep need, which is suggested to rise and accumulate during wake and decline during sleep. The latter, which is independent from sleep and wake, denotes the effects of the 24 h circadian rhythm on the timing and length of everyday sleep opportunity. In humans, since we are diurnal animals, the circadian clock prepares the body to sleep when there is low light and the night falls, but most animals, like mice and rats, are nocturnal and sleep mostly during the daytime, although they can also sleep during the night.

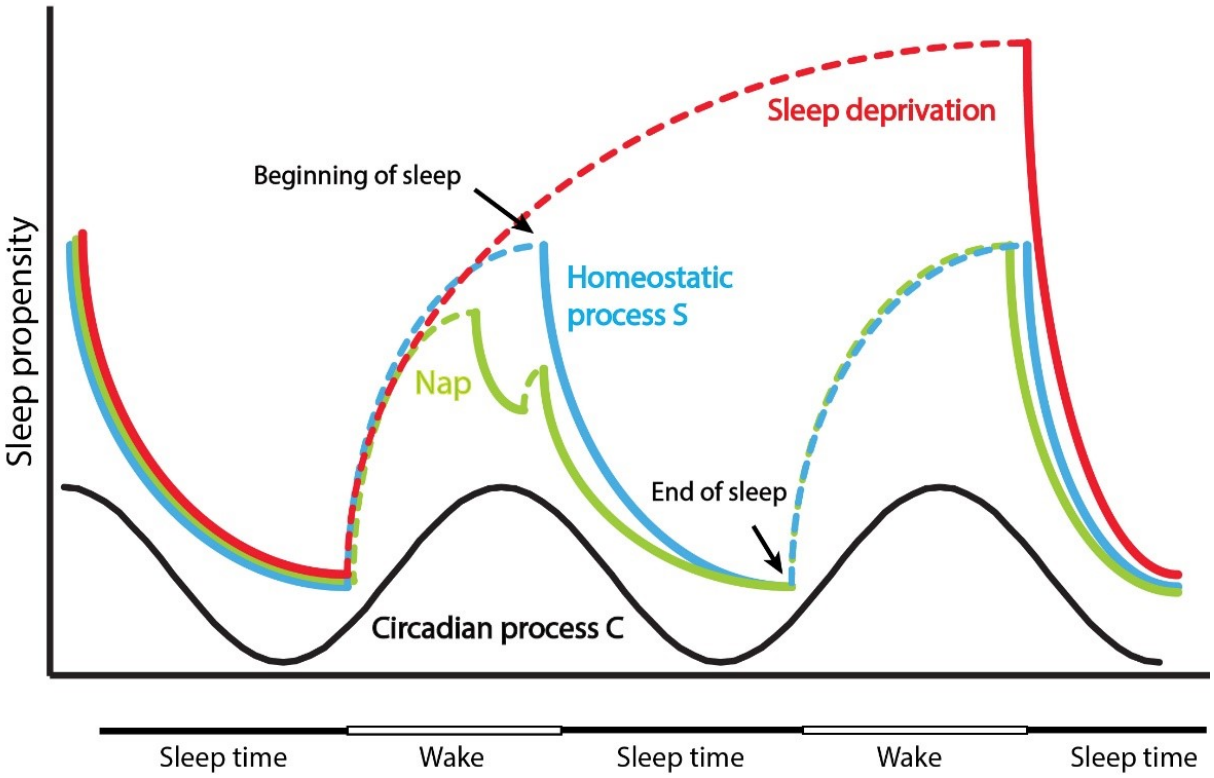

Figure 1.3.1 Sleep and wake cycle regulated by process S and process C.
The process S (blue line) increases with wakefulness and it can be reduced by daytime naps (green line), while process C (black line) oscillates based on day and night time every 24 h. Sleep deprivation increases the sleep propensity over the normal levels (red line). Line corresponding to wakefulness are represented in dashed lines as sleep propensity reflects EEG delta power, not present during wakefulness, and rendering the representation only an estimation. Figure drawn by me.

The homeostatic Process S depends on the levels of slow-wave activity (SWA): the EEG power density in the delta range of 0.5-4.5 Hz. SWA is an indicator of sleep depth, or intensity, and sleep pressure at the onset of sleep time. The levels of SWA at NREM sleep onset are increased as a function of the previous wake episode duration and they decline during sleep [27]. As an example, sleep deprivation induces a homeostatic response increasing the SWA [28]: sleep pressure increases during wakefulness and SWA decreases only when the subject finally sleeps (Figure 1.3.1).

The circadian process C depends on the suprachiasmatic nucleus (SCN) in the hypothalamus, whose neurons are driven by a transcriptional-translational loop that enforces a near-24-hour cycle of activity (Figure 1.3.1). This nucleus is entrained by the external light–dark cycle, firing most rapidly during the light period, under the regulation of a special class of light-sensitive retinal ganglion cells [29, 30]. Cell-specific lesions to this nucleus substantially disrupt the circadian rhythms of sleep and wake [31].

Despite this theory has been used to describe sleep patterns for decades, sleep researchers agree that this model is not sufficient to fully explain sleep time and need. Motivational processes can also affect drastically the time spent awake and asleep, pushing the system to stay awake far beyond the normal sleep time. Hunger, predatory risk, migration patterns and sometimes mating season could affect sleep patterns distribution and have an even bigger effect on sleep regulation than process S and C themselves [32].

1.4 Sleep circuits and networks

In the last few decades, with the advancements of in vivo recording and tracing techniques, the field of sleep circuits has been greatly expanding. Most of the neuronal types have been associated to either sleep or wake regulation, including monoaminergic (releasing molecules as dopamine, histamine, noradrenaline and serotonin), glutamatergic and GABAergic neurons. In this section I will attempt to describe the basics of sleep and wake regulation in the mammalian brain, focusing on areas most relevant to my own research. Both wake, NREM and REM-promoting sleep circuits have been thoroughly described and explained in recent reviews [33-39].

1.4.1 Circuits for wakefulness

Wake-promoting circuits comprise multiple systems and mechanisms working cooperatively to promote higher cortical activity and behavioural arousal. Some of the most relevant circuits associated with wake regulation involve monoaminergic signalling, and show high firing patterns during wakefulness. Both monoaminergic and cholinergic neurons are not only involved in sleep and wake patterns regulation, but their activity is also fundamental in physiological and behavioural functions, such as learning, motivation, reward, locomotor activity and attention [40, 41]. It is therefore important to keep in consideration that manipulation of these pathways might not be a direct effect on wake pathways, but rather a consequence of stimulating other behavioural aspects. Additionally, monoamines act on brain circuits extrasynaptically by volume transmission, causing monoaminergic neurons to activate circuits further away from the terminal networks, potentially affecting a wider and broader range of connections [42]. These wake-promoting neurons frequently co-release GABA and/or glutamate [41], which may as well work extrasynaptically [43], and influence as well both wakefulness and other cognitive and behavioural processes.

The classical view of wake-regulating circuits sees wakefulness controlled by arousal signals ascending through midbrain areas to then split in two separate pathways. The first is a dorsal pathway, and it innervates the thalamus, controlling sensation, cognition and motor activity. This pathways is also referred as thalamo-cortical since the intra thalamic nuclei send widespread projections to the cerebral cortex to stimulate sustained cortical activation [44]. The second pathway is more ventral, and it innervates several nuclei, including tuberomammilary nuclei (TMN), ventral tegmental area (VTA), lateral hypothalamus (LH) and basal forebrain (BF) to then project to the cortex (

Figure **1.4.1**).

One of the major nuclei in the brain postulated to initiate ascending wake signals is the locus coeruleus (LC). The LC is one of the main sources of noradrenaline (NE) in the brain, and it is responsible for inducing wakefulness, in particular in conditions of stress and reward. Photoactivation of NE neurons in the LC causes animals to wake up from sleep; photoinhibition promotes transitions to NREM sleep and administration of drug that reduce NE release have sedative effects in vivo [45].

The serotoninergic (5HT) neurons in the dorsal raphe nucleus (DRN) characterize another set of neurons promoting wakefulness. 5HT neurons directly project and activate wake-promoting circuits, and drugs that increase 5HT tone, as selective serotonin reuptake inhibitors (SSRIs), promote arousal in both animal models and humans. Photoactivation of DRN 5HT neurons causes a dramatic increase in wakefulness and a strong NREM fragmentation [46].

Drugs that increase dopamine (DA) signalling, such as amphetamines and modafinil, have a strong effect on increasing wakefulness and arousal, while drug antagonizing the DA system, as antipsychotics, have a sedating action. Because of these mechanisms, DA neurons have been assumed to be mostly wake promoting. VTA DA neurons, in fact, regulate wakefulness, as their inhibition reduces time spent awake in mice [47]. Interestingly, VTA-DA neurons, when inhibited, do not cause immediate sleep, but they first promote nesting and sleep preparatory behaviours [47]. Additionally, these neurons are not only wake active, but they show a bursting pattern of activity during REM sleep as well [48].

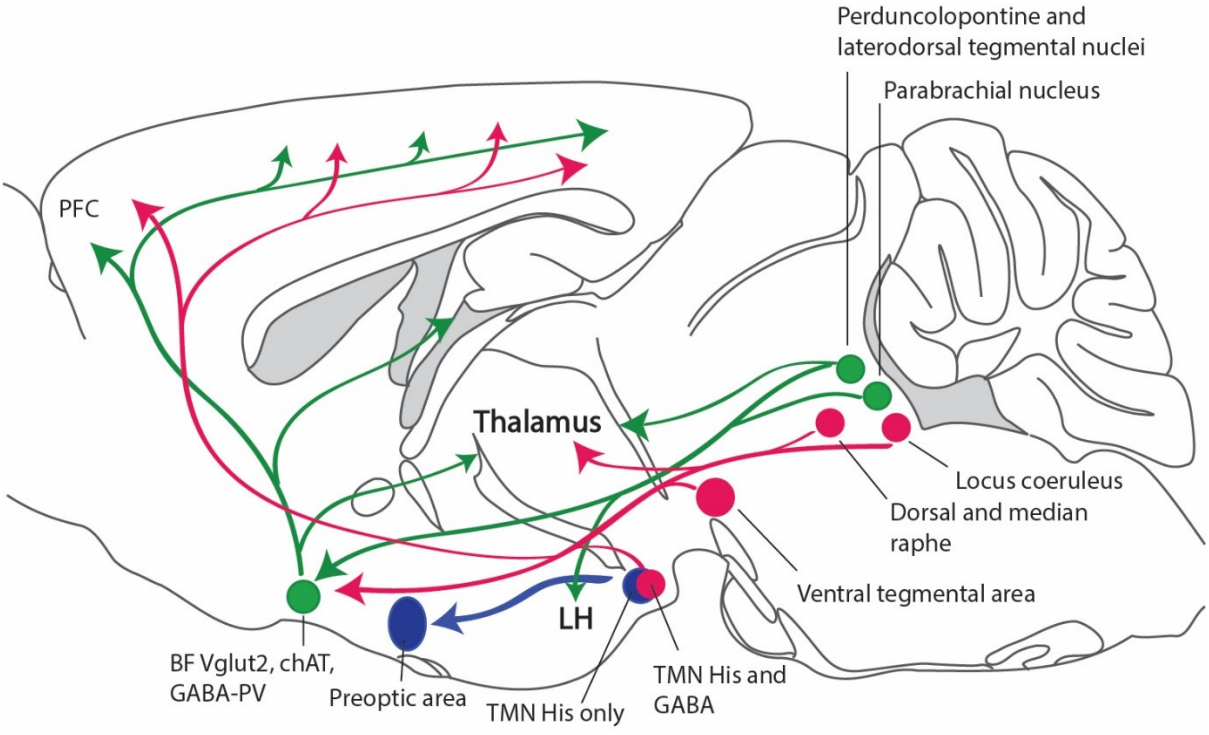

Figure 1.4.1 Ascending wake promoting pathways.
In green is represented the dorsal pathway which from midbrain, including PPT and LDT, innervates thalamus, lateral hypothalamus (LH) orexin neurons, and then cerebral cortex. In pink, the arousing ventral pathway, regulated mostly by monoaminergic

neurons, innervates the lateral hypothalamus and the basal forebrain to then send awakening signals to the cortex. The BF sends cholinergic, glutamatergic and GABAergic-parvalbumin (PV) projections to the cortex, including the prefrontal cortex (PFC) to promote wake [49]. Histamine (His) and GABA neurons from the TMN also send projections to the BF and to the cortex to induce wake, while histamine only TMN neurons project to the preoptic area (POA) to activate local GABAergic neurons and inhibit NREM sleep promoting circuits (in blue) [50, 51]. Figure drawn by me

DRN and ventral periaqueductal grey area (vPAG) DA neurons also take part in maintaining wake, as lesions or inhibition of those neurons cause wake time reduction and more transition to NREM sleep [52, 53].

Our laboratory has recently discovered that not only do VTA DA neurons participate in brain arousal, but also VTA glutamatergic neurons promote wakefulness, sending marked projections to both LH and nucleus accumbens (Figure 1.4.2). Lesioning of these glutamatergic cells impairs wake consolidation especially during lights-OFF, when the animals are mostly awake, while activation of the same neurons increases time spent awake [54].

Another area promoting wakefulness is the TMN, situated in the posterior hypothalamus. It contains a mixed population of neurons, including histamine ones, making it the only source of neuronal histamine in the brain. Histaminergic neurons project widely in the brain and they are active during wakefulness. When activated, these neurons cause an increase in locomotor activity [55], and promote wake in the EEG [43]. Specific lesioning of TMN histamine neurons causes strong sleep-wake fragmentation, and reduces the ability of modafinil to promote wakefulness [56].

Peduncolopontine and laterodorsal tegmental area (PPT and LDT) are two nuclei in between the midbrain and the pons. They contain a cluster of cholinergic (chAT) neurons intermingled with GABAergic and glutamatergic cells. Activation of chAT neurons in the PPT reduces slow EEG activity during NREM [57], but it is not clear whether they can actually promote wake. On the other hand, PPT glutamatergic neurons, when activated, cause sustained wakefulness for hours [57].

The BF as well contains a mixture of chAT, GABAergic and glutamatergic neurons. These neurons project to the cortex to induce arousal and they extend local connection to other BF neurons to control their activity [49, 58]. This nucleus is fundamental for normal sleep-wake behaviours, as lesions to its neurons cause slow waves in the EEG and,

in some cases, coma [59, 60] (Figure 1.4.2). GABArgic neurons from the BF, and specifically the ones co-expressing parvalbumin (PV) [49], are particularly important for wake maintenance, as their activation or inhibition causes either prolonged wakefulness or NREM sleep, respectively [61]. Similarly, GABAergic neurons from the LH and the posterior hypothalamus (PH) promote wakefulness through inhibition of sleep-inducing areas. Activation of these neurons maintains wakefulness for several hours [62].

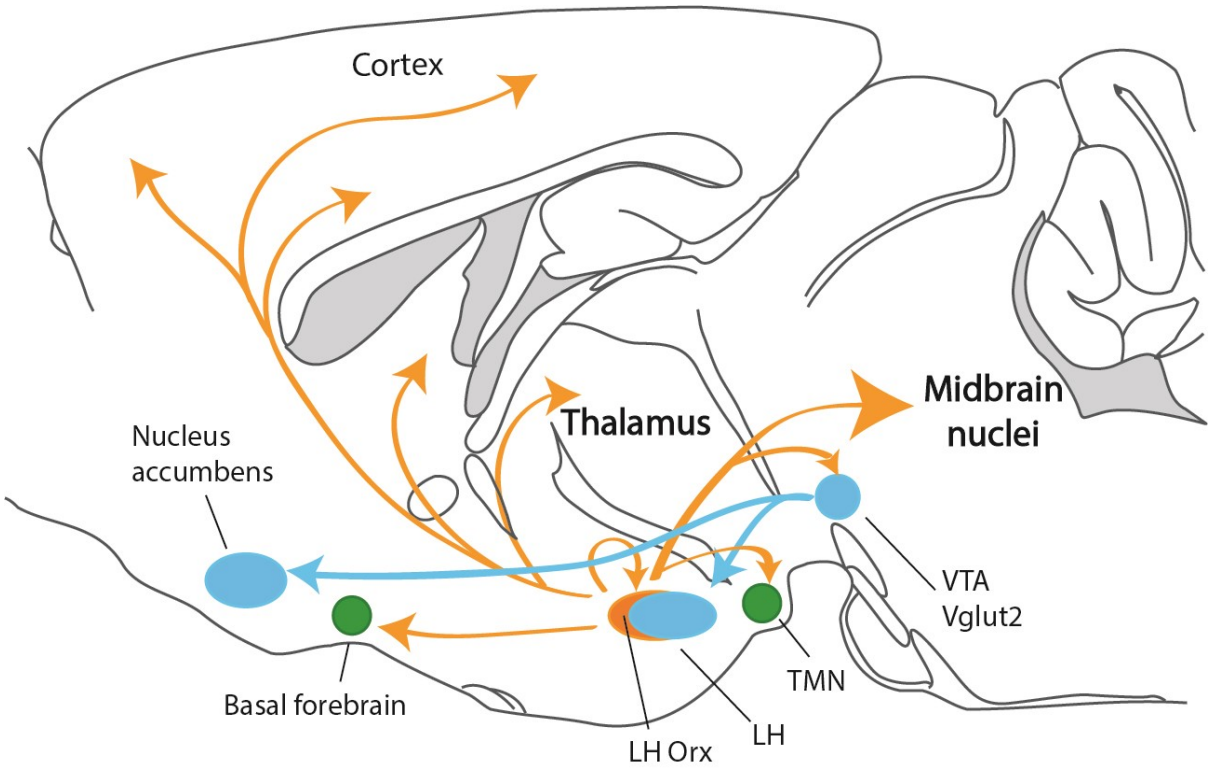

Figure 1.4.2 VTA and LH orexin wake promoting circuits.
VTA glutamatergic neurons project directly to LH and nucleus accumbens to maintain wakefulness. In yellow, LH orexin (Orx) neurons send widespread projections all over the brain to maintain wakefulness, including cortex, BF, TMN, VTA and all wake promoting nuclei in the midbrain. Both BF and TMN (in green) project to the cortex to keep the brain awake, as previously shown in Figure 1.4.1. Figure drawn by me.

Apart from monoaminergic, GABAergic and glutamatergic neurons, there is another essential class of cells that regulates sleep and wake: the hypocretin/orexinergic neurons. These neurons are sparse within the LH and they project to all areas mentioned above, to the thalamus and cortex (Figure 1.4.2). Orexin (orx) neurons are particularly important in maintaining long bouts of wakefulness rather than generating arousal. This can be observed in people suffering from narcolepsy, a common sleep disorder caused by loss of

orx neurons where patients are chronically sleepy. Mouse models of acute loss of orx neurons maintain a normal amount of wakefulness, but they can stay awake only for short periods of time [63]. Manipulation of orx neurons activity have also shown their importance in wake regulation, as their activation causes awakening in experimental animals and increases wake time [64, 65].

1.4.2 Circuits promoting NREM sleep

NREM sleep has been studied at length for decades, but we are still looking for circuits and networks that can truly explain sleep mechanisms and, perhaps, its functions.

An area fundamental for NREM sleep regulation is the preoptic area (PO), situated in the anterior part of the hypothalamus. The importance of this area in NREM sleep regulation was discovered almost a century ago by the scientist Von Economo [66], who found that brain lesions to the anterior hypothalamus caused patients to be constantly sleepy and tired but finding very difficult to fall asleep and stay asleep. Later studies in animals identified the area responsible for this phenotype in the PO [67, 68]. This area is a cluster of different neuronal types, including GABAergic, glutamatergic and galaninergic, all intermingled within each other, making the area quite complex to study and the circuits to dissect.

Using cFos expression, one of the first groups of cells identified for being active during NREM sleep were GABAergic, particularly concentrated in two lateral preoptic (LPO) areas: the ventrolateral preoptic (VLPO) and the median preoptic (MnPO) [69, 70]. Further studies showed how selective damage to VLPO neurons drastically decreased NREM sleep time [71]. In recent years, our laboratory demonstrated how the whole of LPO regulates sleep, as selective reactivation of LPO neurons that expressed cFos during recovery sleep can recapitulate NREM sleep [72].

To regulate and control NREM sleep, the LPO area sends direct inhibitory projections to wake active nuclei. Among these targets there are TMN-His neurons [73], orx neurons in the LH [74], chAT neurons of the BF, 5HT neurons from the DRN, NE neurons in the LC [75], and the vPAG [52] (Figure 1.4.2). At the same time, LPO receives inhibitory inputs from wake promoting areas, as axonal fibres of histaminergic, 5HT and NE neurons are observed in the POA [76]. In particular, His neurons coming from the TMN inhibit the POA through the activation of local GABAergic interneurons [51].

POA neurons are not only active during NREM sleep, as both GABAergic and galaninergic neurons can be activated after periods of predominantly REM sleep [77]. Moreover, some POA neurons, including some GABAergic ones, are wake active [78-80], but the contribution of these POA neurons to REM sleep and wake regulation has still to be elucidated.

In addition to regulating sleep, the POA regulates a diverse range of physiological and behavioural processes, as the MnPO in controlling body temperature [81]. Different sleep active neurons [82] in the POA are, in fact, thermosensitive [83]. Sleep and temperature homeostasis might be regulated from similar brain circuits and structures, and the POA might be a core hub connecting energy balance and appropriate behavioural states. Some galaninergic neurons from the POA also regulate parenting behaviours [84], revealing additional functions of the preoptic neurons.

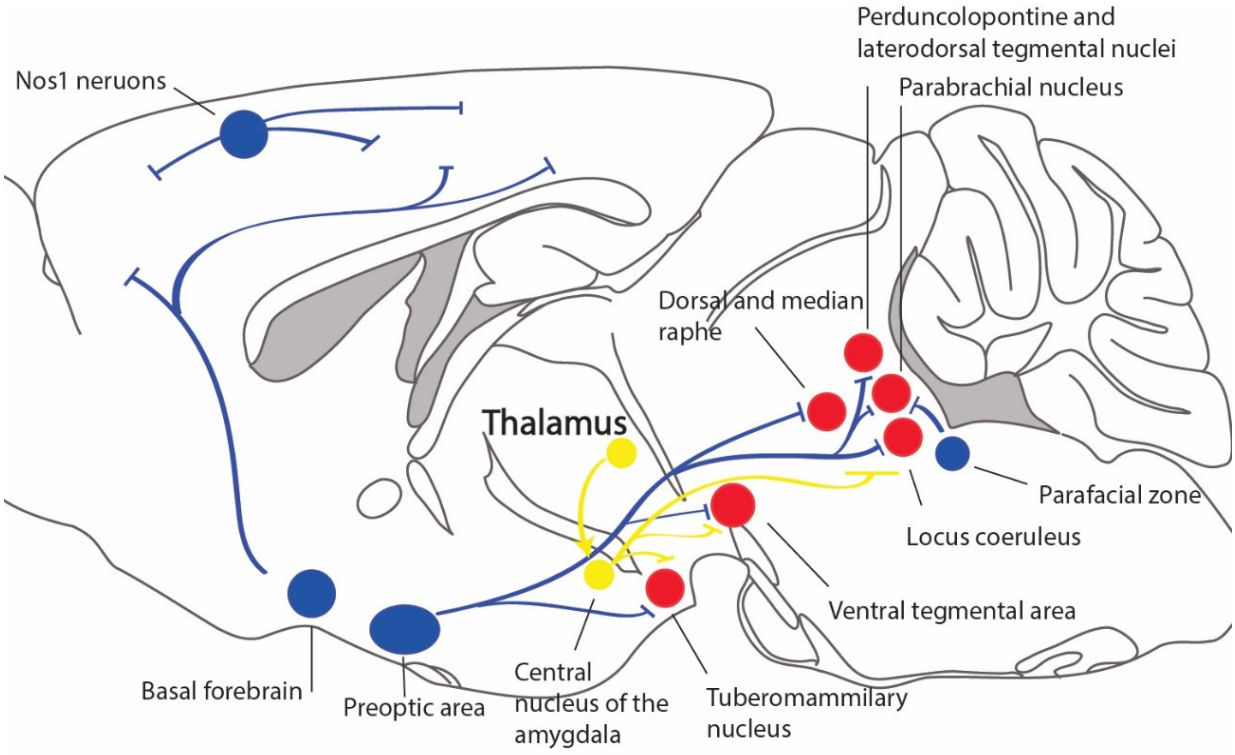

Figure 1.4.3 NREM sleep promoting circuits.
GABAergic and galaninergic neurons from the POA (NREM active nuclei in blue) send inhibitory projections to wake promoting areas (in red), including TMN, VTA, LC, and DRN. In the midbrain, the parafacial zone might act directly on neighbouring wake active nuclei to promote NREM. On the other side, the BF sends projections to the cortex to activate NREM EEG patterns and regulate GABAergic and Nos1 expressing neurons, which they also mediate SWS inhibiting cortical activity. In yellow is the thalamo-amygdala circuit, which inhibits most of the wake-promoting areas. Figure drawn by me.

The parafacial zone (PZ), a small cluster of neurons near the facial nerve in the rostral medulla, also takes part in promoting NREM sleep. Activation of GABA/glycinergic neurons in the PZ causes increased NREM sleep characterized by high SWA, while inhibition of the same circuits causes drastic decrease in NREM sleep time even after sleep deprivation [85]. This area might send inhibitory projections to wake promoting centres, although no work has demonstrated it thoroughly yet.

The BF also contributes to sleep regulation, on top of promoting wakefulness as discussed before, suggesting the presence of local inhibition between sleep and wake active neurons. The BF is cluster of chAT, GABAergic and glutamatergic neurons. The first class promotes wake [58], together with glutamatergic and parvalbumin (PV)-GABAergic neurons, while a subpopulation of somatostatin (SOM)-GABAergic cells are NREM active [49]. These SOM-GABAergic neurons send inhibitory projection to local wake active neurons in order to shift the balance from wake to NREM sleep. In addition to local connection, BF neurons project directly to cortical neurons to promote NREM sleep [86] (Figure 1.4.3 and 1.4.4).

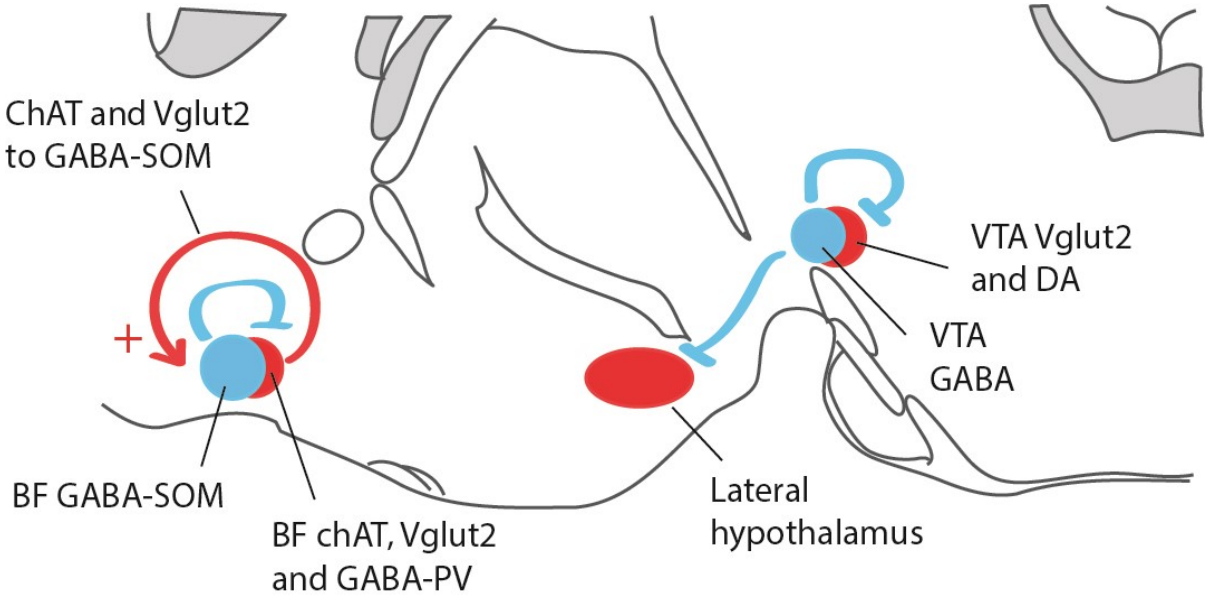

Figure 1.4.4 Basal Forebrain and VTA NREM promoting circuits.
BF GABAergic and somatostatin (SOM) neurons send local inhibitory projections to glutamatergic (Vglut2), ChAT and GABAergic-PV neurons to promote sleep. ChAT and Vglut2 neurons also send excitatory signals to GABA-SOM neurons. VTA GABA neurons also send strong inhibitory connections to local DA and Vglut2 neurons and to LH neurons to promote NREM sleep. Figure drawn by me.

The biggest effect reported on NREM sleep induction comes from both our lab and several others demonstrating that chemogenetic activation of VTA GABAergic neurons induces long-lasting NREM sleep, akin to sedation [54, 87, 88] and lesions to these neurons causes a consistent increase in wakefulness that lasts for more than 4 months. VTA GABAergic neurons could inhibit local DA and glutamatergic neurons as well as LH wake promoting ones to induce NREM sleep (Figure 1.4.4). Interestingly, these neurons are wake and REM sleep active, yet they promote NREM sleep [54].

New areas and clusters of neurons promoting NREM sleep have been recently discovered, using both neuronal projections mapping, selective lesioning, and activation or inhibition of specific circuits using both optogenetic and chemogenetic techniques. Galanin expressing GABAergic neurons in the dorsomedial hypothalamic nucleus (DMH) project to the POA and are NREM active. Their optogenetic activation increased NREM sleep, while decreasing REM sleep time [89]. A different subclass of GABAergic neurons also takes part in NREM sleep regulation. These neurons are in the zona incerta (ZI), and they are identified by selective expression of the LIM homeodomain factor Lhx6. GABAergic/Lhx6 neurons are activated by sleep pressure, and artificial activation of this circuits promotes both NREM and REM sleep [90]. A recent article has also identified a new NREM sleep active pathway connecting the posterior thalamic area to the central nucleus of the amygdala (CeA). Glutamatergic neurons from the thalamus activate GABAergic neurons in the CeA, which then project to and inhibit main wake promoting areas, including TMN, PPT and LC (Figure 1.4.3). Interestingly, both cell groups from the thalamus and the CeA express neurotensin (NTS), and selective KO of NTS in either thalamus or CeA greatly reduce their sleep promoting property [91].

A2A receptor-expressing GABAergic neurons in the nucleus accumbens [92], and A2A neurons in the dorsal striatum [93], and GABAergic neurons in the vPAG [94] also promote NREM sleep. All these circuits might be interconnected to promote behavioural and cortical NREM sleep, but we are still far from understanding how these different circuits communicate together to shift the balance between wake, NREM and REM sleep. Perhaps, such a widespread control of NREM sleep throughout the brain is necessary to communicate to all autonomic and somatomotor activities regulated by different areas of the brain [39]. Alternatively, not only a bottom-up regulation from brain nuclei to the cortex could be responsible for sleep initiation and maintenance, but cortical activity itself might influence behavioural states in a top-down manner.

1.4.3 Circuits promoting REM sleep

REM sleep, or paradoxical sleep, is a fascinating vigilance state. The EEG has a wake-like appearance, yet neural innervation of skeletal (but not breathing or eye muscle) is inhibited, resulting in muscle atonia. Crick and Mitchison speculated that REM sleep was important to reset neuronal networks for reverse learning [95], however, despite this hypothesis, REM sleep has been greatly overlooked over the years, and it is still unclear what are its specific functions in brain physiology. REM sleep and its characteristic eye movements are associated to dreaming, and how and why humans dream has been considered one of the biggest mysteries in science [96]. For now, because of its prominence during early development in mammals, REM sleep has been proposed to be fundamental for immature brain development [97].

REM sleep is partially generated in the pontine and medullary part of the brainstem, where two pathways, a descending and an ascending one, separate to control REM sleep physiology. The first pathway controls postural motor atonia while the second project to different brain centres to generate REM cortical EEG activity (Figure 1.4.5).

The glutamatergic neurons of the sublaterodorsal nucleus (SLD) are fundamental for muscular atonia during REM sleep. These neurons actively fire during REM sleep, as shown by electrophysiology recordings and immunohistochemistry (IHC) for cFos activation. A convincing proof of their role in regulating REM sleep has been shown in case of SLD lesions or inhibition of glutamate signalling in the area: subjects maintain a REM sleep-like EEG but without muscle atonia, exhibiting even complex motor behaviours while asleep [98, 99].

Understanding which cells and nuclei activate the SLD neurons is still a matter of discussion. ChAT neurons from the PPT/LDT are active during both wake and REM sleep and it was believed they were responsible for SLD activation, although recent studies have shown the contrary [100].

An area possibly mediating SLD-generated atonia is the ventromedial medulla (VMM). One of the circuits proposed includes activation from the SLD of glycinergic/GABAergic neurons in the VMM, which would then drive atonia inhibiting motor neurons. This hypothesis is based on the fact that VMM inhibitory neurons disrupt atonia if damaged [101]. An alternative to this pathway includes SLD neurons directly stimulating GABA and glycinergic spinal interneurons, which would then hyperpolarize motor neurons [98]. All

these circuits might coexist and cooperate to drive muscular atonia, but more research would be necessary to clarify functional neuronal connections.

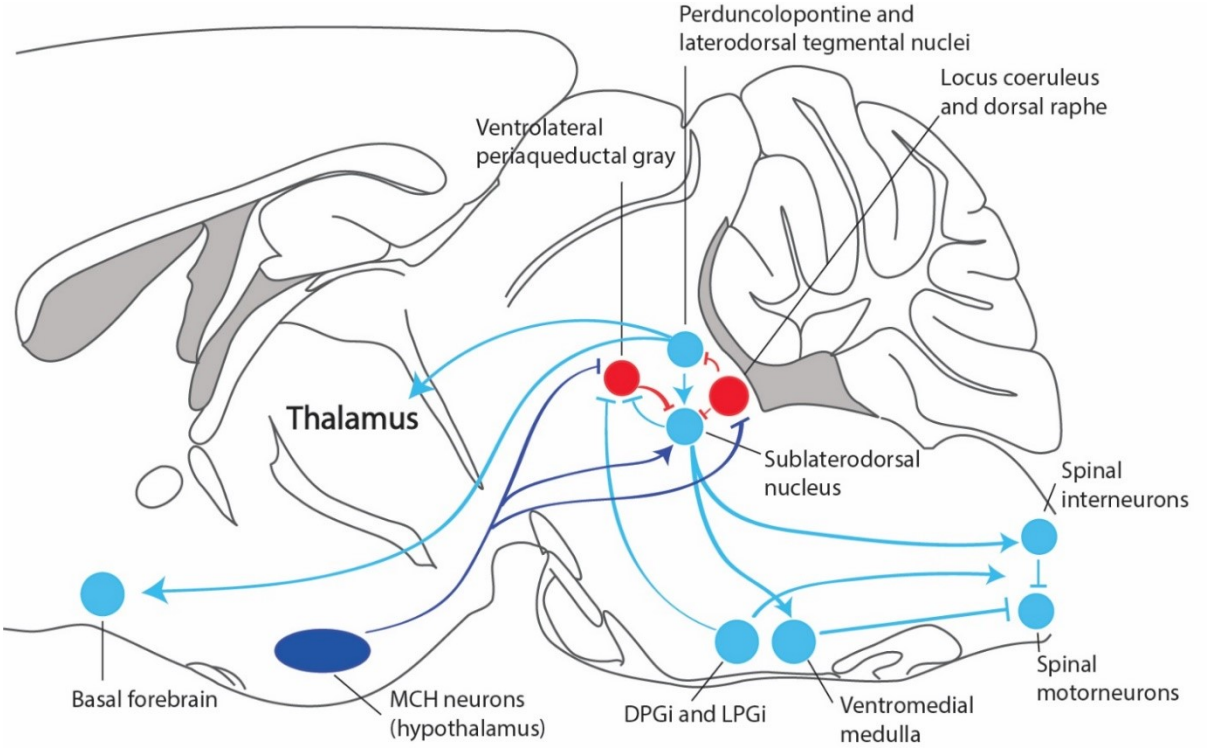

Figure 1.4.5 Ascending and descending pathways controlling REM sleep.
In blue are shown the main brain areas responsible for REM sleep regulation, which inhibit wake promoting areas (in red) to maintain REM sleep. The SLD, fundamental for muscular paralysis, controls directly and indirectly the activity of spinal motor neurons, with the ventromedial medulla (VMM) and the dorsal paragigantocellular reticular nucleus (DPGi). SLD GABAergic neurons might promote REM sleep inhibiting vPAG neurons as well. In dark blue, MCH neurons from the hypothalamus send connection to inhibit vPAG, LC and DRN and to activate the SLDs. LPGi = lateral paragigantocellular nucleus. Graph drawn by me.

Despite controversies previously described in great detail [33], a model possibly explaining SLD activation during REM sleep includes a feed-forward inhibition loop between REM-on GABAergic SLD neurons and REM-off GABAergic projections from the vPAG and the neighbouring lateral pontine tegmentum (LPT) [98]. This flip-flop switch could regulate transitions from REM sleep and wake, but secondary effectors which could regulate both the REM-off and REM-on neurons in a fully described network remain to identify.

The lateral paragigantocellular nuclei (LPGi) are also important for REM sleep activation and atonia. These nuclei in the medulla are cFos labelled during REM sleep [102], and when LPGi GABAergic neurons are activated, more transition to REM from NREM sleep are present and REM sleep episodes last longer compared to controls. The activation of inhibitory LPGi neurons suppresses locomotion [103], since LPGi projects directly to the spinal cord [104, 105].

Researchers are now focusing on REM active neurons not only in the brainstem, but in the hypothalamus as well. As mentioned before, using cFos IHC, some galaninergic and GABAergic neurons appear active during REM sleep in the POA [77]. Additionally, hypothalamic neurons producing melanin-concentrating hormone (MCH) are important for REM sleep maintenance. They fire at highest rates during REM sleep, and, when activated, MCH neurons increase REM sleep time [106]. However, it is still unclear how MCH neurons mediated REM sleep. These neurons project both to REM sleep active areas, including the SLD, and to REM-off nuclei, including the vPAG, LC and DRN. MCH neurons can, in fact, release both GABA and glutamate, and it is possible that they could release inhibitory signals in REM-off nuclei, while sending excitatory projections to REM-on centres [107, 108].

Although great progresses have been achieved in learning the neuronal components of REM descending regulatory pathways, little is still known regarding the ascending pathway, and nuclei and areas which might be responsible for REM sleep cortical activity and dreaming phase. Additionally, researches still do not know why sleep cycles between NREM and REM phase, what regulates the timing of this cycle, and why our brain is wired to wake up from REM sleep rather the NREM.

1.5 Sleep homeostasis and synaptic plasticity

1.5.1 Parameters for sleep homeostasis

Our laboratory has been long interested in understanding the mechanisms regulating the process S, or sleep homeostasis. After decades of sleep research, little is known regarding why the body needs to sleep, and what are the molecular and cellular processes that tell the brain to sleep after a long time spent awake.

As mentioned before, sleep homeostasis refers to the sleep pressure that builds up the longer one has been awake. This pressure has been so far quantified with different parameters, the main one being the SWA, or delta power. However, to understand molecular and/or biochemical factors explaining sleep pressure, more than 100 years ago, researchers discovered that injection of the cerebrospinal fluid from a sleep deprived dog into a normal one induced sleep [109, 110], pioneering the idea that sleep pressure was exerted by substances, or somnogens, that cumulates in the brain during wakefulness. Many laboratories have since been focusing on quantifying brain extracellular substances, which increase during wakefulness to dissipate during the first NREM sleep episode. Among those substances adenosine [111], interleukin-1β [112] and Tumour Necrosis Factor (TNF)-α [113, 114] have been thoroughly studied.

Adenosine has been one of the most discussed molecules amongst the somnogens, as it cumulates during wakefulness in different brain areas, including the BF (Figure 1.5.1, top left) and the hippocampus, to possibly stimulate sleep promoting neurons and induce NREM sleep. This molecule acts on inhibitory A1 and excitatory A2A receptors, and it's possible that adenosine is capable of inhibiting wake promoting neurons via A1 receptors and exciting sleep active circuits through A2A receptor. In a knockout (KO) mouse model of A2A receptor, NREM sleep rebound following sleep deprivation was reduced [115], while conditional KO of A1 receptor in wake promoting area attenuated the SWA rebounds induce by sleep deprivation [116, 117], although a general A1 KO did not affect sleep and SWA homeostatic rebound [118]. More recently, the measurements of adenosine have been criticized, and new requirements focused on reproducing the original adenosine quantification data during wakefulness have yet to be satisfied [119].

Astrocytes, a class of glial cells abundantly present in the brain to regulate neuronal transmission and maintain neuronal health, have been reported to regulate sleep homeostasis, mainly affecting the extracellular levels of adenosine [120]. Astrocytes seem, in fact, to be the main producer of extracellular adenosine following prolonged wakefulness [121], but no clear mechanisms on how wake or sleep affect this cell type has been yet explained.

Neuronal nitric oxide synthase (nNos or Nos1) also regulates sleep homeostasis, in particular the increase in SWA following sleep deprivation: KO of nNos showed attenuated SWA response during sleep [122]. Moreover, GABAergic cortical interneurons expressing nNos seem to be activated in relation to NREM sleep amounts and SWA, as

shown using cFos IHC [122, 123]. Prostaglandin D2 is another potent somnogen, since its injection in sleep regulatory areas as the POA causes increased sleep and neuronal activation [124].

Apart from sleep regulatory substances, some laboratories interested in identifying ties between sleep behaviours and genes functions, have demonstrated how genes of transcriptional factors, circadian clock genes and neurotransmitter receptors subunits, are involved in regulating sleep homeostasis as well, promoting the idea of sleep as genetically encoded [125-131].

All these parameters do not fully explain how sleep regulation and specifically sleep homeostasis work. In fact, debates is still open regarding how sleep is initiated, if on a global cerebral level or from the cellular activity of smaller networks and circuits, more similar to plasticity and inflammation processes [132, 133]. The fact that sleep could be differently regulated and present in different areas of the brain would also change the idea of SWA as universal parameter for sleep pressure and homeostasis, since it has been reported before how SWA could differ drastically based on the position of the EEG electrodes on the cortex. A further problem in relying on SWA quantification as a measure of sleep homeostasis is that SWA could be easily disrupted. In fact, SWA increases after sleep deprivation [134], but with more complex and longer protocols of sleep restrictions SWA does not increase anymore and can no longer explain sleep homeostasis [28, 135, 136]. In addition to this, it is also complicated to justify with a parameter like SWA, calculated only on global cortical neuronal activity, all the changes happening in brain sleep regulatory areas when going from prolonged wakefulness to sleep. In fact, these brain areas and circuits do not seem to be directly affected by cortical SWA increase or decrease and no connection has still been demonstrated between sleep regulatory networks and EEG delta power.

Regarding sleep regulatory substances, the oscillation in their extracellular concertation seems to be related to sleep and wake cycles, but it is difficult to understand whether their oscillation is cause or effect of changes in sleep homeostasis and how the component C could affect their production and release in the brain. Moreover, these molecules have been quantified in areas which are not primarily responsible for sleep regulation. This aspect could fit with the hypothesis of sleep acting separately on a local level, but it is complicated to understand how these molecules could affect changes in the behavioural states alternation without directly affecting sleep regulatory neurons.

In addition, most of the research has been done looking at NREM sleep homeostasis, with almost complete disregard for REM sleep homeostasis. REM sleep is, in fact, homeostatically regulated [137] and molecular and cellular mechanisms responsible for this process are yet to be discovered.

An interesting body of research has, on the other hand, found compelling mechanisms underlying sleep homeostasis in the fruit flies *Drosophila melanogaster*. In this model, it was possible to identify a key circuit responsible for sleep homeostasis in the neurons innervating the dorsal fan-shaped body (dFB) [138, 139]. The activity of these neurons is regulated by two different classes of channels, which cause opposite potassium conductance, and therefore different firing rates, based on the behavioural state the fruit fly is in [140]. During wakefulness, dopaminergic inputs on the dFB neurons cause a hyperpolarization of the circuit. Oxidative stress and increased ATP metabolism regulate the kinetics of these potassium channels' subunits on the dFB neurons. Changes in kinetic based on mitochondrial activity seemed to directly affect sleep and wake amounts by acting on the firing rate and activity of these sleep circuits (Figure 1.5.1, top right) [141].

These recent findings suggest that specific mechanisms in sleep regulatory circuits affect sleep homeostasis. This might be true when analysing circuits and behaviours in different animal models, as rodents. However, a specific circuit solely responsible for sleep homeostasis in mice has not been found yet, and genetic knock outs of mammalian orthologous of the same channels discovered in Drosophila did not show altered sleep phenotypes [142].

For these reasons, I decided to investigate alternative and possible mechanisms which could explain sleep homeostasis, as synaptic plasticity (Figure 1.5.1, bottom). In fact, a promising publication used Drosophila as a model to show how increases in cytosolic calcium (Ca^{2+}) levels, N-methyl-D-aspartate receptor (NMDAr) expression and synaptic strength in target brain circuits corresponded to higher sleep drive after sleep deprivation. In this model, disruption of either intracellular Ca^{2+} levels or of NMDAr expression significantly suppressed homeostatic sleep drive [143]. In addition, another paper has demonstrated the importance of calcium-dependent hyperpolarization and NMDA receptor pathway in regulating sleep duration in mice, using both computational neuronal models and several transgenic mouse lines [144]. These publications suggest that common synaptic plasticity pathway might be fundamental to maintain sleep homeostasis.

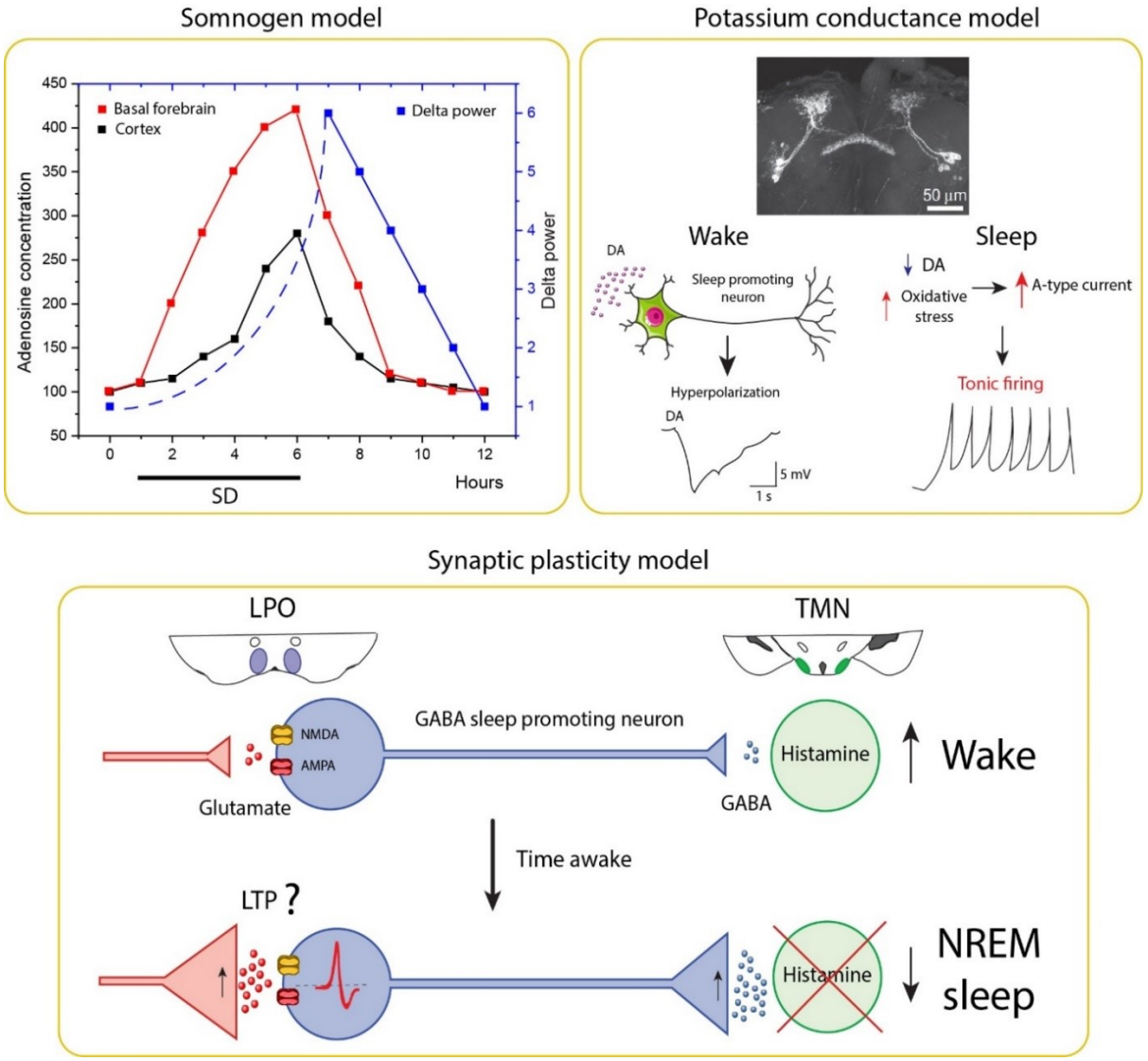

Figure 1.5.1 Three models explaining sleep homeostasis.
From top left, somnogen model with extracellular adenosine increase during sleep deprivation (SD) in both BF (red) and cortex (black). The molecule's levels decrease during recovery sleep, similarly to delta power (blue), however delta power can only be estimated during wakefulness (blue dashed tract). Left, potassium conductance model demonstrated in Drosophila sleep promoting neurons of the dBF. These cells, showed by IHC, receive DA inputs during wake and hyperpolarize. The system allows switches towards sleep by sensing increases in mitochondrial activity and oxidative stress to favour A-type potassium current and generate tonic firing in the sleep promoting neurons. Bottom, synaptic plasticity model: during wake, GABA-LPO neurons are not excited enough to inhibit wake promoting centres, as the histaminergic TMN. Once glutamate synapses on GABA neurons become potentiated enough, they can activate GABA neurons which can then inhibit wake promoting centres. In this case LTP would be happening during wake. Graphs designed by me, dFB IHC from [140].

As for a circuits to study in relation to sleep homeostasis, the POA neurons are particularly active during sleep deprivation and recovery sleep, firing faster than during normal NREM sleep [145], perhaps as a result of sleep homeostasis mechanisms, since it can be hindered by administration of adenosine antagonists [146, 147]. Additionally, our recent paper in press on Current Biology showed how LPO galanin expressing neurons, if deleted, ablate both sleep and delta power rebound following sleep deprivation [148]. I therefore decided to investigate plasticity mechanisms in LPO neurons, firstly starting with targeting all neuronal types, to then narrow down to specific cell types.

In the next paragraph I will discuss the main molecular mechanisms responsible for synaptic plasticity changes involving intracellular Ca^{2+} influx, to then understand whether these pathways might regulate sleep homeostasis.

1.5.2 Synaptic plasticity processes

Brain synapses undergo constant changes and modifications: they can be strengthened, weakened, they can decrease or increase in number for seconds or for years. These processes are referred as long-term potentiation (LTP) and long-term depression (LTD). The former indicates increases in synaptic strength, or up-scaling, while the second denotes weakening of synapses, or downscaling. LTP was firstly discovered in 1973 on glutamate synapses of the hippocampus [149], making researchers believe that synaptic plasticity was reserved to learning and memory processes, happening in fact in the hippocampus. Only later we understood how both LTP and LTD happen in most excitatory synapses in the central nervous system (CNS) and they can be at the base of different brain functions, including addiction [150].

Based on the mechanisms required for plastic changes in synapses, there is a distinction between short-term, intermediate-term and long-term plasticity [151, 152]. Short term plasticity, since it can last only for seconds, relies on post-translational modifications of proteins already presents in the cell. Intermediate-term plasticity lasts between minutes and hours, and it requires *de novo* protein synthesis [153], while long-term plasticity, lasting for hours or more, needs *de novo* gene expression and transcription [154].

One of the most important mechanisms mediating synaptic plasticity is regulated by the glutamate-gated cation channel NMDAr. Together with α-amino-3-hydroxy-5-

methyl-4-isoxazolepropionic acid (AMPA) and kainate receptors, NMDAr is part of the ionotropic glutamate receptors (iGluRs), which respond to transient glutamate release from presynaptic vesicles to generate postsynaptic depolarization.

The NMDAr is present both pre and postsynaptically and it can be found in and outside the synapses. To be activated, NMDAr requires membrane potential depolarization, in order for the voltage dependent magnesium block to be unbound from the receptor [155, 156], and binding of both glutamate and glycine [157]. Once opened, the receptor allows a long duration (e.g. 250 ms) Ca^{2+} influx into the intracellular spaces, which then causes the activation of several intracellular signalling cascades.

The NMDAr is made of two obligatory GluN1 subunits and 2 subunits of GluN2 (NR2A, B, C and D) or GluN3 (NR3A, B). Without GluN1 the receptor cannot be functional or formed [158]. Combinations of different subunits confer a diverse range of properties to the receptor, one being the time the receptor stays open after activation. The receptor can, in fact, be open for few milliseconds, to several seconds [159, 160], with NMDAr containing NR2A subunits being the fastest receptors to close and those containing NR2D subunit the slowest, changing drastically the magnitude of Ca^{2+} influx and duration of the signal sent downstream.

The importance of the receptor in regulating synaptic plasticity has been demonstrated in the hippocampus during memory and learning tasks [161, 162], where synaptic plasticity is consolidated [163]. Ca^{2+} influx in the cellular compartment activates the Ca^{2+}/calmodulin-dependent protein kinase II (CaMKII), which, after auto-phosphorylation, can interact with both NMDAr and AMPAr subunits to mediate synaptic strengthening and upscaling [164, 165]. It is controversial whether NMDAr can modulate not only LTP, but also LTD, and it is still difficult to understand what elements could affect this dual role of the receptors. It is possible that each NR subunit mediates a different outcome to synaptic plasticity [166], but more elements seem to be necessary to justify such drastic changes between LTP and LTD, and the debate remains open.

Another important mechanism capable of mediating LTP and LTD is regulated by the AMPA receptors. In contrast to NMDAr, AMPAr have fast kinetics (1 ms) responding to glutamate release in the extracellular space (Figure 1.5.2).

AMPAr can be composed by the combination of 4 different subunits (GluR1, 2, 3, 4), which can as well modify the properties of the channel. AMPAr with the GluR2 subunit are, in fact, calcium impermeable, and only receptors lacking the GluR2 subunits can

allow calcium influx when the receptor is activated by glutamate. Therefore, combinations of AMPAr subunits generating a calcium permeable receptor, such as GluR1/GluR4, could offer an alternative pathway to the NMDAr in initiating LTP processes dependent on calcium intracellular influx [167], although calcium influx kinetic would be different.

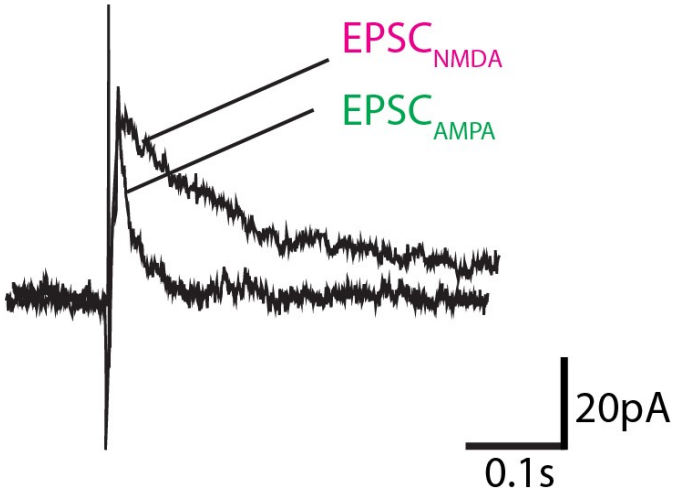

Figure 1.5.2 Excitatory post synaptic currents generated by NMDA or AMPA receptors opening.
Baseline recordings of hypothalamic NMDA or AMPA evoked EPSCs showing differences in the two receptors decay time. Dynamics are recorded after a single spike at *t*=0 and a resting potential of the postsynaptic neuron of -65 mV. Data were recorded from Dr. Kyoko Tossell in the lab.

AMPAr does not regulate synaptic plasticity only by intracellular calcium increases. In fact, phosphorylation and membrane trafficking of AMPAr on postsynaptic membrane and spines are associated to LTP and LTD [168], and diffusion of AMPA receptors on hippocampal neurons is necessary for specific memory processes [169].

A huge volume of research has been carried out on synaptic plasticity, and it is virtually impossible to list all of it here. However, it is important to know that molecular pathways regulating up and downscaling of synapses are not certainly restricted to NMDA and AMPA receptors and to the hippocampus. Mitochondria, for example, play a fundamental role in NMDAr induced LTP [170], and also astrocytes and microglia regulate neuronal plasticity [171, 172].

Synaptic plasticity has also been identified in many different areas of the brain in addition to the hippocampus, such as VTA, amygdala, visual cortex, and thalamus [173-177]. LTP has been detected at different types of synapses, including GABAergic

inhibitory ones [178, 179], and it has been associated with different brain functions, beyond memory, e.g. addiction. The variability itself of the plasticity process, including synaptic potentiation and depression sharing same molecular pathways, and the temporal scale of its effects, spacing from milliseconds to years, make the mechanisms particularly difficult to pinpoint. Because the molecules regulating synaptic plasticity are present possibly on all excitatory and inhibitory synapses in the brain, it is easy to assume that all these neurons undergo a certain level of synaptic plasticity. It is therefore interesting to understand which mechanisms and pathways might connect synaptic plasticity to sleep.

1.5.3 Plasticity mechanisms during sleep

The idea that sleep and synaptic plasticity are interconnected firstly came from the researchers Crick and Mitchison, who hypothesized that REM sleep was necessary for reverse learning, or as they phrase it "*to remove certain undesirable modes of interaction in networks of cells in the cerebral cortex*" [95]. Since then, numerous research groups have started investigating this interaction, although without coming to a unison and agreeable outcome.

Most of the research focusing on explaining the connections between sleep and plasticity has looked at how different sleep patterns, such as SWS, REM sleep and sleep deprivation, might influence synaptic homeostasis, referred as the plasticity mechanisms involved in stabilizing neuronal and circuit activity [180]. One of the most popular and long discussed theories connecting sleep and synaptic plasticity, and related to the Crick and Mitchinson hypothesis, comes from the laboratory of Chiara Cirelli and Giulio Tonini, who have been trying for decades to demonstrate their synaptic homeostasis hypothesis (SHY)[181]. The SHY theory proposes that during wakefulness neurons are active and plastic, learning tasks, regulating behaviour and strengthening connections. These processes are energetically demanding and not sustainable for the brain on the long term. SWS becomes then a necessary step, to downscale neuronal circuits, restore cellular homeostasis and rebalance the brain energy level [182, 183]. Other labs have observed downscaling during sleep, identifying the immediate early gene Homer1a as an essential effector governing synapses homeostasis and scaling-down during sleep. Homer1a can,

in fact, alter the function of glutamate receptors on excitatory synapses during sleep, to weaken or remodel their connections in favour of memory consolidation [184].

A controversy in the SHY theory and supporting articles is that we are still lacking major molecular and cellular pathways which could potentially connect both upscaling during wake and downscaling during sleep. Even though Diering *et al,* explained a potential pathway connecting synaptic plasticity to sleep, Tononi and Cirelli have failed to propose a convincing molecular explanation to their theory, and they do not have a convincing *in vivo* model demonstrating how changes in synaptic plasticity during sleep or wake might affect sleep behaviours.

Another controversy in those publications is the fact that no experiments have been performed on sleep regulatory areas. Researchers have so far looked at neocortex or hippocampus, which are easier to manipulate and where most of the plasticity mechanisms have always been studied. No study has investigated possible plasticity mechanisms in brain areas involved in sleep regulation, and alternative synaptic changes that might happen in NREM, REM and wake active networks. During sleep, circuits responsible for NREM maintenance could undergo short LTP while wake promoting neurons, silenced during NREM, undergo LTD. The opposite could happen during wake, generating a heterogeneity of plastic mechanisms which have not been considered yet.

Apart from criticisms, several studies have also challenged the SHY hypothesis. A study performed on cat brain tissue demonstrated that potentiation of excitatory postsynaptic potential happens during SWS and not during wakefulness, better justifying the idea that SWS controls learning and memory consolidation with both NMDA and AMPA signalling [185]. Another study showed how synaptic downscaling occurs not during NREM sleep episodes but during REM, more in line with Crick and Mitchison original hypothesis. In fact, hippocampal neurons firing rate (FR) decreased during REM sleep [186], allowing networks homeostasis to happen, as REM sleep also allows pruning and strengthening of synapses in the cortex to optimize learning and behavioural tasks consolidation [187].

More research has also been carried out studying FR of primary visual cortex (V1) neurons across behavioural states. No link between FR changes and behavioural states was recorded at baseline levels in V1 neurons. However, when looking at the firing rate homeostasis following visual deprivation, the homeostatic rebound was present only during wake episodes, implying that synaptic homeostasis and plasticity can only happen during wakefulness and not during sleep, opposite to the SHY theory [188].

An additional publication have investigated the neuronal excitability of neocortical neurons during behavioural state. This research group found that the net distribution of FR variation in pyramidal neurons decrease during NREM, as activity of fast-firing neurons decreased, while the one from slow-firing neurons increased, supporting the idea that different neurons have diverse functions in maintaining network homeostasis and excitability [189]. These results partially disagree with the SHY theory, which states that during SWS firing rate is globally reduced [190]. Interestingly, a general and uniform reduction in FR was found during REM sleep, confirming the role of REM sleep in an overall downscaling of network excitability [186].

A different research group found that dendritic spines in the CA1 region of the hippocampus decrease during sleep deprivation and increase during recovery sleep. Specifically, they found that the protein cofilin, which cuts actin filaments, increases in activity with reduced sleep in the CA1 region of the hippocampus. Inhibiting cofilin's molecular pathway in a mouse model averted both signalling and cognitive deficits caused by sleep deprivation [1]. This work is the only one showing a rescue in a memory deficit phenotype targeting a specific molecular pathway in an *in vivo* model, making it a more robust demonstration to their findings.

In addition to research focusing on how sleep might affect synaptic plasticity mechanisms, some researchers have focused on the opposite direction of this tight relationship: how LTP and LTD might affect sleep.

One study has looked at how both AMPA and NMDA receptors are responsible for sleep-dependent memory consolidation, which cannot happen under exposure to glutamate receptor antagonists [191]. Additionally, works mentioned in the previous paragraph, showed NMDA and Ca^{2+} levels are essential for sleep homeostasis maintenance in fruit flies [143], while studies on rodents showed that NMDA receptor pathway is important for regulating sleep duration [144]. No common explanation or theories have been explained in these published works, but they at least offer more insights and ideas on how to approach this very complicated interaction between a behavioural phenomenon like sleep and a molecular process like synaptic plasticity.

1.6 The link between sleep and sedation

For many years, our lab has been interested in how sedatives might promote sleep by selective interaction with the sleep-wake circuitry. At lower doses, anaesthetic drugs cause a sedative state, producing a temporary and reversible loss of consciousness and motor activity, similar to natural sleep. During sedation, the EEG delta power increases, while breathing rate and body temperature decrease, and slow cognitive responsiveness is maintained. Because main autonomic and respiratory functions are not disrupted during this state, sedatives used in intensive care units help reducing delirium and distress from patients, and in promoting sleep. However, the sedative state is not identical to natural sleep, even though some sedatives and sleep promoting drugs act on small local circuits belonging to sleep and wake regulatory networks to induce a NREM-like state [50]. At higher doses, anaesthetic drugs cause general anaesthesia. This state causes unconsciousness, immobility and analgesia. General anaesthesia strongly inhibits reflexes coming from both brainstem and hypothalamus, forcing subjects to be under constant external cardiorespiratory and thermoregulatory support [192]. It also inhibits cortical waves, so that EEG traces appear flat. Because of these characteristics, general anaesthesia cannot be compared to and does not resemble natural sleep [193].

In light of sedation's similarity to NREM sleep, researchers have been trying to identify common pathways activated by the two states, to better understand how both anaesthetic drugs and sleep work. During my studies, I worked with two different types of anaesthetics, dexmedetomidine (Dex) and propofol.

Dex is a α2 adrenergic receptor agonist and it is used as an effective sedation method in intensive care units [194]. Dex causes a state which resembles NREM sleep in rodents and stage 2 of NREM sleep in humans, although it also causes hypothermia and vasodilatation with subsequent reduced blood pressure [195]. Dex was thought to exert its sedative effects by inhibiting NE release from LC neurons [196], however when inhibiting the NE transmission system or knocking down locally the A2A receptor in the LC, mice can still show increased EEG delta power following Dex injection and decreased body temperature [72, 197]. On the other hand, our lab showed by cFos activity tagging that reactivation of LPO neurons tagged by Dex injections recapitulates sleep-like and temperature phenotype induced by Dex [50, 72] (Figure 1.6.1, A). Additionally, the main type of neurons required for Dex's response expresses the galanin peptide, as we showed that lesioning galanin neurons in LPO reduces Dex's sleep and hypothermic-promoting

effects [148]. These results demonstrate that LPO circuit is sufficient to mediate the sedative effects of Dex and, we propose that at higher doses, Dex can inhibit neurons in the LC to induce loss of postural muscle tone [72].

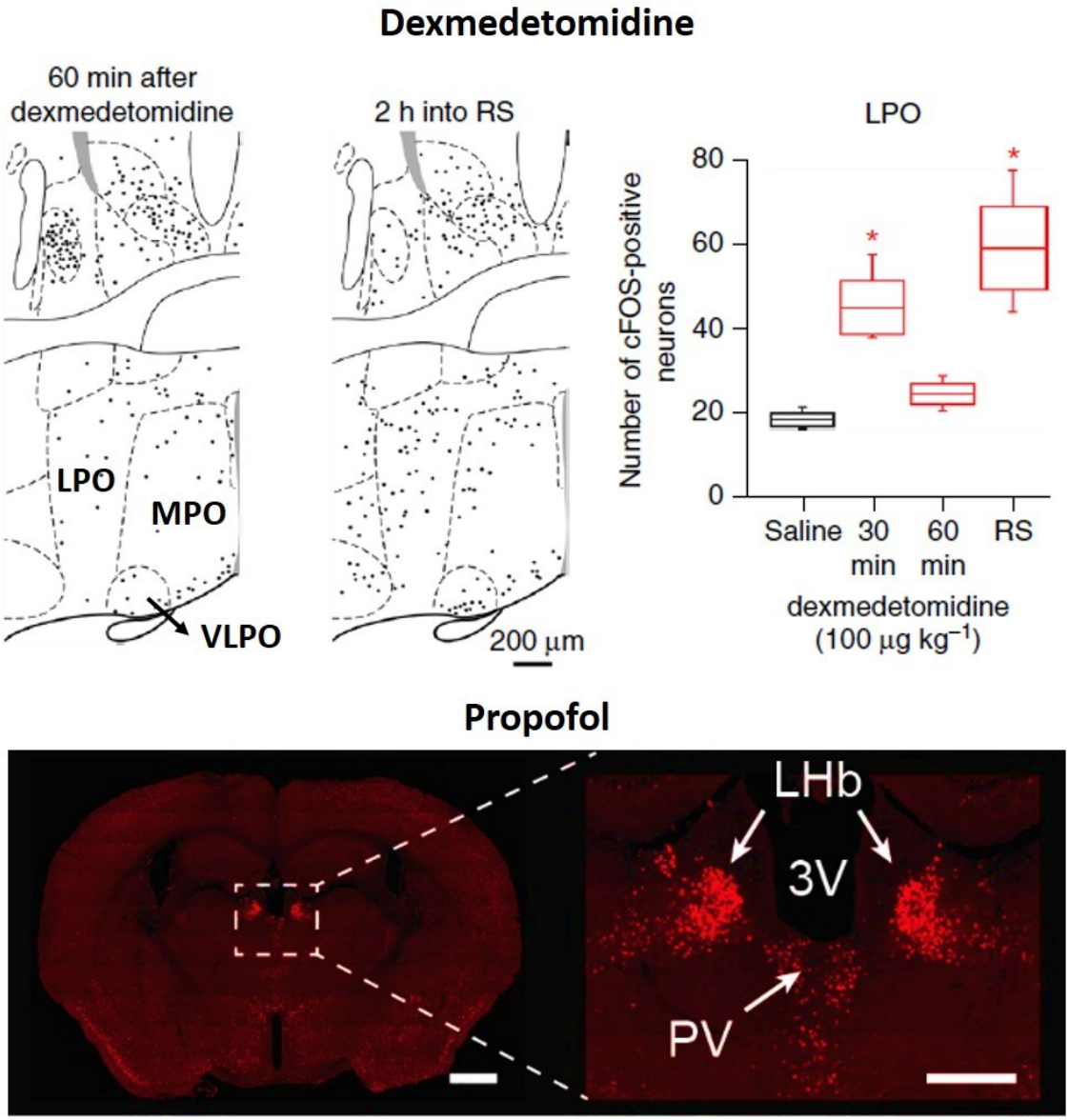

Figure 1.6.1 Dexmedetomidine and Propofol cause cFos activation in LPO and LHb. A, Dexmedetomidine induces cFos expression in the POA following Dex injection or 2 hours of recovery sleep (RS) following 4h sleep deprivation (SD). Reactivation of those tagged cells caused a NREM-like state and reduced body-temperature. Left quantification of cFos positive cells in LPO after saline injection, 30 and 60 minutes after dex injection or following recovery sleep. Graphs from [72]. B, cFos positive neurons in the LHb and not in the MHb following i.p. propofol injections. PV = paraventricular thalamic nucleus. IHC from [198].

Propofol is a strong intravenous anaesthetic, possibly the most widely used nowadays to induce and maintain general anaesthesia. It is a positive allosteric modulator that

interacts with the $GABA_A$ receptor β subunit [199], important to induce anaesthesia, as specific mutations in the receptor's β subunit sequences could reduce, or even remove, sensitivity to propofol [200, 201]. At sedative doses, as opposed to the higher ones used for general anaesthesia, propofol causes thalamocortical oscillations in the EEG, which can be also found during NREM sleep, connecting again the neuronal mechanisms of sedation to sleep [202-204]. To generate such oscillations, propofol might act directly on hypothalamic circuits involved in behavioural states regulation, as the MPA and even the histamine neurons in the TMN. In fact, local infusions of $GABA_A$ receptor agonists in the MPA or TMN induce sleep-like state and sedation [205, 206]; and prolongation of IPSCs on histamine neurons to another $GABA_A$ receptor allosteric modulator zolpidem is sufficient to induce NREM sleep [207].

Interestingly, it has been shown how both GABAergic anaesthetics and α2 adrenergic agonists such as Dex increase cFos activation in sleep promoting areas, as the preoptic area, while reducing it in wake active ones, including cholinergic, monoaminergic and orexinergic neurons [208-210]. Our lab has discovered increased cFos activity under propofol injection in a different area from the ones so far discussed: the lateral habenula (LHb, Figure 1.6.1, B) [209, 211].

The LHb is a small glutamatergic hub located in the epithalamus and involved in different aspects of brain functions and behaviours, from the reward system, to depression, decision making, stress, aversion and pain [212]. This nucleus has been associated to sleep, wake and circadian rhythm regulation, since it receives and sends connections to the 5HT neurons of the DRN and is innervated by SCN projections [213]. Importantly, lesions to the LHb cause a reduction in REM sleep [214], suggesting that its activation would increase REM sleep. The LHb is, in fact, hyperactive in depressed patients, which show increased REM sleep amounts and shorter latency in transitioning to this state [215]. Interestingly, a different publication showed increases in NREM sleep and decreases in REM after short electrical LHb stimulation, proposing that LHb promotes sleep by inhibiting 5-HT wake promoting neurons in the DRN [216].

Apart from playing a role in sleep regulation, one of the main functions of the LHb is to suppress motor activity, which can be controlled by sending inhibitory projection to the VTA [217], where motor responses to aversive stimuli can then be regulated [218].

Because of its involvement in regulating sleep, wake and motor activity, and its activation under anaesthesia, the LHb is an interesting circuit to investigate to

understand how both sleep and anaesthesia work. With propofol, although we know its molecular targets and the brain areas which mediates its effects, little is known regarding complete networks and circuits capable of inducing sedation.

1.7 Projects aims

Because of the lack of knowledge on the mechanisms regulating sleep homeostasis, I have been wanting to find novel and innovative explanations that could justify sleep need and pressure. To do so, I decided to focus on one of the major areas responsible for sleep regulation, the LPO of the hypothalamus. In this area, I investigated whether fundamental pathways responsible for synaptic plasticity, such as the NMDAr pathway, could, via mediating plastic changes, regulate sleep amounts and patterns (Figure 1.5.1). I genetically deleted the NMDA receptor in the mouse LPO hypothalamic area and studied behaviours and sleep phenotype of these experimental animals. I also participated in the publication Ma *et al*. in press in Current Biology, which showed that ablation of galanin neurons in the LPO substantially abolished sleep homeostasis and the sedative and hypothermic actions of dexmedetomidine [148].

In addition to studying plasticity changes related to sleep homeostasis, I also investigated the physiological activity of different neuronal subtypes in LPO during behavioural states. I analysed the activity of both excitatory and inhibitory neurons, identifying different patterns of activation between neuronal subtypes and subareas of the PO region. I also investigated how anaesthetic drugs like Dex could influence LPO activity at the onset of and during sedation.

Finally, to better understand the connections and ties between sleep and sedation, I participated in the work resulted in publication [198] focused on the role of the LHb in mediating propofol induced sedation and in sleep regulation. In this project, I investigated the neuronal activity of the LHb during sleep and wake, and I analysed the effects of LHb optogenetic activation on sleep and wake patterns.

2 Materials and methods

2.1 Animals

I held a personal licence from the UK Home Office, and attended and qualified for all relevant procedures. All experiments were performed in accordance with the United Kingdom Home Office Animal Procedures Act (1986) and were approved by the Imperial College Ethical Review Committee. Wild type C57BL/6N mice were purchased from Charles Rivers at 7/8 weeks of age. $NR1^{flox}$, or fNR1 mice[162], were purchased from The Jackson Laboratory (Jack stock number 005246) after donation of Dr. Susumu Tonegawa, Massachusetts Institute of Technology. The *Grm2-Cre* mouse line was generated by GENSAT and obtained from the Mouse Mutant Resource Center (UC Davis, Davis, CA), stock *Tg*(*Grm2-Cre*) *MR90Gsat/Mmcd* (The Gene Expression Nervous System Atlas - GENSAT - Project, NINDS Contracts N01NS02331 & HHSN271200723701C to The Rockefeller University, New York, NY)[219]. We maintained the line as heterozygotes using as genotyping primers *Grm2*(*34611*)*F* (5'-GGCAGCCACTCTTTGGTTCTACTC-3') and *CreGS-R1* (5'-CGGCAAACGGACAGAAGCATT-3'). Galanin-Cre mice (Tg(Gal-cre)KI87Gsat/Mmucd) were generated by GENSAT and deposited at the Mutant Mouse Regional Resource Center, stock No. 031060-UCD, GENSAT- Project (NINDS Contracts N01NS02331 & HHSN271200723701C to The Rockefeller University, New York)[220]. Vglut2-Cre animals (*Vglut2-ires-Cre: Slc17a6*$^{tm2(cre)Lowl}$*/J*) were kindly provided by B.B. Lowell and purchased from The Jackson Laboratory (JAX stock 016963)[221]. Vgat-Cre mice (*Vgat-ires-Cre: Slc32a1*$^{tm2(cre)Lowl}$*/J*), were kindly provided by B.B. Lowell, and purchased from The Jackson Laboratory (JAX stock 016962)[221]. Nos-Cre animals (*Nos1-ires-Cre*$^{tm1(cre)Mgmj}$/J) were purchased from The Jackson Laboratory (JAX stock 017526)[222]. All mice were housed in maximum five mice per cage with food and water ad libitum and maintained under the same conditions (21±1C, reversed 12h dark/light cycle starting at 5:00 AM). Behavioural experiments were performed during lights-OFF unless otherwise specified, while photometry recordings were performed during lights-ON.

2.2 Plasmids and AAV particles

All AAV particles containing specific plasmids were produced in our laboratory by Raquel Yustos as previously described [43]. Plasmid *pAAV-iCre-2A-Venus* was provided by Thomas Kuner [223]. Plasmid *pAAV-GFP* was a gift from John T. Gray (Addgene plasmid 32396). To create *pAAV-hsyn-GCaMP6s* and the *pAAV-hsyn-flex-GCaMP6s*, the *GCaMP6s* reading frame from *pGP-CMV-GCaMP6s* (Addgene plasmid 40753, gift of Douglas Kim) [224] was mutated into *pAAV-flex-hM3D$_q$-mCHERRY[225],* either removing the *flex-M3-cherry* component or keeping both sets of *loxP* sites (*pAAV-flex* backbone), respectively. In a similar manner, the *AAV-hsyn-ChR2-YFP* virus was produces obtaining the Channelrodhopsin 2 (ChR2) sequence from the plasmid *pAAV-CaMKIIa-hChR2(H134R)-EYFP* (Addgene plasmid 26969)[226] and mutated into into *pAAV-flex-hM3D$_q$-mCHERRY* removing the *flex-M3-cherry* sequence. The flex-ChR2 virus was produced from packaging the viral plasmid *pAAV-EF1a-double floxed-hChR2(H134R)-EYFP-WPRE-HGHpA* (Addgene #20298), gifted by the laboratory of Karl Deisseroth. The *AAV5.GFAP.Cre.WPRE.hGH*, referred as *AAV5-GFAP-Cre* in this thesis, was purchased from Addgene (#105550) and gifted by James M. Wilson.

2.3 Surgeries – EEG and fibres

All surgeries used adult male mice, 8-12 weeks old and were performed under deep general anaesthesia with isoflurane (3% induction/ 2% maintenance) and under sterile conditions. Before starting the surgery, mice were injected subcutaneously (s.c.) with Buprenorphine (Vetergesic 0.3 mg/mL, 1:20 dilution in 0.9% sterile saline solution, final 0.1mg/kg) and Carprofen (Rimadyl 50mg/mL, 1:50 dilution in 0.9% sterile saline solution, final 5 mg/kg) and then places in a stereotaxic frame. Mouse core temperature was constantly checked by rectal probe and respiratory rate by eye.

For AAV injections, the virus was injected using Hamilton microliter #701 10 µL syringes and a stainless-steel needle (33-gauge, 15 mm long). LPO coordinates used for bilateral injection sites were relative to Bregma: AP, +0.40; ML, -/+ 0.75, DV was consecutive, injecting half volume at +5.20 and half at +5.15. A total volume of 0.3 µL each side was injected. After injection, the needle was left in place for additional 5 minutes and then slowly withdrawn. Control AHA coordinates used for bilateral injections sites were relative to Bregma: AP, -0.58; ML, -/+ 0.65; DV, +5.60 and +5.50 for consecutive injections

of 0.15 µL at each DV position, for a total of 0.30 µL of viral solution injected in each side of the brain. The LHb coordinates used for unilateral injection were relative to Bregma: AP, -1.70; ML, + 0.44; DV was consecutive, injecting half volume at +2.90 and half at +2.80, mm for a total volume of 0.4 µL.

For sleep recordings, two or three EEG screw electrodes were chronically implanted on mice skull and 2 EMG wire electrodes were inserted in the neck extensor muscles. The two EEG screws were placed aligned unilaterally on the right side of the skull, one on the frontal bone (-1.5 mm midline, +1.5 mm Bregma) and one on the parietal bone (-1.5 mm midline, -2 mm Bregma). The additional third screw used during photometry and optogenetic recording was placed on the left parietal bone, aligned with the right one (+1.5 mm midline, -2 mm Bregma).

For all surgeries, the wound was sewed around the headstage and the mouse was left recovering in a heat box. All instrumented mice were single-housed to avoid lesions to the headstage. Mice injected with AAVs were allowed 1 month for recovering and for the viral transgenes to adequately express before being fitted with Neurologger 2A devices (see below) and undergoing any experimental procedure.

2.4 EEG/EMG recordings and analysis

EEG and EMG traces were recorded using Neurologger 2A devices as described before [227-229], at a sampling rate of 200 Hz. The data obtained from the Neurolegger 2A were downloaded and visualized using Spike2 Software (Cambridge Electronic Design, Cambridge, UK). The EEG was high pass filtered (0.5Hz, -3dB) using a digital filter, while EMG was band pass filtered between 5-45 Hz (-3dB). To define the vigilance states of Wake, NREM and REM sleep, delta power (0.5-4.5 Hz) and theta ratio (theta power [5-10 Hz]/delta power) were calculated, as well as the EMG integral. Automated sleep scoring was performed using a Spike2 script and the result was manually corrected. For the three vigilance states, amounts percentages were calculate using costume Spike2 scripts. For sleep architecture analysis, costume MATLAB scripts were used. Fast Fourier transformation (512 points) was used to calculate EEG power spectra. Each frequency band was normalized to the sum of the power over the entire frequency range extracted (0-35 Hz).

2.5 Sleep deprivation protocol and dexmedetomidine injections

For fNR1 sleep recordings, mice were fitted with Neurolegger 2A devices and the 24h sleep-wake baseline (BL) was recorded. After BL, mice with Neurologger 2A were sleep deprived from light period onset (5:00pm) for 6 hours, introducing novel objects in their home cage [230]. Constant supervision from the experimenter throughout the 6 hours of SD was necessary to prevent mice falling asleep. When mice were seen nesting or grooming, defined as common signs of sleep preparation, novel objects were immediately introduced to the cage without directly disturbing the animals. In fact, to make the procedure minimally stressful, mice were never touched or pocked apart for changing cages. Sleep recordings were stopped at the end of the dark period of the following day (5:00pm).

Dexmedetomidine injections for sleep and photometry recordings were prepared from stock solution of 0.5 mg/mL (Dexdomitor), diluted in sterile saline before injections. Mice were i.p. injected with the dose of 50 µg/kg at 5:00 pm (lights-ON) to record sleep and *in vivo* calcium signal overnight.

2.6 Open field test

To measure fNR1 mice locomotor activity, mice were left for 30 minutes during the dark period in an open field (50x50 cm), constantly monitored by a video camera. Central zone used for analysis was 4 times smaller than the arena. Mouse tracking and calculation of total distance travelled was performed using ANY-maze software (Ugo Basile, Dublin, Ireland).

2.7 Histology and immunostaining

Before perfusion, animals were injected i.p. with Pentobarbitone (Pentojet, 1:5 dilution in phosphate-buffered saline, PBS) and checked for loss of reflexes before proceeding. When completely not responsive, animals were perfused transcardially with 20 mL of cold PBS at a rate on 4 mL/min, followed by 20 mL 4% paraformaldehyde (PFA, 4mL/min) in PBS. Brains were dissected and post-fixed in 4% PFA overnight, and then transferred in 30% sucrose in PBS until the brain sunk in the solution. After 3 days in sucrose, brains were ready to be cut using a microtome (Leica) after being frozen with dry ice on the microtome stage. 35-µm coronal slices were collected in a 24-well plate with PBS and slices embedding LPO or LHb area were selected for staining. Firstly, slices

were transferred in an epitope retrieval solution (0.05% Tween-20, 10 mM sodium citrate buffer, and pH 6.0) for 20min at 80-85°C, then left at room temperature (RT) for 15min before being washed, to avoid breaking or damaging the heated tissue. After 3 washes of 10min in PBS, brain slices were transferred in 0.2% Triton™ x-100 (Sigma-Aldrich), 20% Normal Goat Serum (NGS, Vector Laboratories) in PBS for 1h at RT, shaking. Primary antibody staining was then performed overnight at 4°C shaking in 0.2% Triton, 2% NGS in PBS. In case of double staining, both primary antibodies were added in the solution unless cross-reactivity was previously observed. The following day, slices were washed 3 times in PBS for 10 minutes and then secondary antibody solution was applied for 1h and 30 min in 0.2% Triton, 2% NGS in PBS, at RT shacking. If double staining was required, washes and another secondary antibody incubation were carried out. For anti-IBA1 staining, donkey normal serum was used instead that NGS with same dilutions. After secondary antibodies incubations, slices were washed again for 3 times for 10min, RT in PBS shacking and DAPI staining (1:5000 in PBS, Hoechst 33342, Life Technologies) was then performed for a maximum of 10min. After at least 1 wash in PBS, slices were ready to be mounted. For mounting, microscope slides (Superfrost PLUS, Thermo Scientific), mounting media ProLong™ Gold Antifade Reagent (Invitrogen) and glass cover slides (24 x 50 mm, VWR Internartional) were used. Slices were left overnight at RT in the dark to ensure that the mounting media was fixed, and then stored at 4°C. Primary antibodies: rabbit anti-GFP (Invotrogen, A6455, 1:1000), chicken anti-GFP (Abcam, ab13970, 1:1000), rabbit anti-GFAP (Dako, Z0334, 1:500), goat anti-IBA-1 (Abcam, ab5076, 1:500), rabbit anti-cFos (Millipore, ABE457, 1:2000). Secondary antibodies (all from Invitrogen): Alexa Fluor-488 goat anti-Chicken (A11039, 1:500), Alexa Fluor-488 goat anti-rabbit (A11008, 1:500), Alexa Fluor-594 goat anti rabbit (A11072, 1:500) and Alexa Fluor-594 donkey anti-goat (A11058, 1:500).

2.8 Brain punches and quantitative PCR

After quick cervical dislocation, the brain from C57BL/6N mice was extracted fresh, and sliced using a brain matrix with 2mm thickness. Punches of LPO area, cortex and cerebellum were performed using two microdissection blades (Fine Science Tools) and transferred immediately in dry ice. Samples were then kept at -80C for at least 24h before RNA extraction, to ensure tissue was completely frozen. Total RNA was extracted using

TRIzol-Reagent protocol (Invitrogen, cat. 15586026). For qPCR assay conditions and controls, Minimal Information for Publication of Quantitative Real-Time PCR Experiments (MIQE) Guidelines were followed [231]. RNA integrity was verified with 1.2% agarose gel and RNA quantity was measured with NanoDrop™ ND-1000 Spectrophotometer (Thermo Fisher). A fixed amount of 600 ng of RNA was then reverse transcribed with High-Capacity cDNA Reverse Transcription Kit (Applied Biosystems, cat. 4368813) using a PCR machine (peqSTAR 96 Universal, Peqlab). The obtained cDNA was then amplified using the buffer from the TaqMan RNA-to-Ct 1-Step Kit (Life Technologies, 4392653) and pre-designed probes for genes of interest TaqMan Gene Expression Assays (GAPDH, Grin1-2a-2b-2c-2d-3a-3b, Gria1-2-3, Thermo Fisher, 4331182) in an Applied Biosystems machine (Foster City, USA). For RT-PCR analysis, the $2^{-\Delta\Delta C_T}$ method [232] was used, using the GAPDH gene as an internal control.

2.9 Acute slice preparation and recordings

Mice were sacrificed by cervical dislocation and subsequent decapitation. The brain was rapidly retrieved to be sliced and placed into cold oxygenated N-Methyl-D-glucamine (NMDG) solution (in mM: NMDG 93, HCl 93, KCl 2.5, NaH2PO4 1.2, NaHCO3 30, HEPES 20, glucose 25, sodium ascorbate 5, Thiourea 2, sodium pyruvate 3, MgSO4 10, CaCl2 0.5). Para-horizontal slices (thickness 300 μm) encompassing the LPO area were obtained using a vibrotome (Vibrating Microtome 7000smz-2; Campden Instruments LTD, UK). Slices were incubated for 15min in NMDG solution at 33 °C with constant oxygenation, and transferred to oxygenated standard aCSF (in mM: NaCl 120, KCl 3.5, NaH2PO4 1.25, NaHCO3 25, glucose 10, MgCl2 1, CaCl2 2) solution for at least 1 hour at room temperature. Slices were transferred to a submersion recording chamber and were continuously perfused at a rate of 4-5ml/min with fully oxygenated aCSF at room temperature. For whole-cell recording, patch pipettes at 4-6 MΩ were pulled from borosilicate glass capillaries (1.5mm OD, 0.86 mm ID, Harvard Apparatus, #GC150F-10) and filled with intracellular solution containing (in mM: 128 $CsCH_3SO_3$, 2.8 NaCl, 20 HEPES, 0.4 EGTA, 5 TEA-Cl, 2 Mg-ATP, 0.5 NaGTP (pH 7.35, osmolality 285mOsm). 0.1% Neurobiotin was included in the intracellular solutions to identify the cell position and morphology following recording. Recordings were performed using a Multiclamp 700B amplifier (Molecular Devices. CA). Access and input resistances were monitored

throughout the experiments. The access resistance was typically < 20 MΩ, and results we discarded if resistance changed by more than 20%.

GFP+ neurons were visually identified and randomly selected. For AMPA and NMDA current, a bipolar stimulus microelectrode (MX21AEW, FHC) was placed 100-200um away from recording site caudally. The intensity of stimulus (10ms) was adjusted to evoke a measurable, evoked EPSC in recording cells. AMPA and NMDA mixed currents were measured at a holding potentials of +40mV. After obtaining at least 10 sweeps of stable mixed currents, D-AP5 (50 μM) was perfused to bath solution for 15min and AMPA currents were measured. NMDA currents were obtained by subtracting AMPA currents from mixed currents off-line. The peak amplitude of both currents were used for AMDA/NMDA ratio analysis. For sEPSCs, GFP+ LPO neurons were voltage clamped at -70mV constantly. A stable baseline recording was obtained for 5-10 min. Frequency, amplitude, rise & decay time constants of sEPSCs were analysed off-line with the Mini Analysis (Synaptosoft). Frequency was obtained from 2 min of recording. All recording were made under the presence of picrotoxin (100 μM).

For immunohistochemistry following electrophysiological recordings, brain slices were post-fixed in 4% PFA overnight at 4 °C. PFA was then washed away 3 times for 10min in PBS and slices were blocked and permeabilized in 20% NGS or 2% Bovine Serum Albumin (BSA) for 3 hours shaking. Primary anti-GFP ab to trace viral distribution was diluted in 2% NGS, 0.5/0.7% TritonX in PBS overnight at 4^{o}C shaking. After 4 washes in PBS fpr 10min each, secondary ab was diluted in 2% NGS and 0.5% TritonX for 3 hour at RT and shaking. After washes and to track Neruobiotin filled neurons recorded by electrophysiology, an Alexa594-conjugated streptavidin (Invitrogen) was diluted 1:500 in 1% NGS, 0.5% TritonX and slices were incubated for 2-3 hours at RT. 4 washes of 15min and subsequent DAPI incubation for 10min were performed before slices were mounted on glass slides as described in Section 2.8.

2.10 *Ex-vivo* extracellular glutamate quantification

Mice were killed by cervical dislocation and subsequent decapitation. The brain was rapidly retrieved to be sliced and placed into cold oxygenated N-Methyl-D-glucamine (NMDG) solution (in mM: NMDG 93, HCl 93, KCl 2.5, NaH2PO4 1.2, NaHCO3 30, HEPES 20, glucose 25, sodium ascorbate 5, Thiourea 2, sodium pyruvate 3, MgSO4 10, CaCl2 0.5).

Coronal slices (thickness 300 μm) encompassing the LPO area were obtained using a vibrotome. Slices of interest were kept to quickly dissect the LPO area using microblades (Fine Science Tools). Once LPO area was cut, these sections were kept in NMDG solution at 33°C for 15min with constant oxygenation, and then transferred to 1 mL of fully oxygenated standard aCSF (in mM: NaCl 120, KCl 3.5, NaH2PO4 1.25, NaHCO3 25, glucose 10, MgCl2 1, CaCl2 2). The slices were maintained in a chamber that was gently and continuously aerated with carbogen gas for 2 hours at room temperature (20–22°C). After 2 hours of incubation, the 1mL of ACSF should contain glutamate, and it was transferred in a clean Eppendorf tube and kept in ice. The brain tissue was kept in a separate Eppendorf previously weighted and left overnight to dry at 37°C before weighting again the tube the day after, to know the weight of the brain tissue used for glutamate collection. The sample containing glutamate was centrifuged at 4°C, 2000 rpm for 5 minutes, and 800 μL was then transferred in a new tube and used for glutamate quantification. For the quantification, the Amplex™ Red Glutamic Acid/Glutamate Oxidase Assay Kit (Invitrogen, A12221) was used and the manufacturer guidelines were followed for the rest of the experiment. For the results analysis, positive and negative controls and an appropriate standard curve were used to analyse the fluorescence optical density of the experimental samples registered with the Amplex™ kit. The fluorescence registered was then normalized by the weight of brain tissue used in each sample, and glutamate quantification was expressed as μg of glutamate per mg of tissue.

2.11 Single cell PCR

For single cell PCR, the brains were quickly removed and placed into cold oxygenated NMDG solution and coronal brain slices (250 μm thickness) encompassing LPO were obtained again with a vibrotome. Slices were prepared as like for electrophysiology recording before collecting RNA samples. To maintain RNase free condition, recording pipette was pulled after autoclaved, and intracellular solution was made in RNase free condition (in mM: 140 K-gluconate, 5 NaCl, 10 HEPES, 0.1 EGTA, 2 MgCl2, 2 Mg-ATP, and 0.3 Na-GTP (pH 7.35, osmolality 285 mOsm)). To maximize RNA recovery, the internal solution in the patch pipette was limited to 1 μl. GFP positive and negative cells for control were randomly selected. Once stable whole-cell status was achieved, their cytoplasm was aspirated into the path pipette, and expelled into a RNase free PCR

tube containing lysate buffer and DNase I solution. All the sample were then processed using the Single-Cell to CT Kit (Invitrogen, #4458237) and RNA Reverse transcription and pre-amplification were performed following manufacturer instructions. Quantitative PCR was performed using the TaqMan Gene Expression Assays, all designed by Invitrogen (ThermoFisher). The probes used were: mSlc17a6 (*Vglut2*), ID Mm00499876_m1; mGad1, ID Mm04207432_g1; mSlc32a1 (*Vgat*), ID Mm00494138_m1; Nos1, ID Mm01208059_m1; Galanin, ID Mm00439056_m1 and GAPDH, ID Mm99999915_g1 for control.

2.12 Photometry and optogenetic set up

To record neurons Ca^{2+} activity of selected neurons, a monofibre (Ø 200 μm, 0.37 NA, Doric Lenses) was chronically implanted in the mouse brain together with EEG and EMG electrodes. The fibre was positioned after AAV injections above the LPO or LHb area following coordinates relative to Bregma. For LPO: AP, +0.10; ML, - 0.90, DV, -5.00 mm. For LHb: AP, -1.70; ML, + 0.44; DV, - 2.60 mm. Following 4 weeks of recovery, mice were acclimatized to the testing environment for at least 2 hours before behavioural experiments and then recorded for 6 hours during the light period. As light source, a Grass SD9 stimulator was used to control a 473 nm Diode-pumped solid state (DPSS) laser with fibre coupler (Shanghai Laser & Optics century Co.) and adjustable power supply (Shanghai Laser & Optics century Co.). A lock-in amplifier (SR810, Stanford Research Systems, California, USA) was used to drive the laser at 125 Hz TTL pulsations with an average power of 80 μW at the tip of the fibre directly connected to the mouse. The light source was joined to a fluorescence cube (FMC_GFP_FC, Doric Lenses) through an optical fibre patch cord (Ø 200 μm, 0.22 NA, Doric Lenses). From the filter cube, an optical patch cords (Ø 200 μm, 0.37 NA, Doric Lenses) was connected to the monofibre chronically implanted in the mouse brain using a ceramic sleeves (Thorlabs). The GCaMP6s output was then filtered at 500-550 nm through the fluorescence cube, converted in Volts by a photodiode (APD-FC, Doric Lenses) and then amplified by the lock-in amplifier with a time constant of 30ms (Figure 2.12.1). Finally, the signal was digitized using a CED 1401 Micro box (Cambridge Electronic Design, Cambridge, UK) and recorded at 200 Hz using Spike2 software (Cambridge Electronic Design, Cambridge, UK). Photometry, EEG and EMG data were aligned offline using Spike2 software and analyzed using custom made MATLAB (MathWorks) scripts. For each experiment, the photometry

signal F was normalized to baseline using the function $\Delta F/F = (F-F_0)/F_0$, where F_0 is the mean fluorescence across the signal analyzed.

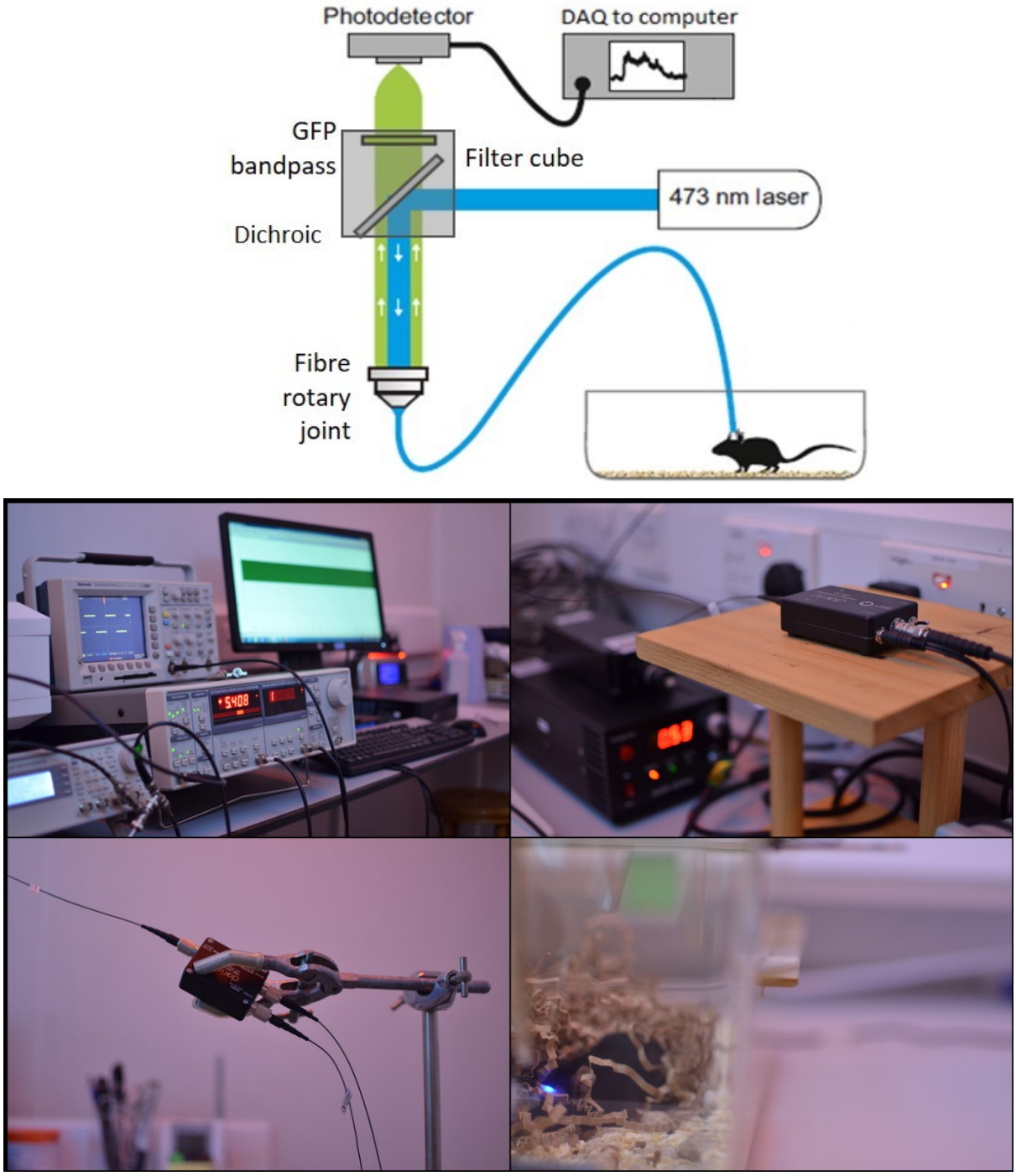

Figure 2.12.1 Representation of the photometry set-up I built and used.
Top, schematic representation of a photometry system used in mice (image modified from Gunaydin et al, 2014). Bottom, example of the photometry set ups. From top left, oscilloscope and signal generator connected to the lock-in amplifier; details of the photodiode; details of the filter cube; sleeping mouse with fibre optic connected and laser light turned on. The animal connected to the fibre is constantly monitored during experiments by a webcam. Video recordings and voltage signal from the photodiode are synchronized with Spike2 software. Photographs by me.

For optogenetics, the chronically implanted monofibre was made in the lab cutting an optical fibre (Ø 200 µm, 0.37 NA, Thorlabs) fixed into a ceramic ferrule (Ø1.25 mm Multimode LC/PC, Thorelabs) by heat curable epoxy glue and hardener (Precision Fiber Products). During the experiments, the laser light was connected directly with an optic fibre to a rotary joint (Doric Lenses), which was then connected to the mouse by a second optic fibre. Stimulation protocols were programed using Signal Software (Cambridge Electronic Design, Cambridge, UK) and laser pulsation was controlled by the CED 1401 Micro box. Laser power was checked at the tip of the last fibre, and was kept in a range between 5-6 mW. Before starting the stimulation protocol, all mice were habituated for at least 30 minutes to the environment.

2.13 Generation of shRNA-NR1

To knock-down (KD) the NR1 subunit using short-interfering RNAs (shRNA), Raquel Yustos and I designed inhibitory RNAs targeting the exons 11 to 18 of the NR1 subunit, 409 to 683 amino acids (aa) in the coding sequence (CDS). Three shRNA sequences were designed through the website *http://katahdin.cshl.org* and amplified using primers (pSM2C Forward: 5'-GATGGCTG-CTCGAG-AAGGTATAT-TGCTGTTGACAGTGAGCG-3'; pSM2C Reverse: 5'-GTCTAGAG-GAATTC-CGAGGCAGTAGGCA-3') obtained from the same source, following the protocol previously described [233].

The three sequences were referred as shRNA-NR1.1, 2 or 3 (the pink sequences represent the mer-22 specific for the NR1 subunit):

- ShRNA-NR1.1 targeted the NR1 sequence at 1800bp (600aa) of the CDS: 3'-TGCTGTTGACAGTGAGCGAACTGACCCTGTCCTCTGCCATTAGTGAAGCCACAGATGTAATGGCAGAGGACAGGGTCAGTGTGCCTACTGCCTCGGA-5'
- ShRNA-NR1.2 matched the NR1 sequence from 2565bp (855aa) of the CDS: 3'-TGCTGTTGACAGTGAGCGCGCCGTGAACGTGTGGAGGAAGTAGTGAAGCCACAGATGTACTTCCTCCACACGTTCACGGCTTGCCTACTGCCTCGGA-5'
- ShRNA-NR1.3 targeted the NR1 sequence at 2215bp (738aa) of the CDS: 3'-TGCTGTTGACAGTGAGCGCGGAGTTTGAGGCTTCACAGAATAGTGAAGCCACAGATGTATTCTGTGAAGCCTCAAACTCCATGCCTACTGCCTCGGA-5'

As control for shRNA-NR1 sequences, a shRNA scramble oligo was also produced, making sure it would not be complementary to any sequences in the mouse DNA. The shRNA-scramble sequence was as following:
3'GCTGTTGACAGTGAGCGAGCTCCCTGAATTGGAATCCTAGTGAAGCCACAGATGTAGGATT CCAATTCAGCGGGAGCCTGCCTACTGCCTCGGA-5'.

The 3 shRNA-NR1 sequences and the shRNA-scramble were cloned into the potent RNA interference using microRNA expression (pPRIME) in the context of the mir30 to be then expressed and tested in HEK293 cells. To check shRNAs efficiencies in knocking down the NMDA receptor in cell culture, a validation plasmid was produced cloning the NR1 sequence, fully matching the shRNA oligos sequences, into a plasmid pcDNA3.1-cherry. Each pPRIME was transfected in HEK293 cells together with the pcDNA3.1-NR1-cherry plasmid and cherry red fluorescence was quantified using a fluorescence microscope.

ShRNA-NR1.3 showed higher inhibition of NR1 expression and lower fluorescence intensity of cherry reporter, and it was therefore chosen to be cloned in the *AAV-pan-Cre-Venus* viral vector, exceeding the Cre recombinase sequence from the virus. The shRNA was then introduced in the reading frame in an inverted orientation (flex-switch), to be expressed only by Cre-expressing neurons. The sequence was then packaged as previously described [43].

2.14 Statistical analysis

Origin and MATLAB ware used for graphs and statistical analysis. Data collection and experimental procedure conditions were randomized. The experimenter was not blinded during the procedures. Data are presented as mean ± standard error of the means (SEM). Data were tested for normality using the Shapiro-Wilk test. If only one value affected the normal distribution, the outlier was excluded from the analysis and the following parametric tests were performed. Unpaired two-tailed Student's *t* test and One-way ANOVA with post-hoc Tukey test were used to compare groups when only one variable was present. For measurement and data collected over time, a 2-way repeated measures ANOVA analysis and post-hoc Tukey or Bonferroni test were performed. For episode number and mean duration analysis with three variables (experimental groups, time and behavioural state) 3-way ANOVA was used. For interpretation of QPCR data, one-way

ANOVA analysis was performed. When data were not normally distributed even if one outlier was excluded from the analysis, non-parametric Mann-Whitney and Friedman test were used. Any additional post-hoc test used for analysis is specified in the corresponding figure legends. Statistical significance was considered when $*p < 0.05$.

3 NMDA receptors in the lateral preoptic are needed for sleep homeostasis and healthy sleep architecture

3.1 Chapter summery and introduction

I deleted the NMDA receptor NR1 subunit from neurons in the lateral preoptic (LPO) area delivering an *AAV-Cre* virus into floxed-NR1 mice. Genetic deletion of the NMDA receptor in LPO neurons using a pan-neuronal promoter for the Cre recombinase (ΔNR1-LPO mice) caused strong hyperactive behaviour and NREM and REM sleep reduction and fragmentation, which did not improve even under high sleep pressure. In fact, ΔNR1-LPO animals appeared sleepy during and after SD, with increased sleep attempts and lower theta waves but higher delta power in their wake EEG spectra. Although these animals showed signs of high sleep pressure and increased delta power rebound following sleep deprivation, they could not catch up on the sleep lost. When targeting with NR1 deletion a different hypothalamic area as the anterior hypothalamus (AHA), ΔNR1-AHA animals did not show any signs of sleep patterns disruption during baseline sleep, or following SD, confirming that the sleep disturbances seen in ΔNR1-LPO mice are only caused by alteration of LPO pathways. My results show that the NMDA receptor is needed in LPO for consolidating sleep and for its rebound following SD. Further work is needed to identify the specific LPO neuronal types responsible for the behaviours observed.

As mentioned in the Introduction (Chapter 1), sleep researchers have been trying to identify possible pathways explaining sleep homeostasis – the process of catching up on lost sleep after sleep deprivation. This has been termed Process S, and involves tracking the time spent awake, and entering a proportionately longer and deeper sleep, referred as recovery sleep. The fact that animals catch up on lost sleep suggests that sleep has a fundamental purpose in survival. On entering recovery sleep after sleep deprivation, SWA is higher, as delta activity in the neocortex is more synchronized and NREM sleep is deeper. This enhanced SWA activity declines during NREM sleep, but over the subsequent 24 hours the animal still catches up on the lost sleep.

The search for a homeostatic mechanism has succeeded in the fruit fly *Drosophila,* where sleep promoting neurons exhibit a switch in potassium channel expression to trigger changes in vigilance states [140]. Additionally, NMDA pathways and Ca^{2+} levels are also essential for sleep homeostasis maintenance in fruit flies [143], and for regulating sleep duration in rodents [144].

Apart from these results, no specific molecular and cellular pathways in sleep regulatory areas have been explained in relation to sleep homeostasis in rodents. We then decided to look into the LPO area, a brain region extremely important for sleep generation and maintenance. This region is an intricate tangle of circuits and networks, with inhibitory and excitatory neurons both involved in sleep and wake promotion. Using cFos-dependent activity tagging, our lab has shown before how this area is active and fires during sleep deprivation and recovery sleep [72], and that reactivation of these neurons induces NREM and recovery sleep, suggesting LPO's involvement in sleep homeostatic mechanisms. Because of these results, I decide to test the hypothesis that NMDA receptors in LPO, and possibly LTP dependent mechanisms on time spent awake, could explain sleep homeostasis (see schematic Figure in Chapter 1).

Thanks to its fundamental subunit NR1, which is essential for the receptor assembly and is present in all NMDA receptors [158], the NMDAr was an easy target to manipulate. We therefore disrupted the NMDA receptor pathway in LPO neurons and analysed sleep patterns and behaviour to understand whether this receptor could be at the base of neuronal changes and signals necessary for sleep homeostasis in mice.

3.2 AMPA and NMDA receptor subunits in LPO

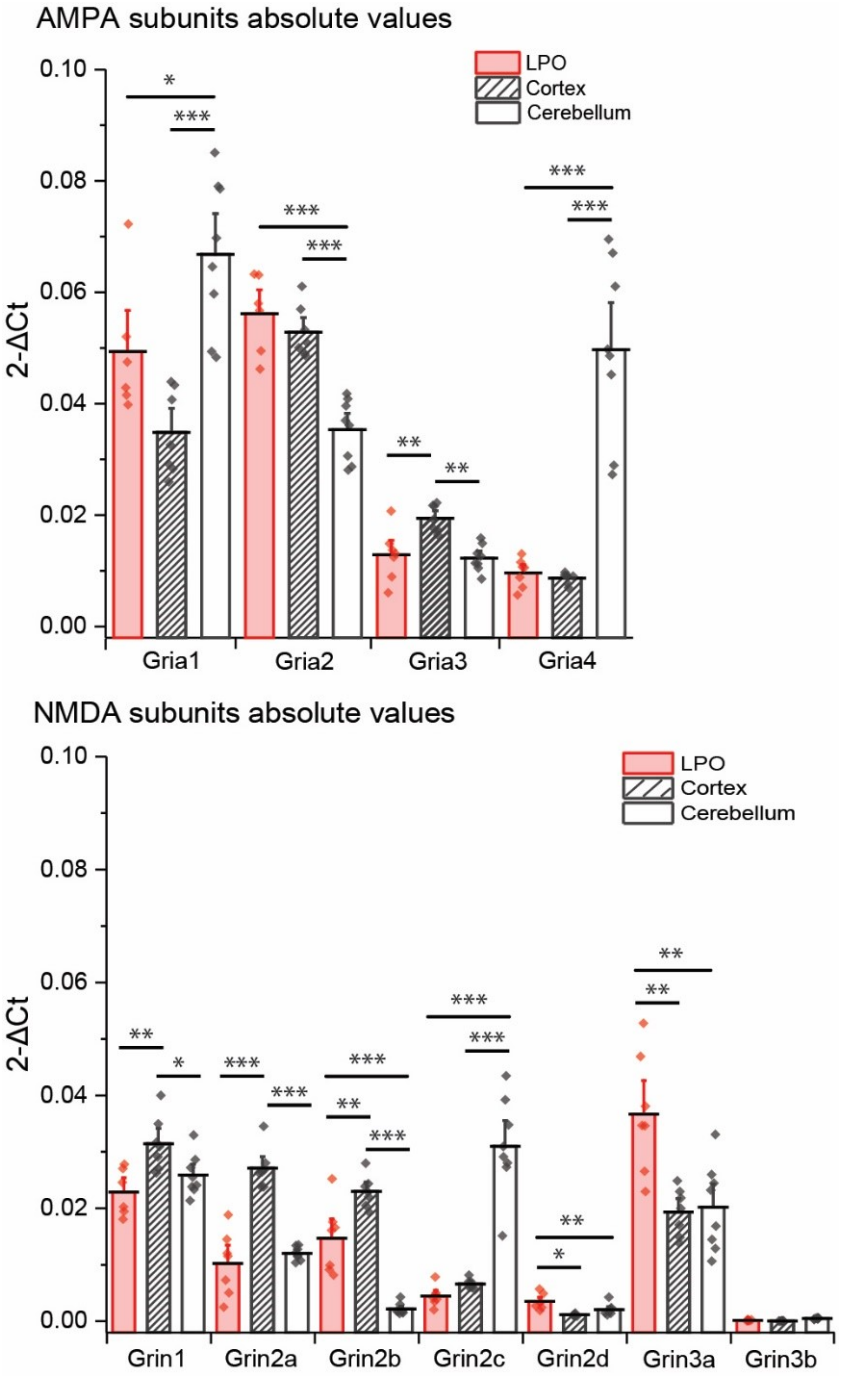

Figure 3.2.1 Quantification of AMPA and NMDA subunit gene expression in LPO. LPO samples were compared to controls cortex and cerebellum. Top, quantification of Gria1, 2, 3, 4 using TaqMan Gene Expression Assays. Calcium impermeable subunit Gria2's gene was significantly expressed more in LPO compared to cerebellum samples. Bottom, quantification of NMDAr subunits Grin1, 2a, 2b, 2c, 2d, 3a and 3b. Both Grin2d and Grin3a were significantly more expressed in LPO compared to controls. N = 8, Significance was calculated with One-way ANOVA, * = p < 0.05, ** = p < 0.005, *** = p < 0.0005.

Before proceeding with targeting the NMDAr pathway in LPO, I quantified the gene expression of different NMDA and AMPA receptors subunits in the region. The receptors have, in fact, a wide range of properties based on the subunits they are made of, which can drastically change their conductance, permeability to cations, sensitivity to blockers, and opening/decay kinetics [160].

Using quantitative PCR, and with the help of Dr Berta Anuncibay-Soto in the lab, I analysed each NMDA and AMPA subunit transcripts in LPO compared to cortex and cerebellum (Figure 3.2.1). Looking at the AMPA receptor subunits expression, we found that all four AMPA receptor subunit genes were expressed in the LPO, meaning that all subtypes of AMPA receptors and subunit combinations could be present in the area. Based on the prevalence of the Gria2 subunit mRNA, calcium impermeable AMPA receptors might be the most common form of AMPAr signalling in LPO, albeit not excluding the presence of calcium permeable AMPAr, e.g. Gria1/Gria4 combinations. For the NMDAr subunit genes, again, all subunit genes were expressed in the LPO area. We found that LPO had strong expression of both Grin2d and Grin3a subunits. The former has the property of maintaining the Grin1a/Grin2d receptor open for the longest time compared to the other subunit combinations [159, 160], while the latter is fundamental during development to finely tune neuronal networks, and its expression is supposed to decay progressively in the adult brain [234]. Interestingly, the 3a subunit has a dominant negative effect on the receptor, reducing its sensitivity to the Mg^{2+} blocking ion, the Ca^{2+} influx through the channel, and the overall NMDA induced-current [235, 236]. Because of its properties, this subunit strongly affects glutamatergic synaptic plasticity and dendritic spines formation, allowing removal of weak and inactive synapses to favour the strengthening and stabilization of more appropriate ones via Grin1/Grin2 conventional receptors signalling [237, 238].

3.3 Generation of ΔNR1-LPO mice

As mentioned before, the NMDAr is a relatively easy target to genetically inactivate, since it can be completely disrupted by affecting only one of its subunit genes, the NR1. I therefore used a floxed-NR1 transgenic mouse line, which carries *LoxP* sites flanking the exons encoding for the C-terminal region of the NR1 subunit (Figure 3.3.1, B). The DNA region included between these two sites is excised and eliminated in presence of Cre recombinase, resulting in a NR1 transcript with a shifted reading frame; consequently, the receptor can no longer be inserted in the cellular membrane and form tetramers. I bilaterally injected in LPO an AAV carrying the Cre-2A-Venus transgene to locally ablate NMDA receptors and to generate ΔNR1-LPO animals (Figure 3.3.1).

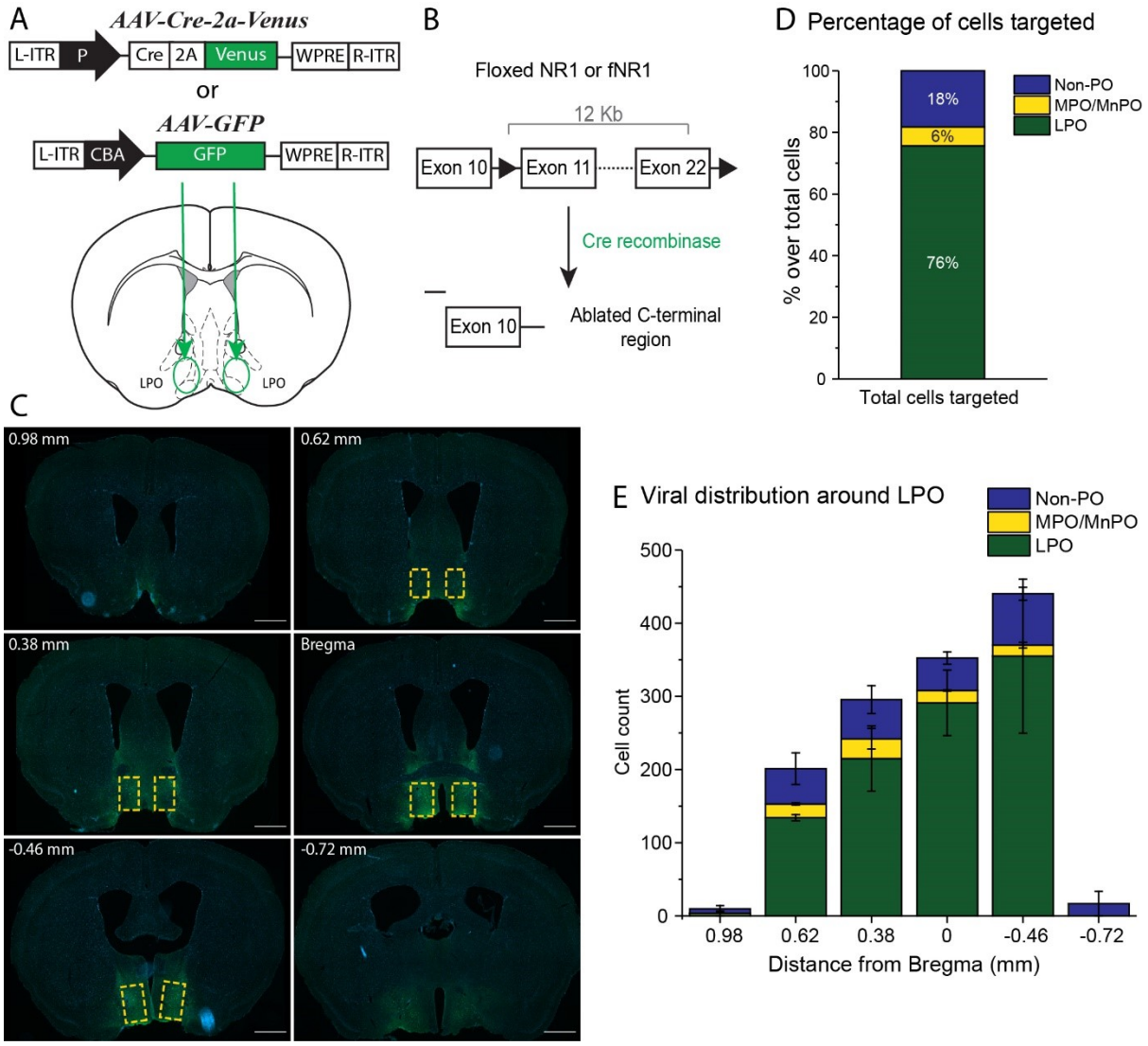

Figure 3.3.1 Generation of ΔNR1-LPO and GFP-LPO mice.
A, schematic representation of *AAV-Cre-Venus* and *AAV-GFP* expression in bilateral LPO. B, injection of Cre recombinase excise the C terminal of the NR1 subunit. C, *AAV-Cre-Venus* viral distribution from basal forebrain to mid thalamus, using green fluorescent protein (GFP) antisera and 4′,6-diamidino-2-phenylindole (DAPI, in blue) to mark all cells and slice structure. D, percentage of cells over total number of cells transduced by the *AAV-Cre-Venus* virus over the 6 coronal slices shown in C, with $N = 3$. 76% of the cells positive to GFP staining were localized in LPO. E, distribution of GFP+ cells over the 6 coronal slices, showing almost no cells transduced anteriorly or posteriorly to LPO. Scale bars in C indicate 100 µm. Error bars in E represent mean ± SEM.

As controls for behavioural analysis, I injected at the same stereotaxic coordinates the AAV viral particles carrying only a GFP marker transgene, to generate the littermate control group GFP-LPO (Figure 3.3.1).

To verify the correct expression and distribution of the virus in the LPO region, I used IHC with GFP antisera, which detects the Venus protein expression from the virus. With a series of coronal slices from basal forebrain to mid thalamus, I could confirm that most of the transgene expression occurred in cell bodies concentrated in LPO (Figure 3.3.1, C, yellow dotted squares), whereas regions anterior and posterior to LPO mostly showed axonal fibres labelling (short range projections), but no transduced cell bodies. GFP positive cell bodies were also counted in 3 different animals and quantified over the 6 coronal slices shown in Figure 3.3.1, panel C. Among all brain slices, 76% of the cell bodies transduced were localized in LPO, while 6% in MPO/MnPO and 18% in neighbouring areas not belonging to the POA (Figure 3.3.1, D). Looking at the viral distribution in more details, we could confirm that the virus transduced cells only in slices where LPO is localized, and there were almost no cell bodies transduced in slices anterior or posterior to LPO (Figure 3.3.1, E). With this data I can conclude that the NR1 deletion was mainly circumscribed to the LPO region.

3.4 Description of the AAV-Cre expression in LPO cell types

To verify that the *AAV-Cre* transgene was not transducing non-neuronal cells in LPO, I performed IHC staining for two classes of glial cells: astrocytes and microglia. For the former, I used the glial fibrillary acidic protein (GFAP), while for the latter I used the ionized calcium binding adaptor molecule 1 (IBA1) marker. I could confirm that the *AAV-Cre-Venus* transgene was not expressed in astrocytes nor microglia (Figure 3.4.1).

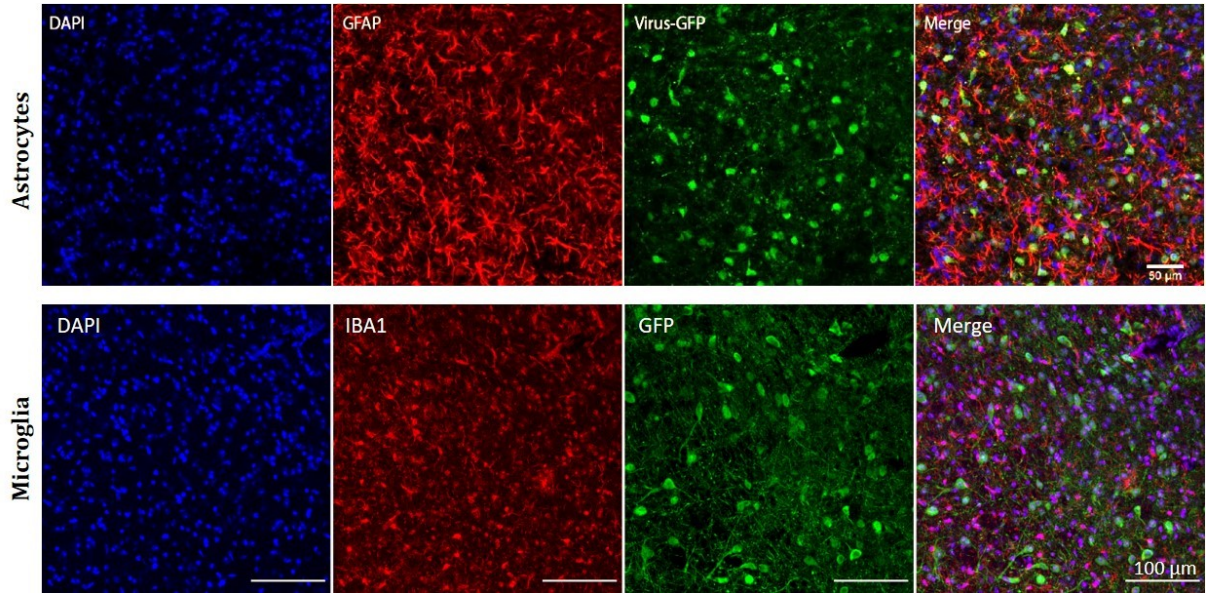

Figure 3.4.1 Confirmation that *AAV-Cre-Venus* virus did not infect glial cells.
Images on the previous page. IHC for GFP virus tag and GFAP astrocytic marker (top row) or microglia IBA1 marker (bottom row). No co-localization between virus and glial markers was observed in any of the animals and brain slices analysed. DAPI = 4′,6-diamidino-2-phenylindole. Scale bars represent 50 μm (top) and 100 μm (bottom).

3.5 Characterization of ΔNR1-LPO neurons by electrophysiology recordings

To confirm that the NMDA receptor currents were deleted from *AAV-Cre-Venus* transduced neurons in NR1-LPO mice, my colleague Dr Kyoko Tossell performed whole-cell electrophysiological recordings and data analysis on acute brain slices prepared from the LPO area. To preserve intact neuronal connections in LPO, para-horizontal slice were used for this analysis (Figure 3.5.1, A). *AAV-Cre-Venus* transduced neurons were visualized under microscope as GFP positive (GFP+). After successful physiological recordings with Neurobiotin-contained patch electrodes, those cells were fixed, stained and their location was mapped by immunohistochemistry (Figure 3.5.1, B).

Evoked excitatory currents were obtained from GFP+ or GFP- neurons in LPO at +40mV holding membrane potential using an electrode filled with a cesium-rich internal solution. Evoked AMPA current was pharmacologically isolated by the bath application of D-AP5, a selective and competitive NMDA receptor antagonist. Inhibitory currents were consistently blocked by Picrotoxin. GFP+ neurons from GFP-LPO animals showed evoked currents for both NMDA and AMPA receptors, with evident differences in the kinetics of the two receptors, although the recordings was noisier (Figure 3.5.1, C, left). In ΔNR1-LPO *ex-vivo* slices, AMPA currents were found preserved, and little or no NMDA current was observed (Figure 3.5.1, C, right). When looking at the levels of NMDA and AMPA currents, there was an evident, but not significant, increase in AMPA currents in ΔNR1-LPO mice compared to controls, whereas the NMDA current seemed only partially reduced (Figure 3.5.1, D). This representation does not account for the variability in excitability of the cells tested, and we therefore also analyse the AMPA/NMDA ratio between the two experimental groups. ΔNR1 GFP+ cells showed a higher AMPA/NMDA current ratio, which appeared not only due to a loss of NMDA current, but also due to a pronounced AMPA current (Figure 3.5.1, E, Unpaired Student's t test). The paired-pulse ratio (PPR) of eEPSC, used to assess pre-synaptic release probability, were briefly

challenged, and it did not have any significant difference compared to control cells (data not shown) [239]. Functional NMDA receptor was therefore successfully knocked-out in neurons from ΔNR1-LPO mice, and AMPA inputs were possibly increased.

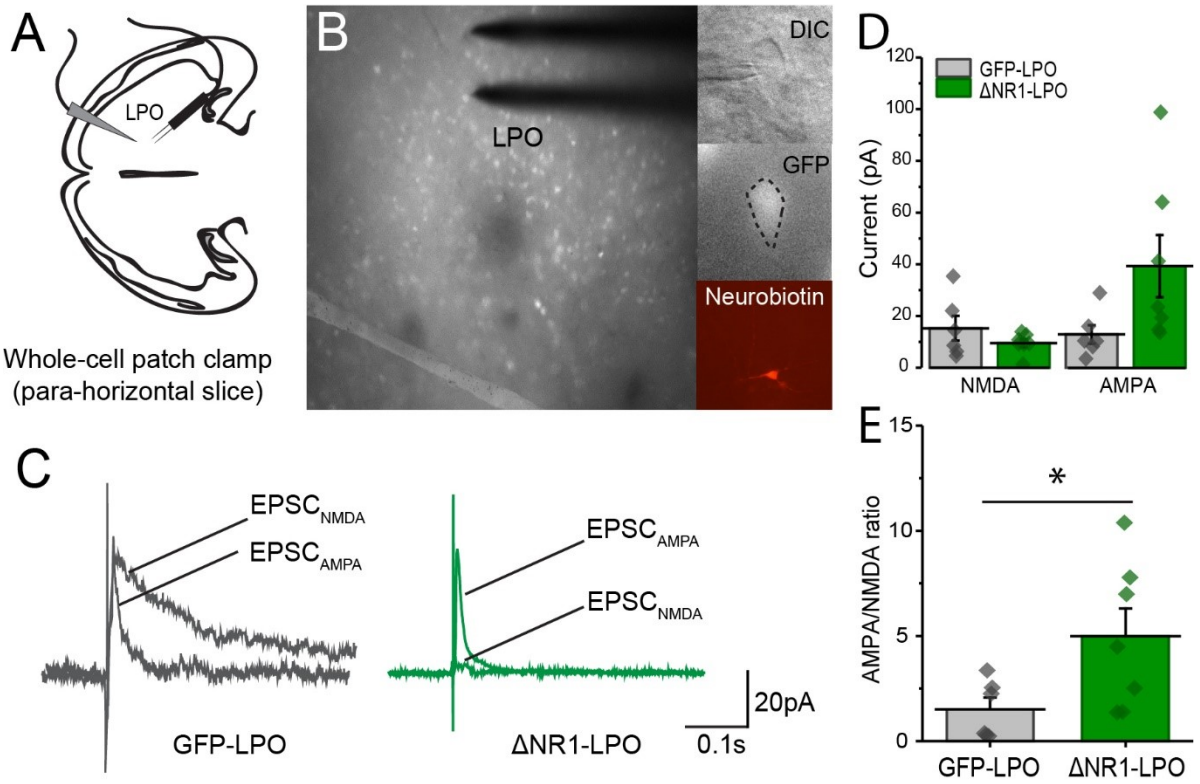

Figure 3.5.1 Electrophysiology recordings confirm successful elimination of NMDA receptors in ΔNR1-LPO mice compared to controls.
A, para-horizontal brain slices used for LPO recordings, with a recording pipette and a bipolar tungsten micro-stimulus electrode. B, microscope images of GFP+ cells infected with *AAV-Cre-Venus* in LPO. The cell successfully patched is shown in differential interface contrast (DIC), grey-scale for GFP and Neurobiotin immune-detection. C, evoked excitatory postsynaptic currents (eEPSCs) of NMDA and AMPA receptor in GFP-LPO (left) and ΔNR1-LPO (right) *ex-vivo* slices. In ΔNR1-LPO GFP+ cells the evoked NMDA current was efficiently eliminated (GFP-LPO recordings was noisier compared to ΔNR1-LPO). D and E, AMPA and NMDA currents (D) and ratio (E). Currents were not significantly different between groups due to variability in levels of excitability among cells tested. To eliminate these difference, the ration showed significant difference, increasing in ΔNR1-LPO (GFP-LPO: 1.51 ±0.56 (n=6 cells), ΔNR1-LPO: 4.99 ± 1.32 (n=7 cells), p=0.04, Mann-Whitney test). In D and E data are shown as mean ± SEM. Ephys recordings and analysis curtesy of Dr Kyoko Tossell.

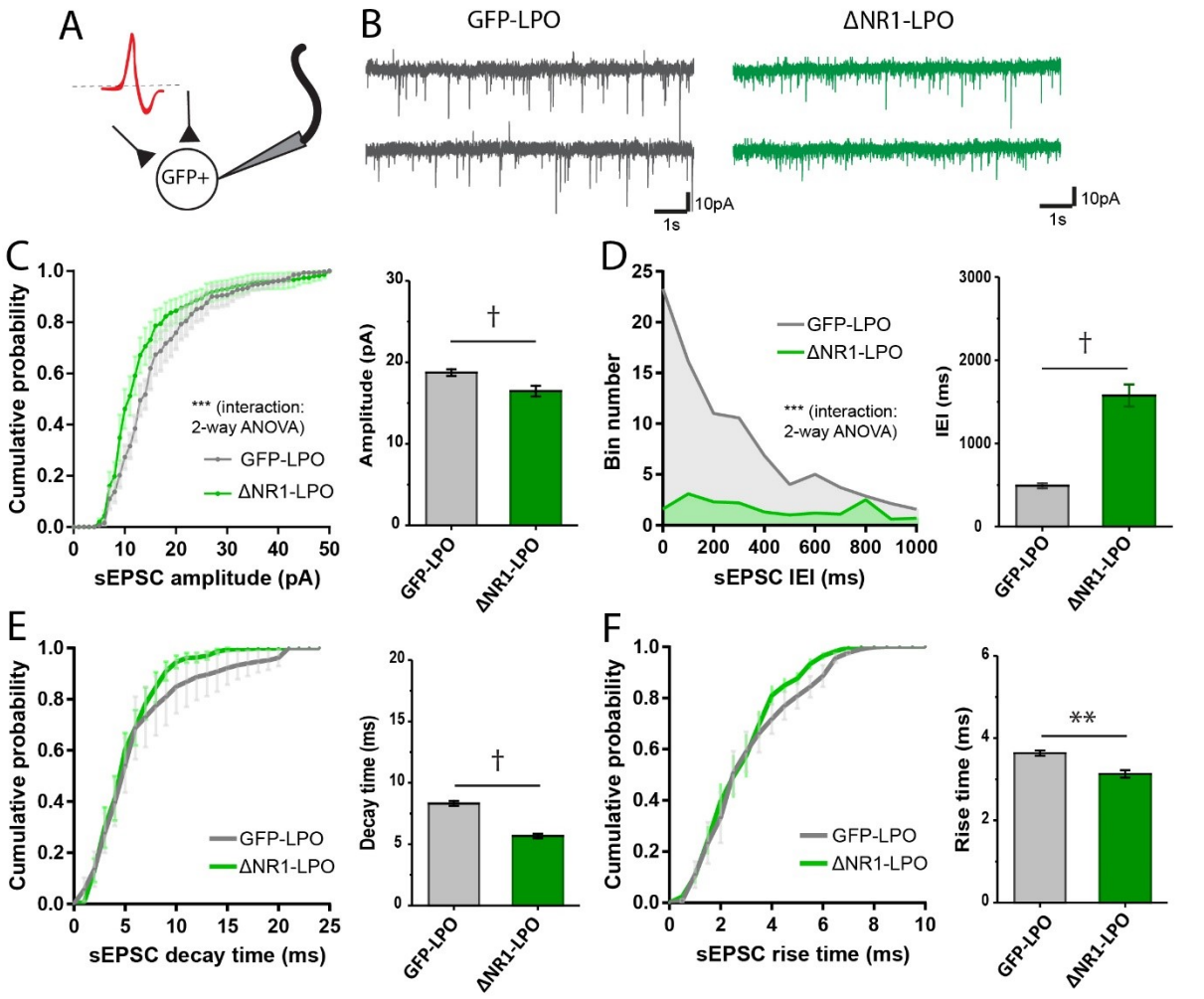

Figure 3.5.2 Spontaneous excitatory postsynaptic currents (sEPSCs) in ΔNR1-LPO mice neurons show a reduced functional AMPA receptors.
A, schematic representation of spontaneous currents recordings. B, example of sEPSC recordings in GFP-LPO and ΔNR1-LPO neurons. C, Cumulative histogram of sEPCSs amplitude (left, GFP-LPO: n=7, ΔNR1-LPO: n=10, p<0.0001 **** (KS test)) and average (right). D, Cumulative histogram of inter interval events (IEI) of sEPSCs (left, GFP-LPO: n=7, ΔNR1-LPO: n=10, p<0.0001 **** (KS test)) and average (right). E, Cumulative histogram of sEPSC decay time (left, GFP-LPO: n=7, ΔNR1-LPO: n=10, p=0.0006 *** (KS test)) and mean decay time (right). F, Cumulative histogram of sEPSC rise time (left, GFP-LPO: n=7, ΔNR1-LPO: n=10, p<0.0001 **** (KS test)) and mean rise time (right). Data are shown as mean ± SEM. Significance for histogram plots was calculated with One-Way repeated measures ANOVA and post-hoc Bonferroni test (** = p < 0.005; † = *p* < 0.00005), and cumulative distribution was analysed by the Kolmogorov-Smirnov test. Recordings, analysis and graphs are curtesy of Dr Kyoko Tossell.

We next investigated the spontaneous excitatory postsynaptic currents (sEPSCs) in GFP-LPO and ΔNR1-LPO acute slices. The size of these currents is related to the average number of functional pre/post synaptic connections. Unlike the currents reported in

hippocampal slices [239], the spontaneous synaptic AMPA currents in ΔNR1-LPO neurons were significantly smaller than controls (Figure 3.5.2, C, left), evident also when comparing the average amplitudes in the two experimental groups (Figure 3.5.2, C, right; One-Way repeated measures ANOVA and post-hoc Bonferroni test). Inter-event-interval (IEI) of sEPSC in ΔNR1-LPO were more widely distributed between a range of duration, but losing the shorter range of intervals compared to controls (Figure 3.5.2, D, left). This was evident when also looking at the average duration of IEI, which appeared much longer in ΔNR1-LPO mice compared to GFP-LPO (Figure 3.5.2, D, right; One-Way repeated measures ANOVA and post-hoc Bonferroni test). Both rise and decay time of these currents were significantly smaller, as well as their mean values, which differ from control cells (Figure 3.5.2, E, F; One-Way repeated measures ANOVA and post-hoc Bonferroni test).

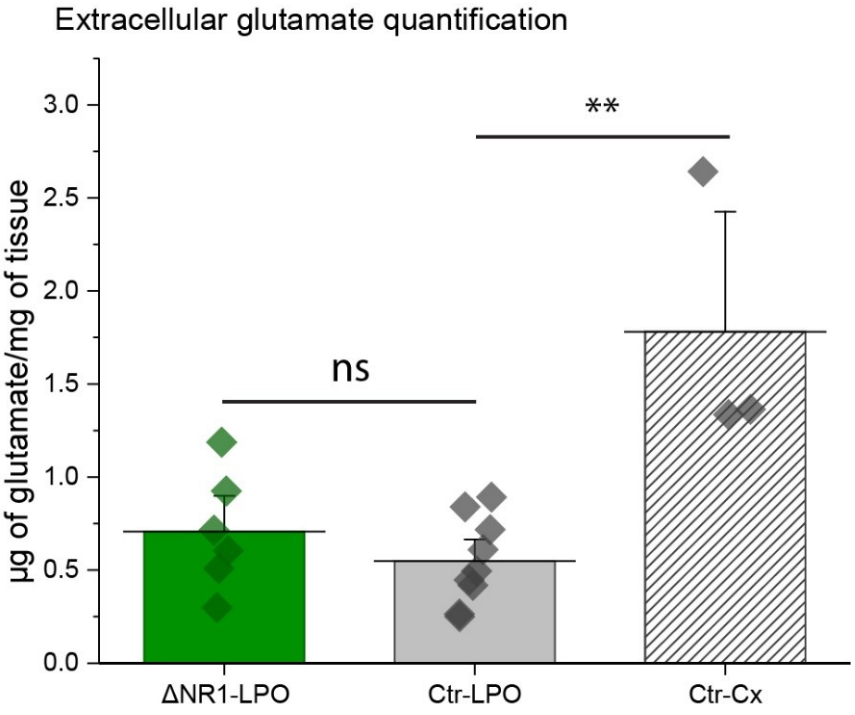

Figure 3.5.3 Extracellular glutamate is not increased in the LPO of ΔNR1-LPO mice. Glutamate was quantified using organotypic brain slices as µg of glutamate per mg of tissue. ΔNR1-LPO, *n*= 6, Control (Ctr)-LPO, *n*= 9, Ctr-Cx, *n*= 3. Data are shown as mean ± SEM, significance was calculated by Paired Student's t test. ** = $p < 0.005$.

In summary, *AAV-Cre-Venus* transduced neurons in ΔNR1-LPO mice had little or no functional NMDA receptors and possible increase of AMPA synaptic inputs, seen from the

eEPSCs. Furthermore, the multiple significant changes in sEPSCs suggest that there is a change in functional AMPA receptors. Further analysis of action-potential independent miniature EPSCs (mEPSCs) is required to answer if this was indeed the change in postsynaptic AMPA receptors itself.

Looking for possible compensatory mechanisms, as accumulation of extracellular glutamate, caused by the NMDAr deletion from LPO neurons, together with both Dr Tossell and Dr Berta Anuncibay-Soto, we quantified extracellular glutamate in LPO from *ex-vivo* organotypic slices. We observed no difference in glutamate levels between ΔNR1-LPO and GFP-LPO samples (ΔNR1-LPO, n= 6, GFP-LPO, n = 9, Figure 3.5.3). As a positive control for the assay, we saw higher levels of the neurotransmitter in the neocortical region compared with samples obtained from the LPO area.

3.6 ΔNR1-LPO are hyperactive

Having confirmed the successful deletion of the NR1 NMDA receptor subunit from LPO neurons, I looked at the behaviour of ΔNR1-LPO animals compared to GFP-LPO control mice in an open field test, to determine their baseline locomotor activity during a 30 minutes period. ΔNR1-LPO mice seemed to run more around the arena compared with controls, almost avoiding the central zone (Figure 3.6.1, A and B, left quadrants). From the average heat map indicating where animals from the two experimental groups were preferentially located during the test, the ΔNR1-LPO animals showed higher preference for the perimeter of the arena compared to controls (Figure 3.6.1, A and B, 2nd quadrants).

Figure 3.6.1 ΔNR1-LPO mice are hyperactive as assessed by open field test.
Figure on the following page. A and B, example traces of GFP-LPO and ΔNR1-LPO animals, respectively (1st quadrants) during 30 minutes of open field test. Heat maps (A and B 2nd quadrants) are the mean for each group (GFP-LPO, n= 8, ΔNR1-LPO, n= 8), showing the arena's central zone in orange. C, total distance travelled in 30 minutes. D, percentage of distance travelled in central zone over total distance. E, number of entries in the central zone. F, total time spent in central zone and latency to the first entry. To verify that central zone size did not affect the results on anxious behaviour, its sides were either doubled or halved. In both cases (G and H respectively), no differences between experimental groups were detected in total time spent in the central zone and in the latency to the first entry. Lines represent mean ± SEM, significance calculated with Unpaired Student's t test in C and Mann-Whitney test for the remaining plots. *** = $p < 0.0005$.

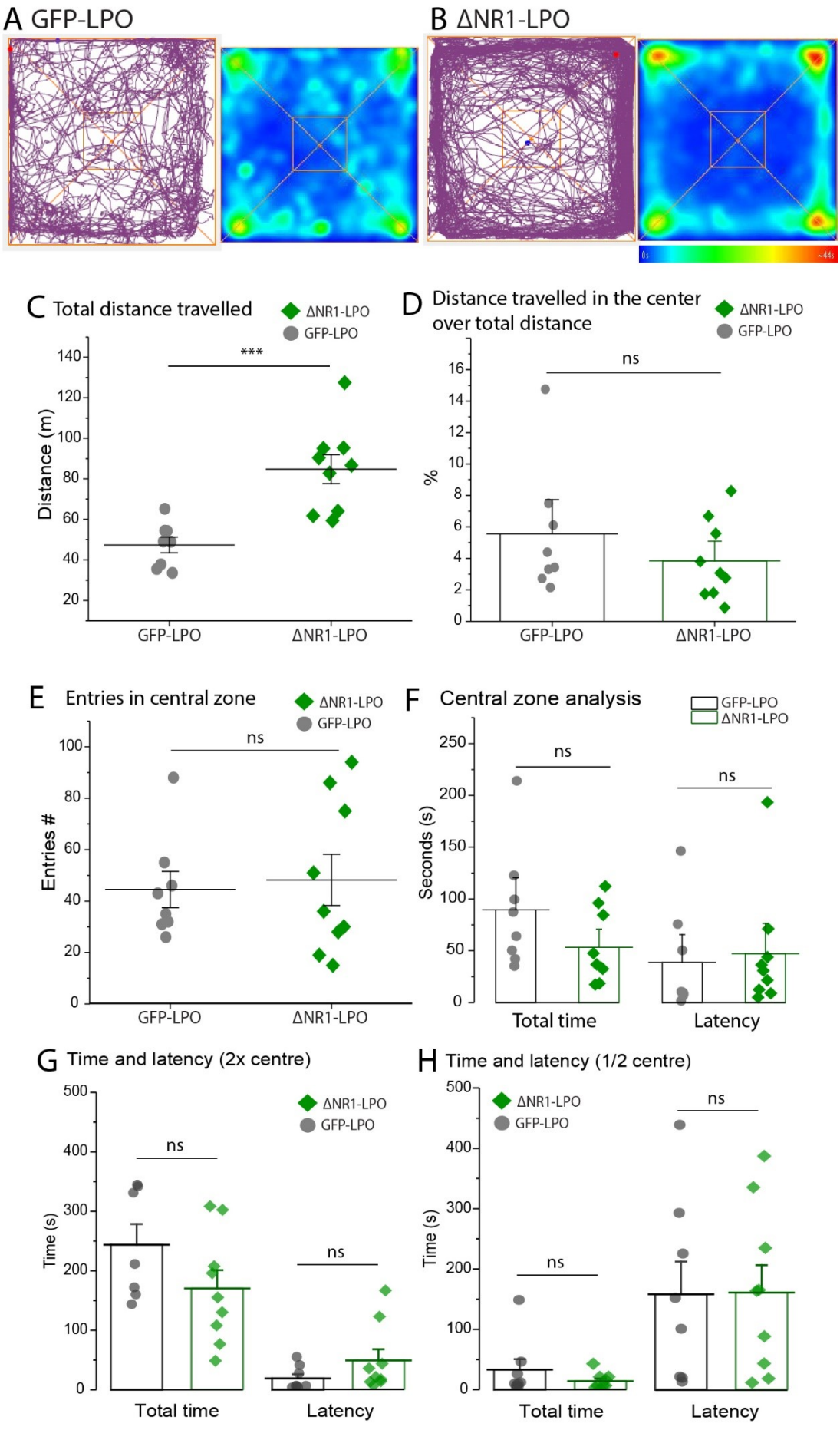
A GFP-LPO
B ΔNR1-LPO
C Total distance travelled
ΔNR1-LPO
GFP-LPO
***
Distance (m)
140
120
100
80
60
40
20
GFP-LPO
ΔNR1-LPO
D Distance travelled in the center over total distance
ΔNR1-LPO
GFP-LPO
ns
%
16
14
12
10
8
6
4
2
0
GFP-LPO
ΔNR1-LPO
E Entries in central zone
ΔNR1-LPO
GFP-LPO
ns
Entries #
100
80
60
40
20
0
GFP-LPO
ΔNR1-LPO
F Central zone analysis
GFP-LPO
ΔNR1-LPO
ns
ns
Seconds (s)
250
200
150
100
50
0
Total time
Latency
G Time and latency (2x centre)
ΔNR1-LPO
GFP-LPO
ns
ns
Time (s)
500
400
300
200
100
0
Total time
Latency
H Time and latency (1/2 centre)
ΔNR1-LPO
GFP-LPO
ns
ns
Time (s)
500
400
300
200
100
0
Total time
Latency

This parameter could indicate that ΔNR1-LPO animals exhibit more anxiety [240]. I therefore firstly quantified the total distance travelled by ΔNR1-LPO and GFP-LPO animals: the first group travelled more compared with controls during the test, showing signs of marked hyperactivity (Figure 3.6.1, A, Unpaired Student's *t* test, $p<0.0005$). To determine if ΔNR1-LPO animals systematically avoided the central zone, I calculated distance travelled in the centre over total distance, number of entries in the central zone during the test, and time spent in the zone and the latency to first enter in it (Figure 3.6.1, B, C and D, respectively). All these values did not show a significant difference compared to controls, indicating that ΔNR1-LPO animals did not display evident signs of anxiety, but rather simple hyperactivity.

When the central zone sides were doubled or halved to check if zone size affected anxiety detection, no significance was calculated in total time spent in the central zone and in the latency to the first entry between ΔNR1-LPO and GFP-LPO animals in any of the two cases (Figure 3.6.1, G and H). No difference was observed also in the number of entries and in the percentage of total distance travelled in the centre over total distance (data not shown), confirming the absence of an anxious behaviour in ΔNR1-LPO mice.

3.7 ΔNR1-LPO mice sleep less and have a highly fragmented sleep-wake pattern

I then looked at 24h baseline (BL) EEG and EMG traces of ΔNR1-LPO animals compared to the GFP-LPO ones.

Figure 3.7.1 ΔNR1-LPO mice have a marked reduction in sleep time.
Figure on the following page. A, example of baseline recordings from GFP-LPO (left) and ΔNR1-LPO (right) animals. From the top, hypnogram, delta power, EMG, and EEG represented as a somnogram and as a trace. B, baseline states distribution in percentage per hour of Wake, NREM and REM over 24h. C and D, percentage of each behavioural state over 12 hours of light (C) and dark period (D). E and F, percentage of wake, NREM and REM sleep in ΔNR1-LPO animals over GFP-LPO animals amount, during light (E) and dark (F) period. ΔNR1-LPO mice lost 50% of REM sleep during the whole baseline. GFP-LPO, $n= 12$, ΔNR1-LPO, $n= 11$. Data are shown as mean ± SEM. Significance in B, C and D was calculated using 2-way ANOVA and post-hoc Tukey test. * = $p < 0.05$; ** = $p < 0.005$; *** = $p < 0.0005$; † = $p < 0.00005$. Grey squares indicate dark period.

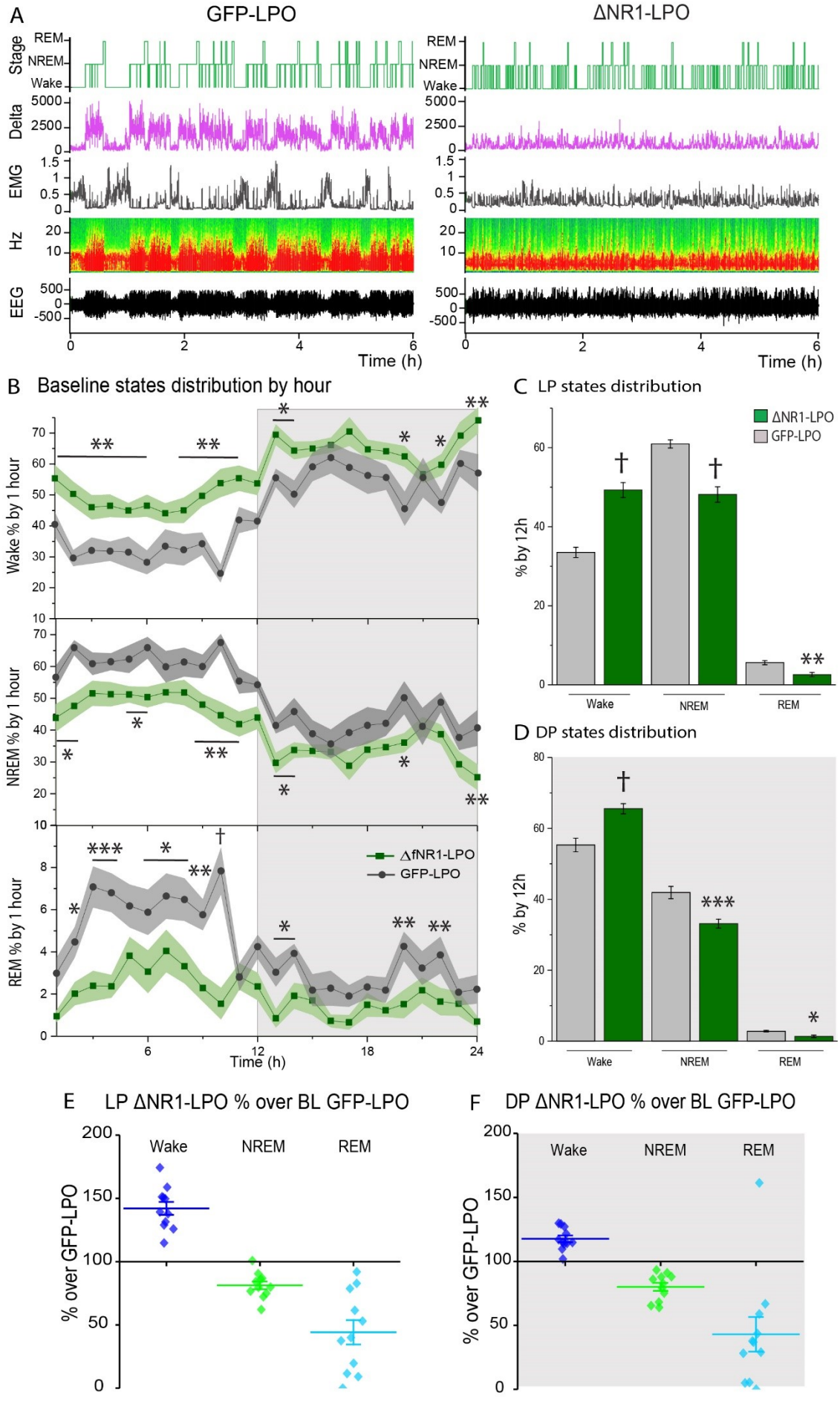
A
GFP-LPO
ΔNR1-LPO
Stage
REM
NREM
Wake
Delta
EMG
Hz
EEG
Time (h)
B Baseline states distribution by hour
Wake % by 1 hour
NREM % by 1 hour
REM % by 1 hour
ΔfNR1-LPO
GFP-LPO
Time (h)
C LP states distribution
ΔNR1-LPO
GFP-LPO
% by 12h
Wake
NREM
REM
D DP states distribution
% by 12h
Wake
NREM
REM
E LP ΔNR1-LPO % over BL GFP-LPO
% over GFP-LPO
Wake
NREM
REM
F DP ΔNR1-LPO % over BL GFP-LPO
% over GFP-LPO
Wake
NREM
REM

ΔNR1-LPO mice showed different patterns than GFP-LPO control mice. For ΔNR1-LPO mice, the hypnogram showed an increased number of transitions between states, and both EEG and EMG traces where altered, and did not show normal NREM sleep bouts as present in the control group (Figure 3.7.1, A). Looking at ΔNR1-LPO animals' states distribution there was a consistent increase in wake time, with a consequent reduction in NREM and REM sleep time compared to controls (Figure 3.7.1, B. 2-way repeated measures ANOVA and post-hoc Tukey test). Plotting the same results as percentage over light period (LP or lights-ON) or dark period (DP, or lights-OFF), revealed that ΔNR1-LPO animals constantly slept less than GFP-LPO controls, with a marked increase in time spent awake (Figure 3.7.1, C. 2-way repeated measures ANOVA and post-hoc Tukey test). To better understand the extent of sleep loss in ΔNR1-LPO animal, I quantified their states distribution during LP and DP as percentage over amounts of sleep and wake in GFP-LPO control animals. NR1 deletion caused a reduction of time spent in REM sleep of 50% and in NREM sleep of 15-20%, during both light and dark period, with a marked increase of wakefulness between 50% during LP and 20% during the DP (Figure 3.7.1, E and F).

I next analysed the sleep architecture, and overall number of transitions between states. ΔNR1-LPO animals had a strong increase in wake and NREM sleep episode numbers, and a decrease in REM sleep episodes, during both the dark and the light phases (Figure 3.7.2, A, 3-way ANOVA and post-hoc Tukey test). Looking at the episode mean duration, ΔNR1-LPO mice showed constant reductions in the duration for all behavioural states, especially for the dark phase during wakefulness and throughout the 24h recorded for NREM and REM sleep (Figure 3.7.2, B, 3-way ANOVA and post-hoc Tukey test). The combination of increased episode numbers and decreased duration is a sign of highly fragmented and poor quality sleep, which can affect sleepiness and cognition in animals [241], as well as in humans [242]. ΔNR1-LPO mice showed almost double the number of transitions between wake and NREM sleep, and an evident reduction in transitions towards REM sleep, especially during the dark phase, confirming the sleep fragmentation phenotype (Figure 3.7.2, C).

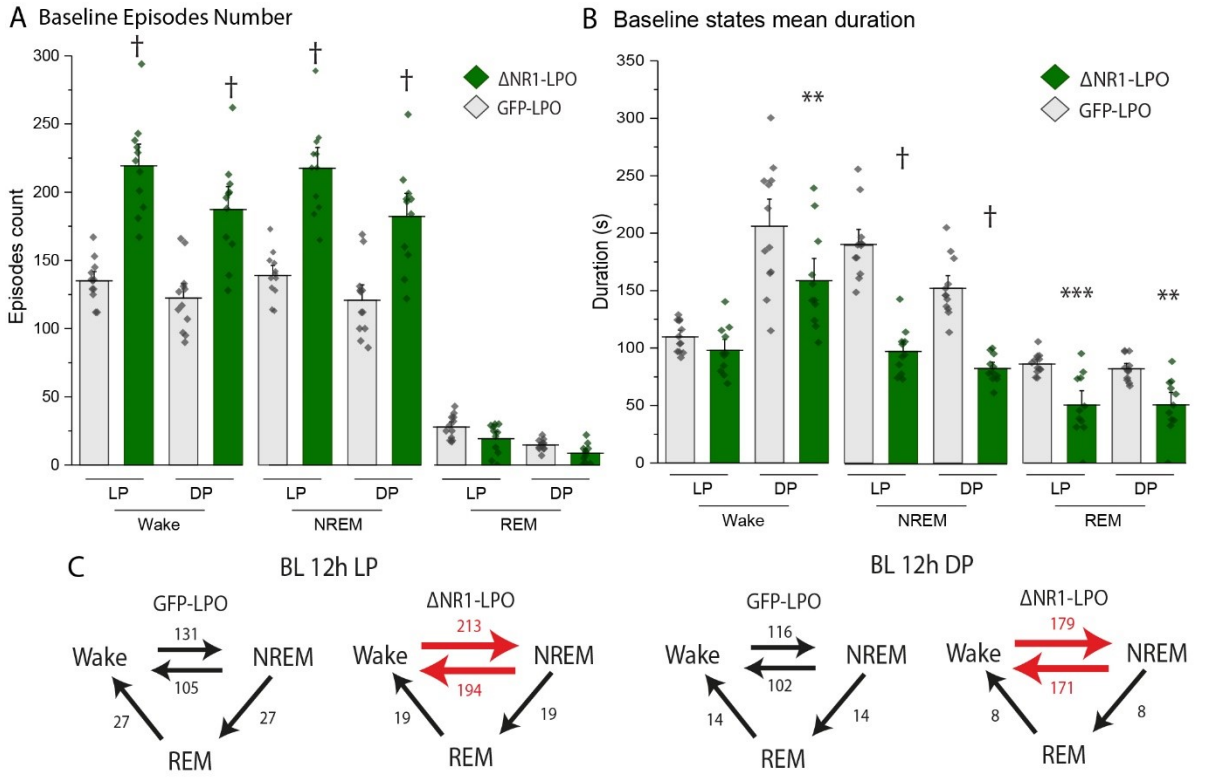

Figure 3.7.2 ΔNR1-LPO animals had a strong increase in NREM sleep and wake episode number, and a decrease in REM sleep.
A, episode number for 24h BL recordings divided by light (LP) and dark period (DP) and behavioural states. B, episode mean duration for each behavioural state during light and dark period. High episodes numbers with low mean durations are a sign of a highly fragmented and poor quality sleep. C, mean of transitions between states in GFP-LPO and ΔNR1-LPO groups representative for sleep fragmentation. Red arrows represent the highest increase in number of transitions in ΔNR1-LPO animals compare to controls. GFP-LPO, *n*= 12, ΔNR1-LPO, *n*= 11. In A and B data are shown are mean ± SEM, significance was calculated by 3-way ANOVA and post-hoc Tukey test. * = $p < 0.05$; ** = $p < 0.005$; *** = $p < 0.0005$; † = $p < 0.00005$.

3.8 ΔNR1-LPO mice did not catch up on lost sleep following sleep deprivation but showed a SWA homeostatic rebound

To test our hypothesis that NMDA receptor input onto LPO neurons tracks the time awake as part of a sleep homeostasis mechanism (see Introduction), sleep recordings were performed under elevated sleep pressure *i.e.* during and after sleep deprivation.
I performed 6h sleep deprivation (6hSD) on both experimental groups using the novel object method, supposedly the least stressful and invasive for the animals. Mice not handled or touched during the whole SD, and they were not poked or moved unless

extremely sleepy and impossible to be kept awake by introducing novel toys. SD was performed during the first 6h of the light phase when sleep pressure is at its highest, while the remaining 18h were left for sleep opportunity and recovery sleep.

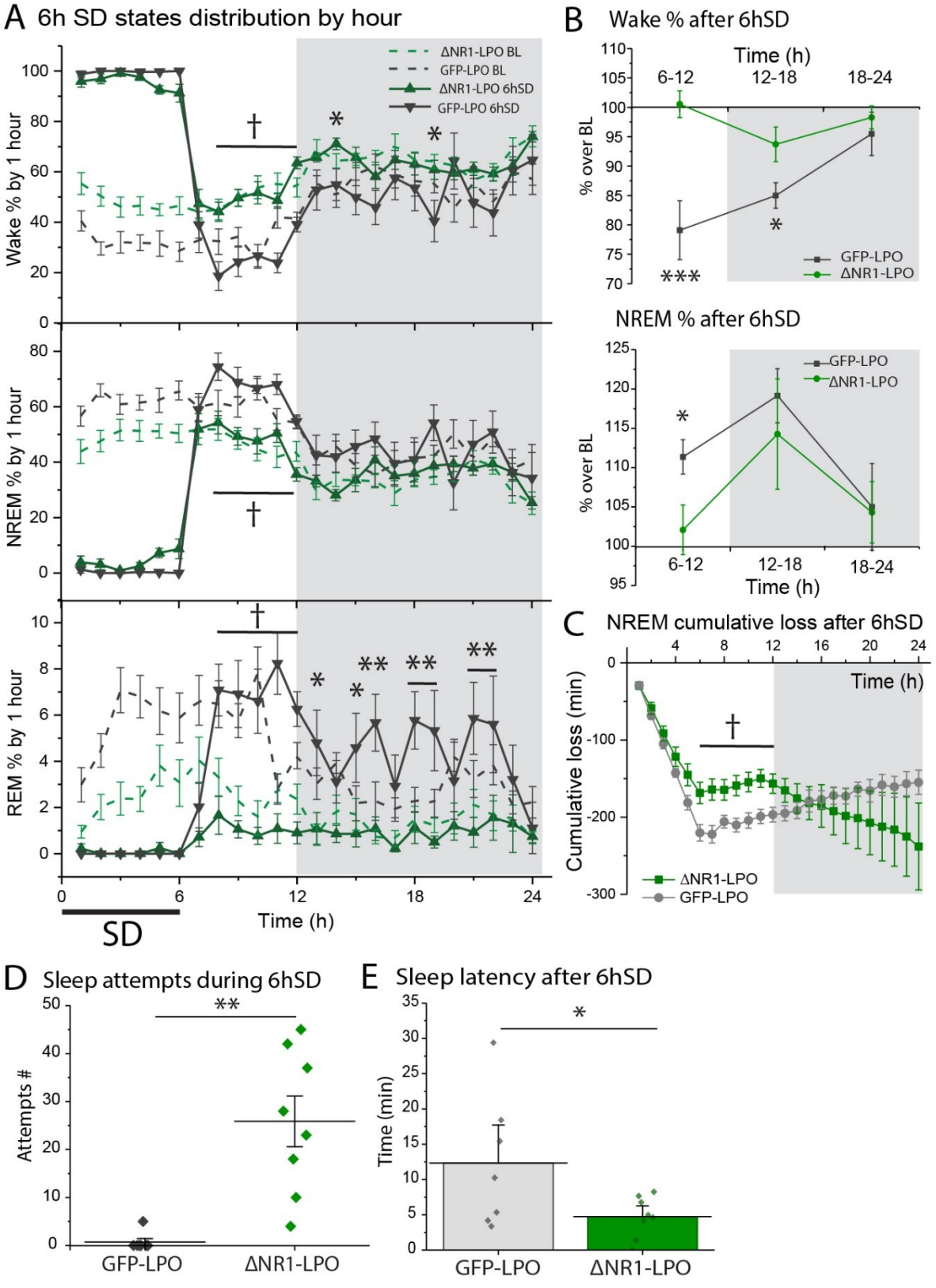

Figure 3.8.1 ΔNR1-LPO mice do not show sleep rebound after sleep deprivation. Figure on previous page. A, Percentage over 1h of wake, NREM and REM sleep including 6h SD. In dotted lines are the BL data. B, percentage over BL amounts of wake (top) and NREM (bottom) amounts by 6h following SD to show sleep rebound. C, cumulative sleep loss following 6hSD plotted over 24h. The sleep loss was calculated compared to the BL NREM sleep amounts. D, sleep attempts number during 6hSD. E, latency to transition to NREM after 6hSD. To be considered, the first NREM sleep bout had to be at least 30 s long. Increased attempts and shorter latency show high sleepiness. Grey background in A, B and C corresponded to dark period. GFP-LPO, n= 8, ΔNR1-LPO, n= 8. Data are shown are mean ± SEM. Significance was calculated in A (only between 6hSD data), B and C with 2-Way repeated measures ANOVA and post-hoc Tukey test for corrections, and in D and E with Unpaired Student's t test. * = $p < 0.05$; ** = $p < 0.005$; *** = $p < 0.0005$; † = $p < 0.00005$.

ΔNR1-LPO animals showed almost the same behavioural states distribution as BL recordings during the 18h following SD, while control mice showed an increase in NREM sleep time after SD as expected (Figure 3.8.1, A, 2-way repeated measures ANOVA and post-hoc Tukey test). Particularly evident was the lack of sleep rebound in the 6h of light period immediately following sleep deprivation, where ΔNR1-LPO animals showed the biggest different in states distribution compare to controls ($p < 0.00005$).

To further analyse the differences in vigilance states distribution between baseline and 6hSD, I quantified the amount of wake and NREM sleep as a percentage over baseline during the 18h after SD. GFP-LPO animals showed a 20% reduction in wake time and a subsequent increase in NREM sleep time, in particular during the remaining 6h of LP. On the other hand, ΔNR1-LPO animals did not change the time spent awake after SD compared to their own baseline, and they did not show an evident increase in NREM sleep following SD, but only a mild increase of 10% NREM during the dark phase (Figure 3.8.1, B, 2-way repeated measures ANOVA and post-hoc Tukey test). Observing the cumulative NREM sleep loss caused by SD and compared to NREM sleep amounts, GFP-LPO animals recuperated almost half of the sleep lost during the 18h of sleep opportunity, whereas ΔNR1-LPO mice kept on losing sleep even if they had been awake for 6 consecutive hours (Figure 3.8.1, C, $p< 0.00005$, 2-way repeated measures ANOVA and post-hoc Tukey test). Interestingly, ΔNR1-LPO animals showed a sharp reduction in NREM sleep rebound when the lights went OFF after SD, suggesting that these animals maintained their hyperactivity during the DP despite their loss of sleep, while control GFP-LPO animals continued

recuperating sleep even during their active phase. It is possible that the markedly active behaviour of ΔNR1-LPO animals participates in reducing sleep opportunity even under conditions of high sleep pressure, and that the NMDA receptor might be needed in LPO to shut down circuits responsible for active behaviour in the brain. These data confirm that ΔNR1-LPO mice did not have a sleep rebound following SD.

To better characterize the phenotypical loss of sleep rebound, I quantified the number of sleep attempts during the 6hSD and the latency to the first 30s NREM sleep bout after SD termination. ΔNR1-LPO mice had highly increased sleep attempts during SD and a shorter latency to fall asleep (Figure 3.8.1, C and D, Unpaired Student's t test), showing a dramatic sleepy behaviour, although they seemed incapable of catching up on the sleep loss. ΔNR1-LPO mice maintained a marked sleep fragmentation following SD. Episodes number of wake and NREM sleep were still substantially increased with respect to controls, while REM sleep bouts were still decreased (Figure 3.8.2, A, 3-way ANOVA and post-hoc Tukey test). Episodes were constantly shorter for all states in ΔNR1-LPO animals for the 18h of sleep opportunity, with half NREM sleep bouts length and a third of REM sleep episodes duration compared to controls (Figure 3.8.2, B, 3-way ANOVA and post-hoc Tukey test). ΔNR1-LPO mice had more than double the transitions between wake and NREM sleep, and half of the transitions towards REM sleep when compared to GFP-LPO animals (Figure 3.8.2, C). ΔNR1-LPO animals, although they could show signs of sleep pressure and sleepiness, they were incapable of recovery sleep loss and to temporarily increase their sleep quality following 6hSD.

Figure 3.8.2 Sleep fragmentation persisted in ΔNR1-LPO mice even after increased sleep pressure caused by 6hSD.

Figure on the following page. A, episodes number calculated by 6h following 6hSD. From left to right, wake, NREM and REM sleep. B, episodes mean duration of wake, NREM, REM calculated in periods of 6h following SD. Sleep fragmentation persisted in ΔNR1-LPO even after increased sleep pressure. C, mean values of transitions between states calculated over the 18h following SD for GFP-LPO (left) and ΔNR1-LPO (right) groups. ΔNR1-LPO animals showed more than double transitions between wake and NREM compared to controls. GFP-LPO, n= 8, ΔNR1-LPO, n= 8. In A and B data are shown are mean ± SEM. Significance was calculated by 3-way ANOVA and post-hoc Tukey test in A and B. * = p < 0.05; ** = p < 0.005; *** = p < 0.0005; † = p < 0.00005.

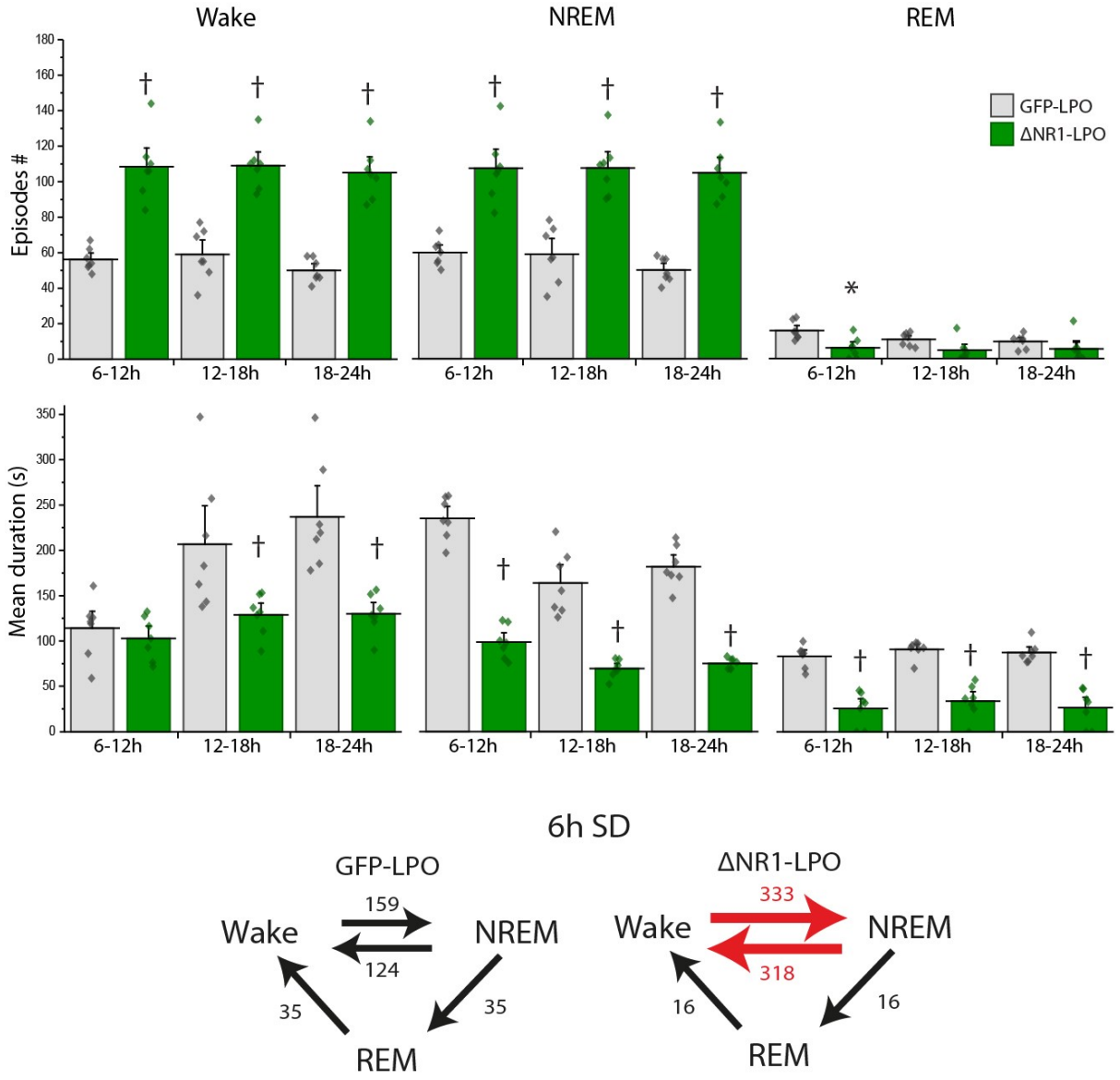

As mentioned in the Introduction, a standard criterion to quantify sleep homeostasis is to measure the delta power (SWA) rebound under increased sleep pressure. Normally, SWA is increased in the first part of the recovery sleep that follows sleep deprivation, reflecting a deeper sleep, as the neurons in the neocortex generating the EEG are firing more synchronously. I therefore analysed the NREM EEG power spectra for the first 1 hour after SD in both ΔNR1-LPO and GFP-LPO groups, comparing the SD results to the baseline EEG spectra at the same circadian time. Both experimental groups showed a similar delta power rebound compared to their baseline levels (**Error! Reference source not found.**, A, left and right panels, 2-way repeated measures ANOVA and pot-hoc Tukey test), demonstrating how this phenomenon of deeper sleep following sleep deprivation was not affected by the NMDAr deletion in LPO.

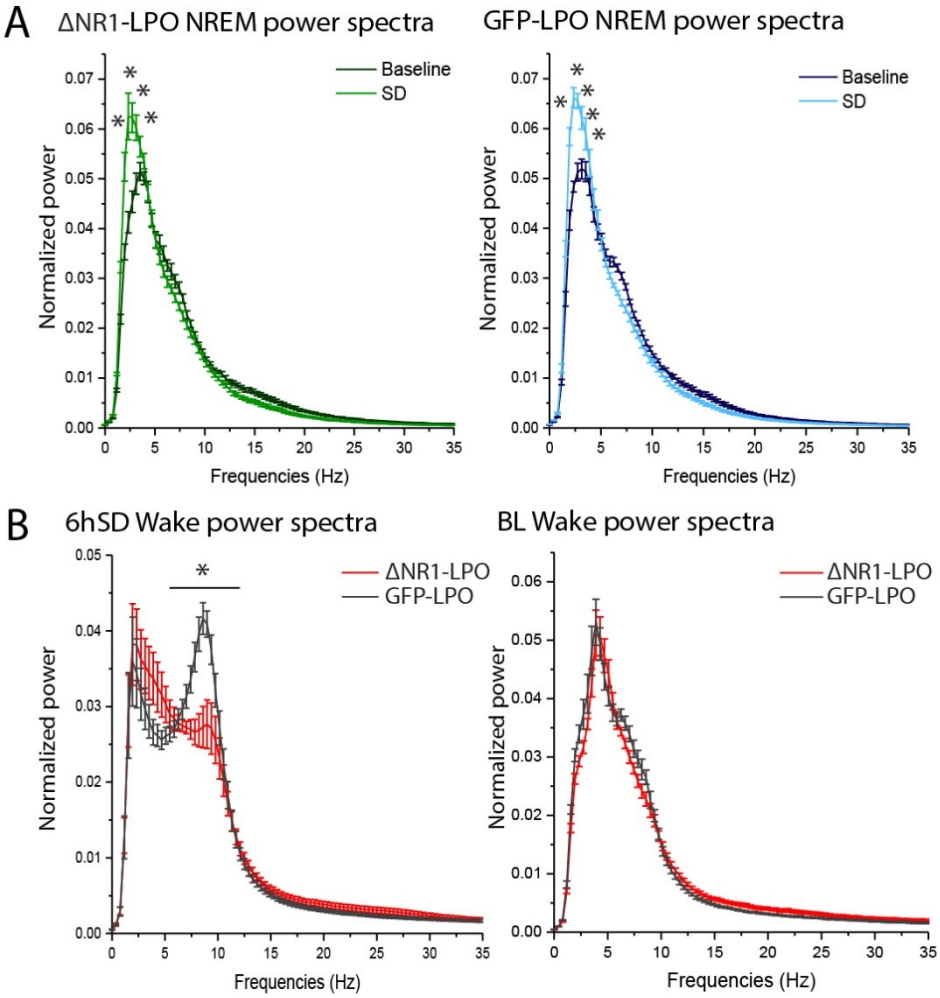

Figure 3.8.3 ΔNR1-LPO mice have a SWA rebound following 6hSD.
A, NREM EEG power spectrum calculated over 1h following 6hSD. Both ΔNR1-LPO (left) and GFP-LPO (right) mice showed delta power rebound compared to baseline values (showed in darker colours) at the same circadian time. B, wake EEG power spectrum during 6hSD (left) and corresponding 6h baseline recordings (right). On the left, ΔNR1-LPO animals (here in red) wake EEG power spectrum showed most of the power was concentrated in the Delta range, showing a diminishment of theta power in wake episodes. GFP-LPO, n= 8, ΔNR1-LPO, n= 8. Data were normalized over the total EEG power and are shown are mean ± SEM. Significance was calculated by 2-way repeated measures ANOVA and pot-hoc Tukey test. * = $p < 0.05$.

Even though ΔNR1-LPO animals had a delta power rebound, I wanted to investigate their wake EEG power spectra during SD, since under conditions of high sleep pressure, SWA can increase even during episodes of prolonged wakefulness [243, 244]. Both ΔNR1-LPO and GFP-LPO animals had enhanced delta power in the EEG wake power spectra

during SD (**Error! Reference source not found.**, B, left, 2-way repeated measures A NOVA and pot-hoc Tukey test) compared to baseline wake spectra (**Error! Reference source not found.**, B, right). However, while GFP-LPO had still higher EEG wake power in the theta waves range, ΔNR1-LPO animals had diminished EEG power in the theta waves frequency band (**Error! Reference source not found.**, B, left), although they a ppeared awake and active for almost all the 6hSD. Deletion of the NR1 subunit from LPO neurons causes a dramatic sleep loss, while maintaining the accumulation of sleep pressure, as shown by the increased number of sleep attempts during SD and the shorter latency to fall asleep (Figure 3.8.1, D and E respectively). This suggests that ΔNR1-LPO animals are constantly sleep deprived and needing sleep. The 6hSD imposed on them worsens their sleepy phenotype and their sleep pressure, causing delta power to accumulate to a level that has to be dissipated even during wakefulness. This phenotype suggests that cortical delta power in ΔNR1-LPO animals is constantly higher compared to controls, even before sleep deprivation. 24h baseline analysis of both raw and normalized data of delta power levels and their dissipation rate throughout the day in ΔNR1-LPO animals and control GFP-LPO could give a better understanding of the effects of NR1 deletion from LPO neurons and of constant sleep deprivation.

3.9 Specificity control: ΔNR1-LPO sleep phenotype is not generated by targeting a neighbouring hypothalamic area, the AHA

I wanted to verify whether the ΔNR1 sleep phenotype observed targeting LPO neurons was specific to that area or could be generated by targeting a closely neighbouring region. I decided to target the anterior hypothalamic area (AHA), a region immediately posterior to LPO. This area has a similar structure compared to LPO, as it is a major cluster of GABAergic neurons. The AHA integrates different behavioural, autonomic and endocrine responses [245, 246], including stress and food intake [247], which might have an effect on sleep patterns if the physiology of its circuits are altered by NMDAr deletion. I therefore generated ΔNR1-AHA and GFP-AHA animals using the same viral particles that were injected in ΔNR1-LPO and GFP-LPO groups (Figure 3.9.1, top). I confirmed that the LPO region was not transduced with *AAV-Cre-Venus* (Figure 3.9.1, bottom).

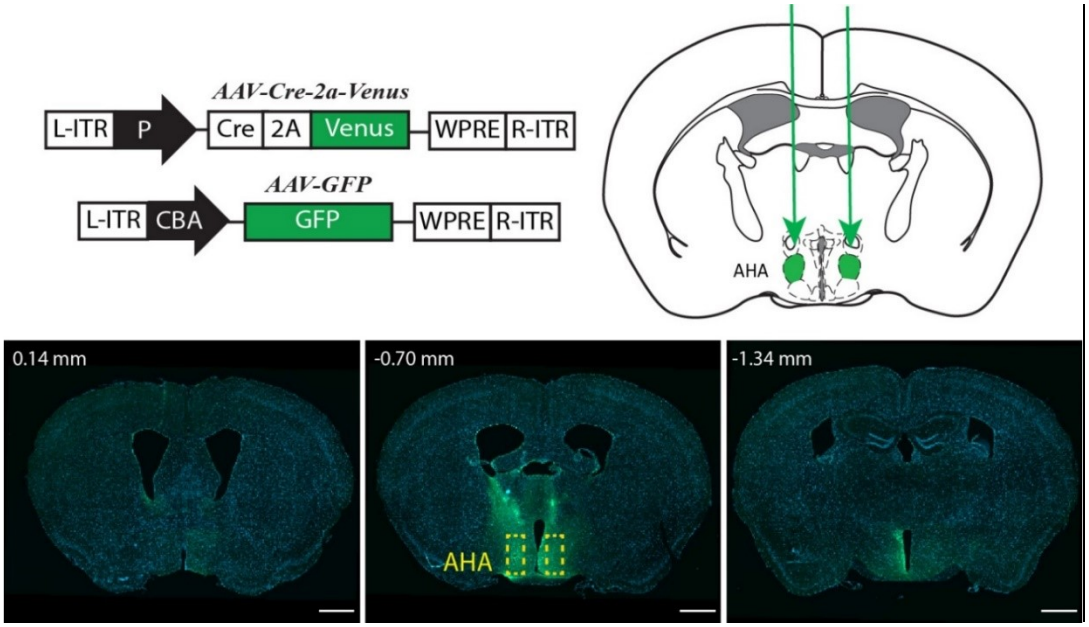

Figure 3.9.1 Generation of ΔNR1-AHA and GFP-AHA mice.
Top, representation of *AAV-Cre-Venus* or *AAV-GFP* injected in bilateral AHA, indicated by dotted squares. Bottom, viral distribution from LPO to mid thalamus to show virus was concentrated in the AHA (showed by the dashed yellow squares). Scale bars represents 1 mm, positions relative to Bregma.

For ΔNR1-AHA animals, there was no significant difference in the behavioural states amounts during both LP and DP (Figure 3.9.2, A, 2-way repeated measures ANOVA and

post-hoc Tukey test). There was also no difference in the amount of transitions, with ΔNR1-AHA showing even less transitions between NREM and wake than GFP-AHA animals (Figure 3.9.2, B). Episodes number and mean duration (Figure 3.9.2, C and D, 3-way ANOVA and post-hoc Tukey test) during both LP and DP were also not significantly different between the experimental groups, showing no signs of sleep fragmentation.

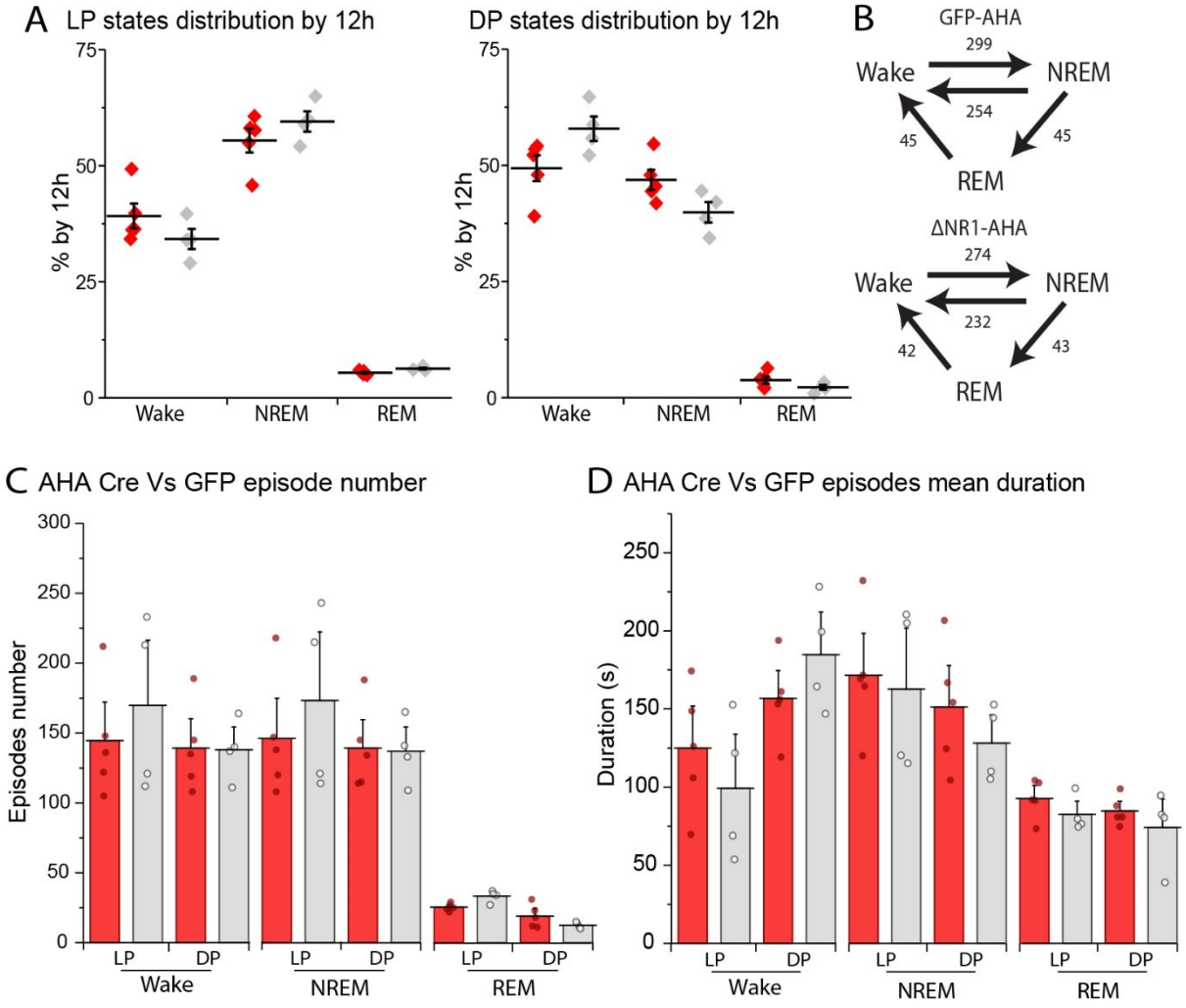

Figure 3.9.2 Baseline sleep is unaffected by removing NMDA receptors from the AHA.

Figure on the following page. A, states distribution showed as % over 12h during LP and DP. Only REM sleep during LP appeared significantly reduced compared to GFP-AHA, although it was no significant when calculating it over 24h (data not shown). B, number of transitions between states over 24h. Episode numbers (C) and mean duration (D) divided by state and by light and dark period. No significance was present when calculated with 2-way ANOVA and post-hoc Tukey test for plot A and with 3-way ANOVA in plots C and D. GFP-AHA, *n*= 4, ΔNR1-AHA, *n*= 5. Data are shown as mean ± SEM.

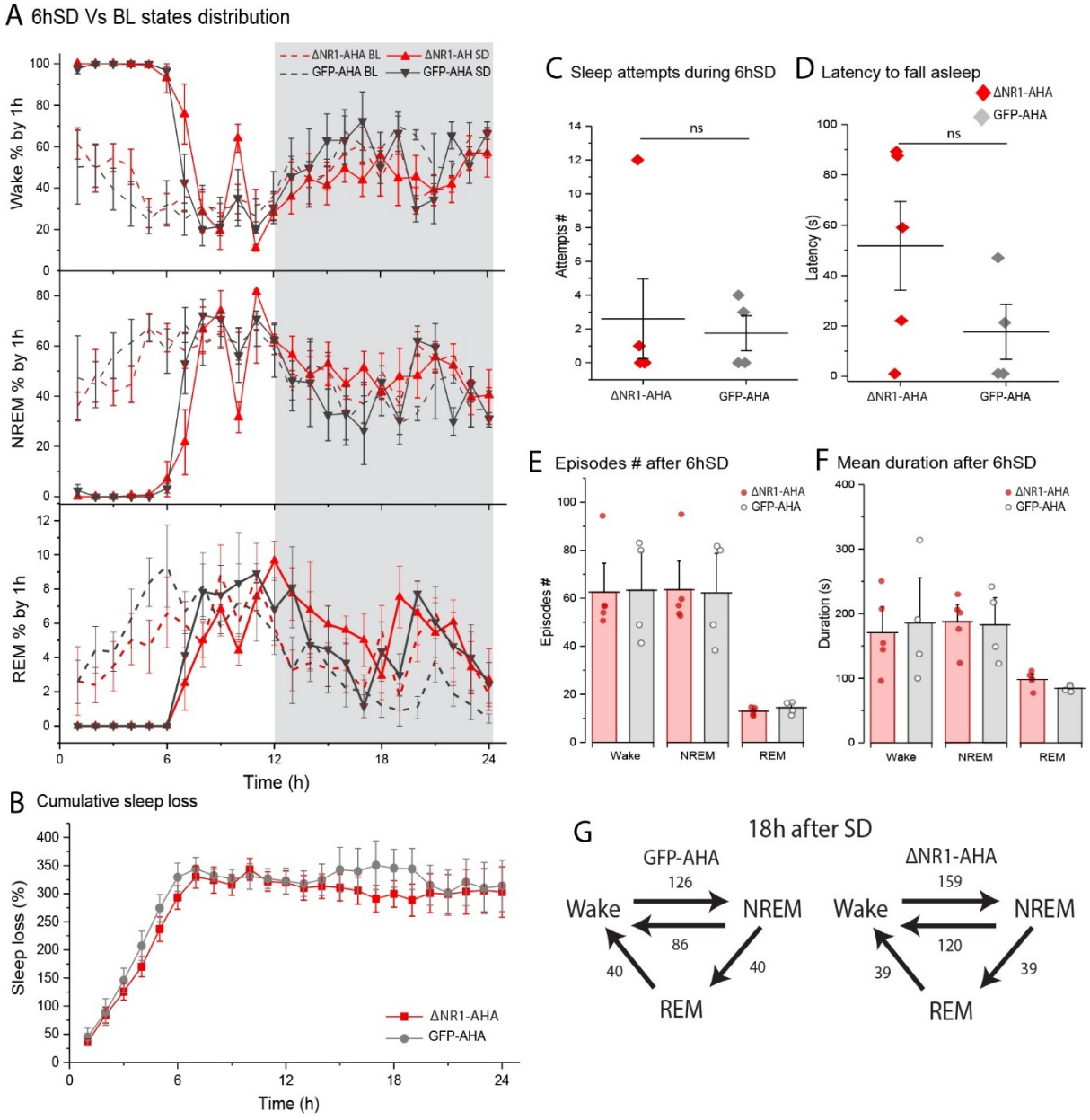

Figure 3.9.3 Sleep patterns following 6hSD are unaffected by removal of the NMDA receptor from the AHA.

A, 24h states distribution showed as % over 1h, comparing BL distribution (dotted) to SD quantification. B, Cumulative sleep loss compared to BL NREM sleep amounts following SD showed no differences between the two groups. C, Sleep attempts during 6hSD. D, latency to fall asleep once SD was ended (first 30s long NREM episode). Episodes number (E) and mean duration (F) during the 18h following 6hSD showed no sleep fragmentation. G, Number of transitions between states over the 18h of sleep opportunity. There was no significance for any of the parameters quantified when calculated by 2-way repeated measures ANOVA and post-hoc Tukey test in A, B, E, and F and with Mann-Whitney test for C and D. GFP-AHA, *n*= 4, ΔNR1-AHA, *n*= 5. Data are shown as mean ± SEM.

I then performed 6hSD on ΔNR1-AHA and GFP-AHA animals with the same protocol used for ΔNR1-LPO and GFP-LPO experimental groups. State distributions represented as percentage by hour following sleep deprivation did not show any differences between control and experimental groups (Figure 3.9.3, A, 2-way repeated measures ANOVA and post-hoc Tukey test). Neither group showed a complete recuperation of the sleep lost (Figure 3.9.3, B, 2-way repeated measures ANOVA and post-hoc Tukey test) similarly to GFP-LPO animals (Figure 3.8.1, C), suggesting a peculiar phenotype of the floxed-NR1 animals used, which seems to not fully recuperate sleep loss after 6hSD. Additionally, I did not find any differences in number of sleep attempts during SD and in the latency to fall asleep following 6h of prolonged wakefulness compared to controls (Figure 3.9.3, C and D, Mann-Whitney test). No differences in episode number or average episodes duration were present for any of the behavioural states when comparing ΔNR1-AHA animals to controls GFP-AHA (Figure 3.9.3, E and F, 2-way repeated measures ANOVA and post-hoc Tukey test). The number of transitions between states during the 18h of sleep opportunity also did not show signs of alteration from controls levels or of sleep fragmentation (Figure 3.9.3, G).

Finally, ΔNR1-AHA and GFP-AHA both had a similar and significant delta power rebound compared to their own baseline recordings (Figure 3.9.4, A and B, 2-way repeated measures ANOVA and post-hoc Tukey test), confirming that the sleep homeostasis mechanisms were conserved. Both ΔNR1-AHA and GFP-AHA had a similar distribution of the EEG power across different frequency bands, with the most relevant EEG power distributed within the theta waves frequency band, characteristic of wake (Figure 3.9.4, C, 2-way repeated measures ANOVA and post-hoc Tukey test).

These data demonstrate how the specific behavioural and sleep phenotype caused by the deletion of the NMDA receptor from LPO neurons is specific to LPO circuits and cannot be explained when targeting the same pathway in different hypothalamic areas.

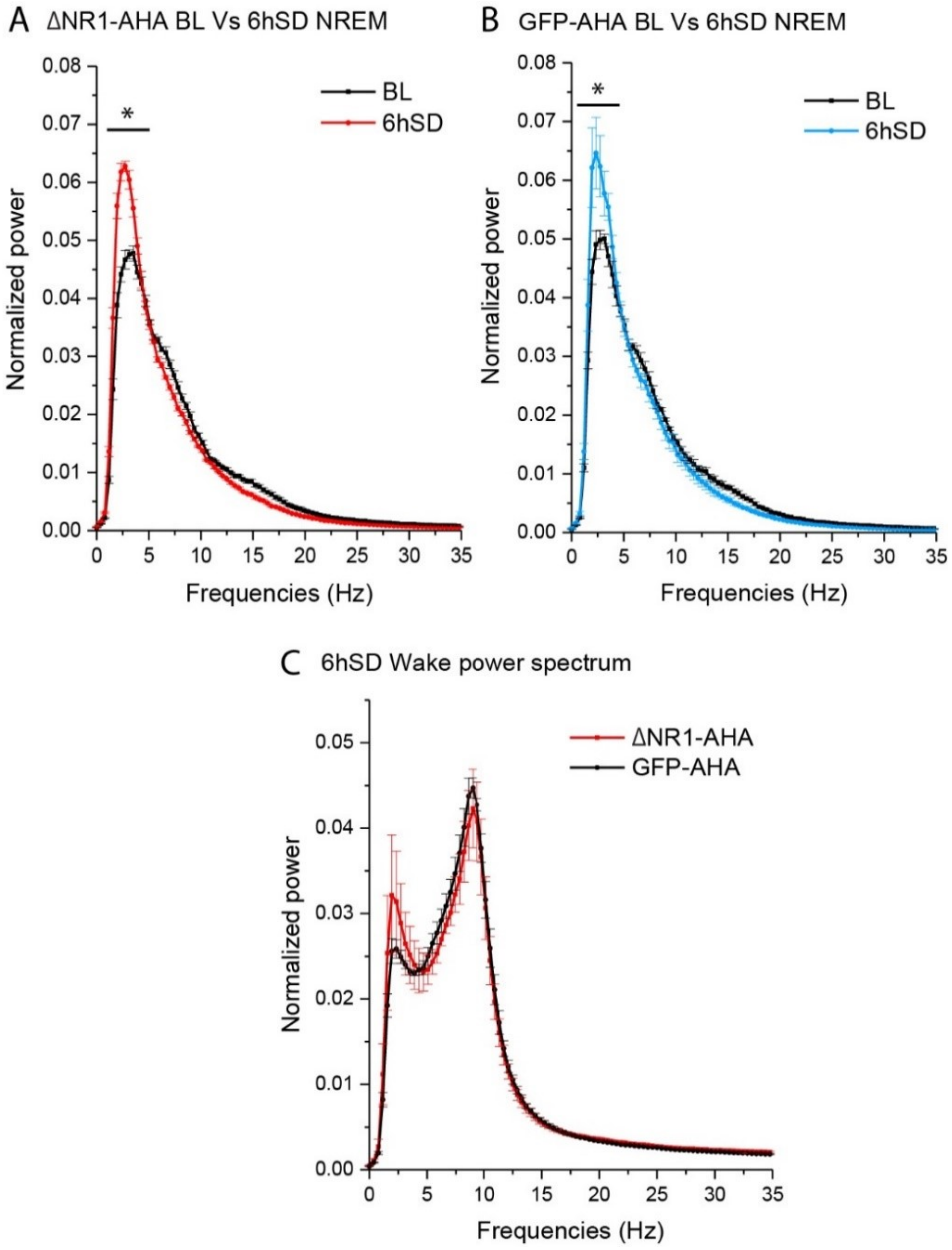

Figure 3.9.4 NREM delta power rebound and wake power spectrum is not affected by deleting NMDA receptors from the AHA

Figure on the following page. A and B, NREM delta power rebound comparing 1h following SD to BL recordings at the same circadian time. Both ΔNR1-AHA and GFP-AHA mice showed delta power rebound. C, Wake power spectrum during 6h SD to quantify delta waves leakage. No difference was detected between the two experimental groups. Significance was calculated with 2-way repeated measures ANOVA and post-hoc Tukey test. GFP-AHA, n= 4, ΔNR1-AHA, n= 5. Data are shown as mean ± SEM.

3.10 Single-cell gene expression profiling of ΔNR1-LPO cells

To understand the cell types predominantly affected by the *AAV-Cre-Venus* virus, I selected different cellular markers to characterize the targeted cells by single cell PCR. I screened for the expression of: glutamate decarboxylase 1 (GAD1), vesicular GABA transporter (Vgat), vesicular glutamate transporter 2 (Vglut2), nitric oxide synthase (Nos1) and galanin.

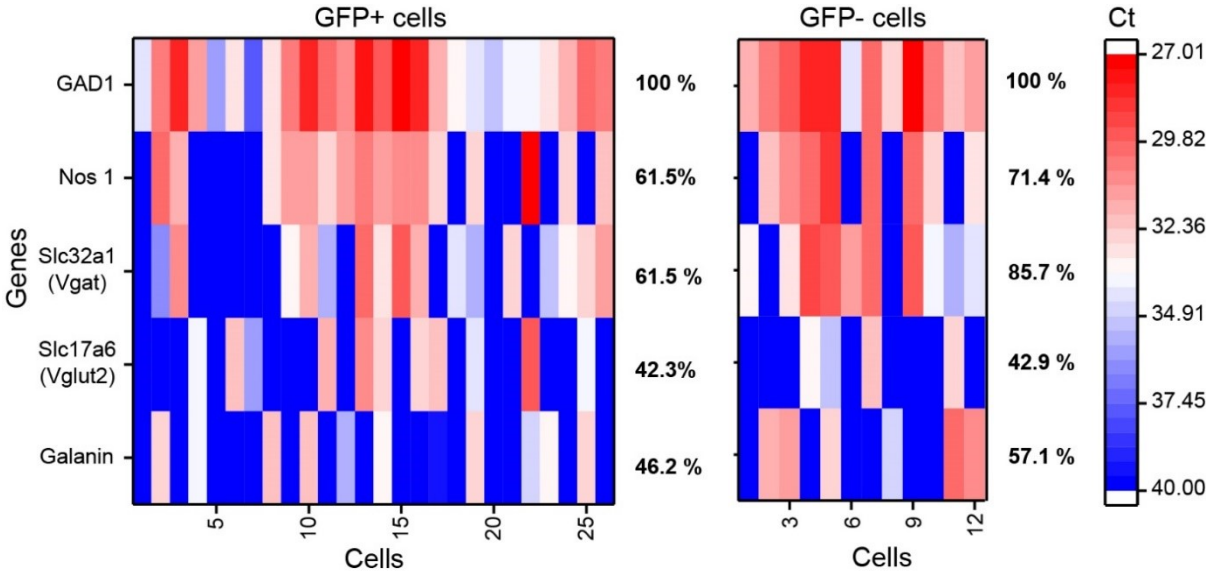

	Tot cells	Tot Vgat	Tot Vglut	Vgat+Vglut	Vgat only	Vglut only
GFP +	26	16	11	6	10	5
GFP -	12	10	4	4	6	0

Figure 3.10.1 Single-cell PCR in ΔNR1-LPO mice to identify transduced cells.
Figure on the following page. Heat map representing levels of expressions of GAD1, Nos1, Slc32a1 (Vgat), Slc17a6 (Vglut2) and galanin genes in preoptic cells infected by *AAV-Cre-Venus* virus (left, GFP+) or by neighbouring control cells not infected by the virus (right, GFP-). GFP+, *n*= 26, GFP-, *n*= 12. Bottom, table quantifying number of cells expressing and/or Vgat and Vglut to show majority of infected cells were Vgat expressing.

To perform this screening, Dr Tossell made acute slices from ΔNR1-LPO animals and collected the cytosol of single cells either transduced by the virus and GFP+, or GFP- (as

controls). Dr Anuncibay-Soto contributed to the amplification and data collection from the single cells' RNA, which included 26 GFP+ cells and 12 GFP- from 4 different animals.

We noticed that GAD1 gene expression was not an ideal marker to discriminate excitatory from inhibitory cells (Figure 3.10.1) [248]. Over 60% of the cells tested were Vgat-positive, with a third of them co-expressing Vglut2 among the GFP+ neurons. LPO neurons, in fact, often co-express the two markers, giving to these cells a hybrid function [248]. Less than half of the cells tested (46%) were galanin positive, indicating that the specific location targeted by the viral injection might not have been centred on galaninergic neuronal clusters. Nos1 transcripts were also present in just above 60% of the neurons analysed. This marker is common in the POA [81, 249].

3.11 Appendix 1: Deletion of NMDA receptors caused increased astrocytic activation in LPO

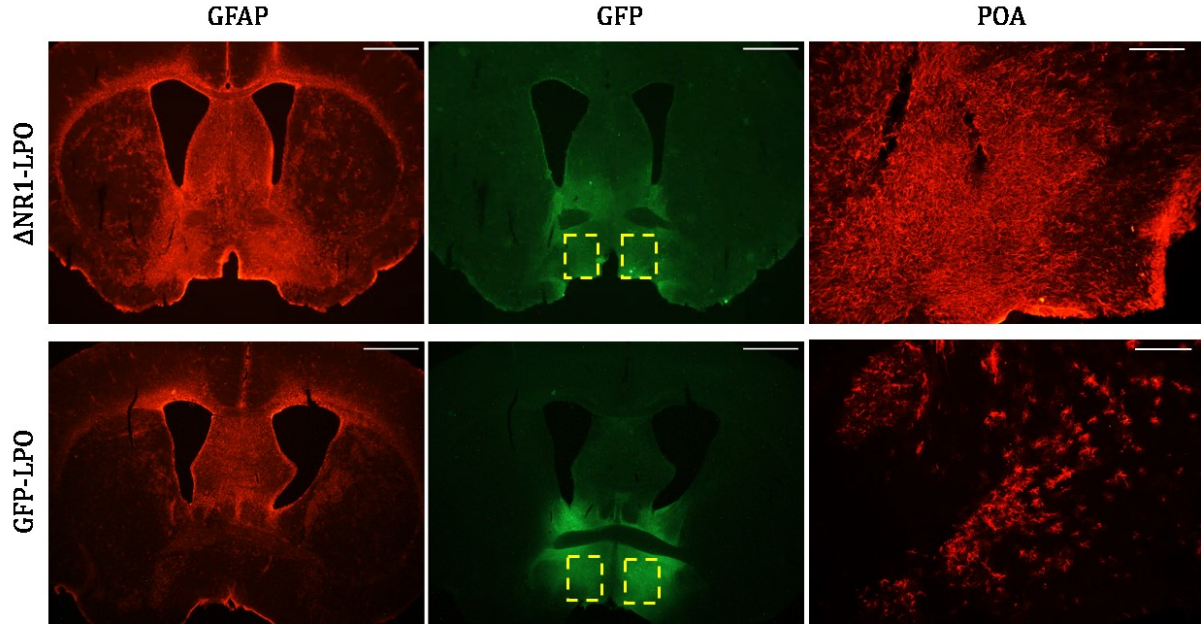

Figure 3.11.1 GFAP+ astrocytes activation following NMDA deletion in LPO.
Left, 2x magnification of ΔNR1-LPO (top) and GFP-LPO (bottom) for astrocytes marker GFAP (red) and green fluorescent protein (GFP viral tag, green). On the left, x10 image of the POA (indicated by dotted squares) to show differences in astrocytes proliferation. Scale bars represent 1 mm on the left, and 200 μm on the right.

I recently obtained some further interesting, but preliminary, data on the ΔNR1-LPO mice. Under my supervision, my undergraduate student Fergus Wade compared astrocytes staining in fNR1 animals injected with either *AAV-Cre-Venus* or *AAV-GFP* viruses. Using the astrocyte-specific marker GFAP and GFP staining to mark AAV transgene expression, we observed that astrocytes staining appeared considerably brighter around the viral injection area in ΔNR1 tissue slices compared to GFP-LPO controls. This seemed to be due to either increase astrocytic activation or proliferation, although the latter might be a less plausible possibility (Figure 3.11.1).

To quantify this result, we analysed brain slices belonging to either ΔNR1-LPO or GFP-LPO animals and calculated the ratio between GFAP staining over GFP intensity, to demonstrate that GFAP+ astrocytes activation, and possibly proliferation, was specific to the NMDA deleted samples (Figure 3.11.2).

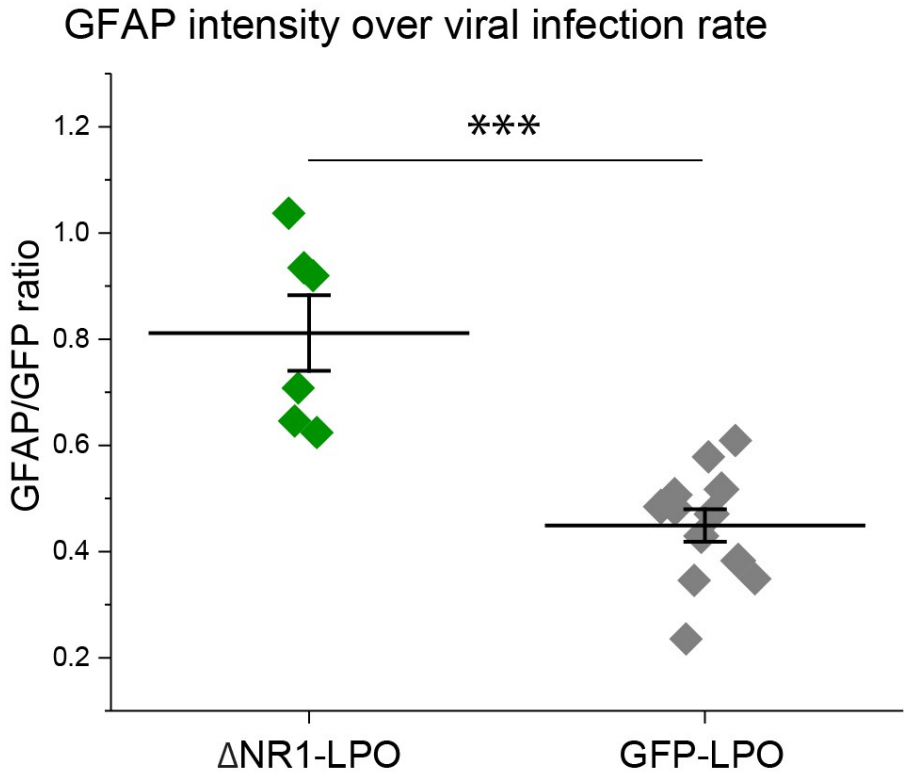

Figure 3.11.2 NMDA deletion from LPO neurons caused astrocytes activation.
GFAP intensity quantification as a ratio over GFP fluorescence indicating viral transduction. GFP-LPO, *n*= 13, ΔNR1-LPO, *n*= 6. Data are shown as mean ± SEM, significance was calculated by Unpaired Student's t test, ***= $p < 0.0005$.

3.12 Discussion

Sleep homeostasis, together with the circadian rhythm, are two of the main processes responsible for governing sleep time and need [26], although other factors, such as hunger, predatory risks and mating also partially determine sleep timing and duration [32]. Sleep homeostasis is an indicator of sleep pressure an intensity, and it increases during wakefulness to dissipate during sleep. The more an organism stays awake, the more sleep pressure accumulates, and the sleep intensity is higher when sleep finally sets in. This process is presumably related to the function of sleep, otherwise catching up on the sleep loss would not be necessary. The sleep homeostasis mechanism somehow tracks the time spent awake, but in mammals it is not yet clear how this happens. Different parameters have been used to identify and possibly quantify sleep homeostasis and the accumulation of sleep need. For mammals, delta power, as the NREM EEG power spectrum in the frequency range of 0.5-4.5 Hz (or SWA), is one of the main analysis performed by sleep researchers in relation to sleep homeostasis, as it increases proportionally to the duration of the preceding wake episode to decrease throughout NREM sleep [250]. In other words, the longer an animal has been awake, the deeper, or more synchronized is in the neocortex the subsequent NREM recovery sleep, reflected as an increase in delta power. Sleep regulatory substances, such as adenosine, TNF-α, IL-1β and prostaglandin-D2 [111, 112, 114, 124], have been shown to increase in the extracellular space in different brain areas during prolonged wakefulness to decrease during sleep. However, the increase in adenosine with time spent awake has proved controversial. First, it only increases in two brain areas with time spent awake, and second, the measurements are quite variable [119].

Synaptic plasticity has been progressively under more attention from sleep researchers in relation to sleep homeostasis and for tracking time awake [141, 143, 144]. The debate is still open on whether synapses strength increases during wake and decreases during sleep, or *vice versa* [1, 181, 184], and whether this mechanism is applicable in mammals and is responsible for sleep homeostasis. Controversies aside, studies done on synaptic homeostasis and sleep have been performed mostly on cortical and hippocampal tissues, where it is easier to track and observe neuronal and network dynamics due to their cellular alignment. This means that no data related to synaptic plasticity and sleep homeostasis have been observed in sleep regulatory areas, once again

ignoring the importance of these networks in inducing and maintaining sleep. Moreover, no clear signalling pathway or molecular explanation have been identified as responsible for changes in synaptic homeostasis based on sleep patterns in mammals.

For all these reasons, I decided to focus on one sleep regulatory area and one specific molecular pathway and signalling involved in tracking the time the animal spends awake, to understand the reciprocal effects of changes in synaptic strength and sleep amounts and behaviours. As for the circuit, I decided to investigate LPO. LPO is part of a more extended area, the POA, which is fundamental for sleep onset and maintenance [67, 68]. Our lab has demonstrated that LPO neurons are active during both sleep deprivation and recovery sleep, and once artificially reactivated, these same neurons recapitulate NREM sleep [251]. Our lab has also shown that galanin neurons in the LPO area are needed for sleep homeostasis [148].

As synaptic plasticity mechanisms, I decided to target the NMDA receptor, one of the major receptors responsible for LTP in the brain. The NDMAr is fundamental for memory consolidation and learning [162]. This receptor is an easy target to manipulate, since the disruption of only one of its subunits, the NR1, is sufficient to ablate completely the NMDAr assembly and functions [158]. Using a floxed-NR1 transgenic mouse line and the selective injection of a Cre recombinase transgene into LPO region, I was able to disrupt the NMDAr by interrupting the production of the NR1 subunit in LPO neurons, generating ΔNR1-LPO animals. These mice were compared to controls GFP-LPO animals, where littermates received a control virus carrying only the green fluorescent protein (GFP). Both groups underwent sleep and behavioural analysis to understand the effects of synaptic plasticity disruption on sleep homeostasis.

3.12.1 NMDAr pathway in LPO is fundamental for sleep regulation

When tested in an open field arena, ΔNR1-LPO animals appeared highly hyperactive, running almost double the distance compared to controls. ΔNR1-LPO mice did not show signs of anxiety, as reluctance to explore the central zone of a brightly lit open space [240] (Figure 3.6.1). Compared to controls GFP-LPO mice, ΔNR1-LPO mice showed an extremely fragmented sleep phenotype, with a 15-20% constant sleep loss during both LP and DP (Figure 3.7.1 and Figure 3.7.2). These data suggest that the NMDAr regulates LPO circuits necessary to maintain sleep, and that the sleep phenotype observed in ΔNR1-

LPO animals is not a simple consequence to other primary effects of the deletion, as, for example, anxiety.

As shown with QPCR analysis of AMPA and NMDA receptors subunits, LPO has a higher expression compared to cortex and cerebellum of the NMDA subunit NR2D (Figure 3.2.1), which is responsible for keeping the receptor open for the longest time [159, 160], allowing even minutes of calcium influx in neurons. Because of this peculiarity, it is possible that LPO neurons need longer excitatory signalling and stimulations to maintain and sustain sleep downstream in the circuit. With NMDA deletion, LPO neurons can still receive glutamatergic excitatory signals from AMPA receptors, which have characteristic fast kinetics of just a few milliseconds (Figure 1.5.2). Perhaps, fast AMPAr signalling can cause sleep-promoting neurons to initiate sleep, but sustained integrative excitatory inputs on the same circuit via NMDAr might be necessary to maintain sleep. In fact, from electrophysiology recordings performed on ΔNR1 neurons, we noticed that the spontaneous excitatory postsynaptic activity of these neurons is greatly reduced, meaning that the cells will send less downstream signals to their postsynaptic connections (Figure 3.5.2). Because one of the main classical roles of LPO neurons is to inhibit through GABAergic projections wake promoting areas [75], it is possible that those inhibitory neurons are not activated enough, or perhaps long enough, to keep wake centres inhibited and supress wakefulness. The sleep fragmentation phenotype would then be a consequence of frequent intrusions of wakefulness into sleep time. This phenotype would also explain the considerate reduction in time spent asleep in ΔNR1-LPO compared to controls, as sleep cannot be maintained.

3.12.2 NMDA pathway connects sleep rebound to cortical delta power

To understand the role of the NMDAr in affecting sleep homeostasis, we performed 6hSD on ΔNR1-LPO animals and GFP-LPO controls, to increase sleep pressure. Following SD, sleep fragmentation and sleep loss were not improved in ΔNR1-LPO animals compared to controls. ΔNR1-LPO animals, although showed numerous signs of sleepiness, as increased sleep attempts during SD, shorter latency to fall asleep after SD, and higher leakage of delta waves during SD wakefulness, they could not recover the sleep loss (Figure 3.8.1 and Figure 3.8.2). This lack of sleep rebound was present even though the NREM EEG power spectra showed a delta power rebound following sleep

deprivation (**Error! Reference source not found.**). NMDAr deletion revealed then a de-c oupling of phenotypical sleep rebound and cortical EEG power spectra. Consequently, the lack of NMDAr in the group of neurons driven by the "pan neuronal" promoter in LPO does not cause a complete elimination of sleep homeostasis mechanisms. This data could be elucidating a disconnection between sleep phenotype and homeostatic parameters, which can happen under chronic sleep restriction [136]. Perhaps, sleep homeostasis parameters and sleep rebound are not connected at all, and they might be regulated by separate areas and circuits. This would mean that deletion of the NMDAr might not be affecting the neuronal connections between delta power and sleep phenotype, but only reduce the sleep rebound component after prolonged wakefulness.

Postsynaptic neurons, if affected themselves by the NMDA deletion, might not only received less inputs caused by the reduction of sEPSCs in presynaptic neurons, but might also be affected by the lack of plasticity mechanisms regulating their synaptic strength. If synaptic strength increases during wakefulness as proposed by the SHY theory [181], and it facilitates sleep rebound following sleep deprivation, lack of LTP caused by NMDA deletion would not allow LPO neuronal circuits to strengthen enough to induce and initiate sleep. On the other side, if synaptic upscaling happens during NREM as previously suggested [1], lack of NMDA driven synaptic strengthening might drastically reduce sleep duration. In other words, for sleep to be maintained, LTP-like mechanisms should be initiated in sleep promoting neurons to favour sleep recovery over wakefulness, in particular in a condition of elevated sleep need.

Figure 3.12.1 Changes in synaptic homeostasis based on behavioural state.
Figure on following page. A, representation of NREM sleep regulation through synaptic upscaling, taking the POA as an example. During sleep, NREM promoting circuits undergo LTP to maintain sleep and inhibit wake promoting centres (in red). LPO local inhibitory connections might undergo synaptic upscaling as well and can successfully inhibit sleep promoting neurons. B, more detailed representation of possible local LTP and LTD mechanisms. Top, during wakefulness, monoaminergic and glutamatergic wake-promoting neurons are potentiated and activate local LPO inhibitory neurons to silence NREM-circuits, which undergo LTD. Local inhibitory neurons in wake-promoting areas also undergo LTP, allowing a state switch. During NREM sleep, NREM-promoting neurons can now undergo LTP, as well as their local inhibitory neurons, while wake-promoting cells downscale. Local inhibition permits state switches by undergoing LTP or LTD based on the vigilance state. Figures drawn by me.

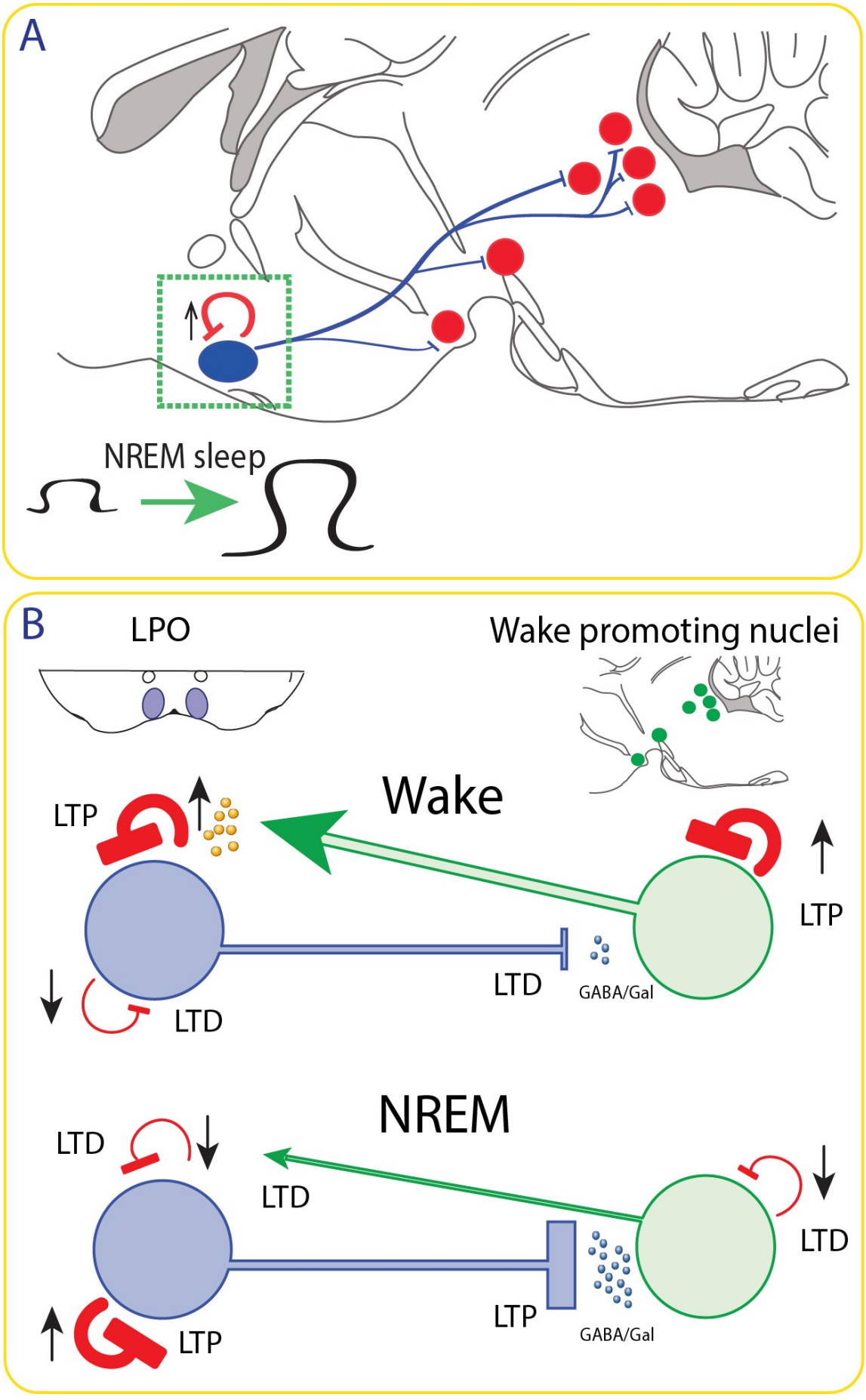
A
NREM sleep
B
LPO
Wake promoting nuclei
Wake
LTP
LTD
GABA/Gal
LTP
LTD
NREM
LTD
LTD
LTP
GABA/Gal
LTD
LTP

Perhaps synaptic up and downscaling coexist in the brain based on the behavioural states, brain areas, circuits, and neuronal types we are observing. It might be possible that during sleep, NREM promoting circuits undergo LTP to maintain the brain asleep, while wake promoting neurons, which receive massive inhibitory inputs from sleep circuits, undergo LTD to be silenced (Figure 3.12.1, A). This would explain why studies performed on cortical tissues showed synaptic upscaling during wakefulness and downscaling during sleep. The cortex, in fact, peaks in its activity during wake episodes, and under sustained stimulation its neurons undergo LTP. During NREM sleep, and under delta power slow oscillations, the cortex is at rest, and circuits and neuronal connections could downscale [252]. If up and downscaling coexist in different areas based on the behavioural stage and neuronal type, it would be interesting to understand how the brain networks can flip the process to induce states transitions. Circadian components can intervene in balancing vigilance states but sleep and wake circuits would need inhibitory inputs to regulate their activity. These inhibitory neurons forming a negative loop might as well undergo synaptic strengthening during a specific state. When potentiated enough during one of the behavioural states, they could send sustained signals to inhibit wake or sleep promoting neurons, to favour a state transition. In case of a sleep regulatory circuits for example, both sleep promoting neurons and local inhibitory cells can undergo synaptic upscaling, and sleep promoting neurons would continue inhibiting wake promoting centres until their local inhibitory signals become sustained enough to block the sleep neurons. Wake centres would than no longer be inhibited, and the brain could be woken up (Figure 3.12.1, B).

It is still unclear how NMDAr-driven LTP can affect sleep regulatory circuits, but the possibility that different mechanisms coexist based on brain area and neuronal type seem more plausible than thinking the whole brain undergoes the same mechanisms under a specific behavioural state.

3.12.3 The ΔNR1 phenotype is specific to the LPO area

To make sure that the behaviour observed in ΔNR1-LPO animals was specific to LPO and was not an artefact caused by deletion of the NMDAr from neurons, I performed the same experiments targeting a different hypothalamic area, the AHA. The AHA is a dense structure, with high prevalence of GABAergic neurons, and involved in a wide range of

physiological responses [247]. I generated ΔNR1-AHA and GFP-AHA animals and observed their sleep patterns and behaviours (Figure 3.9.1). These animals did not show any drastic changes in sleep amounts and architecture during baseline recordings (Figure 3.9.2), and did not show any alterations in sleep homeostatic mechanisms compared to controls after 6hSD (Figure 3.9.3 and Figure 3.9.4). These data confirm that the phenotype observed in ΔNR1-LPO animals derives from the specific targeting of sleep regulatory circuits and not from a non-specific disruption of glutamatergic signalling.

Interestingly, ΔNR1-AHA animals did not show any signs of behavioural alteration: they did not appear smaller or with evident loss or gain of weight and they did not appear to have anxious of stressed behaviour neither in the home cage nor when handled. The effects of NMDAr deletion on a circuit might therefore be specific for the area targeted. In the AHA, conversely to LPO, the AMPAr signalling might be enough to maintain a normal functioning of the networks, while for LPO neurons both AMPA and NMDA signals might be necessary to keep neurons activity intact. Electrophysiological recordings of both evoked and spontaneous EPSCs might be useful to verify AMPAr compensation in AHA NMDAr deleted neurons.

3.12.4 Single cell PCR reveals most of the ΔNR1 cells in LPO were expressed the Vgat mRNA

To understand what types of neurons the *AAV-Cre-Venus* virus transduced, we performed single cell PCR comparing GFP+ and GFP- negative cells. More than 60% of the cells analysed resulted positive to the GABAergic neuronal marker Vgat. . Looking at the excitatory marker Vglut2, more than 40% of GFP+ cells expressed this marker, often together with the Vgat one (**Error! Reference source not found.**), as previously shown ADDIN EN.CITE [248]. Among the GFP- cells, no cells were positive for Vglut only, and 4 showed a co-expression with Vgat (**Error! Reference source not found.**, bottom table). We can conclude that the ΔNR1-LPO phenotype was for most part generated by the deletion of the NMDAr from GABAergic neurons or neurons using GABA/glutamate co-transmission. Specific targeting of GABA-releasing neurons might clarify which circuits is behind sleep patterns regulation and homeostatic responses. One option would be to target galanin neurons in LPO, as they are needed for sleep homeostasis [148]. These neurons are also needed for sleep homeostasis in zebra fish [253], and activation of LPO

galanin neurons induces NREM sleep [148, 254]. Perhaps part of the results I obtained from the NMDAr deletion from LPO neurons comes from removing it from galanin neurons. As excitation increases with time spent awake on galanin cells, they are more likely to fire to induce NREM sleep. However, around 10 distinct types of galanin neuron have now been identified in the PO area [248], making this a difficult problem to further dissect.

3.12.5 NMDA deletion causes astrocytic activation

Because astrocytes are highly involved in glutamate regulation in the brain [255], and in gating NMDAr activity through the release off the gliotransmitters D-serine [256], I wanted to understand whether NMDA deletion in LPO neurons could affect this class of glial cells. I used the astrocytes selective marker GFAP in IHC staining in association with staining of GFP to trace viral injection. NMDA deletion caused a marked GFAP positive astrocytic activation in ΔNR1-LPO animals compared to controls GFP-LPO. This phenotype was not caused by the AAV injection, since *AAV-GFP* alone did not cause the same astrocytic reaction (Figure 3.11.1), as also shown by the intensity ratio between GFAP and GFP staining (Figure 3.11.2).

Different reasons could explain the activation observed in ΔNR1-LPO mice. First, ΔNR1-LPO brain slices had no increase in extracellular glutamate (Figure 3.5.3). Neuronal NMDAr deletion might cause higher release of glutamate by the presynaptic neurons to compensate the lack in postsynaptic glutamatergic signals. Extracellular glutamate can be excitotoxic for the neurons and astrocytes can capture the neurotransmitter from the synaptic cleft and reduce its availability to neurons [255]. Astrocyte increased activity might then be a consequence of increased need for glutamate buffering upon NMDAr deletion from neurons.

Additionally, astrocytes have been shown to be involved in regulating sleep patterns and homeostasis [257]. As mentioned in the introduction, astrocytes in the brain are the main producer of adenosine. Through their actions on A1 and A2A receptors, astrocytes can affect sleep homeostasis, maintaining delta power rebounds following sleep deprivation [120]. Perhaps in ΔNR1-LPO animals astrocytes proliferation might be useful to produce more extracellular adenosine, which can act on A2A excitatory receptors on sleep promoting neurons to compensate the reduction of spontaneous EPSCs caused by NMDAr deletion (Figure 3.5.2). In addition to their role in adenosine release, astrocytes

control behavioural states through glucose and lactate trafficking to neurons, as impairments to the Gap junctions connecting the two cell types reduce wake maintenance and time [258]. It would be useful to quantify extracellular adenosine concentration and energetic levels of lactate and glucose in both astrocytes and neurons after NMDA deletion in LPO to understand why astrocytes increase their activity, and perhaps their number, in ΔNR1-LPO animals, and what is the exact function of these cells following NMDAr deletion.

3.12.6 Conclusions and future work

With the data shown in this chapter I have demonstrated that the NMDAr pathway and its downstream signals are fundamental for sleep patterns and homeostatic regulation in LPO. More work ought to be carried out to understand whether synaptic up and downscaling driven by the NMDAr are really the molecular basis for sleep regulation. More electrophysiological recordings performed right after prolonged wakefulness or sleep might help us study the activity of LPO neurons and their synaptic plasticity during behavioural states. With these experiments, we would be able to test whether LTP mechanisms have been happening during wake or NREM sleep in LPO and whether they are driven for the most part by NMDAr pathways.

Additionally, to tackle the question of whether LPO neurons need longer stimulations to maintain sleep and inhibit downstream wake promoting targets, manipulations of the subunit NR2D might explain with more precision the phenotype observed in ΔNR1-LPO animals and the physiology of LPO sleep promoting circuits. Using a flox-NR2D mouse and injections of a Cre recombinase in LPO it would be possible to analyse the effects of ablating only specific properties of the NMDA receptors.

Regarding the role of astrocytes in ΔNR1-LPO animals, quantification of extracellular adenosine and metabolic substrates as glucose and lactate in astrocytes and neurons might help us understand this reaction observed upon NMDA deletion from neurons. Additionally, to elucidate the role of astrocytes in sleep and wake regulation, chemogenetic activation of these glial cells might explain astrocytes function in LPO. To do so, I am currently using a *GFAP-hM3-cherry* virus to artificially activate astrocytes and observe the effects on sleep patterns.

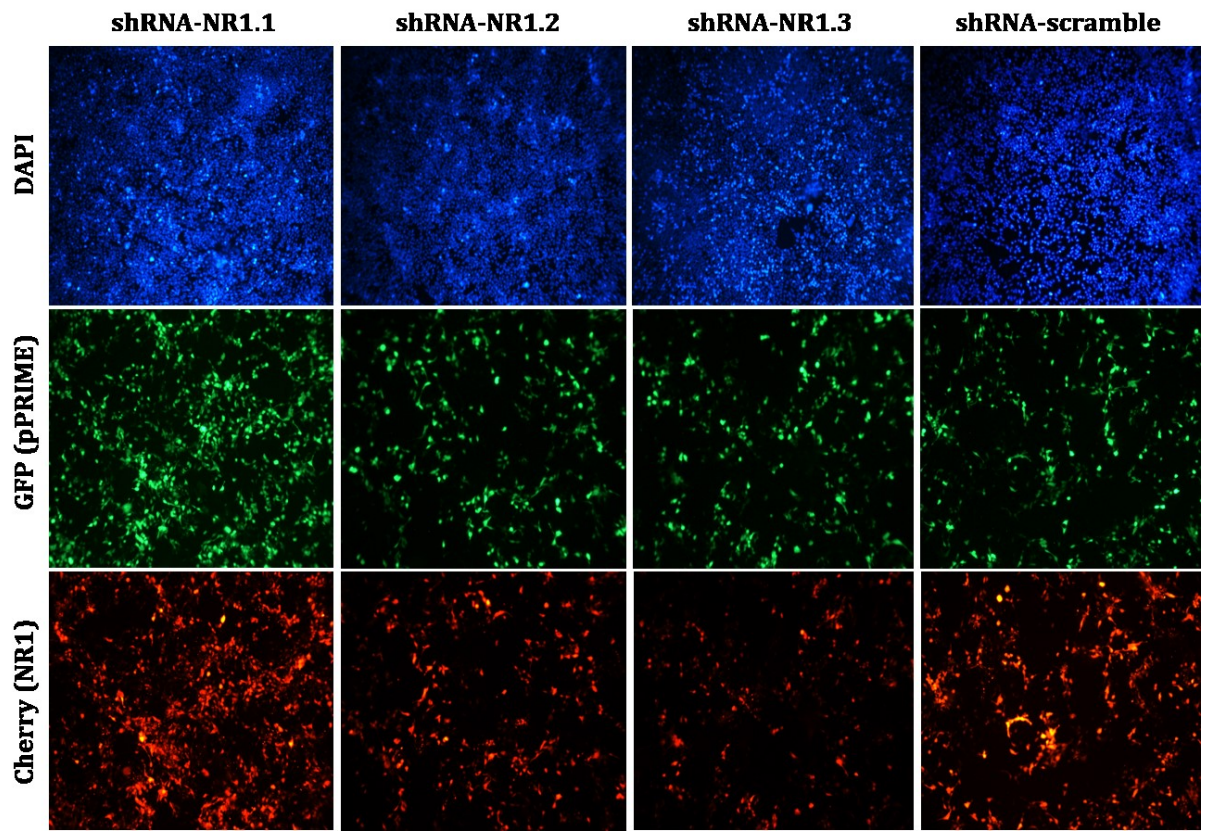

Figure 3.12.2 Comparison of three shRNA-NR1 and shRNA-scramble in knocking down NR1 expression.
Fluorescent images of HEK293 cells showing DAPI (top row, in blue), GFP reporter for expression of shRNA-NR1 and scramble pPRIMEs (second row, in green), and cherry reporter, indicating expression of the plasmid carrying the NR1 sequence (third row, in red). ShRNA-NR1.3 in third column showed to be the most efficient in inhibiting NR1 expression.

Since most of the GFP+ cells characterized in ΔNR1-LPO animals were expressing Vgat, with my colleague Raquel Yustos, we produced a short interfering RNA (shRNA) capable of inhibiting the expression of the NR1 subunit of the NMDA receptor. Three different sequences of shRNA-NR1 have been tested in cultured HEK293 cells to verify their ability to inhibit NR1 expression, offering the possibility to choose the most efficient sequence, in comparison to a control shRNA scramble oligo. The three shRNA.NR1 and a shRNA-scramble sequence were cloned into a pPRIME plasmid and co-transfected in HEK293 cells together with a cherry reporter plasmid carrying the NR1 subunit gene. The cell culture sample with lowest cherry fluorescence detected indicated the best shRNA efficiency in inhibiting the NR1 gene expression (Figure 3.12.2). The third sequence tested resulted to be the most effective in inhibiting the expression of the cherry reporter

(Figure 3.12.3) and it was therefore mutated in an AAV viral vector under flex direction to be expressed in specific neuronal types expressing the Cre recombinase, e.g. Vgat-Cre animals.

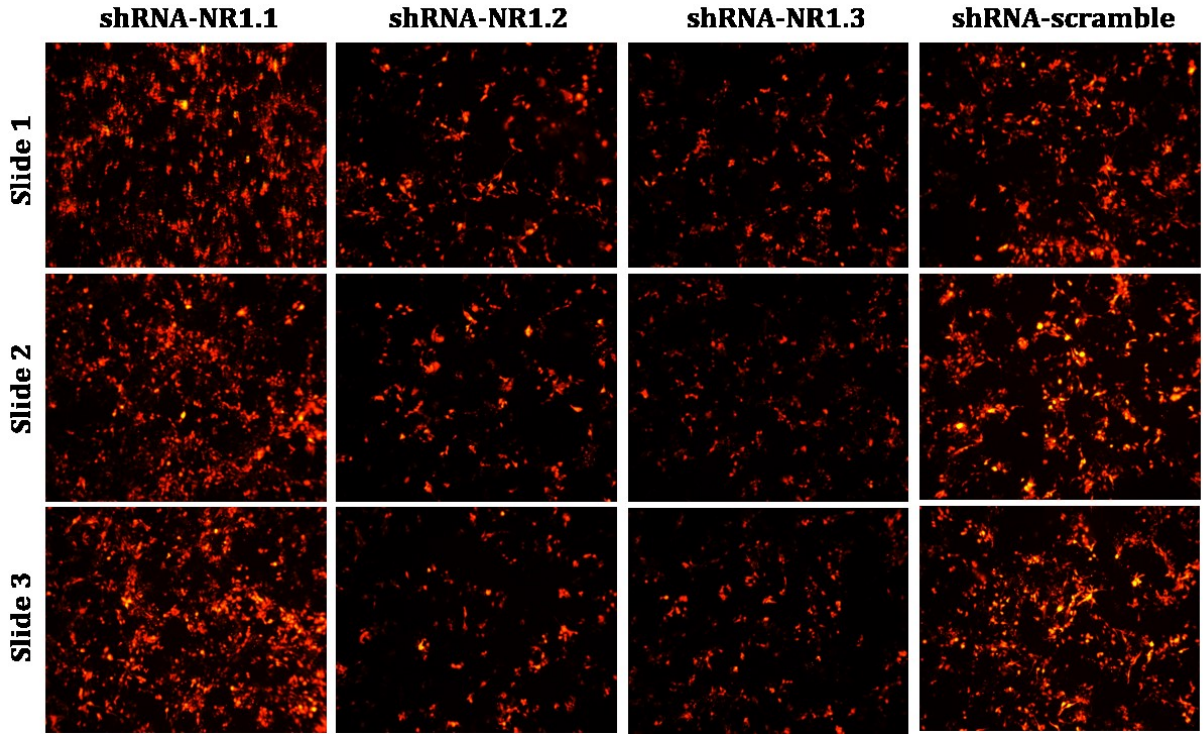

Figure 3.12.3 Confirmation of shRNA-NR1.3 as most efficient in inhibiting NR1 expression in HEK293 cells.
Additional fluorescence images on 3 separate cells fixed slices showing the inhibition of the NR1-cherry plasmid expression after addition of, from left to right, shRNA-NR1.1, 2, 3 and shNRA-scramble to the cultured HEK293 cells.

Using a Vgat-Cre transgenic mouse line, I am currently analysing the effects of the shRNA-NR1 silencing on Vgat expressing neurons only, with the intent of identifying a specific neuronal circuit responsible for the phenotypes observed under NMDAr deletion.

Finally, alternative mechanisms related to synaptic plasticity might be investigated, to understand whether the phenotype I observed was specific for NMDAr pathways, or whether any type of signalling regulating synaptic homeostasis might affect sleep regulation in a similar manner. For example, deletion of the Gria1 subunit of AMPAr can interfere with LTP mechanisms in the hippocampus, but not in cortical pyramidal neurons [259], and it would be interesting to test its involvement in regulating synaptic homeostasis in sleep regulatory circuits.

4 Vigilance state-dependent neuronal activity in LPO

4.1 Chapter summary and introduction

To characterize their activity during vigilance states, I performed in vivo photometry with ultra-sensitive calcium sensors (GCaMP6s) to record LPO neurons in freely behaving animals together with EEG and EMG traces. Using hysn-GCaMP6s or flex-GCaMP6s transgenes, I recorded the activity of all LPO neurons, or of Vgat, Vglut2, Nos1 and galanin only. All LPO neurons appeared to be REM active, with frequent spiking during NREM sleep and almost no activity during wake. A similar profile was observed in Vgat, Nos1 and Vglut2 neurons, while galaninergic ones showed little activity during NREM sleep and no calcium fluctuations during wake. Following Dex sedation, Vgat, Nos1 and a third of the Vglut2 neurons showed regular 0.1 Hz spiking at the onset of the sedative state. After at least 90 minutes from Dex injections, a third of Vgat and Nos1 neurons were silenced, while the remaining maintained a slow frequency GCaMP6s signal. Only the Vglut2 neurons active at the onset of sedation maintained a slower activity during deep sedation, while the rest remained silenced. Interestingly, a group of Vglut2 neurons in MPO showed activity only during wakefulness. These data reveal a possible role of LPO neurons in REM sleep regulation and suggest that Vgat and Nos1 neurons might be important for the induction Dex sedation. The use of more specific markers for exclusively excitatory or inhibitory LPO neurons might help us better understand the role of this area in sleep regulation.

The preoptic area of the hypothalamus (PO) is a dense area of intermingled and diverse neuronal types [248]. Traditionally, the PO has been divided into different subareas e.g. ventral lateral preoptic (VLPO), lateral preoptic (LPO) and medial preoptic

(MPO) areas, which regulate individually, and sometimes cooperatively, many behaviours, including parenting [260], temperature regulation [81, 261], aggression [262], sleep and sedation [71, 72]. However, these anatomical subdivisions have no clear basis in gene expression [248].

A way to understand how LPO regulates sleep is to investigate its neuronal activity during behavioural states. So far, only changes in neuronal discharges have been studied in the PO area, showing how MnPO [263] and VLPO [78] neurons actively discharge during both NREM and REM sleep, while LPO neurons are mainly REM active, although all sleep active neurons from these areas discharge at even higher frequencies during sleep deprivation and enhanced delta power during recovery sleep [145]. Apart from these unit recordings in rats, there has been little reported about how genetically specified subtypes of PO neurons change their activity during vigilance states. From Von Economo's studies in the XX century [66], to more recent attempts to understand LPO circuitries involved in sleep [254], we only partially comprehend how the PO area works. For this reason, I decided to investigate the role of PO neurons and their baseline activity during vigilance states. Using different transgenic mouse lines, I was able to investigate the activity of PO neurons as a whole area, and then to single out the activity of GABAergic, glutamatergic, Nos1-expressing and galaninergic neurons, which are all present in the PO area, as previously discussed (Chapter 3, Section 10.4). To do so, I used photometry techniques and ultra-sensitive protein calcium sensors (GCaMP) [264]. This technique allows the recording of fluorescent signals from neuronal calcium activity in freely behaving animals, while simultaneously recording EEG and EMG data [265]. It is assumed that an increase in intracellular calcium corresponds to increased neuronal excitation and membrane depolarization, which would result in action potentials [266].

Many different variants of GCaMP6 sensors are available, with differences in sensitivity, affinity for calcium and kinetic. For our experiments, we used GCaMP6slow (GCaMP6s), the most sensitive of the variants, with a high affinity to calcium and a higher threshold for saturated fluorescence [224], so that we could perform longer polysomnographic recordings. Raquel Yustos in the lab generated and packaged two different AAV transgenes, one expressing GCaMP6s under a human synapsin (hsyn) promoter (Hsyn-GCaMP6s) and one with the GCaMP6s reading frame in an inverted orientation (flex-switch), allowing the expression of the calcium sensor only in Cre recombinase positive cells. The latter AAV was used in transgenic mouse lines, expressing

the Cre recombinase under specific promoters: Vgat-Cre, Vglut2-Cre, Nos-Cre and Galanin (Gal)-Cre.

4.2 LPO neurons in LPO-hsyn-GCaMP6s mice are mostly REM active

First, I wanted to observe the overall physiological activity of the LPO area during vigilance states in C57Bl/6 mice. Using a localized injection of *AAV-hsyn-GCaMP6s* virus into the LPO hypothalamic area and subsequent implantation of optic fibre, only the calcium activity from LPO neurons was recorded.

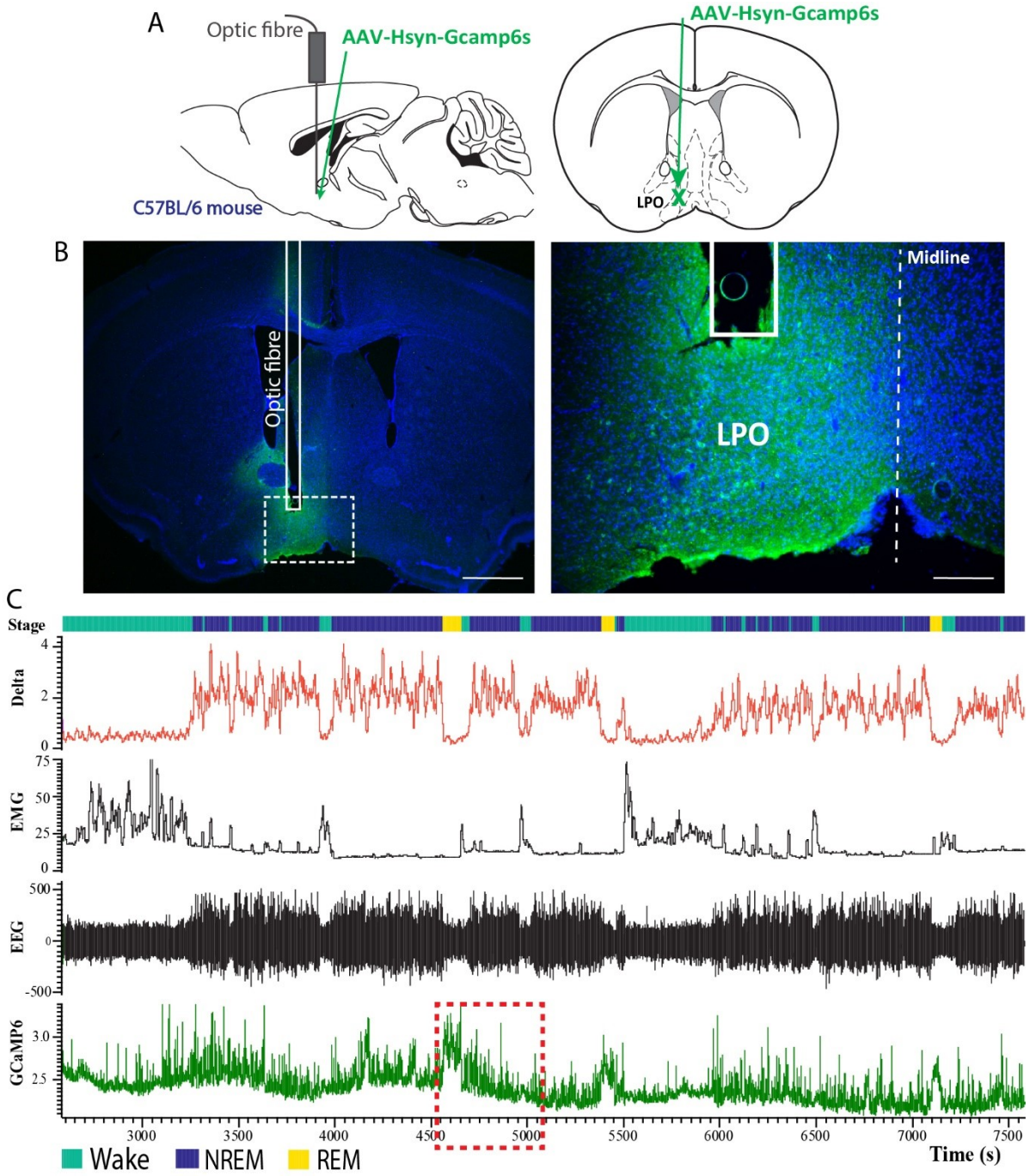

Figure 4.2.1 LPO hsyn-GCaMP6s mice and *in vivo* photometry recordings.
Figure on previous page. (A) Schematic representation of the *AAV-hsyn-GCaMP6s* injection and fibre optic implantation in LPO. (B) IHC of hsyn-GCaMP6s expression and visible fibre track. Dotted square on the left indicates zoomed-in area shown on the right. Scale bars represent on the left 1 mm, on the right 200 µm. (C) Example of Hsyn-GCaMP6s photometry recording aligned to EEG/EMG data. Graph shows from the top: stage (green = wake, blue = NREM, yellow = REM), delta power, EMG, EEG and GCaMP6s fluorescence converted in Volts. Red dotted square indicates zoomed in area showed in Figure 4.2.2.

The highest peaks in the GCaMP6s photometry traces aligned to EEG and EMG traces corresponded to REM sleep episodes (Figure 4.2.1), however during NREM sleep frequent high intensity Ca^{2+} spikes were also recorded, suggesting a more sporadic firing rate of LPO neurons during NREM compared with REM sleep, and confirming the activity of this area in regulating or responding to both behavioural states (Figure 4.2.2). For wake episodes, almost no change in the photometry signal was registered when drift and basal noise were subtracted.

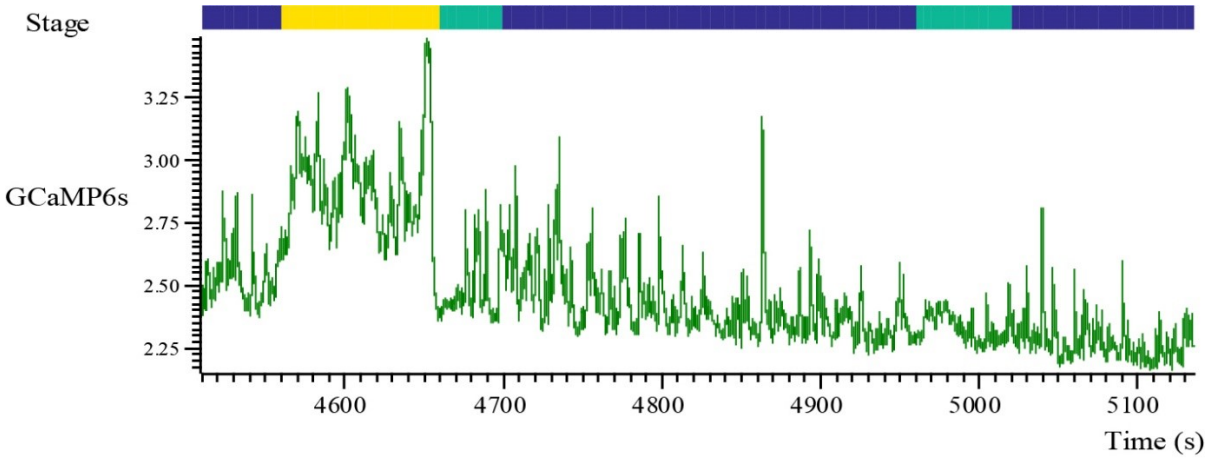

Figure 4.2.2 LPO hsyn-GCaMP6s mice: high calcium activity in LPO during NREM and REM sleep.
Zoomed in representation from Figure 4.2.1 showing high GCaMP6s signal spikes during NREM sleep and more sustained increases in calcium activity during REM sleep. No major changes in the signal were recorded during wake episodes.

To analyse the data, the photometry signal was normalized as ΔF/F:

$$\Delta F/F(t) = \frac{F(t) - mean(F)}{mean(F)}$$

Using ΔF/F data 30 seconds before and after Wake → NREM, NREM → Wake, NREM → REM and REM → Wake transitions, photometry signals from each animal were aligned and observed to determine when the highest calcium activity occurred.

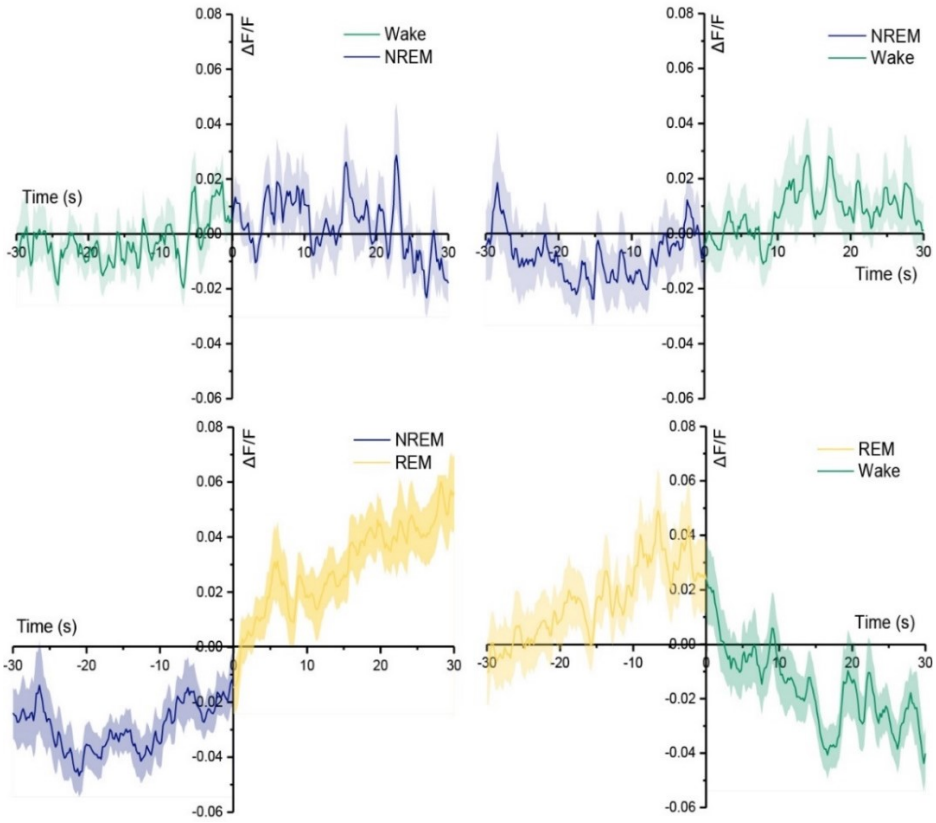

Figure 4.2.3 ΔF/F ratio across state transitions in LPO hsyn-GCaMP6s mice.
GCaMP6s signal 30s before and after each transition was normalized as ΔF/F. Each transition was considered only if the animals were for at least 30s in the selected vigilance state before and after transition. N= 3 mice; trials, W-N = 26; N-W = 23; N-R = 28; R-W = 27. Data are shown as mean of ΔF/F and error bars represents ± SEM.

These data confirmed that the highest activity recorded from LPO neurons corresponded to REM sleep episodes, in particular when transitioning from NREM sleep. The photometry signal of NREM sleep episodes following periods of wake also showed a slight increase over the average signal, indicating a possible increase in calcium activity in LPO when it initiates NREM sleep (Figure 4.2.3). Interestingly, photometry signal at the onset and at the end of REM sleep episodes seems to climb, indicating higher level of calcium signaling shynchronizations in those phases. These results were also confirmed when plotting the single ΔF/F traces for each transition instead that the mean, excluding possible averaging artefacts (data not shown).

To our surprise, LPO neurons were most active during REM rather than NREM sleep. To investigate further the role of this area in regulating or responding to sleep, calcium activity from genetically sepecified neuronal subtypes was recorded.

4.3 LPO Vgat, Vglut2, Galanin and Nos1-expressing neurons are mostly REM sleep-active with spikey NREM-sleep activity

I first looked at GABAergic neurons in the LPO area. These neurons take an active part in regulating sleep, in particular NREM [37]. They project to wake active areas to inhibit them and favour state transitions towards NREM sleep [267]. Using a *AAV-flex-hsyn-GCaMP6s* virus injected in LPO of Vgat-Cre mice and follwing fibre optic and EEG/EMG headstage implantation, calcium activity and somnographic traces were recorded.

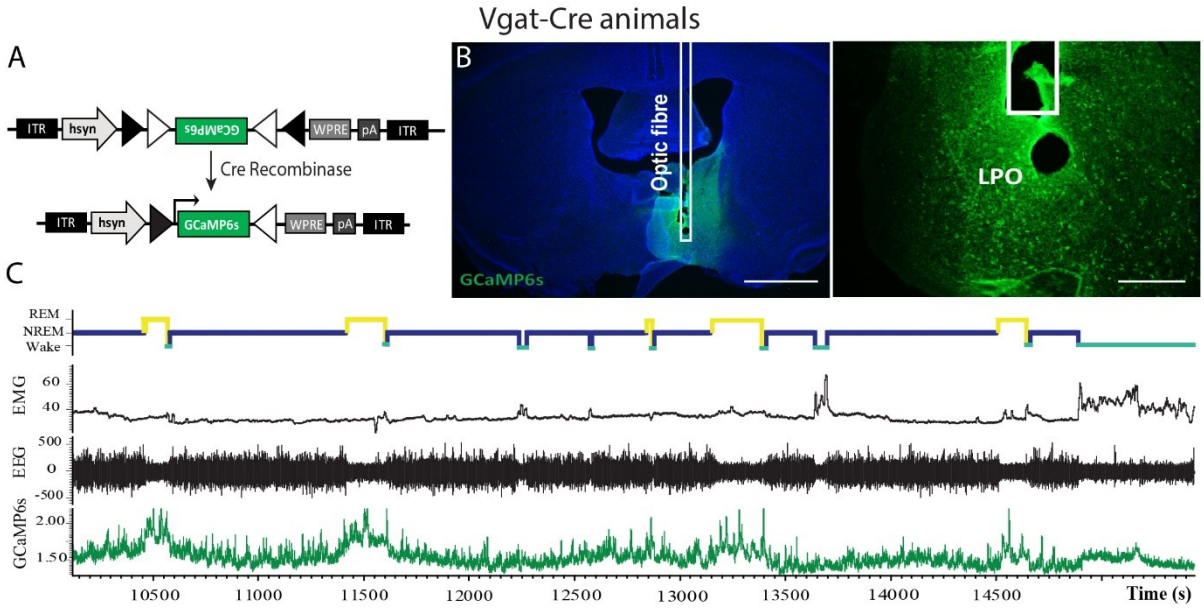

Figure 4.3.1 LPO Vgat-GCaMP6s mice: Vgat neurons show highest activity during REM sleep.
(A) Schematic representation of *AAV-flex-hsyn-GCaMP6s* virus. GCaMP6s gene can be expressed only in presence of the Cre recombinase. (B) IHC of GCaMP6s (green = GFP; blue = DAPI) and fibre optic track centred in LPO. Scale bars represent on the left 1 mm, on the right 200 µm. (C) Example of EEG/EMG recordings aligned to GCaMP6s traces to show that high photometry signal corresponds to REM episodes. From top to bottom: hyphogram, EMG, EEG and GCaMP6s.

For non-normalized signals, the highest calcium activity was recorded during REM sleep (Figure 4.3.1). During NREM sleep, the Ca^{2+} signal increased above baseline, while during wake no spikes or increased fluorescence was detected.

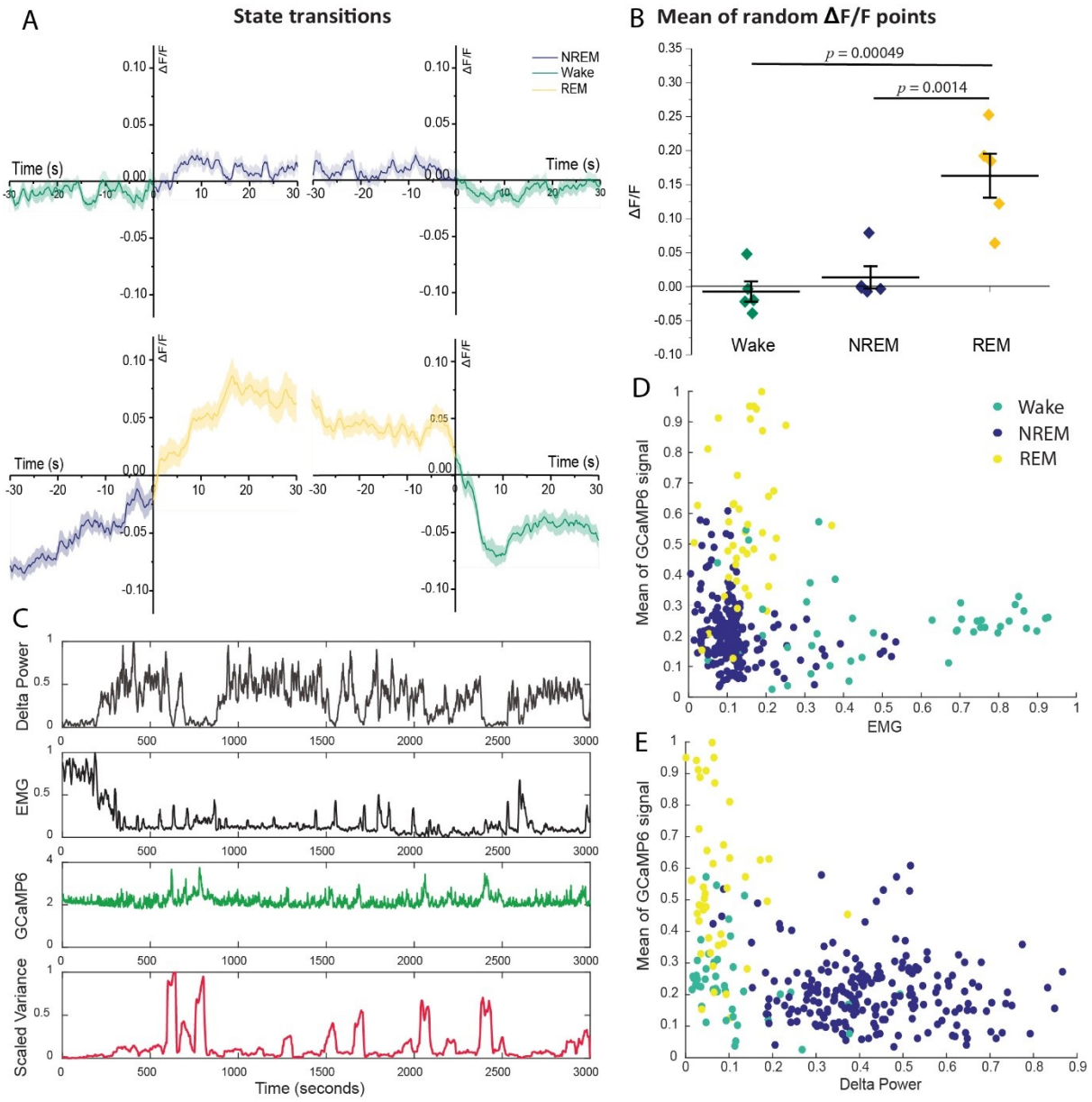

Figure 4.3.2 LPO Vgat-expressing neurons are most active during REM sleep.
(A) GCaMP6s signal 30s before and after state transitions; signal was normalized as ΔF/F (n= 5; trials, W-N = 49; N-W = 43; N-R = 51; R-W = 46). (B) Mean of 10 ΔF/F points randomly chosen for each state in order to represent photometry signal activity during longer episodes (One-way ANOVA and post-hoc Tukey Test). (C) Scaled EEG delta power, EMG, GCaMP6s signal and photometry signal variance. Variance was calculated with a rolling window of 50s. (D, E) Scaled mean of GCaMP6s signal plotted against scaled EMG (D) and scaled delta power (E) showing Ca^{2+} photometry signal is consistently higher during REM sleep (yellow). Rolling analysis window of 50s, points plotted every 10s. Data in A and B are shown as mean of ΔF/F and error bars represents ± SEM.

Using ΔF/F normalization 30s before and after each trasition and at the mean of random ΔF/F points for each state, highest values corresponded to REM episodes. NREM

episodes showed higher photometry signals compared to wakefulness, but the difference was not significant (Figure 4.3.2, A, B). Overall, looking at scaled variance and mean of GCaMP6s signal during 1 hour of recording, and plotting EMG and delta power against mean of GCaMP6s signal, Vgat-expressing LPO neurons were most active in REM sleep (Figure 4.3.2, C, D, E).

Similar GCaMP6s photometry experiments were then carried out in the LPO area of Gal-Cre and Nos-Cre animals. With both genotypes, the highest calcium activity was again registered during REM sleep (Figure 4.3.3 and Figure 4.3.5).

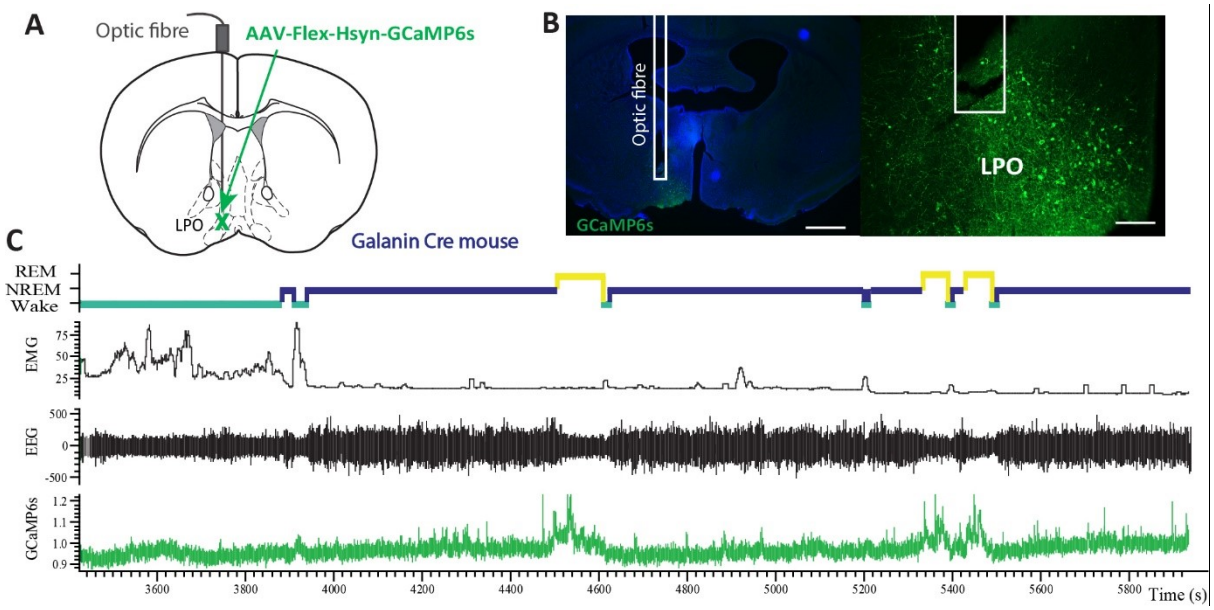

Figure 4.3.3 Flex-GCaMP6s injection and fibre implantation in Gal-Cre mice.
(A) Schematic representation of *AAV-flex-hsyn-GCaMP6s* virus injection in LPO. (B) IHC of GCaMP6s (green = GFP; blue = DAPI) and fibre optic track centred in LPO. Scale bars represent on the left 1 mm, on the right 200 µm. (C) Example of EEG/EMG recordings aligned to GCaMP6s traces to show high photometry signal from Gal-Cre neurons corresponds to REM episodes. From top to bottom: hyphogram, EMG, EEG and GCaMP6s.

For galanin-positive neurons, almost no activity was detected during wake and NREM sleep (Figure 4.3.3, C). For the ΔF/F signals around states transitions, although higher values still corresponded to REM sleep time, the photometry signal increased during wake when compared to NREM time (Figure 4.3.4, A). However, in the mean of random ΔF/F points, NREM sleep showed higher values compared to wake episodes (Figure 4.3.4, B), justified by the fact that during NREM sleep, some Gal-Cre neurons showed high amplitude and low frequency Ca^{2+} spikes (data not shown).

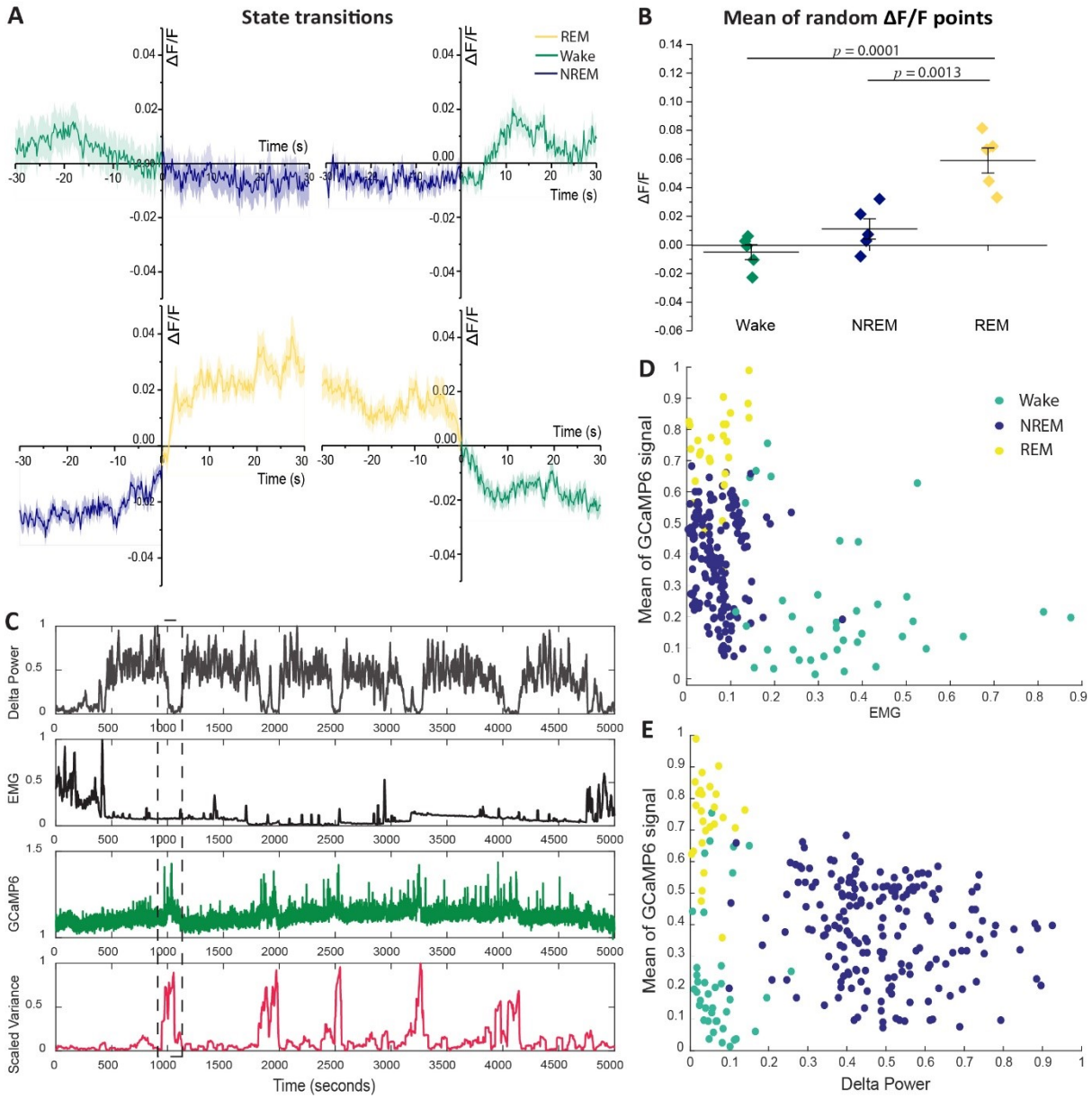

Figure 4.3.4 LPO-Gal-GCaMP6s mice showed most activity during REM sleep.
(A) GCaMP6s signal 30s before and after state transitions; signal was normalized as ΔF/F and increased with REM sleep episodes (n= 5, trials, W-N = 37; N-W = 33; N-R = 52; R-W = 51). (B) Mean of 10 ΔF/F points randomly chosen for each state. REM sleep points were significantly higher compared to NREM and wake (One-way ANOVA and post-hoc Tukey Test). (C) Scaled EEG delta power, EMG, GCaMP6s signal and photometry signal variance. Variance was calculated with a rolling window of 50s. (D, E) Scaled mean of GCaMP6s signal plotted against scaled EMG (D) and scaled delta power (E) showing Ca^{2+} photometry signal is consistently higher during REM sleep (yellow). Rolling analysis window of 50s, points plotted every 10s. Data in A and B are shown as mean of ΔF/F and error bars represents ± SEM.

Analysing the variance (Figure 4.3.4, C, dotted square) and then mean (Figure 4.3.4, D and E) of GCaMP6s signals in relation to EMG and delta power, REM sleep points

corresponded to high calcium activity values, while even though NREM and wake shared a similar range of mean GCaMP6s signal, NREM sleep points were mostly concentrated towards higher values compared to wake.

These activity data on LPO galanin neurons are unexpected, and do not support the data previously published demonstrating how LPO-gal neurons are necessary for NREM sleep maintenance and regulation [148, 254]. In fact, a recent publication from our laboratory has shown how galanin neurons, at the same brain coordinates I targeted, promote NREM sleep. However, this photometry data are more in line with other publications, which reported high cFos staining in LPO-gal neurons following REM sleep [89, 254] and high firing or LPO neurons during REM sleep in unit recordings data on rats [145].

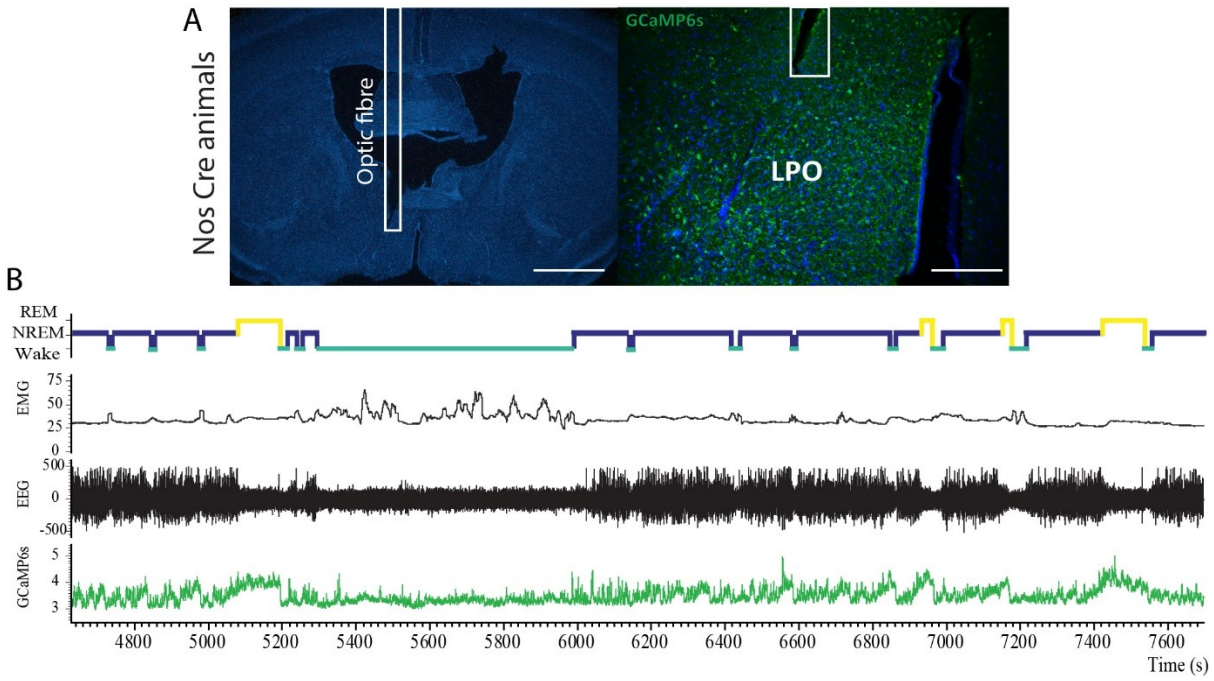

Figure 4.3.5 Generation of LPO-Nos1-GCaMP6s mice.
(A) IHC of GCaMP6s (green = GFP; blue = DAPI) and fibre optic track centred in LPO. Scale bars represent on the left 1 mm, on the right 200 µm. (B) Example of EEG/EMG recordings aligned to GCaMP6s traces to show high photometry signal from Nos-Cre neurons corresponds to REM episodes. From top to bottom: hyphogram, EMG, EEG and GCaMP6s.

I next looked at LPO-Nos1-GCaMP6s mice. Similar to the Vgat and galanin neurons, Nos1 neurons in LPO had their highest Ca^{2+} signal during REM sleep (Figure 4.3.5, B). With ΔF/F values analysis around state transitions, the REM sleep Ca^{2+} signal was markedly above baseline fluorescence activity, and the ΔF/F values corresponding to wake were higher than during NREM sleep (Figure 4.3.6, A).

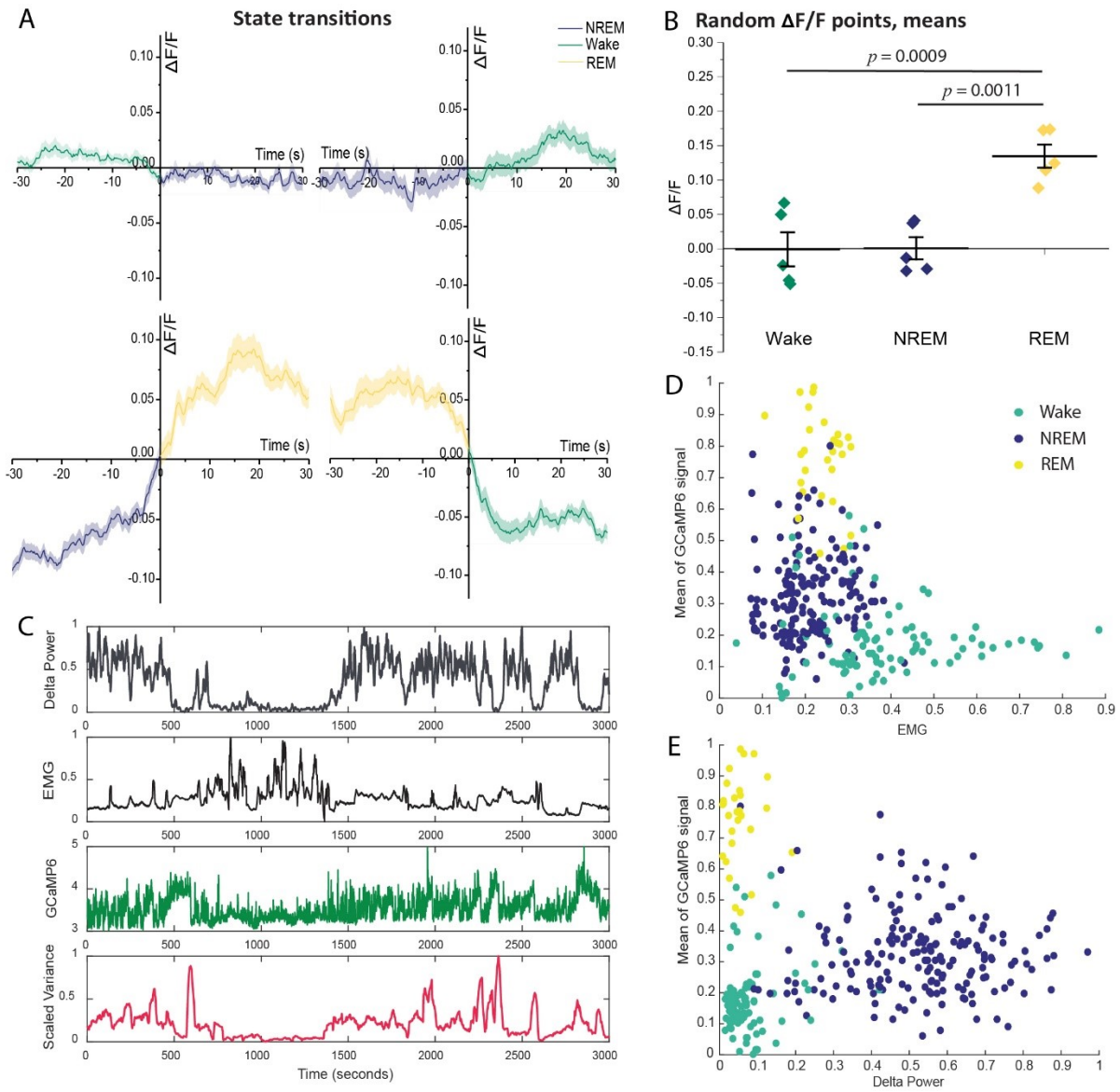

Figure 4.3.6 LPO-Nos1 neurons are most active during REM sleep.
(A) GCaMP6s signal 30s before and after state transitions; signal was normalized as ΔF/F and increased with REM sleep episodes (n= 5, trials, W-N = 46; N-W = 41; N-R = 46; R-W = 48). (B) Mean of 10 ΔF/F points randomly chosen for each state (One-way ANOVA and post-hoc Tukey Test). (C) Scaled EEG delta power, EMG, GCaMP6s signal and photometry signal variance, calculated with a rolling window of 50s. (D, E) Scaled mean of GCaMP6s signal plotted against scaled EMG (D) and scaled delta power (E) showing Ca^{2+} photometry signal is higher during REM sleep (yellow). Rolling analysis window of 50s, points plotted every 10s. Data in A and B are shown as mean of ΔF/F and error bars represents ± SEM.

With the mean of random ΔF/F points, there was a significant difference between wake and REM and NREM and REM sleep points, with no differences between wake and NREM sleep. This result, however, was not confirmed by the variance (Figure 4.3.6, C) or the

mean of GCaMP6s signal plotted against EMG and delta power values (Figure 4.3.6, D and E). During wake episodes the GCaMP6s variance was almost 0, while during NREM sleep was higher. These data suggest that during wake Nos1 expressing neurons are more active only if preceding or following NREM sleep.

Following Vgat and Nos1 neuronal recordings, I looked at Vglut2+ neurons in LPO. I checked the expression of *AAV-flex-hsyn-GCaMP6s* virus in LPO (Figure 4.3.7, A), and then observed that these neurons appeared to be active during REM sleep, with no differences in the signal between wake and NREM sleep (Figure 4.3.7, B).

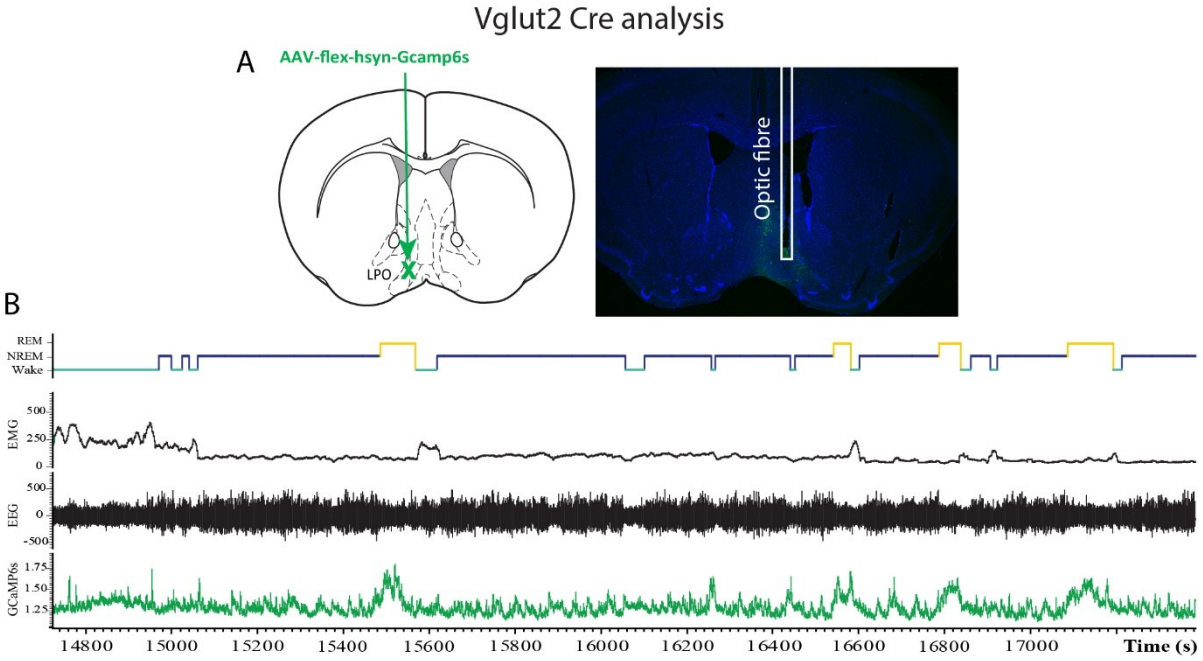

Figure 4.3.7 Generation and recording from LPO-Vglut2-GCaMP6s mice.
(A) Left, schematic representation of *AAV-flex-hsyn-GCaMP6s* virus injection in the LPO area of Vglut2-Cre animals. Right, IHC of GCaMP6s (green = GFP; blue = DAPI). Scale bars represent 1 mm. (B) Example of EEG/EMG recordings aligned to GCaMP6s traces to show high photometry signal from Vglut2 neurons corresponding to REM sleep episodes. From top to bottom: hyphogram, EMG, EEG and GCaMP6s.

The ΔF/F ratio over state transitions for Vglut2 expressing neurons and the mean of random ΔF/F points for each state confirmed how REM sleep correlated to higher GCaMP6s activity, significantly different to NREM and wake (Figure 4.3.8, A and B). During wakefulness, calcium activity seemed to be higher compared to NREM sleep episodes, but not significantly different. Variance (Figure 4.3.8, C) and mean (Figure 4.3.8,

D and E) of GCaMP6s signal demonstrated that low EMG and delta power points corresponded to higher calcium activity and to REM sleep.

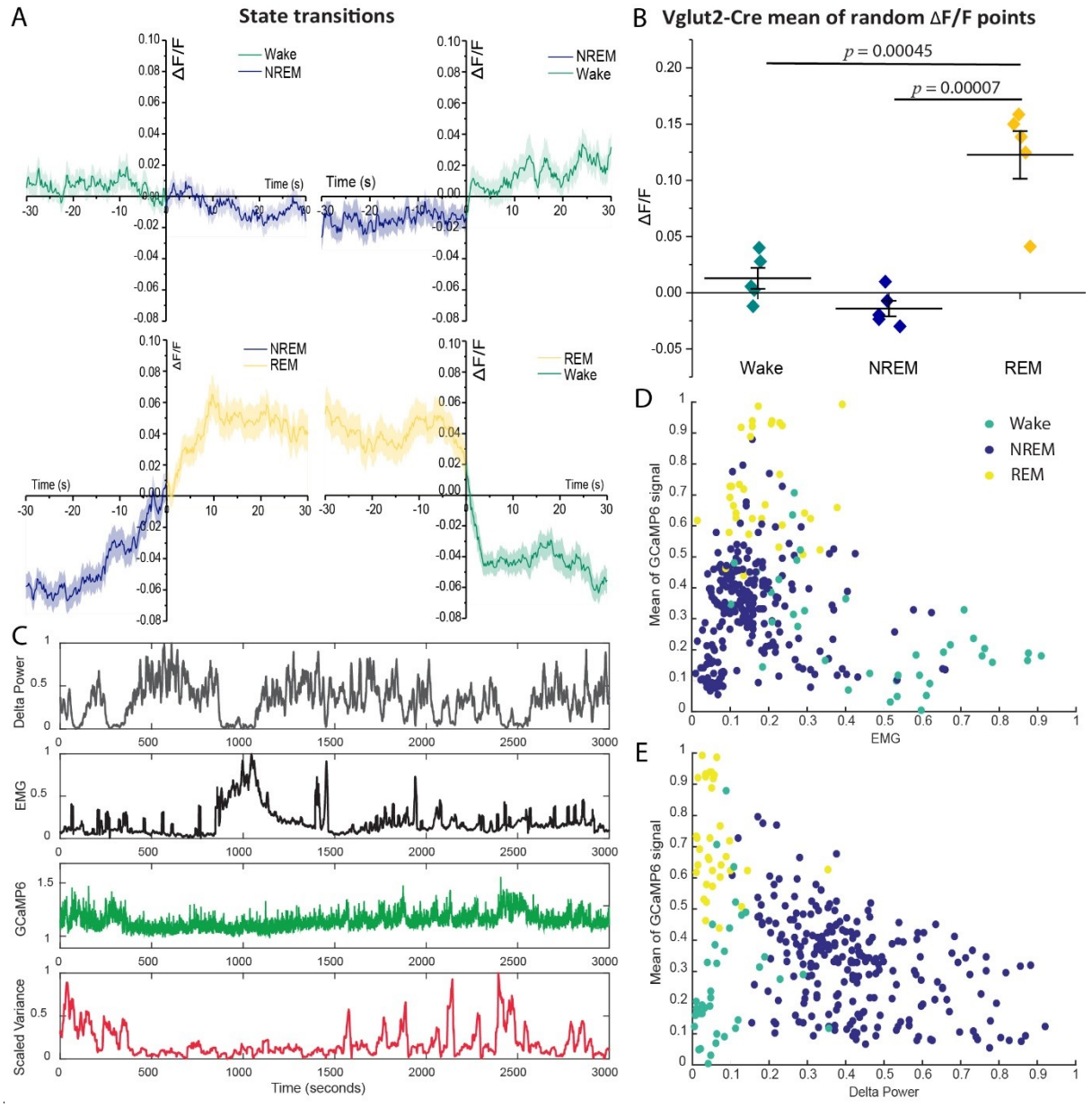

Figure 4.3.8 LPO-Vglut2 neurons are most active during REM sleep.
(A) GCaMP6s signal 30s before and after state transitions; signal was normalized as ΔF/F and increased with REM sleep episodes (n= 5, trials, W-N = 39; N-W = 33; N-R = 49; R-W = 50). (B) Mean of 10 random ΔF/F points for each state. REM sleep points were significantly higher compared to NREM and wake (One-way ANOVA and post-hoc Tukey Test). (C) Scaled EEG delta power, EMG, GCaMP6s signal and photometry signal variance, calculated with a rolling window of 50s. (D, E) Scaled mean of GCaMP6s signal plotted against scaled EMG (G) and scaled delta power (H). Rolling analysis window of 50s, points plotted every 10s. Data in A and B are mean of ΔF/F and error bars represents ± SEM.

No difference in the range of variance and mean of GCaMP6s signal was present between NREM and wake values, however the majority of data points corresponding to NREM sleep appeared to be associated to low clacium activity, in particular in relation to EMG values (Figure 4.3.8, D), while for wake points there was a more even distribution between low and high mean GCaMP6s values. This could explain why ΔF/F values around transitions and mean of random points looked slightly increased during wake.

In summary, Vgat, Vglut2, galanin and Nos1-expressing LPO neurons are mostly REM sleep rather than NREM sleep active, although these neurons did have sporadic NREM activity. These results are surprising, since our lab and others have found that activation of LPO galanin neurons induces NREM sleep [148, 254], and lesioning galanin neurons causes fragmented sleep-wake patterns without affecting REM sleep [148]. However, galanin neurons in LPO could perhaps still regulate REM sleep. Damaging LPO neurons reduces REM sleep, but not NREM sleep [71], and LPO galanin neurons are cFos posistive following periods of predominantly REM sleep [77], although no behavioral state specificity could be guaranteed in this last publication. Importantly, some of these results might be coming from GABAergic neurons, has they can co-express galanin mRNA in the LPO area [73]. In fact, it is possible that I have recorded cells co-expressing a combination of Vgat, Vglut2, Nos1 and galanin [248], explaining the similar activation pattern during REM sleep, with slight differences in the Ca^{2+} activity between NREM and wake episodes. Dual transmitter neurons (GABA/Glutamate) are not, in fact, uncommon in the PO area [248] (**Error! Reference source not found.**). Perhaps using intersectional genetics, new a nd more specific neuronal markers could be used to further dissect the function and activity of inhibtory and excitatory neurons in LPO.

4.4 Dexmedetomidine activates Vgat, Nos1 and Vglut2 neurons in LPO

Earlier in this Chapter, I showed that LPO neurons are, surprisngly, selectively REM sleep-active, and only have sporadic NREM activity. Previous publications from our lab demonstrated that cFos-dependent activity tagged neurons in LPO were required for Dex-induced sedation and NREM like state to occur [72], and that lesioning of LPO galanin neurons with caspese abolishes Dex's ability to induce high power delta oscillations and hypothermia [148]. LPO neurons are therefore fundamental to exert the sedative action of dexmedetomidine (Dex). Dex is a selective agonist at α2 adrenergic receptors and induces a NREM sleep-like state in humans [268] and rodents [269]. Dex can excite neurons directly by adra2a receptors coupled to Gi and HCN channel inhibition [270], and it does not induce REM sleep, contradicting the REM-active nature of LPO cells. I therefore investigated the activation pattern of LPO neurons when mice were given sedative doses of Dex. I injected *i.p.* 50 μg/kg of Dex and recorded the photometry signal, EEG and EMG for 6 hours in the LPO of Vgat-Cre, Nos1-Cre and Vglut2-Cre animals.

30min after Dex injection, LPO Vgat-expressing neurons had low frequency and high amplitude single-pointed Ca^{2+} activity spikes. Each spike seemed to represent a single and distinct activation, resembling an action potential (Figure 4.4.1, A, bottom row). Plots of the ΔF/F ratio from 100s recordings of all 3 mice tested showed a similar pattern, with an average of 1 spike every 10 seconds, *i.e.* 0.1 Hz (Figure 4.4.1, B, left panel).

I then looked at the activity of these neurons after approximately 2h from injection time. In this case, I observed a more heterogeneous neuronal activation between animals. One showed almost no activity, with no changes in the baseline levels of Ca^{2+} until Dex's sedative effect faded off (Figure 4.4.1, C). In the ΔF/F ratio of 100s of recordings, neurons from two animals showed 2-5 spikes, and a similar frequency of activation throughout the sedative action of Dex, while one animal did no longer show Ca^{2+} signal (Figure 4.4.1, D, left graph). In this case, the mean of the three recordings was not explicative of the diversity in GABAergic activity under Dex induced sedation (Figure 4.4.1, D, right panel).

This analysis was also performed for Nos1-Cre neurons. 30 minutes immediately following Dex injection, LPO Nos1 neurons had a similar activation pattern as Vgat neurons. In 100s ΔF/F ratio, all 3 mice showed high amplitude calcium activity spikes, with an average frequency of 1 spike/10s, *i.e.* 0.1 Hz (Figure 4.4.2, A and B, left).

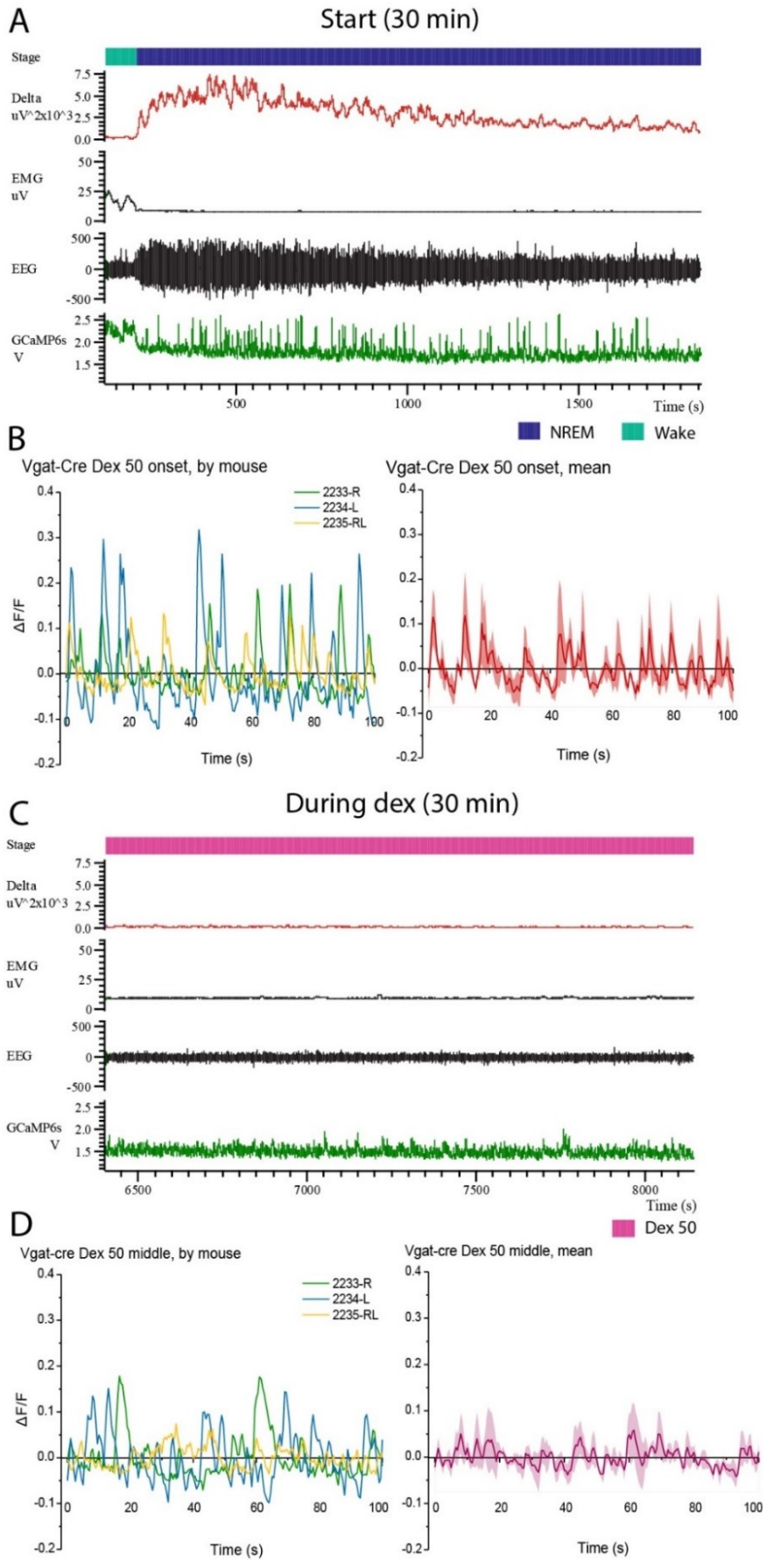

Figure 4.4.1 LPO Vgat neurons are most active immediately after Dex injection. (A, C) 30 minutes example of somnographic and photometry recordings immediately following (A) or 2 hours after (C) i.p. injection of Dex 50 µg/kg. From the top: stage, delta power, EMG, EEG and GCaMP6s signal. (B) Left, 100s ΔF/F ratio immediately after Dex injection. Lines represent individual animals (n = 3). Right, mean of ΔF/F ratio between all animals tested. (D) Left, 100s ΔF/F ratio 2h after Dex injection. Right, mean of 30min signals to show how overall Vgat neurons activity under Dex sedation is greatly reduced. Where shown, error bars represent ± SEM.

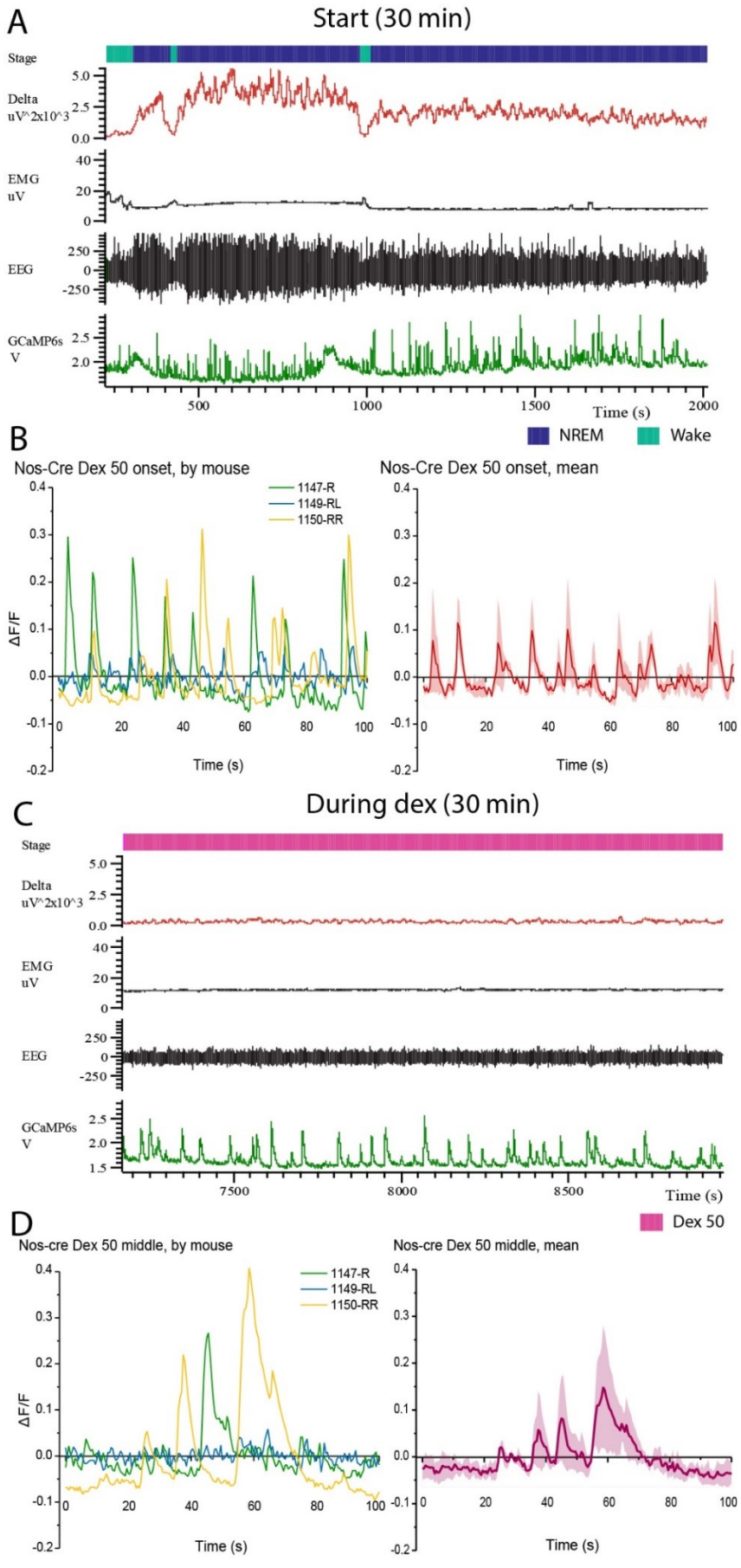

Figure 4.4.2 LPO Nos1 neurons are most active immediately after Dex injection.
(A, C) 3min example of somnographic and photometry recordings immediately following (A) or 2h after (C) i.p. injection of Dex 50 µg/kg. From the top: stage, delta power, EMG, EEG and GCaMP6s signal. (B) Left, 100s ΔF/F ratio after Dex injection. Lines represent each individual animal (n = 3). Right, mean of ΔF/F ratio between all animals tested. (D) Left, 100s ΔF/F ratio 2h after Dex injection. Mice showed a heterogeneous pattern of activation. Right, mean of 100s ΔF/F signals. Where shown, error bars represent ± SEM.

The mean of the 3 trials clearly showed the activation pattern of Nos1+ neurons, confirming the 0.1 Hz activity spikes (Figure 4.4.2, B, right panel). Looking at the calcium activity of this neuronal group 2 hours after Dex injection, there was a diverse range of activation, from slow frequency spikes, between 1 and 3 spikes every 100 s, to no signal at all in one animal (Figure 4.4.2, C and D). In summary, both Vgat- and Nos1-expressing neurons are active during the initial stages of Dex induced-sedation, but these cells slow down or almost completely reduce their calcium activity during deeper stages of Dex-induced sedation.

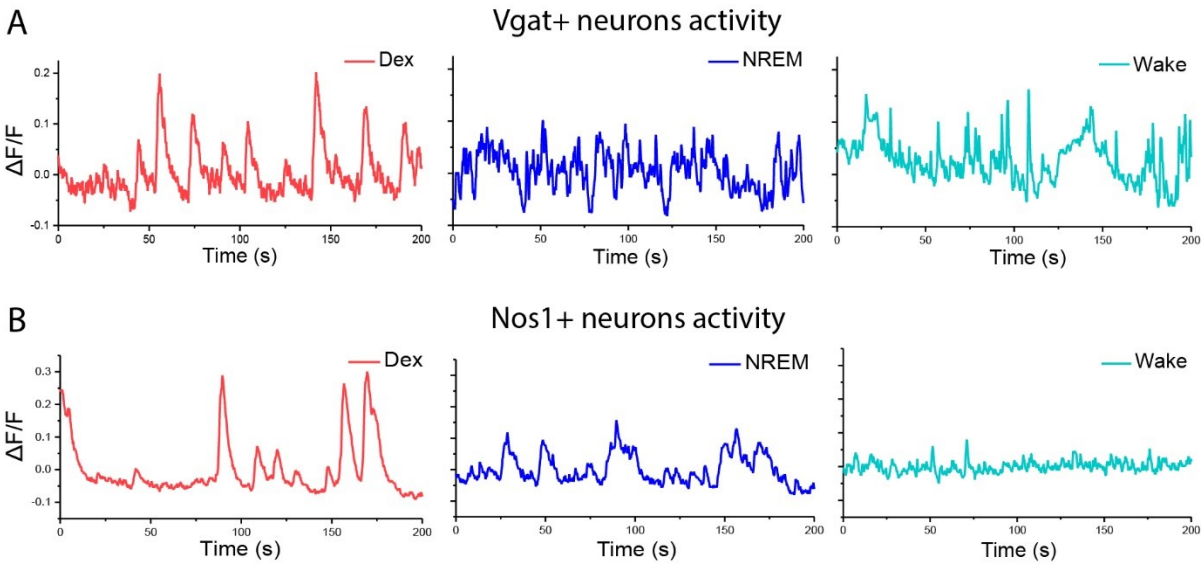

Figure 4.4.3 Vgat+ and Nos1+ neurons show different calcium activity patterns under sedation compared to BL NREM and wake.
A and B, examples of 200s ΔF/F from GCaMP6s signals sampled at 5Hz in Vgat+ (A) and Nos1+ (B) neurons during Dex sedation (left), baseline NREM sleep (centre) and baseline wakefulness (right). For both neuronal types, calcium activity spikes under sedation are much higher compared to the activity observed during wake and NREM sleep recordings. Baseline signal is also less noisy under sedation compared to the other behavioural states, confirming that sedation reduces the general activity of LPO neurons maintaining only essential ones active to control the sedative state.

To better understand how Dex-induced sedation would alter baseline calcium activity of LPO neurons, I compared 200s of GCaMP6s recordings obtained during sedation to baseline sleep and wake activity in Vgat-Cre and Nos-Cre animals (Figure 4.4.3). When looking at the ΔF/F signal during Dex-induced sedation (Figure 4.4.3, A and B, left panels), both Vgat+ and Nos1+ neurons showed an overall reduction of baseline calcium

fluctuations compared to the signals corresponding to NREM and wakefulness, suggesting that Dex might inhibit the overall activity of LPO neurons, maintaining a constant, almost rhythmic spikey calcium activation only in few neurons. These neurons might therefore be sufficient to drive the sedative state from LPO. Focusing on Vgat+ neurons, the baseline levels of the GCaMP6s trace during Dex sedation appeared much less variable compared to NREM and wake traces (Figure 4.4.3, A, left compared to central and right panel). On the other hand, when looking at Nos1+ neurons, the highest peaks of calcium activity are reached during sedation, suggesting a specific role of these cells in inducing this state through LPO circuits (Figure 4.4.3, B, left compared to central and right panels).

Interestingly, it is evident how Vgat expressing neurons have an overall higher baseline calcium activity than Nos1+, suggesting that either more cells were recorded in Vgat-Cre animals, increasing the baseline noise when compared to Nos-Cre mice, or that Vgat+ cells are generally more active and show more minor intracellular calcium fluctuations than Nos1+. A similar pattern was observed amongst all Vgat-Cre and Nos-Cre animals (data not shown), suggesting that this difference was not unique to the examples shown in Figure 4.4.3. An estimation of the number of cells recorded in Vgat-Cre and Nos-Cre animals could help better understand the differences in neuronal activity between neuronal types.

I then tested the effects on neuronal calcium activity of Dex-induced sedation in Vglut2-Cre animals. For the 30 minutes immediately after Dex injection, Vglut2-positive neurons showed heterogeneous activities, in contrast to Vgat- and Nos1-expressing ones. Out of the three mice tested, two showed no signs of significant calcium activity under sedation (Figure 4.4.4, A), whereas one showed a pronounced activation pattern, with again high amplitude and 0.1 Hz spikes (Figure 4.4.4, B). Zooming into the 100 s of ΔF/F ratio, the diversity between Vglut2 neurons activity was evident, and was better explained representing the individual ΔF/F ratios rather than their mean (Figure 4.4.4, C).

For the 30 min photometry signal 90 min after injection, neurons which did not show activity at the onset of Dex sedation showed no signs of major calcium activity (Figure 4.4.5, A), whereas the animal with active Vglut2 neurons in the first 30 min after Dex injection showed calcium activity even though the spike frequency was reduced (Figure 4.4.5, B). Looking at the ΔF/F ratio of the same recoridngs, the animal with calcium

activity 90 min after Dex injection showed a frequncy of 3 spikes /100s throughout the whole sedation period, whereas no activity was recorded for the other 2 subjects until sedation faded (Figure 4.4.5, C).

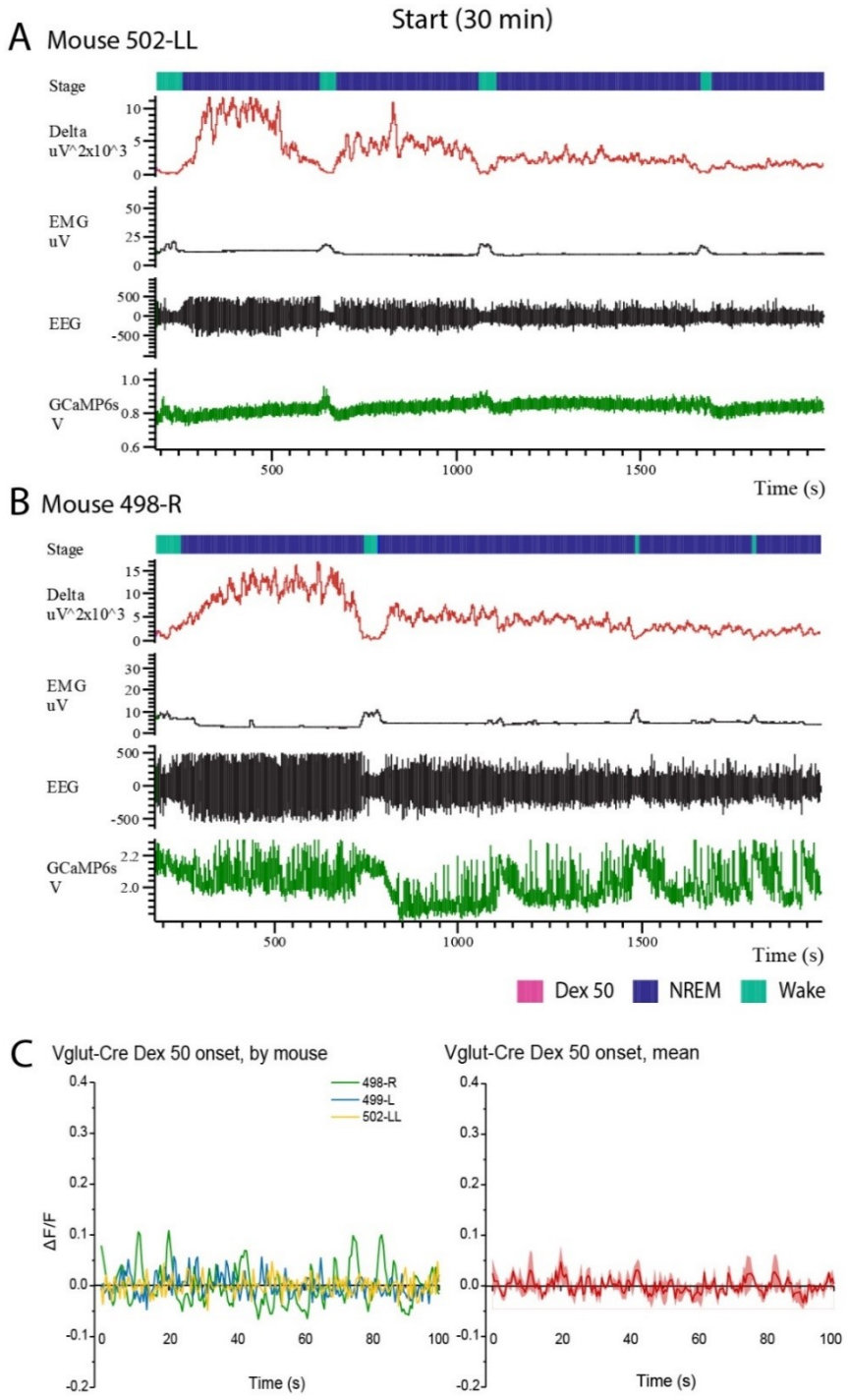

Figure 4.4.4 LPO Vglut2 neurons show heterogeneous activity immediately after Dex injection. (A, B) Example of two different 30 minutes recordings from animals which showed an either flat (A) or very high calcium signal (B) after i.p. injection of Dex 50 µg/kg. From the top: stage, delta power, EMG, EEG and GCaMP6s signal. (C) Left, 100 s ΔF/F ratio immediately after Dex injection. Lines represent each individual animal (n = 3) showing different calcium activity patterns. Right, mean of ΔF/F ratio between all animals tested. The mean was not representative of group variability. Where shown, error bars represent ± SEM.

Note: all animals tested under Dex sedation were first recorded for activity patterns during sleep and wake, and all showed consistent photometry activity during all

recordings. Before Dex injections, mice were tested for at least 1 hour for habituation and to verify that their photometry signal was not bleached from previous tests. In all experimental groups, recovery of the normal sleep-wake photometry signal after Dex sedation was recorded to ensure that negative values observed during the sedation time were not caused by bleaching or artefacts but represented a true reduction in the calcium activity of the neuronal population.

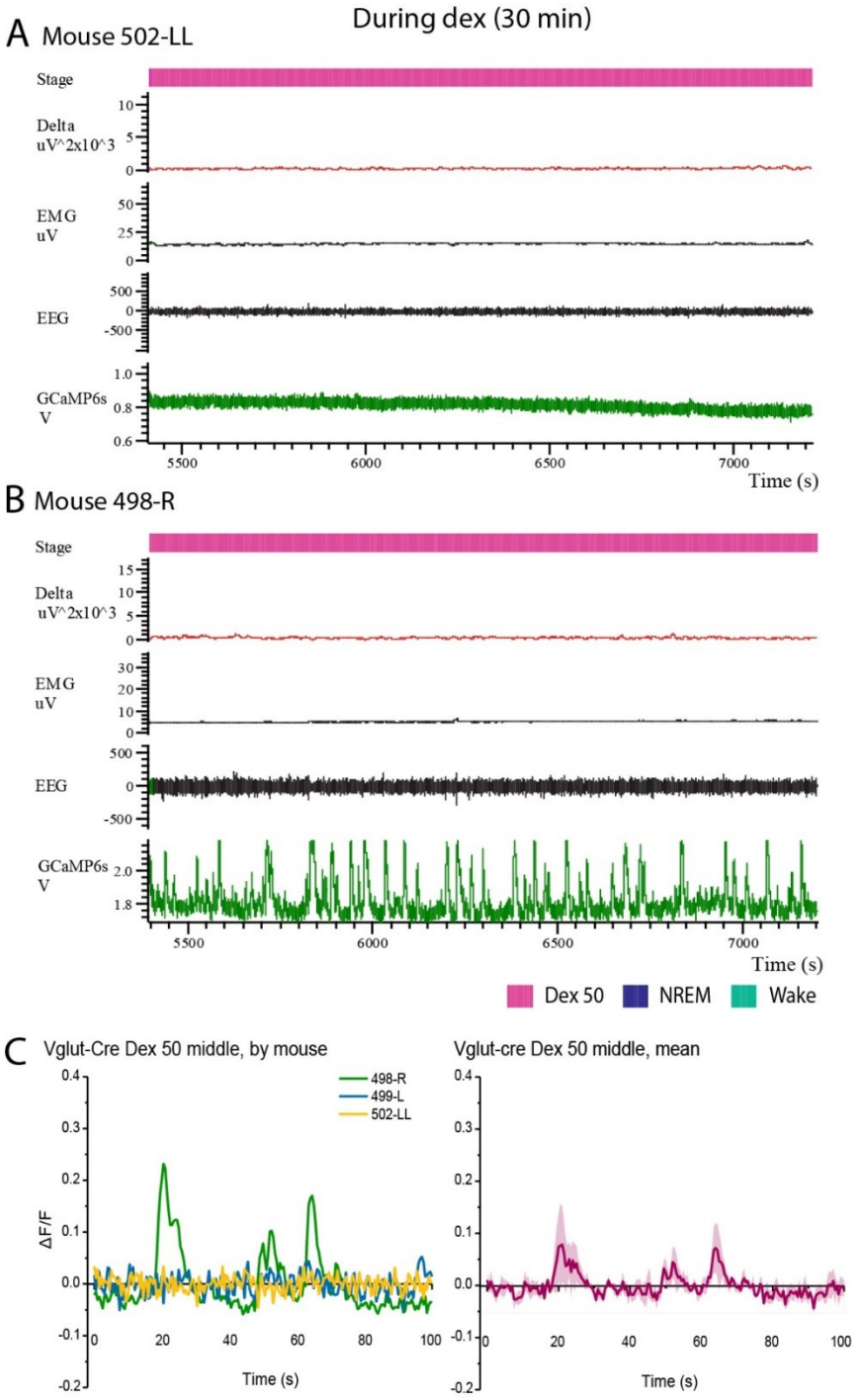

Figure 4.4.5 Only one animal showed activity in LPO Vglut2 neurons 90 minutes after Dex injection.
(A, B) Example of two different 30 minutes recordings from animals which showed an either flat (A) or very high calcium signal (B) under Dex sedation. From the top: stage, delta power, EMG, EEG and GCaMP6s signal. (C) Left, 100 s ΔF/F ratio immediately after Dex injection. Lines represent each individual animal (n = 3) showing different calcium activity patterns between subject. Right, mean of ΔF/F ratio between all animals tested. Where shown, error bars represent ± SEM.

Alltogether, these data confirm the active participation in Dex-induced sedation of Vgat, Nos1 and Vglut2 neurons in the LPO area. It could be that the active Vglut2 neurons recorded during Dex-induced sedation was a dual transmitter (Vgat/Vglut2) cell type [248], hence it resembled the activity of the Nos1 and Vgat neuronal recordings. Bigger *N* numbers for all groups could better elucidate how each neuronal subtype responds to Dex.

4.5 Appendix: MPO-Vglut2 neurons are wake-active

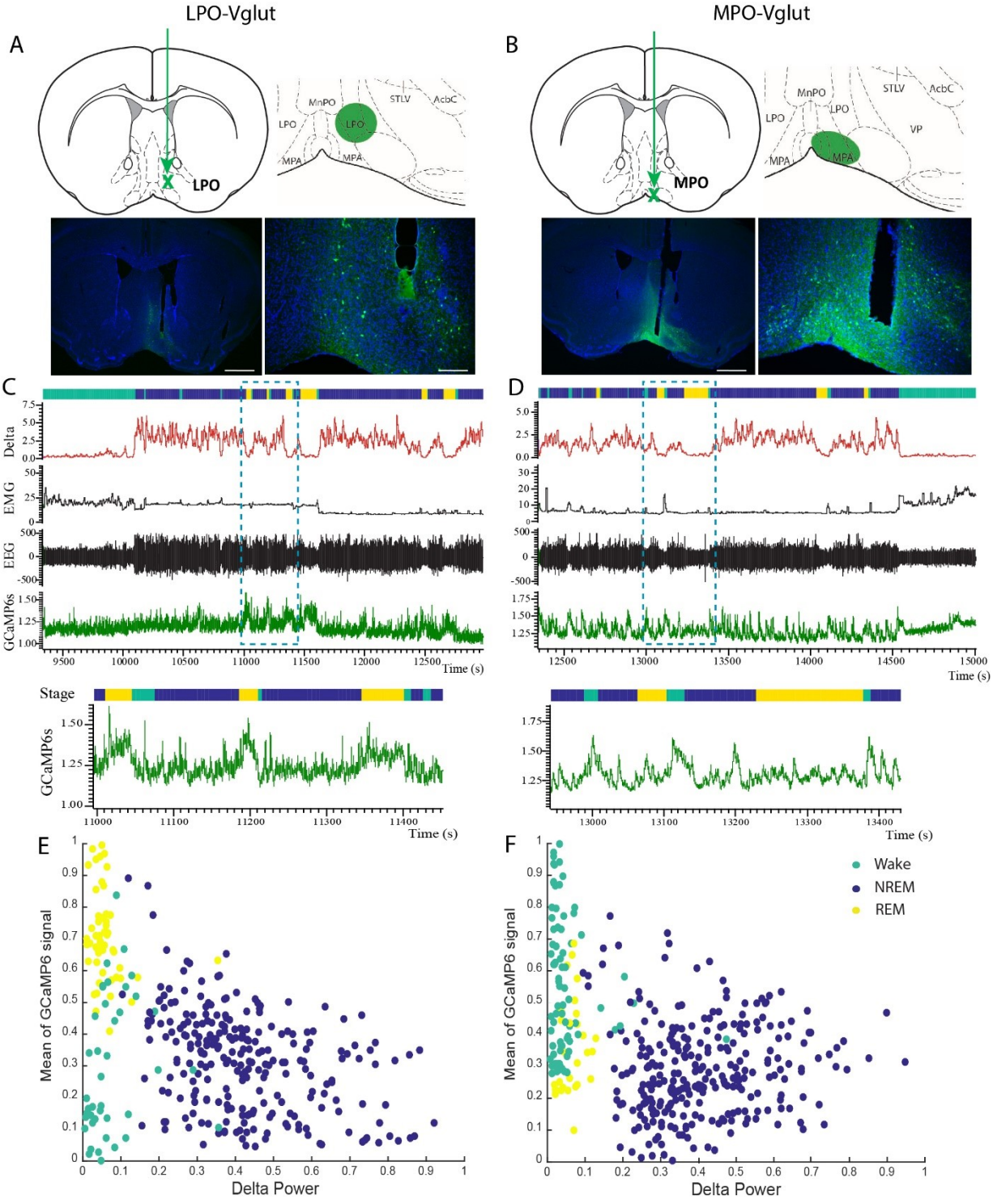

Figure 4.5.1 Ca^{2+} activity of Vglut2 neurons changes in different subareas of the PO. Calcium levels in the two neuronal populations are inverted between REM sleep and wake, whole photometry signal during NREM sleep was small for both groups.
(A, B) Top, representation of viral injection in LPO (A) or MPO (B). Bottom, IHC of GCaMP6s (green = GFP; blue = DAPI) and fibre optic track centred in the two different areas. Scale bars represent on the left 1 mm, on the right 200 µm. (C, D) From the top,

stage, delta power, EMG, EEG and photometry signal aligned. The dotted squares indicate areas zoomed in and represented at the bottom (stage and photometry signal only). (E, F) EEG delta power plotted against scaled mean of GCaMP6s signal to show different distribution of points between REM active (E) and wake active (F) neurons. Variance was calculated with a rolling window of 50s and plotted every 10s.

I investiagted the vigliance dependent activity of Vglut2-Cre neurons in the anterior medial preoptic (MPO), the area in the hypothalamus which neighbours LPO, but closer to the midiline (Figure 4.5.1, A and B). This MPO area and the central MnPO part contains Nos1/Vglut2 neurons which inititiate body cooling and sleep induction [81, 271], as well as regulating parenting [260] and hunting behavior [272].

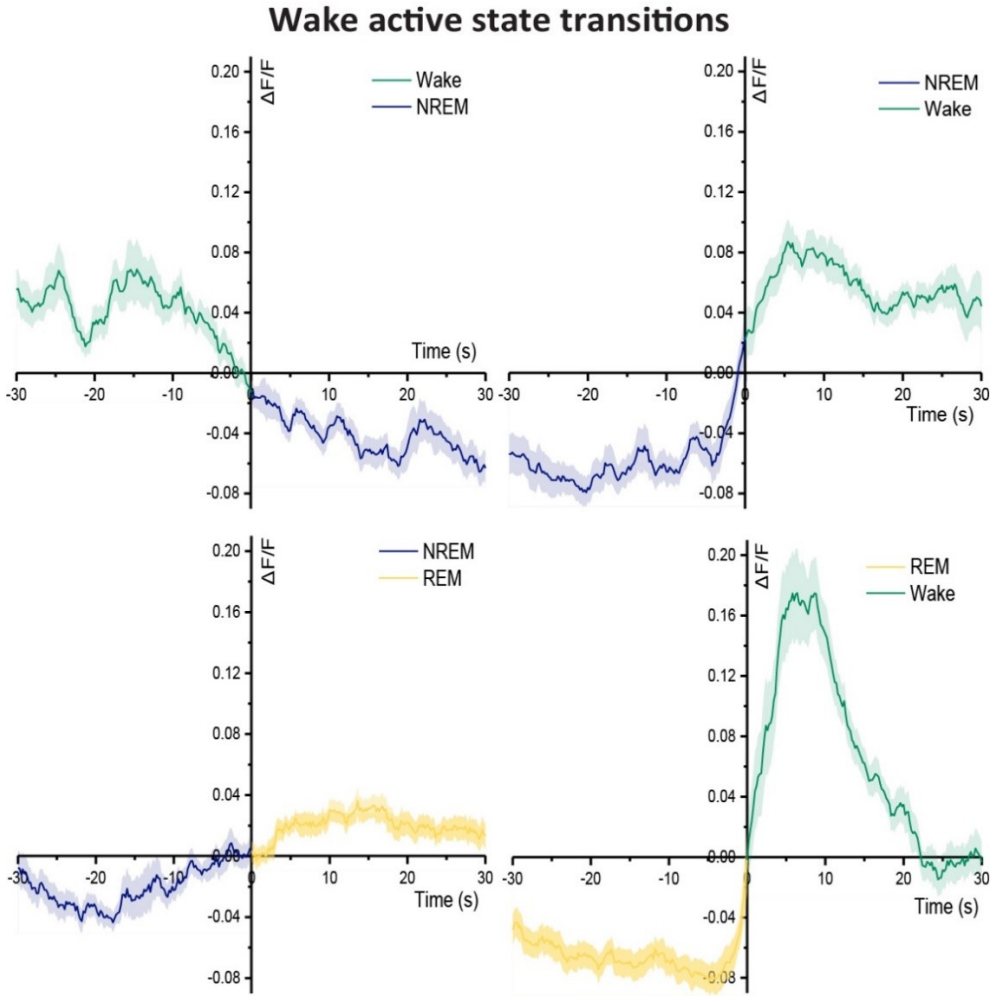

Figure 4.5.2 MPO-Vglut2 neurons are wake active: ΔF/F ratio across transitions. GCaMP6s signal 30s before and after each transition was normalized as ΔF/F and aligned in order to have the beginning of the transition at time 0. Signal increased during wakefulness, in particular following REM sleep episodes (n= 3; trials, W-N = 34; N-W = 32; N-R = 36; R-W = 40). Data are shown as mean of ΔF/F and error bars represent ± SEM.

MPO-Vglut2 neurons calcium signaling had a different activity pattern compared to Vglut2 neurons in LPO, as they showed higher activity during wake rather than REM sleep (Figure 4.5.1**Error! Reference source not found.**, C and D), with higher peaks of calcium a ctivity recorded at the beginning of a wake epoch, following both NREM and REM sleep. These spikes in the calcium activity at the beginning of a wake epoch were more visibile by zooming into the photometry fluorescence signal (Figure 4.5.1, C and D bottom panels). Wake episodes showed higher photometry signals both following and preceding NREM sleep, but the highest and most consistent peaks were recorded when mice woke up from REM sleep, as confirmed when looking at the ΔF/F ratio across transitions(Figure 4.5.2).

Plotting EEG delta power against the mean of GCaMP6s signal for LPO-Vglut2 and MPO-Vglut2 neurons, it was clear that the latter were active mosty during wake, with rather low levels of calcium activity during REM sleep (Figure 4.5.1, E and F). Calcium levels in the two neuronal populations seemed to be inverted between REM and wake states, whereas the photometry signal during NREM sleep was small for both groups.

4.6 Discussion

In this Chapter, I showed how LPO neurons are mostly active during REM sleep, with high steady calcium increases; these neurons have more variable patterns of activation during REM and are mostly inactive during wake. Given the huge amount of data supporting the role of LPO neurons in inducing NREM sleep [71], it was unexpected to see how all LPO neuronal types (galaninergic, GABAergic, glutamatergic and Nos1-expressing neurons) were invariably REM-active, rather than NREM sleep active. However, equally surprising given their REM specificity, I also found that all these neurons fired at a distinctive 0.1. Hz pattern during dexmedetomidine-induced sedation, even though this drug produces a NREM-like sleep [148].

4.6.1 Highest activity of LPO neurons is during REM sleep

All LPO neurons assayed with Hsyn-GCaMP6s showed high calcium activity during REM sleep, a marked spikey pattern of calcium signalling during NREM sleep, and variable patterns, from almost no activity to relatively high, during wakefulness (Figure 4.2.2). GCaMP6s signals recorded from Vgat, galanin, Vglut2 and Nos1-expressing neurons using a flex-GCaMP6s virus showed similar patters to the pan signal (Figure 4.3.2 and Figure 4.3.6), whereas galaninergic neurons had almost no signal during NREM sleep and wake (Figure 4.3.3 and Figure 4.3.4). This last result might be caused by the low number of galaninergic neurons in the area recorded, and by their possibly higher distance from the photometry probe (galaninergic neurons generally constitute a small percentage of LPO, making the photometry recordings of this neuronal type particularly hard to achieve). Nevertheless, we and others found that chemogenetic activation of LPO galanin neurons induces NREM sleep and hypothermia, but no changes in REM sleep [148, 254]. Additionally, lesions to LPO-gal neurons cause a strong increase in NREM sleep-wake fragmentation and hypothermia [148], with a reduced ability of Dex to induce sedation and hypothermia. These data suggest that galanin neurons could fire actively during NREM sleep, and my *in vivo* calcium recordings were possibly not sensitive enough to record only few cells and their smaller calcium activity changes.

LPO-Vglut2 neurons showed a similar pattern to Vgat and Nos1 expressing neurons when looking at photometry traces aligned (Figure 4.3.7), however random ΔF/F point showed how Vglut2 neurons might be more active during wakefulness than NREM sleep

(Figure 4.3.8). Overall, it is difficult to judge how many neuronal types I have studied in LPO with these calcium recordings. There are multiple intermingled cell types in the PO area that co-express these markers, and some neurons express both Vglut2 and Vgat [248].

The high neuronal activity recorded predominantly during REM sleep across all neuronal types in LPO might be indicating a new pathway responsible for REM sleep regulation, or alternatively, a passive response of LPO to REM sleep-promoting circuitry.

REM sleep circuits have been well studied in the pons and midbrain to dissect neuronal connections controlling REM atonia, but less is known regarding ascending pathways regulating the characteristic cortical theta activity. A subset of galaninergic dorsomedial hypothalamic neurons have been reported to be REM active, and to receive inhibitory signals from POA-galaninergic neurons [89]. However, different subsets of LPO neurons, with different transcription profiles, might be directly involved in this REM regulatory pathway, and possibly connect to ascending signals which stimulate theta waves through the hippocampus and REM-active septal neurons [273].

4.6.2 Conclusion and future experiments

The data here presented showed LPO activity is higher during REM sleep, and that LPO neurons are active especially during the onset of Dex-induced sedation.

More refined analysis can be carried out on the data here represented. First, the scaled variance shown in multiple figures (see for example Figure 4.3.2, Figure 4.3.4, Figure 4.3.6 and Figure 4.3.8, panel C, bottom row) is not fully descriptive of the actual activity of LPO neurons, as it simplifies neuronal dynamics and reduces their resolution. In this thesis, it has been used to highlight and better visualize major and more consistent changes in calcium activity, in particular around transitions towards REM sleep, when baseline activity around these transitions was particularly low. However, in cases as shown in Figure 4.4.4, bottom line of panel B, the scaled variance would not be applicable: higher variance would correspond to segments of the trace where spiky activity is predominant, and would be lower when the calcium signal is consistently higher, misrepresenting the actual neuronal activity in the experiment. For these reasons, traces normalized over mean or median of the photometry trace would be a more generally applicable (as $\Delta F/F$). Additionally, to improve the overall analysis of the calcium activity, smoothing algorithms

to correct baseline drift would be necessary, as ΔF/F calculation alone cannot eliminate these visible changes in baseline signal over hours of recordings. To address this issue, I am currently working together with my colleague Dr Mathieu Nollet in the lab on writing a Matlab script which would automatically subtract an exponential curve fitted to the baseline drift of each photometry recoding, so that the baseline calcium activity could be at the same level throughout an entire recording.

In addition to further analysis of the data already obtained, more experiments carried out with higher resolution technologies might be necessary to dissect in more details LPO circuits and dynamics. Implantation of GRIN lenses in deep brain areas might be useful experiments to not only record, but also observe the activation patterns of LPO excitatory and inhibitory neurons. These experiments could be also performed during sleep deprivation and recovery sleep, to understand whether there is a differential activation under higher sleep need.

It is interesting to consider the meaning of the intracellular calcium increase in LPO during REM sleep and dexmedetomidine-induced sedation. The NMDAr might be one effector for the increase in intracellular calcium observed during REM sleep, and these influxes of calcium might be necessary for REM sleep to be maintained. In fact, as shown in the previous chapter, deletion of the NMDAr causes a consistent reduction in REM sleep both during baseline and after sleep deprivation (Figure 3.7.1 and Figure 3.8.1). It will be interesting to use fNR1 mice and delete the NMDA receptor with a Cre recombinase and co-transduce the neurons with a flex-GCaMP6s virus. This experiment would show how NMDAr deletion could affect the overall cellular firing patterns during baseline recordings, as well as during Dex-induced sedation.

Multiple electrodes activity recordings in both LPO and its projection sites might aid understanding whole brain circuits' dynamics, and how LPO neurons communicate with target areas to promote either sleep, wake, or behavioural state changes and sedation. Using retrograde tracers injected in LPO, it would be possible to identify areas that send excitatory projections to LPO neurons. Activity recordings of these projecting nuclei might help identify activation patterns throughout the brain, and possible functional connections regulating REM sleep.

5 Investigation of lateral habenula neuronal activity in vigilance states

5.1 Chapter summary and introduction

The LHb is a glutamatergic hub reported by cFos IHC to be activated by propofol induced sedation. Outputs blockage from its glutamatergic neurons Grm2 caused a reduction in sensitivity to propofol induced sedation and a marked NREM sleep fragmentation. To understand LHb role in sleep-wake patterns regulation, I recorded the calcium activity of all LHb neurons or of only Grm2 expressing ones during different vigilance states using *in vivo* fibre photometry. LHb neurons were active during wakefulness compared to NREM sleep, while Grm2-expressing neurons showed marked calcium increase during both wake and REM sleep. Optogenetic activation of the same neurons revealed how sustained short activations of all LHb neurons caused prolonged wakefulness, while longer but more sporadic excitations promote REM sleep. When activating Grm2 neurons only, longer stimulations (40-60s) promoted REM sleep, and allowed NREM sleep to occur between stimulations, which was not observed when activating all LHb neurons. These results confirm LHb involvement in regulating both wake and REM sleep, and Grm2-expressing neurons role in permitting NREM sleep. Further studies on Vglut2 neurons with a better spatial resolution might be useful to further characterize LHb circuits in sleep and wake.

The LHb is a cluster of glutamatergic neurons located in the epithalamus controlling a vast range of behaviours. The LHb regulates behavioural responses to fear, aversion and pain by suppressing motor responses and inducing analgesia; its malfunctioning

correlates to cases of depression and schizophrenia [274]. Several studies have showed how the LHb is important for REM sleep maintenance, as lesions to its neurons reduces REM sleep time [214], however short electrical LHb stimulations cause an increase in NREM and decrease in REM sleep [216], suggesting how this glutamatergic hub might be regulating more aspects of sleep-wake patterns. In fact, the LHb projects to numerous targets in the brain, including areas which control wake and arousal [213]. Because of its activation quantified by cFos IHC [209], we know that LHb fires under propofol-induced sedation, a commonly used anaesthetic that potentiates $GABA_A$ receptor responses.

Because of its activity under sedation, and its possible role in regulating sleep and wake patterns, the LHb is a fascinating target to study not only to understand sleep and anaesthesia individually, but also to determine how the networks regulating these mechanisms overlap.

In the paper published in 2018, I and Dr Cigdem Gelegen investigated the role of a specific population of neurons expressing the metabotropic glutamate receptor 2 (Grm2). After surveying the GENSAT database of Cre lines, we noticed that this Grm2 marker is expressed in the LHb but is absent in the adjacent medial habenula (MHb), allowing us to specifically target the LHb. Using a mouse line with the Cre recombinase expressed under the Grm2 promoter, we targeted only neurons in the LHb. To understand the role of the LHb in regulating sleep and sedation, Dr Gelegen used an AAV virus expressing the Tetanus-Toxin Light-Chain (TeLC). The TeLC reading frame was in an inverted orientation that could be placed in sense orientation downstream of the promoter using Cre recombinase (flex switch), so that only Cre expressing neurons could produce the transgene. Once expressed, TeLC cleaves the protein synaptobrevin-2, required for the association of neurotransmitter vesicles to the cell membrane [275], and blocks neurotransmitter release. In this way, Dr Gelegen blocked any output from Grm2-expressing neurons and observed sleep patterns and sensitivity to propofol. I complimented her analysis with GCaMP6s recordings form the LHb neurons, as well as preliminary optogenetic analysis.

5.2 Grm2 neurons are needed for NREM sleep and propofol sedation

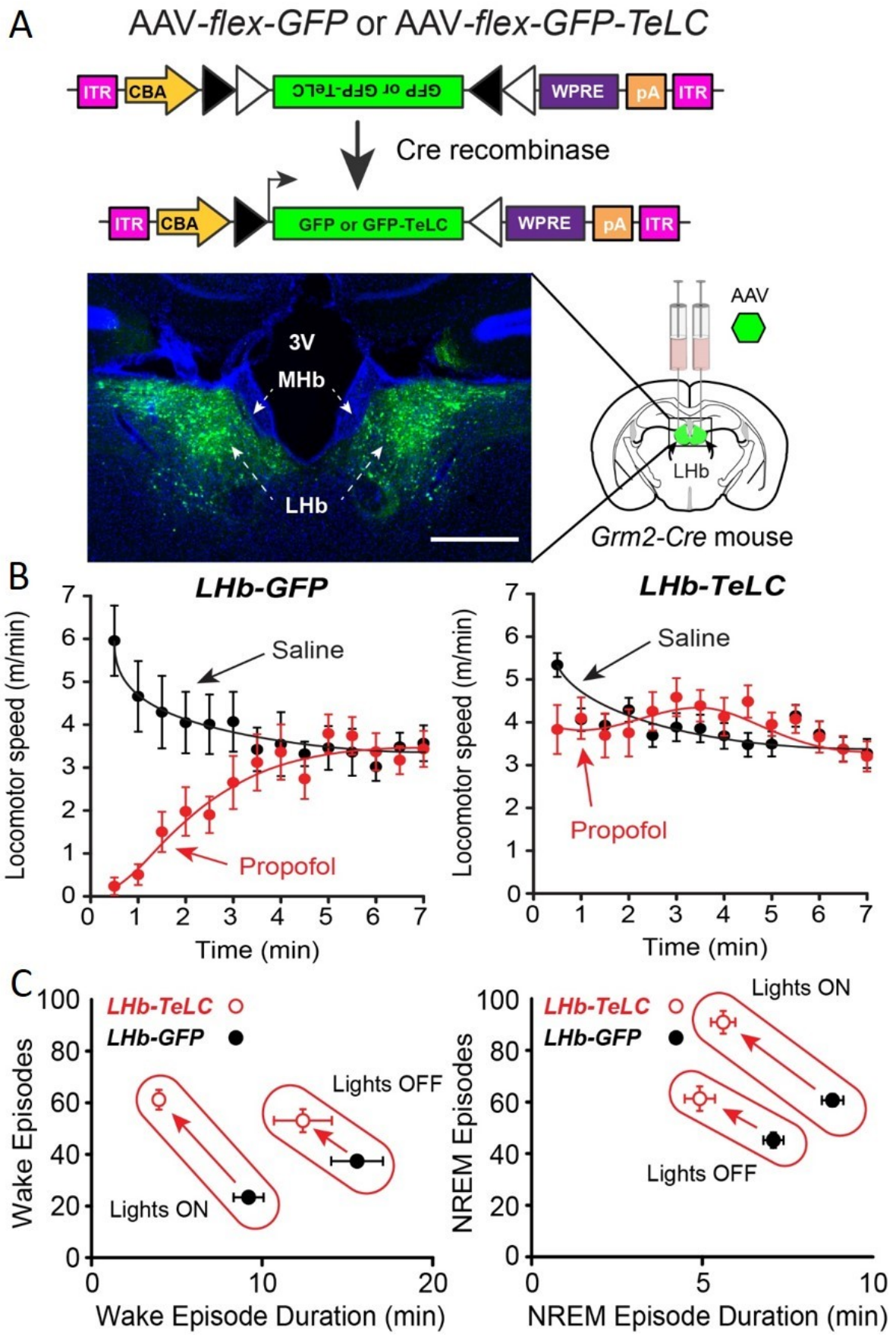

Figure 5.2.1 Blockage of Grm2 neuronal output reduces sensitivity to propofol and causes sleep-wake fragmentation.
Figure on previous page. A, bilateral injection of *AAV-flex-GFP* or *AAV-flex-GFP-TeLC* in LHb of Grm2-Cre mice to silence outputs from Grm2 neurons. Black arrowheads indicate loxP sites. Bottom, coronal section showing GFP expression in LHb area and not in the medial habenula (MHb). Scale bar, 500 μm. B, Propofol-induced sedation in LHb-GFP (left, saline, n= 11; propofol n= 14) and LHb-TeLC mice (right, saline, n= 21; propofol, n= 23). Locomotion in LHb-TeLC was unaffected (means ± SEM, p= 0.26). C, compared to LHb-GFP mice (n = 13), LHb-TeLC mice (n = 9) showed a significant increase in episodes number and a significant decrease in episodes duration in both wake (left) and NREM sleep (right, unpaired two-tail t test). Symbols are mean ± SEM, $p< 0.05$. Figured modified from publication [198].

My colleague Dr Cigdem Gelegen and I investigated the role of LHb neurons in regulating sleep and sedation [198].

Dr Gelegen showed that Grm2-Cre-positive neurons are glutamatergic (data not shown here), and she blocked their outputs using a TeLC to test their sensitivity to propofol. TeLC-LHb mice were less responsive to propofol induced sedation, with almost no effects on their locomotor activity following tail injections of the anaesthetic (Figure 5.2.1, B). These animals not only showed no motor suppression, but also did not have the typical thalamo-cortical delta oscillations caused by sedative doses of propofol, which can be easily distinguished in EEG recordings (data not shown here) under propofol sedation [203]. TeLC-LHb mice also had a marked NREM sleep fragmentation, especially during the lights-ON phase, when mice normally sleep more (Figure 5.2.1, C).

To confirm the results obtained within the TeLC experimental group, Dr Gelegen manipulated these neurons using chemogenetics. To target only Grm2-expressing neurons, she injected into the LHb an *AAV-flex-hM3Dq-mCherry* virus. Activation of Grm2 expressing neurons after *i.p.* injection of CNO significantly reduced locomotion (Figure 5.2.2), without altering sleep and wake time. This is a rare example where a glutamatergic excitatory circuit causes an inhibition of locomotor activity rather than a general activation, the other being that Vglut2/Nos1 neurons in MPO/MnPO hypothalamus also induce NREM sleep [81].

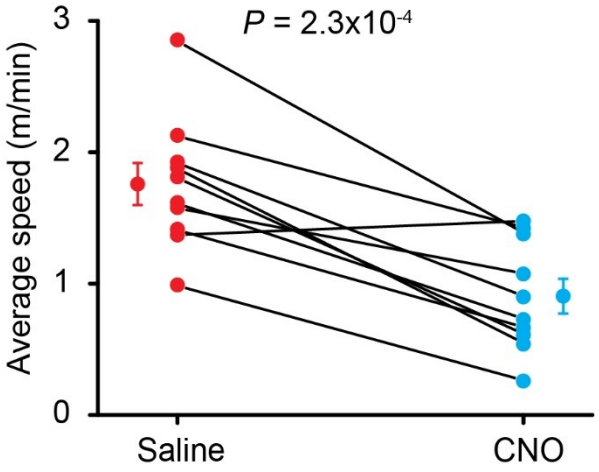

Figure 5.2.2 DREADD receptor activation in Grm2-Cre neurons reduces locomotion.
After bilateral injection of AAV-flex-hm3Dq-mCHERRY in LHb, a 2-fold reduction of locomotor speed was observed in 20 minutes open field test after CNO (5 mg/kg, i.p.) or saline injection (paired two-tailed t test; n = 10). Symbols are mean ± SEM. Figure from publication [198], performed by Dr Gelegen.

To elucidate whether LHb Grm2-Cre neurons were actively responsible in regulating sleep and wake, I first investigated their baseline activity using the calcium signal sensor GCaMP6s during different vigilance states. Second, I activated the same neurons using optogenetics, expressing Channel Rhodopsin 2 (ChR2) in either all LHb neurons or only Grm2 expressing ones, to better investigate how artificial activation of Grm2 neurons can affect sleep and wake patterns.

5.3 LHb Grm2 expressing neurons are wake and REM sleep active

To investigate how the LHb regulates sleep behaviours, I looked at the activity and functions of either all LHb neurons or only Grm2-expressing ones using photometry recordings. As described in Chapter 4, we generated two different AAVs, one carrying the GCaMP6s transgene under a human synapsin (hsyn) promoter and the other expressing the hsyn-GCaMP6s transgene with a flex-switch, to be expressed in Grm2-expressing neurons (Figure 5.3.1).

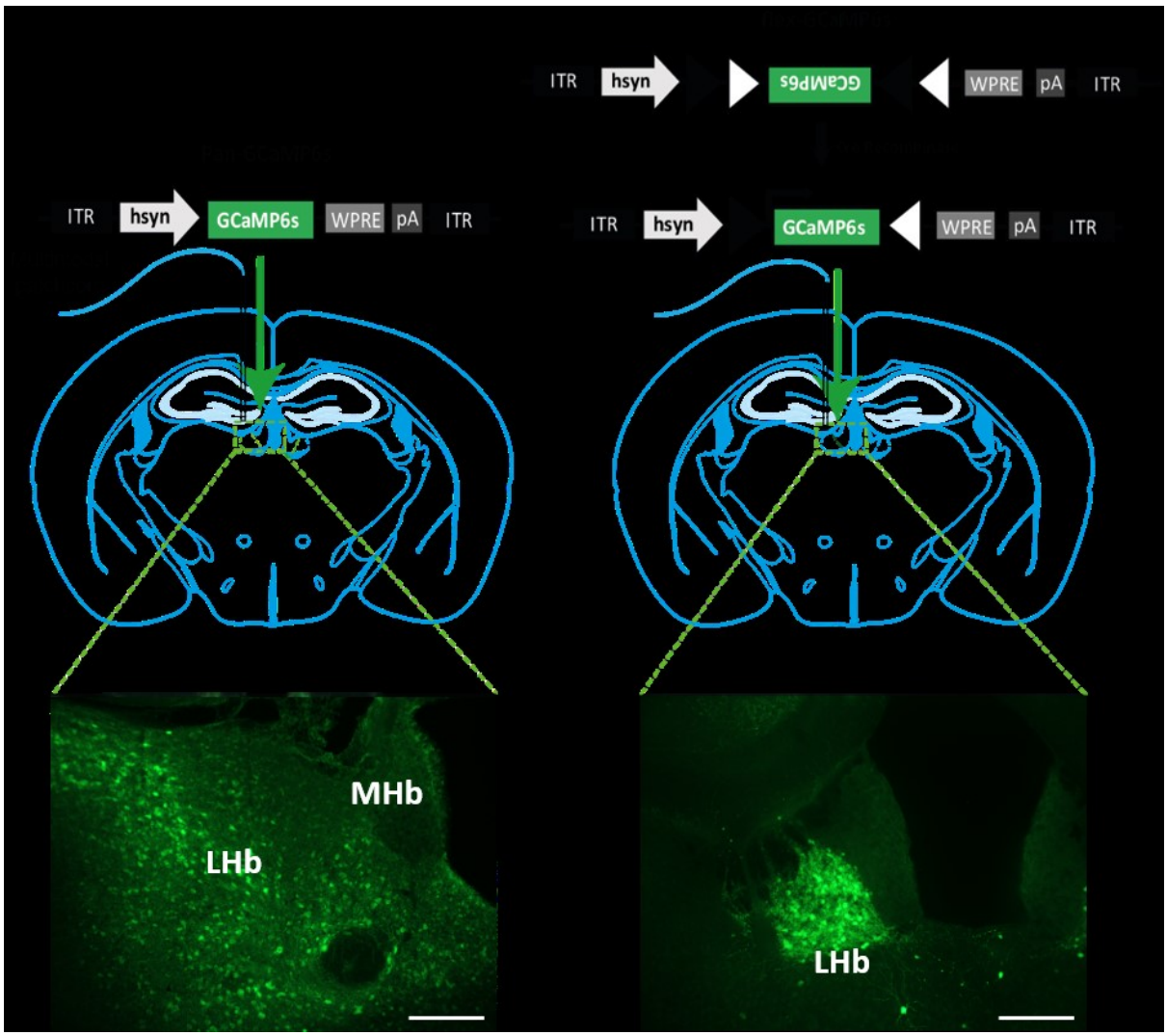

Figure 5.3.1 Generation of Pan-GCaMP6s and Flex-GCaMP6s mice.
Top, schematic representation of the AAV transgenes carrying the GCaMP6s gene under a pan promoter (left) or in a flex-switch direction (right). ITR, inverted terminal repeats; pA, polyadenylation signal; WPRE, woodchuck-post transcriptional-regulatory element; 3V. The viruses were injected unilaterally in the LHb and mice were chronically implanted in the same area with a fibre optic. Centre, schematic representation of a coronal section at -1.70mm from Bregma. Bottom, GFP IHC of a pan-GCaMP6s (left) and flex-GCaMP6s (right). MHb, medial habenula. Scale bars represent 200 µm.

AAV-flex-hsyn-GCaMP6s was injected in Grm2-Cre positive mice (Flex-GCamp6s) and *AAV-hsyn-GCaMP6s* (pan-GCaMP6s) in wild type littermates (Figure 5.3.1). At the same time, mice were implanted with a permanent fibre optic (Ø 200 µm, 0.37 NA) in the LHb area and an EEG/EMG headstage. After 4 weeks of recovery, GCaMP6s fluorescence and EEG and EMG traces were simultaneously recorded.

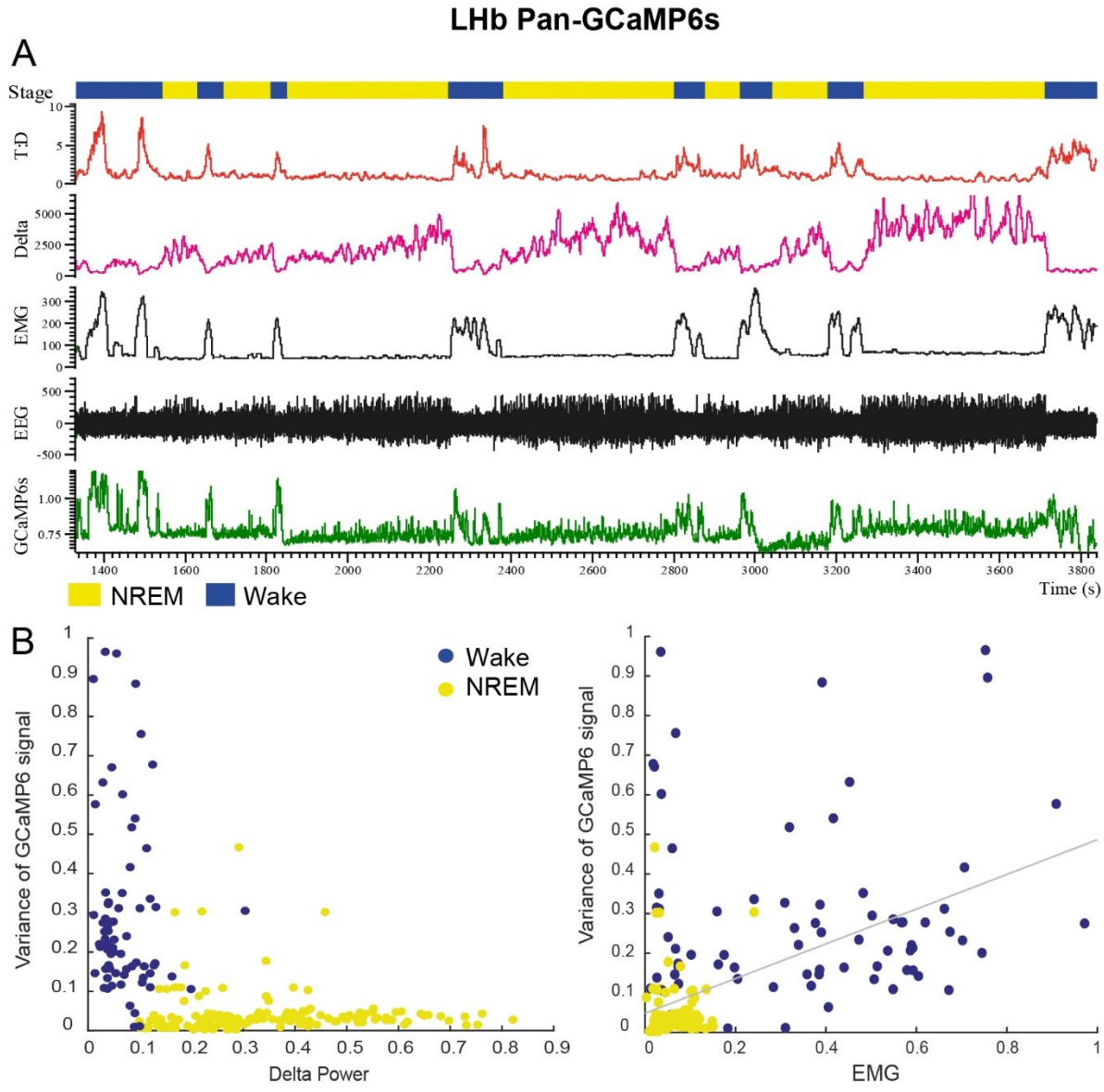

Figure 5.3.2 LHb Pan-GCaMP6s signal is higher during wake episodes.
A, example of a recording from n=8 animals tested, showing from top to bottom a hypnogram (blue=wake, yellow=NREM), theta/delta power ratio (T: D), delta power (0.5-4 Hz), EMG, EEG and GCaMP6s signal. B, plot of GCaMP6s signal variance against delta power (left) or EMG signal (right), showing how higher variance corresponds to low delta power and correlates to high EMG (blue= wake, yellow=NREM). Each point represents 10 seconds of data.

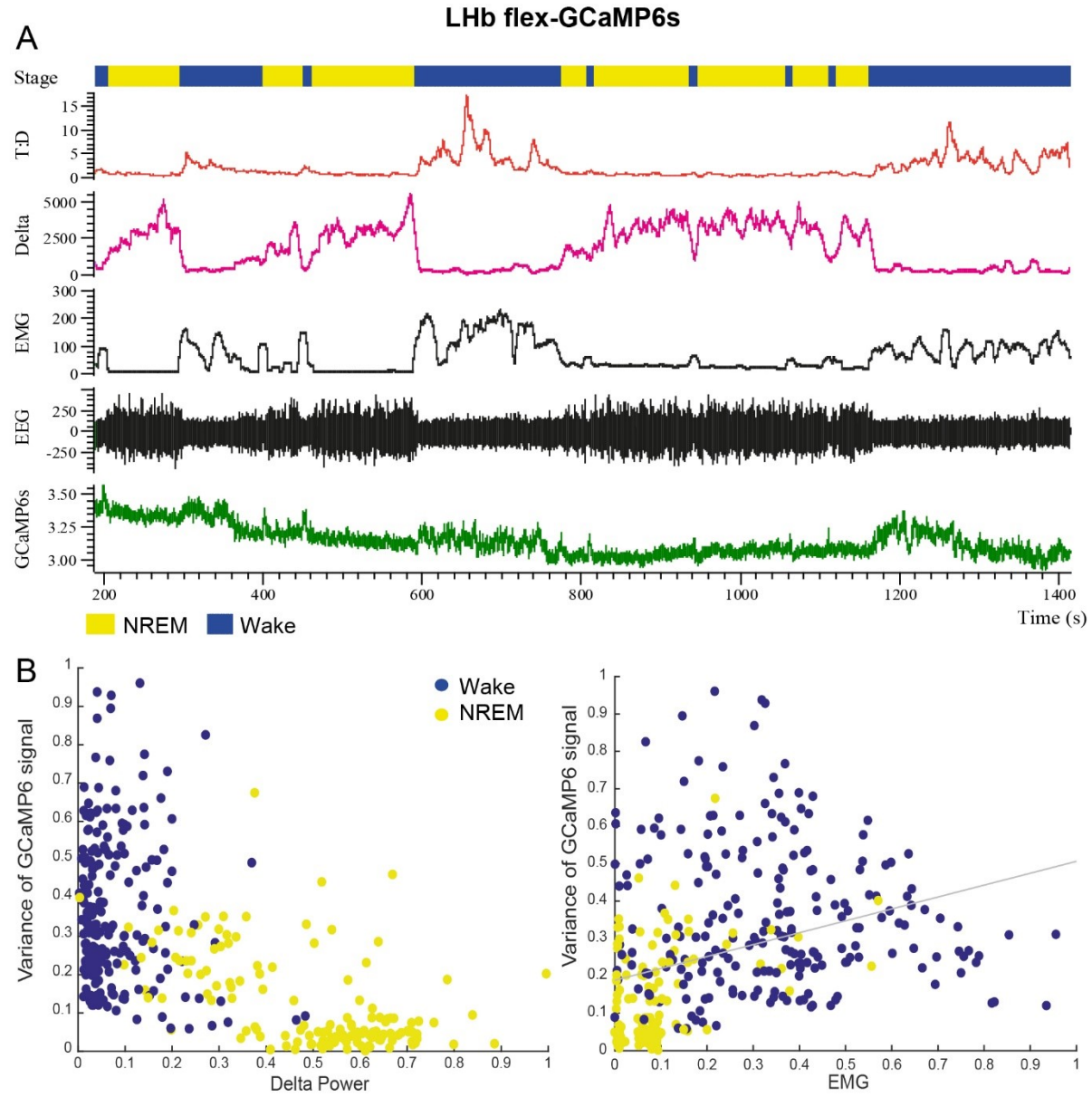

Figure 5.3.3 The activity of Grm2-expressing neurons is highest during wakefulness.

A, example of a recording from n=3 animals tested, showing from top to bottom an hypnogram (blue=Wake, yellow=NREM), theta/delta power ratio (T:D), delta power , EMG, EEG and GCaMP6s signal. B, plot of GCaMP6s signal variance against delta power (left) or EMG signal (right, blue= wake, yellow= NREM). Data were plotted every 5s. C, mean of random ΔF/F points during wake and NREM sleep. N= 5, error bars are mean ± SEM with One-way ANOVA and post-hoc Tukey Test.

During the light and dark periods, both pan-GCaMP6s and flex-GCaMP6s expressing neurons in the LHb showed a markedly higher GCaMP6s signal during wakefulness episodes compared to NREM sleep (Figure 5.3.2, A and Figure 5.3.3, A). For these analyses, variance rather than mean of GCaMP6s signal was considered to exclude basal GCaMP6s signal noise and drift observed during recordings. A similar drift was previously reported [47]. Plotting the variance of the GCaMP6s signal against either EMG or delta power confirmed how both all LHb neurons and in particular Grm2 expressing ones were active during wakefulness (Figure 5.3.2, B and Figure 5.3.3, B). Looking at the mean of random ΔF/F points during NREM or wake, I could confirm that highest calcium activity was registered during wakefulness rather than NREM sleep (Figure 5.3.3, C, paired Student's *t* test).

Grm2-Cre neurons also showed higher Ca^{2+} activity during REM sleep (Figure 5.3.4, A), and the fluorescence signal was higher even compared to wake episodes. In fact, plotting the variance of the GCaMP6s signal against the theta to delta power ratio (Figure 5.3.4, B), a direct correlation between these two variables was observed, with the highest values of variance corresponding to REM epochs. This correlation was confirmed when looking also at the GCaMP6s variance plotted against the EMG (Figure 5.3.4, C) or against delta power (Figure 5.3.4, D), showing how lowest values for these two variables, indicating REM sleep data points, corresponded to the highest levels of GCaMP6s variance. The average of random ΔF/F points during the three behavioural states also confirmed that the highest calcium activity in Grm2 expressing neurons corresponds to periods of REM sleep and wakefulness (Figure 5.3.4, E). These data demonstrate the activity of LHb Grm2 neurons during REM sleep episodes, fitting with other previously published works. In fact, the LHb controls motor suppression and freezing responses to fear, aversion and stress. Similarly, it is possible that the LHb neurons participate in the generation of muscular atonia during REM sleep [276, 277].

Figure 5.3.4 Grm2-Cre neurons are most active during REM sleep.
Figure on following page. A, representative recording from n=3 animals tested during REM sleep, showing from top to bottom T:D ratio, delta power, EMG, GCaMP6s signal and scaled GCaMP6s variance. B-D, plots of GCaMP6s signal variance against T:D ratio (B), EMG (C) or delta power (D). (blue= wake, yellow=NREM, light blue= REM). Data were plotted every 5s. E, mean of random ΔF/F points during wake, REM and NREM sleep, showing highest levels of calcium signalling during REM sleep. N= 5, error bars indicate mean ± SEM with significance calculated by One-way ANOVA and post-hoc Tukey Test.

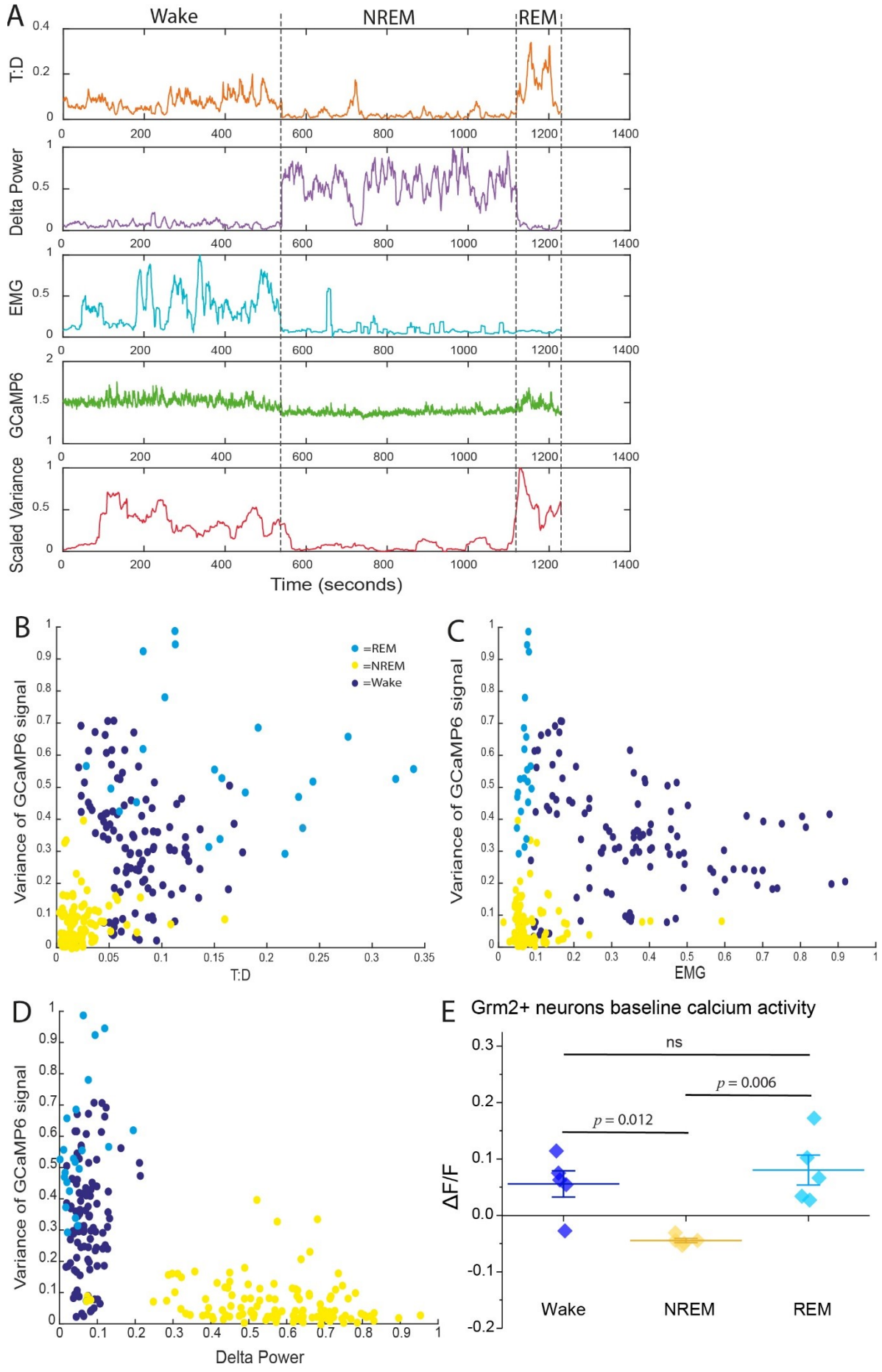
A
Wake
NREM
REM
T:D
Delta Power
EMG
GCaMP6
Scaled Variance
Time (seconds)
B
=REM
=NREM
=Wake
Variance of GCaMP6 signal
T:D
C
Variance of GCaMP6 signal
EMG
D
Variance of GCaMP6 signal
Delta Power
E
Grm2+ neurons baseline calcium activity
ns
p = 0.006
p = 0.012
ΔF/F
Wake
NREM
REM

As a control, the GCaMP6s signal from Cre-negative mice was also recorded, and *Flex-GCaMP6s* virus was injected into the LHb of wild-type Grm2-Cre negative littermates. In this case, no difference in the GCaMP6s signal based on the behavioural state was observed (Figure 5.3.5, A). There was no state-dependent increase or decrease in the GCaMP6s variance, thus giving confidence in any changes obtained in the experimental groups (Figure 5.3.5, B).

Altogether, these data confirmed how the LHb and specifically the Grm2 expressing neurons, are involved in regulating behavioural states, being active during wakefulness and REM sleep.

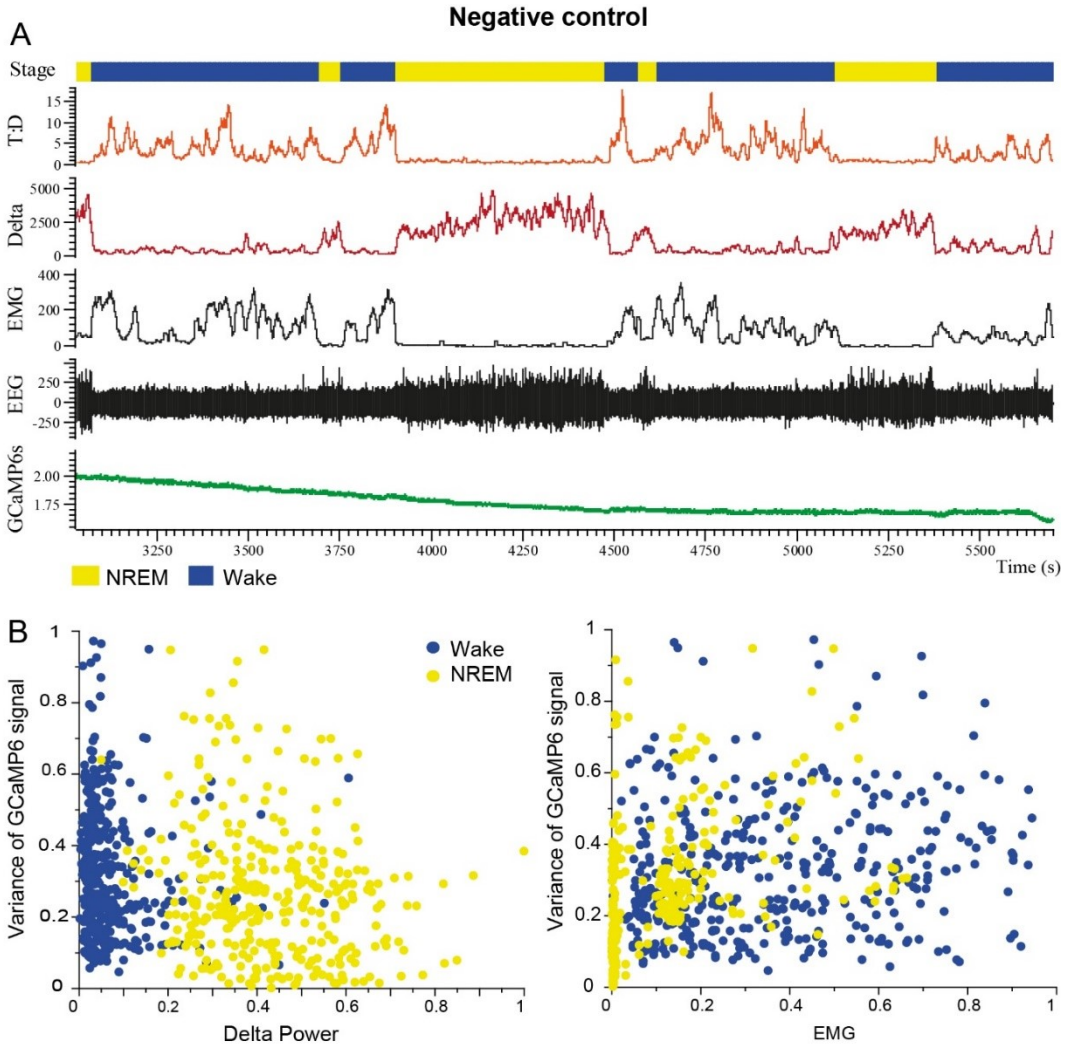

Figure 5.3.5 Negative control for Flex-GCaMP6s in the LHb shows no changes in GCaMP6s fluorescence.

The flex-GCaMP6s virus was injected in a Cre negative littermates. A, example of a recording from n=2 animals tested, showing from top to bottom an hypnogram (blue=wake, yellow=NREM), T:D ratio, delta power, EMG, EEG and GCaMP6s signal. Plot of Ca^{2+} signal variance against delta power (B) or EMG signal (C), showing no correlations between the variables (blue= wake, yellow=NREM). Data were plotted every 5s.

5.4 Optogenetic stimulation of LHb neurons

To complement the chemogenetic activation results in our publication, we used optogenetics to selectively activate LHb neurons.

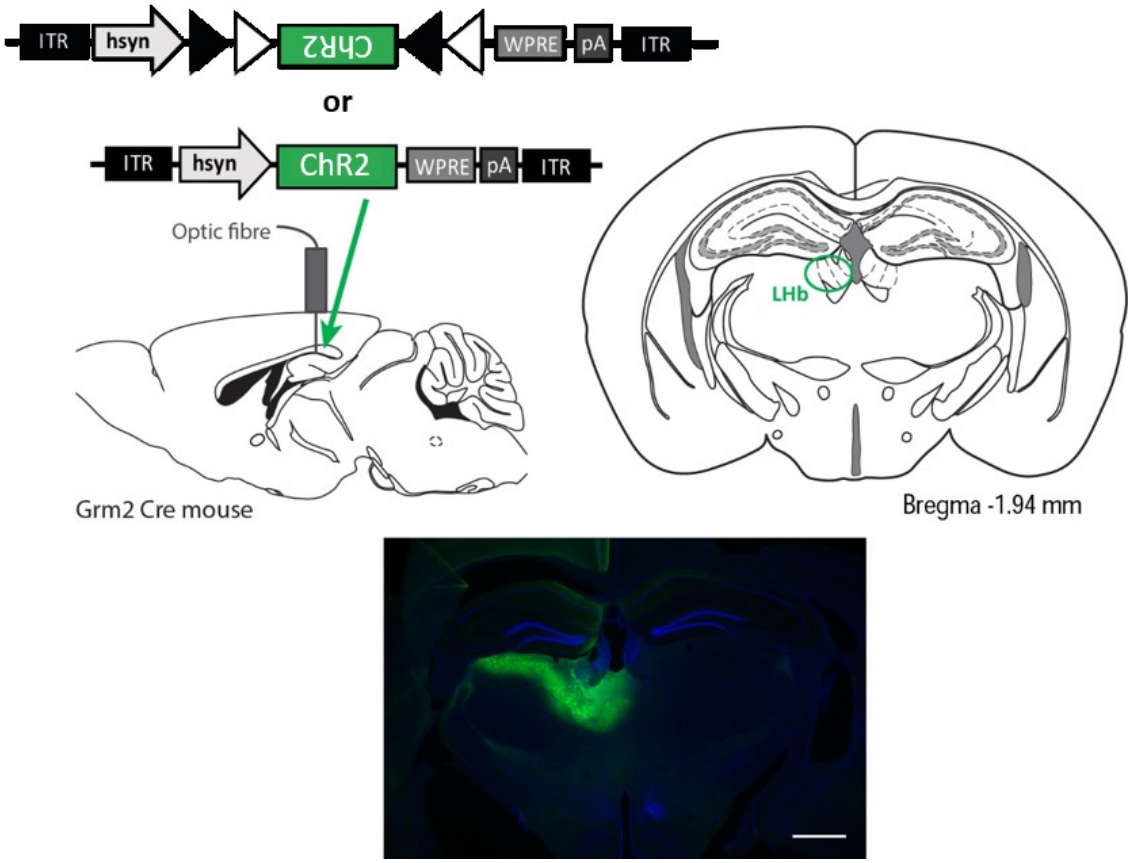

Figure 5.4.1 ChR2 expression on the LHb neurons and generation of Hsyn and Flex-ChR2 mice.
Top, schematic representation on sagittal (left) and coronal (right) slices of *AAV-Flex-hsyn-ChR2* and *AAV-hsyn-ChR2* viral injections in left LHb and implantation of optic fibre in Grm2-Cre positive or negative littermates, respectively. Bottom, GFP IHC to mark *AAV-hsyn-ChR2* virus expression. Scale bar represents 500 µm.

Channelrhodopsin 2 (ChR2) is activated by the absorption of photons with a wavelength between 450-480 nm, and, when opened, the channel allows influx of cations in the intracellular space, causing the neurons to depolarize [278].

With the help of Raquel Yustos in the lab, we produced AAVs carrying the ChR2 transgene under a human synapsin promoter (hsyn-ChR2), while the Flex-ChR2 virus, expressed in Grm2 positive cells only (Figure 5.4.1), was packaged in the lab after purchasing the Addgene plasmid *pAAV-EF1a-double floxed-hChR2(H134R)-EYFP-WPRE-HGHpA* (#20298).

After viral injection, an optic fibre was permanently implanted in the animals in order to deliver specific protocols of laser stimulations at 473 nm, with a power at the fibre tip of 6mW.

5.4.1 Optogenetic activation of LHb neurons produces sustained wakefulness and partially REM sleep

For hsyn-ChR2 animals, two different stimulation protocols were tested to identify an activation pattern more similar to the physiological neuronal firing of the area. The first protocol (Protocol 1) included frequent stimuli of 20 ms pulses at 25 Hz for 2 seconds every minute, whereas the second protocol (Protocol 2) had spaced stimulations of 10 ms pulses at 10 Hz for 10, 20, 40 and 60 seconds with a 10 minutes break between each set. Both protocols were tested during dark period, so that NREM and REM episodes could not be caused by sleepiness during the light period.

During Protocol 1, hsyn-ChR2 mice were kept awake for the whole 1 hour stimulation, shifting to NREM sleep only towards the end of the protocol (Figure 5.4.2). Using video recordings, mice were observed during the whole set of stimulations and appeared hyperactive, continuously running in their home cage as previously described [279]. No episodes of quite waking, as grooming, drinking and feeding, were observed as it can also be denoted by very high EMG signals in EEG/EMG recordings (Figure 5.4.2, A, third row). This protocol seemed to cause an overstimulation of the whole neuronal system surrounding the LHb rather than mimicking a physiological activation patter of its neurons, and it was therefore not tested in Flex-ChR2 animals.

After at least a week of recovery, the hsyn-ChR2 experimental group was then tested with Protocol 2. With this protocol, mice had 10 minutes between stimulations to recover. For each set in the protocol, laser was ON for an increasing amount of time to understand whether different patterns and durations of stimulations were needed to induce either sleep or wake. In fact, from Protocol 1 tests data, we observed that short and frequent stimulations promoted exclusively a state of hyperactive wakefulness, but it is possible that longer and less frequent stimulations could favour a less active behaviour. During Protocol 2 testing, it was clear that when laser was kept ON for only 10 s, wake was predominantly present, but when laser was kept ON for longer, as for 40 and 60 s, mice shifted to REM sleep, even during a wake episode (Figure 5.4.3).

In between stimulations, wakefulness seemed to be the predominant state, while almost no NREM sleep was recorded either with laser ON or OFF. Therefore, Protocol 2 seemed a more appropriate set of stimulations to study LHb activity during different vigilance states. In Hsyn-ChR2 group, activation of the LHb area caused a general brain activation, favouring theta waves over delta in the EEG not only during stimulations, but also when laser was kept OFF.

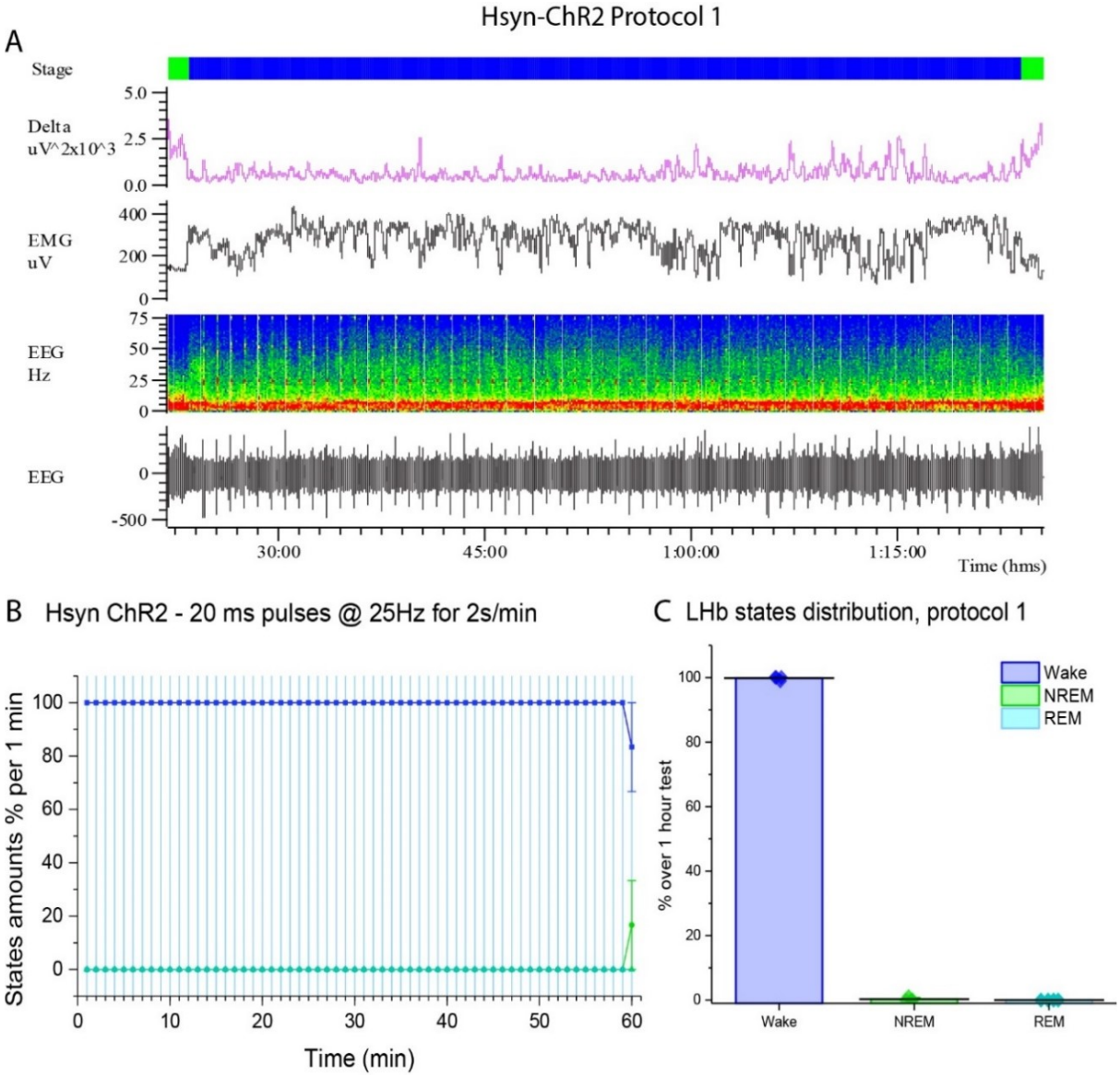

Figure 5.4.2 Protocol1 stimulations of LHb neurons caused prolonged wakefulness. A, example of one 1 hour recording of optogenetic stimulation at 25 Hz, 20 ms pulses for 2 seconds every minute. From the top, each line denotes state (blue = wake; green= NREM), delta power, EMG and EEG represented as a somnogram and waveform. B, percentage of states amounts per minute over the 1 hour stimulation. All mice tested (n= 5) did not sleep during the whole testing time. Blue lines indicate laser stimulation at 473 nm. C, states distribution during 1 hour stimulation. Data are presented as mean and scale bars represent ± SEM.

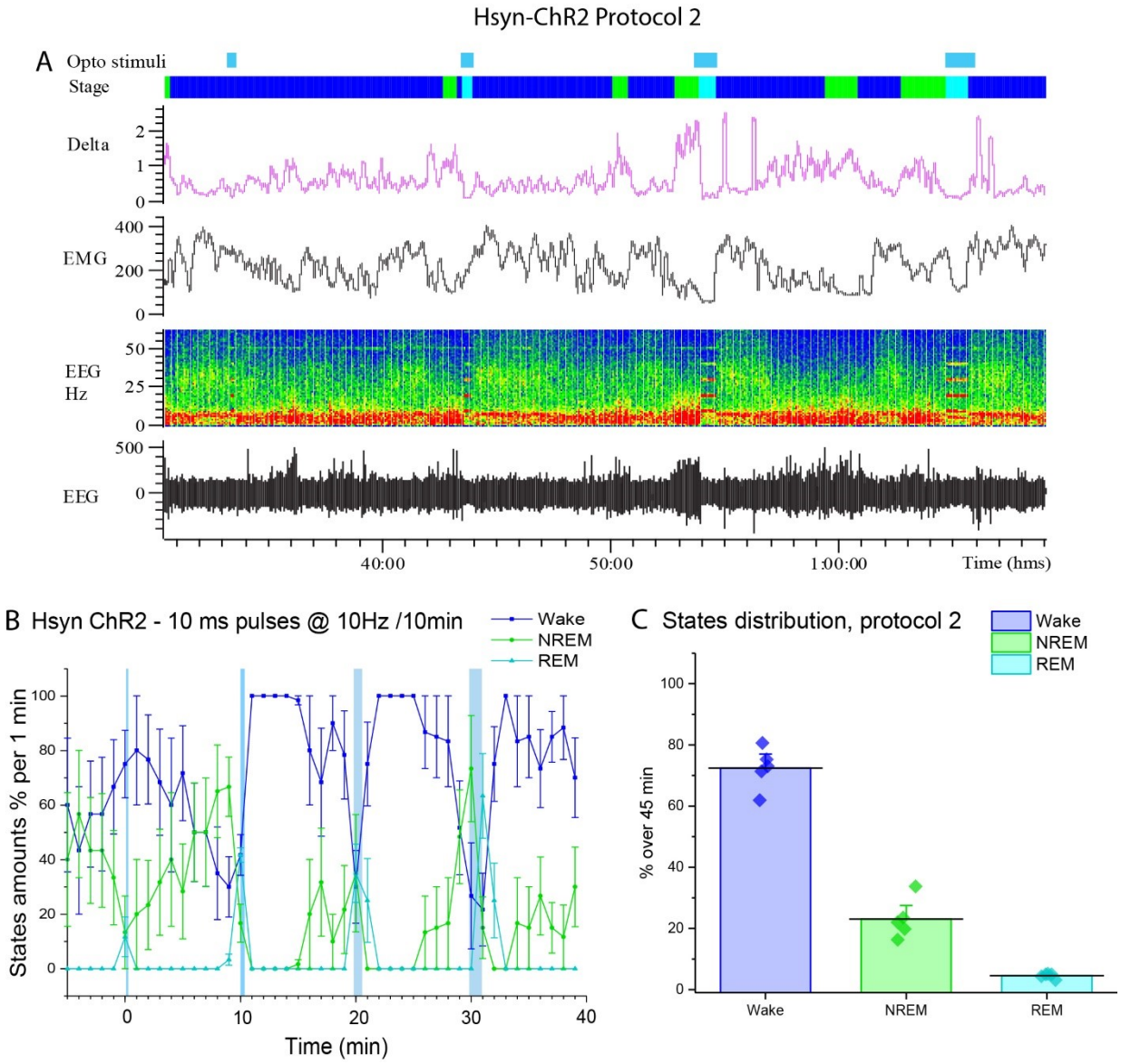

Figure 5.4.3 Protocol 2 short stimulations of LHb neurons caused wake while longer stimulations promoted REM sleep.

A, example of 1 recording with optogenetic stimulation at 10 Hz, 10 ms pulses for 10, 20, 40, 60s every 10 minutes. From the top, state (blue = wake; green= NREM, light blue = REM), delta power, EMG and EEG represented as a somnogram and waveform. B, percentage of states amounts per 1 minute over the 45 minutes length of the protocol, including 5 minutes before first stimulus and 10 minutes after each stimulus. All mice tested (n= 5) showed increased REM sleep, particularly during longer stimulations, and reduced NREM sleep when laser was OFF. Blue lines indicate laser stimulation at 473 nm. C, states distribution for 45 minutes showing an increase in REM sleep compared to the previous stimulation protocol. Data are presented as mean ± SEM.

Interestingly, stimulation of the LHb at 10 Hz caused harmonics in the EEG exclusively during stimulation time. This phenotype could be due to the tight connection between LHb and hippocampus in controlling and generating theta oscillations (between 5-10 Hz) [214]. Because the EEG screws implanted on the animal skull span over the hippocampus, the EEG traces are strongly composed by the electrical activity of hippocampal neurons. Stimulations of the LHb at 10 Hz could therefore affect the hippocampus and cause these oscillations visible in the EEG. It is important to note that these oscillations are not caused by instrumental noise or interference, as control animals subjected to the same light pulses but lacking the ChR2 gene did not show harmonics in the EEG (data not shown).

5.4.2 Optogenetic activation of Grm2 expressing neurons induced REM sleep and permits NREM sleep between stimulations

Protocol 2 was tested in Grm2-Cre mice, injecting a flex-ChR2 virus in the LHb area. Mice were tested at the same circadian time as the Hsyn-ChR2 group, with the same laser power and set of optogenetic stimulations. For Flex-ChR2 animals, mice were mostly awake during short 10 s stimulations and were woken up if laser turned ON during a NREM episode. When the laser was kept ON for longer, particularly for 60s, mice showed an increase in REM sleep, which was maintained even if laser was turned ON during a REM sleep episode (Figure 5.4.4). During all stimulations, NREM sleep regularly decreased, with again an evident shift from delta to theta waves in the EEG. In contrast to the Hsyn-ChR2 group, Flex-ChR2 animals did not have an overall inhibition of NREM sleep, and they were able to fall back asleep right after the laser was ON, or, in some cases, even during the longer stimuli, right after being woken up by the stimulation.

Figure 5.4.4 Protocol 2 stimulations of Grm2 expressing neurons increased wake and REM sleep during stimuli and NREM sleep when laser was OFF.
Figure on the following page. A IHC of flex-GCaMP6s injection in the LHb (green = GFP; blue = DAPI). Scale bars represent 1 mm (left) and 200 μm (right). B, example of 1 recording during optogenetic stimulation at 10 Hz, 10 ms pulses for 10, 20, 40, 60 s every 10 min. From the top, state (blue = wake; green= NREM, light blue = REM), delta power, EMG and EEG represented as a somnogram and waveform. C, percentage of states amounts per minute over 45 minutes. All mice tested (n= 5) showed an increase in REM sleep and wake only during the laser stimulus. Blue lines indicate laser ON at 473 nm. D, states distribution for 45 minutes protocol showing how optogenetic neuronal activation did not reduce NREM sleep in between stimuli. Data are presented as mean ± SEM.

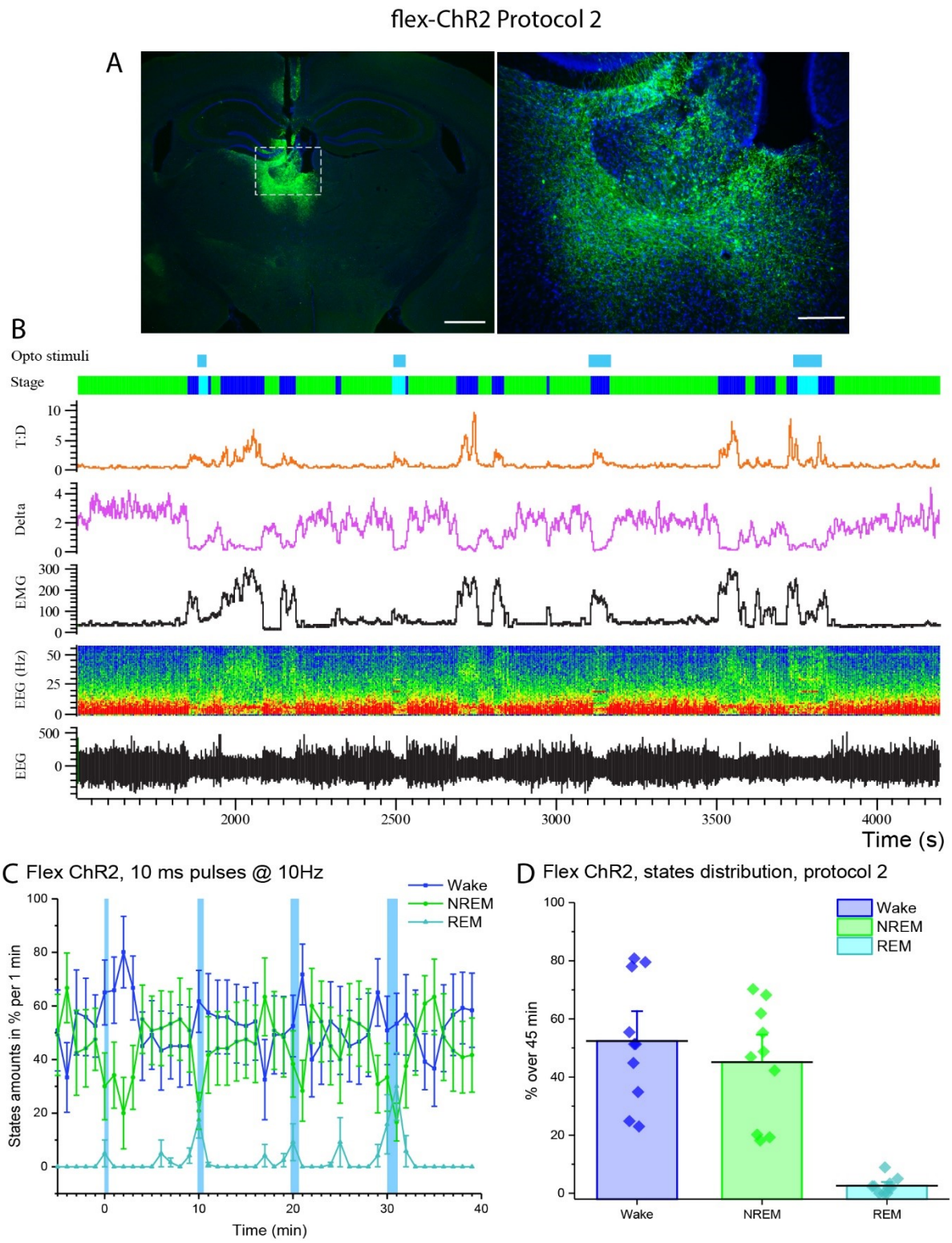

These data suggest that Grm2 expressing neurons are not responsible for causing a general cortical activation resulting in hyperactivity, and they seem rather permissive for NREM sleep to occur and be maintained in between direct neuronal activation.

5.5 Discussion

To investigate the role of the LHb glutamatergic neurons expressing the Grm2 gene in maintaining sleep and sensitivity to sedation, I used *in vivo* photometry recordings and optogenetic stimulations in combination with EEG and EMG recordings. With the first technique, I observed the baseline activity of LHb neurons during different behavioural states, while with the second I artificially activated the same circuits through the expression of the ChR2 channel. I demonstrated that the LHb neurons promote wake and REM sleep induction, while Grm2 expressing cells seem to also be permissive for NREM sleep. It is possible that Grm2 negative neurons are responsible for inducing prolonged wakefulness and might activate circuits regulating hyperactivity and stress behaviours. Overall, these data suggest that Grm2 neurons do not directly induce NREM sleep, but it is possible that they contribute in its maintenance, as suggested in our publications, as they allow NREM in between or even during longer optogenetic laser stimulations. Grm2 positive neurons seemed more convincingly to induce REM sleep initiation, in particular when stimulated less intensely and for a longer time. Short bursts of activation could cause brief wake episodes, activating circuits of fear and aversion, but longer excitations could favour the system towards a REM like state, characterized by motor suppression and atonia [274].

5.5.1 LHb role in behavioural stages generation

My recordings of *in vivo* calcium activity using the sensor GCaMP6s have shown how both all neurons in LHb and only Grm2 expressing ones are active during wake and REM sleep (Figure 5.3.2, Figure 5.3.3 and Figure 5.3.4), with no signs of significant activity during NREM sleep. Optogenetic activation of the LHb caused a diverse distribution of vigilance states, depending on the precise opto-activation protocol. Short but sustained stimulations of LHb neurons caused marked hyperactivity in all mice tested for the whole length of the experiment (Figure 5.4.2). On the other hand, less frequent stimulations caused in both Hsyn-ChR2 and Flex-ChR2 animals wake during short laser light trains and REM sleep during longer ones (Figure 5.4.3 and Figure 5.4.4). Interestingly, NREM sleep did not take place even between stimulations in Hysn-ChR2 animals, while it was present when stimulating only Grm2-expressing neurons. These data might suggest that the LHb controls wake and REM sleep, as its neurons are important to generate

hippocampal theta oscillations [214], whereas Grm2-positive neurons are permissive for NREM sleep to occur and be maintained. In fact, blocking their outputs using targeted expression of TeLC caused NREM sleep fragmentation [198].

Because LHb is a small neuronal cluster, and Grm2 is expressed in both hippocampal dentate granule cells and in the central medial thalamus, which are respectively dorsal and ventral to the LHb, contaminations from these two areas might also have affected photometry and optogenetic recordings. Animals that in IHC resulted having the fibres positioned in the wrong brain areas were excluded from the analysis, but I could not be sure that no signal from neighbouring neurons might have participated to the behaviours and phenotypes observed.

However, after I finished this work, Dr Wei Ba in the lab started studying the LHb using Vglut2 as a marker to drive GCaMP6s and DREADD receptor expression in Vglut2-Cre animals. Vglut2 proved to be a more selective marker for the LHb compared to Grm2, as it is not expressed in the hippocampus or thalamic relay cells, which use Vglut1 instead. Dr Ba found that the LHb Vglut2-expressing neurons are selectively wake and REM sleep active, in agreement with my results (unpublished, confidential), and she demonstrated that chemogenetic activation of the same neurons induces first NREM and then REM sleep (unpublished, confidential).

5.5.2 Concluding remarks and future experiments

With the data presented here, and the ones previously published [198], we have demonstrated that the LHb regulates propofol-induced sedation and that it participates in sleep patterns regulation.

To better analyse the functions of LHb, it would be interesting to record the activity and manipulate only LHb projections in different brain areas, to understand how these connections are regulating sleep and sedation in their downstream targets. Both optogenetic and photometry techniques could be used on projection sites.

Alternative silencing techniques could also be used, as the inhibitory archaerhodopsin T (ArchT), a proton pump that inhibits neurons when activated by yellow light [280]. ArchT would offer a reversible silencing method, to understand whether the results obtained using TeLC were not caused by a secondary effect of a general and permanent silencing of Grm2 expressing neurons.

6 Final discussion

With my research, I have studied circuits' functions and connections in different areas of the brain, to understand how sleep and sedation are regulated.

In the first results Chapter (Chapter 3) I have demonstrated how the NMDAr is fundamental for LPO neurons to maintain sleep during both the light and dark period. Deletion of the NMDA receptor exclusively from LPO neurons using genetic ablation of its fundamental subunit NR1 caused marked hyperactivity in mice (ΔNR1-LPO animals). This extremely active behaviour was associated to constant sleep loss of both NREM and especially REM sleep compared to controls and very marked sleep fragmentation throughout the 24 hours baseline recordings. When animals lacking the NMDAr in LPO were sleep deprived for 6 consecutive hours (6hSD) at the beginning of the light phase, their sleep period, they showed an increased number of sleep attempts during the SD, and they also fell asleep much faster compared to controls once the deprivation ended, suggesting a highly sleepy phenotype. Despite the sleepiness, ΔNR1-LPO animals could not catch up on the lost sleep, and when the dark period began after 6hSD and 6h of sleep opportunity, these animals maintained their baseline hyperactive behaviour, while control animals kept on catching up the lost sleep even during their active phase. However, ΔNR1-LPO animals showed a delta power rebound, parameter often used to quantify sleep pressure and homeostasis, meaning that these animals could feel the sleep need, but they could not maintain longer sleep bouts.

These results suggest that the NMDA receptor in LPO is fundamental for maintaining the brain asleep, and without it wake signals can constantly intrude into sleep episodes causing state transitions. Additionally, the NMDA pathways do not directly regulate sleepy phenotypes and cortical delta power rebounds. The inhibition of these pathways shows that the intensity of slow wave activity, as sleep depth, and sleep rebound, as recuperating lost sleep, might be regulated by separate circuits in the brain.

Further experiments focused on understanding which LPO neuronal pathway is responsible for this phenotype could be useful to understand how LPO regulates sleep. First, I will use selective NR1 deletion exclusively in neuronal subtypes, as GABAergic and glutamatergic neurons. Second, using viral tracing technique, I will observe and possibly

manipulate target regions of these neuronal populations, to observe whether one specific pathway is the most relevant for controlling sleep maintenance and rebound in the brain. Finally, more questions should be answered to understand whether synaptic plasticity does occur in sleep regulatory areas and under which mechanism; if cortical delta power and local sleep regulatory circuits are or not connected to synchronize rebounds following sleep deprivation; and whether astrocytes might actively participate in regulating sleep in the LPO area.

In the second results Chapter (Chapter 4), *in vivo* calcium recordings in freely moving animals has allowed me to investigate the Ca^{2+} activity of LPO neurons during behavioural states and Dex induced sedation. Different subtypes of LPO neurons showed marked synchronized Ca^{2+} activity during REM sleep rather than during NREM sleep. The PO area has been mostly studied in association to NREM sleep regulation, although some reports have shown, either by cFos IHC or by local unit recordings [77, 145], that LPO neurons are active during REM sleep. These published data together with my new findings might be suggesting a new role of LPO in mediating an ascending pathway for REM sleep generation. Interestingly, PO neurons expressing Vgat or Nos1 have also a synchronised 0.1 Hz Ca^{2+} activation pattern under Dex injection, in particular at the onset of the sedative state. These results confirm LPO neurons role in inducing NREM-like sedation, although it is still unclear how these calcium activity patterns fit with the selectively REM-active nature of LPO neurons during baseline conditions.

More experiments performed with higher resolution could also be important to better elucidate LPO neurons activity. Using both fluorescent voltage sensors and electrodes implanted directly in LPO, I could record action potentials and neuronal activation more reliably. Also, it would be interesting to connect the calcium activity data to the effects caused by the deletion of the NMDA receptor from LPO neurons. The NMDAr is, in fact, one of the major sources of intracellular calcium influxes in neuronal cells, and its deletion from LPO neurons causes a very dramatic reduction in REM sleep, when I observed the highest calcium activity in LPO. It is possible that the synchronized increase in intracellular calcium in LPO neurons during REM sleep is the necessary mechanism that maintains this behavioural state. Photometry recordings obtained exclusively from neurons lacking the NMDA receptor could help us understanding whether REM sleep can still occur under low intracellular calcium concentrations.

In the third and final results Chapter (Chapter 5), I have studied the role of the LHb neurons, and the Grm2 expressing ones, in regulating sleep and sedation. Using *in vivo* photometry recordings I observed that LHb circuits are active during wake and REM sleep, with almost no signal recorded during NREM sleep. Using *in vivo* optogenetic, I artificially stimulated the same circuits to understand whether LHb increased neuronal calcium activity was only a passive effect or whether these neurons were actively involved in generating wake and REM sleep. When activated by blue pulsating light, LHb neurons induced wakefulness mostly during shorter trains of stimulations, and REM sleep during longer ones. When Grm2 neurons were stimulated, NREM sleep occurred in between simulations, something that was not observed when stimulating all LHb neurons. These data suggest that Grm2 neurons are permissive to NREM sleep while they actively participate in the generation of REM sleep and wakefulness.

These data can once again be related to the results obtained in the previous chapters. Both LPO and LHb neurons increase their intracellular calcium during REM sleep, and these two areas are tightly connected to each other, with reciprocal direct projections [198]. It is possible that LPO is the upstream node to the LHb in the ascending pathway regulating REM sleep, and that increased intracellular calcium is one of the main signals activating this circuit, possibly through the NMDA receptor. Activity manipulations of LHb neurons receiving afferent projections from LPO and *vice versa* could demonstrate whether these two areas are connected in regulating REM sleep and what is their hierarchical position in the ascending circuits regulating cortical theta activity.

With future projects and experiments, and with the collaboration of my colleagues, we will attempt to give an answer to all these questions.

References

1. Havekes, R., et al., *Sleep deprivation causes memory deficits by negatively impacting neuronal connectivity in hippocampal area CA1.* Elife, 2016. **5**.
2. Rasch, B. and J. Born, *About sleep's role in memory.* Physiol Rev, 2013. **93**(2): p. 681-766.
3. Killgore, W.D., *Effects of sleep deprivation on cognition.* Prog Brain Res, 2010. **185**: p. 105-29.
4. Lo, J.C., et al., *Effects of partial and acute total sleep deprivation on performance across cognitive domains, individuals and circadian phase.* PLoS One, 2012. **7**(9): p. e45987.
5. Nollet, M., et al., *REM sleep's unique associations with corticosterone regulation, apoptotic pathways, and behavior in chronic stress in mice.* Proc Natl Acad Sci U S A, 2019. **116**(7): p. 2733-2742.
6. Xie, L., et al., *Sleep drives metabolite clearance from the adult brain.* Science, 2013. **342**(6156): p. 373-7.
7. Tononi, G. and C. Cirelli, *Sleep and synaptic down-selection.* Eur J Neurosci, 2019.
8. Arrigoni, E., et al., *Long-term synaptic plasticity is impaired in rats with lesions of the ventrolateral preoptic nucleus.* Eur J Neurosci, 2009. **30**(11): p. 2112-20.
9. Davies, S.K., et al., *Effect of sleep deprivation on the human metabolome.* Proc Natl Acad Sci U S A, 2014. **111**(29): p. 10761-6.
10. Besedovsky, L., T. Lange, and J. Born, *Sleep and immune function.* Pflugers Arch, 2012. **463**(1): p. 121-37.
11. McAlpine, C.S., et al., *Sleep modulates haematopoiesis and protects against atherosclerosis.* Nature, 2019. **566**(7744): p. 383-387.
12. Basner, M., et al., *Sleep deprivation and neurobehavioral dynamics.* Curr Opin Neurobiol, 2013. **23**(5): p. 854-63.
13. Watson, N.F., et al., *Sleep duration and depressive symptoms: a gene-environment interaction.* Sleep, 2014. **37**(2): p. 351-8.

14. O'Leary, K., et al., *Sleep quality in healthy and mood-disordered persons predicts daily life emotional reactivity.* Cogn Emot, 2017. **31**(3): p. 435-443.
15. Shan, Z., et al., *Sleep duration and risk of type 2 diabetes: a meta-analysis of prospective studies.* Diabetes Care, 2015. **38**(3): p. 529-37.
16. Cappuccio, F.P., et al., *Meta-analysis of short sleep duration and obesity in children and adults.* Sleep, 2008. **31**(5): p. 619-26.
17. Blask, D.E., *Melatonin, sleep disturbance and cancer risk.* Sleep Med Rev, 2009. **13**(4): p. 257-64.
18. Cappuccio, F.P., et al., *Sleep duration predicts cardiovascular outcomes: a systematic review and meta-analysis of prospective studies.* Eur Heart J, 2011. **32**(12): p. 1484-92.
19. Zhu, Y., et al., *Chronic Sleep Disruption Advances the Temporal Progression of Tauopathy in P301S Mutant Mice.* J Neurosci, 2018. **38**(48): p. 10255-10270.
20. Zhu, Y., et al., *Degeneration in Arousal Neurons in Chronic Sleep Disruption Modeling Sleep Apnea.* Front Neurol, 2015. **6**: p. 109.
21. Keene, A.C. and E.R. Duboue, *The origins and evolution of sleep.* J Exp Biol, 2018. **221**(Pt 11).
22. Kim, E.J., et al., *Improved Monosynaptic Neural Circuit Tracing Using Engineered Rabies Virus Glycoproteins.* Cell Rep, 2016. **15**(4): p. 692-699.
23. Lin, R., et al., *Cell-type-specific and projection-specific brain-wide reconstruction of single neurons.* Nat Methods, 2018. **15**(12): p. 1033-1036.
24. Dana, H., et al., *High-performance calcium sensors for imaging activity in neuronal populations and microcompartments.* Nat Methods, 2019.
25. Bayguinov, P.O., et al., *Imaging Voltage in Genetically Defined Neuronal Subpopulations with a Cre Recombinase-Targeted Hybrid Voltage Sensor.* J Neurosci, 2017. **37**(38): p. 9305-9319.
26. Achermann, P. and A.A. Borbely, *Mathematical models of sleep regulation.* Front Biosci, 2003. **8**: p. s683-93.
27. Borbely, A.A., et al., *The two-process model of sleep regulation: a reappraisal.* J Sleep Res, 2016. **25**(2): p. 131-43.
28. Leemburg, S., et al., *Sleep homeostasis in the rat is preserved during chronic sleep restriction.* Proc Natl Acad Sci U S A, 2010. **107**(36): p. 15939-44.

29. Gooley, J.J., et al., *Melanopsin in cells of origin of the retinohypothalamic tract.* Nat Neurosci, 2001. **4**(12): p. 1165.
30. Sollars, P.J., et al., *Melanopsin and non-melanopsin expressing retinal ganglion cells innervate the hypothalamic suprachiasmatic nucleus.* Vis Neurosci, 2003. **20**(6): p. 601-10.
31. Mistlberger, R.E., *Circadian regulation of sleep in mammals: role of the suprachiasmatic nucleus.* Brain Res Brain Res Rev, 2005. **49**(3): p. 429-54.
32. Eban-Rothschild, A., W.J. Giardino, and L. de Lecea, *To sleep or not to sleep: neuronal and ecological insights.* Curr Opin Neurobiol, 2017. **44**: p. 132-138.
33. Arrigoni, E., M.C. Chen, and P.M. Fuller, *The anatomical, cellular and synaptic basis of motor atonia during rapid eye movement sleep.* J Physiol, 2016. **594**(19): p. 5391-414.
34. Weber, F. and Y. Dan, *Circuit-based interrogation of sleep control.* Nature, 2016. **538**(7623): p. 51-59.
35. Luppi, P.H., C. Peyron, and P. Fort, *Not a single but multiple populations of GABAergic neurons control sleep.* Sleep Med Rev, 2017. **32**: p. 85-94.
36. Peever, J. and P.M. Fuller, *The Biology of REM Sleep.* Curr Biol, 2017. **27**(22): p. R1237-R1248.
37. Scammell, T.E., E. Arrigoni, and J.O. Lipton, *Neural Circuitry of Wakefulness and Sleep.* Neuron, 2017. **93**(4): p. 747-765.
38. Eban-Rothschild, A., L. Appelbaum, and L. de Lecea, *Neuronal Mechanisms for Sleep/Wake Regulation and Modulatory Drive.* Neuropsychopharmacology, 2018. **43**(5): p. 937-952.
39. Liu, D. and Y. Dan, *A Motor Theory of Sleep-Wake Control: Arousal-Action Circuit.* Annu Rev Neurosci, 2019.
40. Lorincz, M.L. and A.R. Adamantidis, *Monoaminergic control of brain states and sensory processing: Existing knowledge and recent insights obtained with optogenetics.* Prog Neurobiol, 2017. **151**: p. 237-253.
41. Ma, S., et al., *Dual-transmitter systems regulating arousal, attention, learning and memory.* Neurosci Biobehav Rev, 2018. **85**: p. 21-33.
42. Fuxe, K. and D.O. Borroto-Escuela, *Volume transmission and receptor-receptor interactions in heteroreceptor complexes: understanding the role of new concepts for brain communication.* Neural Regen Res, 2016. **11**(8): p. 1220-3.

43. Yu, X., et al., *Wakefulness Is Governed by GABA and Histamine Cotransmission.* Neuron, 2015. **87**(1): p. 164-78.
44. Jones, E.G., *A new view of specific and nonspecific thalamocortical connections.* Adv Neurol, 1998. **77**: p. 49-71; discussion 72-3.
45. Carter, M.E., et al., *Tuning arousal with optogenetic modulation of locus coeruleus neurons.* Nat Neurosci, 2010. **13**(12): p. 1526-33.
46. Ito, H., et al., *Analysis of sleep disorders under pain using an optogenetic tool: possible involvement of the activation of dorsal raphe nucleus-serotonergic neurons.* Mol Brain, 2013. **6**: p. 59.
47. Eban-Rothschild, A., et al., *VTA dopaminergic neurons regulate ethologically relevant sleep-wake behaviors.* Nat Neurosci, 2016. **19**(10): p. 1356-66.
48. Dahan, L., et al., *Prominent burst firing of dopaminergic neurons in the ventral tegmental area during paradoxical sleep.* Neuropsychopharmacology, 2007. **32**(6): p. 1232-41.
49. Xu, M., et al., *Basal forebrain circuit for sleep-wake control.* Nat Neurosci, 2015. **18**(11): p. 1641-7.
50. Yu, X., N.P. Franks, and W. Wisden, *Sleep and Sedative States Induced by Targeting the Histamine and Noradrenergic Systems.* Front Neural Circuits, 2018. **12**: p. 4.
51. Williams, R.H., et al., *Optogenetic-mediated release of histamine reveals distal and autoregulatory mechanisms for controlling arousal.* J Neurosci, 2014. **34**(17): p. 6023-9.
52. Lu, J., T.C. Jhou, and C.B. Saper, *Identification of wake-active dopaminergic neurons in the ventral periaqueductal gray matter.* J Neurosci, 2006. **26**(1): p. 193-202.
53. Cho, J.R., et al., *Dorsal Raphe Dopamine Neurons Modulate Arousal and Promote Wakefulness by Salient Stimuli.* Neuron, 2017. **94**(6): p. 1205-1219 e8.
54. Yu, X., et al., *GABA and glutamate neurons in the VTA regulate sleep and wakefulness.* Nat Neurosci, 2019. **22**(1): p. 106-119.
55. Yu, X., et al., *Circadian factor BMAL1 in histaminergic neurons regulates sleep architecture.* Curr Biol, 2014. **24**(23): p. 2838-44.
56. Yu, X., et al., *Genetic lesioning of histamine neurons increases sleep-wake fragmentation and reveals their contribution to modafinil-induced wakefulness.* Sleep, 2019. **42**(5).

57. Kroeger, D., et al., *Cholinergic, Glutamatergic, and GABAergic Neurons of the Pedunculopontine Tegmental Nucleus Have Distinct Effects on Sleep/Wake Behavior in Mice.* J Neurosci, 2017. **37**(5): p. 1352-1366.
58. Zant, J.C., et al., *Cholinergic Neurons in the Basal Forebrain Promote Wakefulness by Actions on Neighboring Non-Cholinergic Neurons: An Opto-Dialysis Study.* J Neurosci, 2016. **36**(6): p. 2057-67.
59. Buzsaki, G., et al., *Nucleus basalis and thalamic control of neocortical activity in the freely moving rat.* J Neurosci, 1988. **8**(11): p. 4007-26.
60. Fuller, P.M., et al., *Reassessment of the structural basis of the ascending arousal system.* J Comp Neurol, 2011. **519**(5): p. 933-56.
61. Anaclet, C., et al., *Basal forebrain control of wakefulness and cortical rhythms.* Nat Commun, 2015. **6**: p. 8744.
62. Venner, A., et al., *A Novel Population of Wake-Promoting GABAergic Neurons in the Ventral Lateral Hypothalamus.* Curr Biol, 2016. **26**(16): p. 2137-43.
63. Branch, A.F., et al., *Progressive Loss of the Orexin Neurons Reveals Dual Effects on Wakefulness.* Sleep, 2016. **39**(2): p. 369-77.
64. Adamantidis, A.R., et al., *Neural substrates of awakening probed with optogenetic control of hypocretin neurons.* Nature, 2007. **450**(7168): p. 420-4.
65. Sasaki, K., et al., *Pharmacogenetic modulation of orexin neurons alters sleep/wakefulness states in mice.* PLoS One, 2011. **6**(5): p. e20360.
66. Von Economo, C., *Sleep as a problem of localization.* The Journal of Nervous and Mental disease, 1930. **71**(3): p. 249-259.
67. Nauta, W.J., *Hypothalamic regulation of sleep in rats; an experimental study.* J Neurophysiol, 1946. **9**: p. 285-316.
68. McGinty, D.J. and M.B. Sterman, *Sleep suppression after basal forebrain lesions in the cat.* Science, 1968. **160**(3833): p. 1253-5.
69. Sherin, J.E., et al., *Activation of ventrolateral preoptic neurons during sleep.* Science, 1996. **271**(5246): p. 216-9.
70. Gong, H., et al., *Activation of c-fos in GABAergic neurones in the preoptic area during sleep and in response to sleep deprivation.* J Physiol, 2004. **556**(Pt 3): p. 935-46.
71. Lu, J., et al., *Effect of lesions of the ventrolateral preoptic nucleus on NREM and REM sleep.* J Neurosci, 2000. **20**(10): p. 3830-42.

72. Zhang, Z., et al., *Neuronal ensembles sufficient for recovery sleep and the sedative actions of alpha2 adrenergic agonists.* Nat Neurosci, 2015. **18**(4): p. 553-561.
73. Sherin, J.E., et al., *Innervation of histaminergic tuberomammillary neurons by GABAergic and galaninergic neurons in the ventrolateral preoptic nucleus of the rat.* J Neurosci, 1998. **18**(12): p. 4705-21.
74. Yoshida, K., et al., *Afferents to the orexin neurons of the rat brain.* J Comp Neurol, 2006. **494**(5): p. 845-61.
75. Steininger, T.L., et al., *Subregional organization of preoptic area/anterior hypothalamic projections to arousal-related monoaminergic cell groups.* J Comp Neurol, 2001. **429**(4): p. 638-53.
76. Chou, T.C., et al., *Afferents to the ventrolateral preoptic nucleus.* J Neurosci, 2002. **22**(3): p. 977-90.
77. Lu, J., et al., *Selective activation of the extended ventrolateral preoptic nucleus during rapid eye movement sleep.* J Neurosci, 2002. **22**(11): p. 4568-76.
78. Szymusiak, R., et al., *Sleep-waking discharge patterns of ventrolateral preoptic/anterior hypothalamic neurons in rats.* Brain Res, 1998. **803**(1-2): p. 178-88.
79. Takahashi, K., J.S. Lin, and K. Sakai, *Characterization and mapping of sleep-waking specific neurons in the basal forebrain and preoptic hypothalamus in mice.* Neuroscience, 2009. **161**(1): p. 269-92.
80. Modirrousta, M., L. Mainville, and B.E. Jones, *Gabaergic neurons with alpha2-adrenergic receptors in basal forebrain and preoptic area express c-Fos during sleep.* Neuroscience, 2004. **129**(3): p. 803-10.
81. Harding, E.C., et al., *A Neuronal Hub Binding Sleep Initiation and Body Cooling in Response to a Warm External Stimulus.* Curr Biol, 2018. **28**(14): p. 2263-2273 e4.
82. Alam, M.N., D. McGinty, and R. Szymusiak, *Preoptic/anterior hypothalamic neurons: thermosensitivity in rapid eye movement sleep.* Am J Physiol, 1995. **269**(5 Pt 2): p. R1250-7.
83. Boulant, J.A. and J.B. Dean, *Temperature receptors in the central nervous system.* Annu Rev Physiol, 1986. **48**: p. 639-54.
84. Wu, Z., et al., *Galanin neurons in the medial preoptic area govern parental behaviour.* Nature, 2014. **509**(7500): p. 325-30.

85. Anaclet, C., et al., *The GABAergic parafacial zone is a medullary slow wave sleep-promoting center.* Nat Neurosci, 2014. **17**(9): p. 1217-24.
86. Manns, I.D., A. Alonso, and B.E. Jones, *Discharge properties of juxtacellularly labeled and immunohistochemically identified cholinergic basal forebrain neurons recorded in association with the electroencephalogram in anesthetized rats.* J Neurosci, 2000. **20**(4): p. 1505-18.
87. Takata, Y., et al., *Sleep and Wakefulness Are Controlled by Ventral Medial Midbrain/Pons GABAergic Neurons in Mice.* J Neurosci, 2018. **38**(47): p. 10080-10092.
88. Chowdhury, S., et al., *GABA neurons in the ventral tegmental area regulate non-rapid eye movement sleep in mice.* Elife, 2019. **8**.
89. Chen, K.S., et al., *A Hypothalamic Switch for REM and Non-REM Sleep.* Neuron, 2018. **97**(5): p. 1168-1176 e4.
90. Liu, K., et al., *Lhx6-positive GABA-releasing neurons of the zona incerta promote sleep.* Nature, 2017. **548**(7669): p. 582-587.
91. Ma, C., et al., *Sleep Regulation by Neurotensinergic Neurons in a Thalamo-Amygdala Circuit.* Neuron, 2019.
92. Oishi, Y., et al., *Slow-wave sleep is controlled by a subset of nucleus accumbens core neurons in mice.* Nat Commun, 2017. **8**(1): p. 734.
93. Yuan, X.S., et al., *Striatal adenosine A2A receptor neurons control active-period sleep via parvalbumin neurons in external globus pallidus.* Elife, 2017. **6**.
94. Weber, F., et al., *Regulation of REM and Non-REM Sleep by Periaqueductal GABAergic Neurons.* Nat Commun, 2018. **9**(1): p. 354.
95. Crick, F. and G. Mitchison, *The function of dream sleep.* Nature, 1983. **304**(5922): p. 111-4.
96. Kennedy, D. and C. Norman, *What don't we know?* Science, 2005. **309**(5731): p. 75.
97. Marks, G.A., et al., *A functional role for REM sleep in brain maturation.* Behav Brain Res, 1995. **69**(1-2): p. 1-11.
98. Lu, J., et al., *A putative flip-flop switch for control of REM sleep.* Nature, 2006. **441**(7093): p. 589-94.
99. Krenzer, M., et al., *Brainstem and spinal cord circuitry regulating REM sleep and muscle atonia.* PLoS One, 2011. **6**(10): p. e24998.

100. Grace, K.P., L.E. Vanstone, and R.L. Horner, *Endogenous cholinergic input to the pontine REM sleep generator is not required for REM sleep to occur.* J Neurosci, 2014. **34**(43): p. 14198-209.

101. Holmes, C.J. and B.E. Jones, *Importance of cholinergic, GABAergic, serotonergic and other neurons in the medial medullary reticular formation for sleep-wake states studied by cytotoxic lesions in the cat.* Neuroscience, 1994. **62**(4): p. 1179-200.

102. Sapin, E., et al., *Localization of the brainstem GABAergic neurons controlling paradoxical (REM) sleep.* PLoS One, 2009. **4**(1): p. e4272.

103. Capelli, P., et al., *Locomotor speed control circuits in the caudal brainstem.* Nature, 2017. **551**(7680): p. 373-377.

104. Magoun, H.W. and R. Rhines, *An inhibitory mechanism in the bulbar reticular formation.* J Neurophysiol, 1946. **9**: p. 165-71.

105. Schenkel, E. and J.M. Siegel, *REM sleep without atonia after lesions of the medial medulla.* Neurosci Lett, 1989. **98**(2): p. 159-65.

106. Vetrivelan, R., et al., *Melanin-concentrating hormone neurons specifically promote rapid eye movement sleep in mice.* Neuroscience, 2016. **336**: p. 102-113.

107. Jego, S., et al., *Optogenetic identification of a rapid eye movement sleep modulatory circuit in the hypothalamus.* Nat Neurosci, 2013. **16**(11): p. 1637-43.

108. Chee, M.J., E. Arrigoni, and E. Maratos-Flier, *Melanin-concentrating hormone neurons release glutamate for feedforward inhibition of the lateral septum.* J Neurosci, 2015. **35**(8): p. 3644-51.

109. Ishimori, K., *True cause of sleep: a hypnogenic substance as evidenced in the brain of sleep-deprived animals.* Tokyo Igakkai Zasshi, 1909. **23**: p. 429-457.

110. Legendre, R.P., H, *Recherches sur le besoin de sommeil consécutif à une veille prolongée.* Z. Allg. Physiol., 1913. **14**: p. 235-262.

111. Clasadonte, J., et al., *Chronic sleep restriction disrupts sleep homeostasis and behavioral sensitivity to alcohol by reducing the extracellular accumulation of adenosine.* J Neurosci, 2014. **34**(5): p. 1879-91.

112. Davis, C.J., et al., *The neuron-specific interleukin-1 receptor accessory protein is required for homeostatic sleep and sleep responses to influenza viral challenge in mice.* Brain Behav Immun, 2015. **47**: p. 35-43.

113. Imeri, L. and M.R. Opp, *How (and why) the immune system makes us sleep.* Nat Rev Neurosci, 2009. **10**(3): p. 199-210.

114. Rockstrom, M.D., et al., *Tumor necrosis factor alpha in sleep regulation.* Sleep Med Rev, 2018. **40**: p. 69-78.
115. Urade, Y., et al., *Sleep regulation in adenosine A2A receptor-deficient mice.* Neurology, 2003. **61**(11 Suppl 6): p. S94-6.
116. Bjorness, T.E., et al., *Control and function of the homeostatic sleep response by adenosine A1 receptors.* J Neurosci, 2009. **29**(5): p. 1267-76.
117. Bjorness, T.E., et al., *An Adenosine-Mediated Glial-Neuronal Circuit for Homeostatic Sleep.* J Neurosci, 2016. **36**(13): p. 3709-21.
118. Stenberg, D., et al., *Sleep and its homeostatic regulation in mice lacking the adenosine A1 receptor.* J Sleep Res, 2003. **12**(4): p. 283-90.
119. Leenaars, C.H.C., et al., *Intracerebral Adenosine During Sleep Deprivation: A Meta-Analysis and New Experimental Data.* J Circadian Rhythms, 2018. **16**: p. 11.
120. Halassa, M.M., et al., *Astrocytic modulation of sleep homeostasis and cognitive consequences of sleep loss.* Neuron, 2009. **61**(2): p. 213-9.
121. Schmitt, L.I., et al., *Wakefulness affects synaptic and network activity by increasing extracellular astrocyte-derived adenosine.* J Neurosci, 2012. **32**(13): p. 4417-25.
122. Morairty, S.R., et al., *A role for cortical nNOS/NK1 neurons in coupling homeostatic sleep drive to EEG slow wave activity.* Proc Natl Acad Sci U S A, 2013. **110**(50): p. 20272-7.
123. Gerashchenko, D., et al., *Identification of a population of sleep-active cerebral cortex neurons.* Proc Natl Acad Sci U S A, 2008. **105**(29): p. 10227-32.
124. Scammell, T., et al., *Activation of ventrolateral preoptic neurons by the somnogen prostaglandin D2.* Proc Natl Acad Sci U S A, 1998. **95**(13): p. 7754-9.
125. Franken, P., D. Chollet, and M. Tafti, *The homeostatic regulation of sleep need is under genetic control.* J Neurosci, 2001. **21**(8): p. 2610-21.
126. Franken, P., *A role for clock genes in sleep homeostasis.* Curr Opin Neurobiol, 2013. **23**(5): p. 864-72.
127. Hasan, S., et al., *A human sleep homeostasis phenotype in mice expressing a primate-specific PER3 variable-number tandem-repeat coding-region polymorphism.* FASEB J, 2014. **28**(6): p. 2441-54.
128. Funato, H., et al., *Forward-genetics analysis of sleep in randomly mutagenized mice.* Nature, 2016. **539**(7629): p. 378-383.

129. Mang, G.M., et al., *Altered Sleep Homeostasis in Rev-erbalpha Knockout Mice.* Sleep, 2016. **39**(3): p. 589-601.
130. Holst, S.C., et al., *Cerebral mGluR5 availability contributes to elevated sleep need and behavioral adjustment after sleep deprivation.* Elife, 2017. **6**.
131. Wang, Z., et al., *Quantitative phosphoproteomic analysis of the molecular substrates of sleep need.* Nature, 2018. **558**(7710): p. 435-439.
132. Siclari, F. and G. Tononi, *Local aspects of sleep and wakefulness.* Curr Opin Neurobiol, 2017. **44**: p. 222-227.
133. Krueger, J.M., et al., *Local sleep.* Sleep Med Rev, 2019. **43**: p. 14-21.
134. Deboer, T., *Behavioral and electrophysiological correlates of sleep and sleep homeostasis.* Curr Top Behav Neurosci, 2015. **25**: p. 1-24.
135. Kim, Y., et al., *Repeated sleep restriction in rats leads to homeostatic and allostatic responses during recovery sleep.* Proc Natl Acad Sci U S A, 2007. **104**(25): p. 10697-702.
136. Stephenson, R., A.M. Caron, and S. Famina, *Behavioral sleep-wake homeostasis and EEG delta power are decoupled by chronic sleep restriction in the rat.* Sleep, 2015. **38**(5): p. 685-97.
137. Benington, J.H. and H.C. Heller, *REM-sleep timing is controlled homeostatically by accumulation of REM-sleep propensity in non-REM sleep.* Am J Physiol, 1994. **266**(6 Pt 2): p. R1992-2000.
138. Donlea, J.M., et al., *Inducing sleep by remote control facilitates memory consolidation in Drosophila.* Science, 2011. **332**(6037): p. 1571-6.
139. Donlea, J.M., D. Pimentel, and G. Miesenbock, *Neuronal Machinery of Sleep Homeostasis in Drosophila.* Neuron, 2014. **81**(6): p. 1442.
140. Pimentel, D., et al., *Operation of a homeostatic sleep switch.* Nature, 2016. **536**(7616): p. 333-337.
141. Kempf, A., et al., *A potassium channel beta-subunit couples mitochondrial electron transport to sleep.* Nature, 2019. **568**(7751): p. 230-234.
142. Steinberg, E.A., et al., *The role of K(2)p channels in anaesthesia and sleep.* Pflugers Arch, 2015. **467**(5): p. 907-16.
143. Liu, S., et al., *Sleep Drive Is Encoded by Neural Plastic Changes in a Dedicated Circuit.* Cell, 2016. **165**(6): p. 1347-60.

144. Tatsuki, F., et al., *Involvement of Ca(2+)-Dependent Hyperpolarization in Sleep Duration in Mammals.* Neuron, 2016. **90**(1): p. 70-85.

145. Alam, M.A., et al., *Neuronal activity in the preoptic hypothalamus during sleep deprivation and recovery sleep.* J Neurophysiol, 2014. **111**(2): p. 287-99.

146. Chamberlin, N.L., et al., *Effects of adenosine on gabaergic synaptic inputs to identified ventrolateral preoptic neurons.* Neuroscience, 2003. **119**(4): p. 913-8.

147. Gallopin, T., et al., *The endogenous somnogen adenosine excites a subset of sleep-promoting neurons via A2A receptors in the ventrolateral preoptic nucleus.* Neuroscience, 2005. **134**(4): p. 1377-90.

148. Ma Y., M.G., Yu X., Harding E., Miao A., Yustos R., Vyssotski A., Franks N.P., Wisden W., *Galanin neurons in the hypothalamus link sleep homeostasis, body temperature and actions of the a2 adrenergic agonist dexmedetomidine.* Curr Biol, 2019. **29**: p. 1-8.

149. Bliss, T.V. and T. Lomo, *Long-lasting potentiation of synaptic transmission in the dentate area of the anaesthetized rabbit following stimulation of the perforant path.* J Physiol, 1973. **232**(2): p. 331-56.

150. van Huijstee, A.N. and H.D. Mansvelder, *Glutamatergic synaptic plasticity in the mesocorticolimbic system in addiction.* Front Cell Neurosci, 2014. **8**: p. 466.

151. Goelet, P., et al., *The long and the short of long-term memory--a molecular framework.* Nature, 1986. **322**(6078): p. 419-22.

152. Baltaci, S.B., R. Mogulkoc, and A.K. Baltaci, *Molecular Mechanisms of Early and Late LTP.* Neurochem Res, 2019. **44**(2): p. 281-296.

153. Sutton, M.A., et al., *Interaction between amount and pattern of training in the induction of intermediate- and long-term memory for sensitization in aplysia.* Learn Mem, 2002. **9**(1): p. 29-40.

154. Kukushkin, N.V. and T.J. Carew, *Memory Takes Time.* Neuron, 2017. **95**(2): p. 259-279.

155. Mayer, M.L., G.L. Westbrook, and P.B. Guthrie, *Voltage-dependent block by Mg2+ of NMDA responses in spinal cord neurones.* Nature, 1984. **309**(5965): p. 261-3.

156. Nowak, L., et al., *Magnesium gates glutamate-activated channels in mouse central neurones.* Nature, 1984. **307**(5950): p. 462-5.

157. Johnson, J.W. and P. Ascher, *Glycine potentiates the NMDA response in cultured mouse brain neurons.* Nature, 1987. **325**(6104): p. 529-31.

158. Forrest, D., et al., *Targeted disruption of NMDA receptor 1 gene abolishes NMDA response and results in neonatal death.* Neuron, 1994. **13**(2): p. 325-38.
159. Attwell, D. and A. Gibb, *Neuroenergetics and the kinetic design of excitatory synapses.* Nat Rev Neurosci, 2005. **6**(11): p. 841-9.
160. Traynelis, S.F., et al., *Glutamate receptor ion channels: structure, regulation, and function.* Pharmacol Rev, 2010. **62**(3): p. 405-96.
161. Morris, R.G., et al., *Selective impairment of learning and blockade of long-term potentiation by an N-methyl-D-aspartate receptor antagonist, AP5.* Nature, 1986. **319**(6056): p. 774-6.
162. Tsien, J.Z., P.T. Huerta, and S. Tonegawa, *The essential role of hippocampal CA1 NMDA receptor-dependent synaptic plasticity in spatial memory.* Cell, 1996. **87**(7): p. 1327-38.
163. Bliss, T.V. and G.L. Collingridge, *A synaptic model of memory: long-term potentiation in the hippocampus.* Nature, 1993. **361**(6407): p. 31-9.
164. Lisman, J., R. Yasuda, and S. Raghavachari, *Mechanisms of CaMKII action in long-term potentiation.* Nat Rev Neurosci, 2012. **13**(3): p. 169-82.
165. Chang, J.Y., et al., *Mechanisms of Ca(2+)/calmodulin-dependent kinase II activation in single dendritic spines.* Nat Commun, 2019. **10**(1): p. 2784.
166. Shipton, O.A. and O. Paulsen, *GluN2A and GluN2B subunit-containing NMDA receptors in hippocampal plasticity.* Philos Trans R Soc Lond B Biol Sci, 2014. **369**(1633): p. 20130163.
167. Cull-Candy, S., L. Kelly, and M. Farrant, *Regulation of Ca2+-permeable AMPA receptors: synaptic plasticity and beyond.* Curr Opin Neurobiol, 2006. **16**(3): p. 288-97.
168. Huganir, R.L. and R.A. Nicoll, *AMPARs and synaptic plasticity: the last 25 years.* Neuron, 2013. **80**(3): p. 704-17.
169. Penn, A.C., et al., *Hippocampal LTP and contextual learning require surface diffusion of AMPA receptors.* Nature, 2017. **549**(7672): p. 384-388.
170. Divakaruni, S.S., et al., *Long-Term Potentiation Requires a Rapid Burst of Dendritic Mitochondrial Fission during Induction.* Neuron, 2018. **100**(4): p. 860-875 e7.
171. Parkhurst, C.N., et al., *Microglia promote learning-dependent synapse formation through brain-derived neurotrophic factor.* Cell, 2013. **155**(7): p. 1596-609.

172. Allen, N.J. and C. Eroglu, *Cell Biology of Astrocyte-Synapse Interactions.* Neuron, 2017. **96**(3): p. 697-708.
173. Whitlock, J.R., et al., *Learning induces long-term potentiation in the hippocampus.* Science, 2006. **313**(5790): p. 1093-7.
174. Doyere, V., et al., *Synapse-specific reconsolidation of distinct fear memories in the lateral amygdala.* Nat Neurosci, 2007. **10**(4): p. 414-6.
175. Tye, K.M., et al., *Rapid strengthening of thalamo-amygdala synapses mediates cue-reward learning.* Nature, 2008. **453**(7199): p. 1253-7.
176. Cooke, S.F. and M.F. Bear, *Visual experience induces long-term potentiation in the primary visual cortex.* J Neurosci, 2010. **30**(48): p. 16304-13.
177. Vashchinkina, E., et al., *GABAA receptor drugs and neuronal plasticity in reward and aversion: focus on the ventral tegmental area.* Front Pharmacol, 2014. **5**: p. 256.
178. Kullmann, D.M. and K.P. Lamsa, *LTP and LTD in cortical GABAergic interneurons: emerging rules and roles.* Neuropharmacology, 2011. **60**(5): p. 712-9.
179. Chiu, C.Q., A. Barberis, and M.J. Higley, *Preserving the balance: diverse forms of long-term GABAergic synaptic plasticity.* Nat Rev Neurosci, 2019. **20**(5): p. 272-281.
180. Turrigiano, G., *Homeostatic synaptic plasticity: local and global mechanisms for stabilizing neuronal function.* Cold Spring Harb Perspect Biol, 2012. **4**(1): p. a005736.
181. Tononi, G. and C. Cirelli, *Sleep and the price of plasticity: from synaptic and cellular homeostasis to memory consolidation and integration.* Neuron, 2014. **81**(1): p. 12-34.
182. Liu, Z.W., et al., *Direct evidence for wake-related increases and sleep-related decreases in synaptic strength in rodent cortex.* J Neurosci, 2010. **30**(25): p. 8671-5.
183. de Vivo, L., et al., *Ultrastructural evidence for synaptic scaling across the wake/sleep cycle.* Science, 2017. **355**(6324): p. 507-510.
184. Diering, G.H., et al., *Homer1a drives homeostatic scaling-down of excitatory synapses during sleep.* Science, 2017. **355**(6324): p. 511-515.
185. Chauvette, S., J. Seigneur, and I. Timofeev, *Sleep oscillations in the thalamocortical system induce long-term neuronal plasticity.* Neuron, 2012. **75**(6): p. 1105-13.
186. Grosmark, A.D., et al., *REM sleep reorganizes hippocampal excitability.* Neuron, 2012. **75**(6): p. 1001-7.

187. Li, W., et al., *REM sleep selectively prunes and maintains new synapses in development and learning.* Nat Neurosci, 2017. **20**(3): p. 427-437.
188. Hengen, K.B., et al., *Neuronal Firing Rate Homeostasis Is Inhibited by Sleep and Promoted by Wake.* Cell, 2016. **165**(1): p. 180-191.
189. Watson, B.O., et al., *Network Homeostasis and State Dynamics of Neocortical Sleep.* Neuron, 2016. **90**(4): p. 839-52.
190. Vyazovskiy, V.V., et al., *Cortical firing and sleep homeostasis.* Neuron, 2009. **63**(6): p. 865-78.
191. Gais, S., et al., *Visual-procedural memory consolidation during sleep blocked by glutamatergic receptor antagonists.* J Neurosci, 2008. **28**(21): p. 5513-8.
192. Brown, E.N., R. Lydic, and N.D. Schiff, *General anesthesia, sleep, and coma.* N Engl J Med, 2010. **363**(27): p. 2638-50.
193. Akeju, O. and E.N. Brown, *Neural oscillations demonstrate that general anesthesia and sedative states are neurophysiologically distinct from sleep.* Curr Opin Neurobiol, 2017. **44**: p. 178-185.
194. Adams, R., et al., *Efficacy of dexmedetomidine compared with midazolam for sedation in adult intensive care patients: a systematic review.* Br J Anaesth, 2013. **111**(5): p. 703-10.
195. Bol, C., et al., *Pharmacokinetic-pharmacodynamic characterization of the cardiovascular, hypnotic, EEG and ventilatory responses to dexmedetomidine in the rat.* J Pharmacol Exp Ther, 1997. **283**(3): p. 1051-8.
196. Correa-Sales, C., B.C. Rabin, and M. Maze, *A hypnotic response to dexmedetomidine, an alpha 2 agonist, is mediated in the locus coeruleus in rats.* Anesthesiology, 1992. **76**(6): p. 948-52.
197. Segal, I.S., et al., *Dexmedetomidine diminishes halothane anesthetic requirements in rats through a postsynaptic alpha 2 adrenergic receptor.* Anesthesiology, 1988. **69**(6): p. 818-23.
198. Gelegen, C., et al., *Excitatory Pathways from the Lateral Habenula Enable Propofol-Induced Sedation.* Curr Biol, 2018. **28**(4): p. 580-587 e5.
199. Franks, N.P., *General anaesthesia: from molecular targets to neuronal pathways of sleep and arousal.* Nat Rev Neurosci, 2008. **9**(5): p. 370-86.

200. Belelli, D., et al., *The interaction of the general anesthetic etomidate with the gamma-aminobutyric acid type A receptor is influenced by a single amino acid.* Proc Natl Acad Sci U S A, 1997. **94**(20): p. 11031-6.

201. Mihic, S.J., et al., *Sites of alcohol and volatile anaesthetic action on GABA(A) and glycine receptors.* Nature, 1997. **389**(6649): p. 385-9.

202. Purdon, P.L., et al., *Electroencephalogram signatures of loss and recovery of consciousness from propofol.* Proc Natl Acad Sci U S A, 2013. **110**(12): p. E1142-51.

203. Baker, R., et al., *Altered activity in the central medial thalamus precedes changes in the neocortex during transitions into both sleep and propofol anesthesia.* J Neurosci, 2014. **34**(40): p. 13326-35.

204. Flores, F.J., et al., *Thalamocortical synchronization during induction and emergence from propofol-induced unconsciousness.* Proc Natl Acad Sci U S A, 2017. **114**(32): p. E6660-E6668.

205. Tung, A., B. Bluhm, and W.B. Mendelson, *Sleep inducing effects of propofol microinjection into the medial preoptic area are blocked by flumazenil.* Brain Res, 2001. **908**(2): p. 155-60.

206. Nelson, L.E., et al., *The sedative component of anesthesia is mediated by GABA(A) receptors in an endogenous sleep pathway.* Nat Neurosci, 2002. **5**(10): p. 979-84.

207. Uygun, D.S., et al., *Bottom-Up versus Top-Down Induction of Sleep by Zolpidem Acting on Histaminergic and Neocortex Neurons.* J Neurosci, 2016. **36**(44): p. 11171-11184.

208. Nelson, L.E., et al., *The alpha2-adrenoceptor agonist dexmedetomidine converges on an endogenous sleep-promoting pathway to exert its sedative effects.* Anesthesiology, 2003. **98**(2): p. 428-36.

209. Lu, J., et al., *Role of endogenous sleep-wake and analgesic systems in anesthesia.* J Comp Neurol, 2008. **508**(4): p. 648-62.

210. Moore, J.T., et al., *Direct activation of sleep-promoting VLPO neurons by volatile anesthetics contributes to anesthetic hypnosis.* Curr Biol, 2012. **22**(21): p. 2008-16.

211. Abulafia, R., V. Zalkind, and M. Devor, *Cerebral activity during the anesthesia-like state induced by mesopontine microinjection of pentobarbital.* J Neurosci, 2009. **29**(21): p. 7053-64.

212. Proulx, C.D., O. Hikosaka, and R. Malinow, *Reward processing by the lateral habenula in normal and depressive behaviors.* Nat Neurosci, 2014. **17**(9): p. 1146-52.

213. Zhao, H., et al., *The role of lateral habenula-dorsal raphe nucleus circuits in higher brain functions and psychiatric illness.* Behav Brain Res, 2015. **277**: p. 89-98.

214. Aizawa, H., et al., *The synchronous activity of lateral habenular neurons is essential for regulating hippocampal theta oscillation.* J Neurosci, 2013. **33**(20): p. 8909-21.

215. Aizawa, H., et al., *Hyperactivation of the habenula as a link between depression and sleep disturbance.* Front Hum Neurosci, 2013. **7**: p. 826.

216. Goldstein, R., *A GABAergic habenulo-raphe pathway mediation of the hypnogenic effects of vasotocin in cat.* Neuroscience, 1983. **10**(3): p. 941-5.

217. Faget, L., et al., *Afferent Inputs to Neurotransmitter-Defined Cell Types in the Ventral Tegmental Area.* Cell Rep, 2016. **15**(12): p. 2796-808.

218. Jhou, T.C., et al., *The rostromedial tegmental nucleus (RMTg), a GABAergic afferent to midbrain dopamine neurons, encodes aversive stimuli and inhibits motor responses.* Neuron, 2009. **61**(5): p. 786-800.

219. Gong, S., et al., *A gene expression atlas of the central nervous system based on bacterial artificial chromosomes.* Nature, 2003. **425**(6961): p. 917-25.

220. Schmidt, E.F., et al., *BAC transgenic mice and the GENSAT database of engineered mouse strains.* Cold Spring Harb Protoc, 2013. **2013**(3).

221. Vong, L., et al., *Leptin action on GABAergic neurons prevents obesity and reduces inhibitory tone to POMC neurons.* Neuron, 2011. **71**(1): p. 142-54.

222. Leshan, R.L., et al., *Leptin action through hypothalamic nitric oxide synthase-1-expressing neurons controls energy balance.* Nat Med, 2012. **18**(5): p. 820-3.

223. Abraham, N.M., et al., *Synaptic inhibition in the olfactory bulb accelerates odor discrimination in mice.* Neuron, 2010. **65**(3): p. 399-411.

224. Chen, T.W., et al., *Ultrasensitive fluorescent proteins for imaging neuronal activity.* Nature, 2013. **499**(7458): p. 295-300.

225. Krashes, M.J., et al., *Rapid, reversible activation of AgRP neurons drives feeding behavior in mice.* J Clin Invest, 2011. **121**(4): p. 1424-8.

226. Lee, J.H., et al., *Global and local fMRI signals driven by neurons defined optogenetically by type and wiring.* Nature, 2010. **465**(7299): p. 788-92.

227. Anisimov, V.N., et al., *Reconstruction of vocal interactions in a group of small songbirds.* Nat Methods, 2014. **11**(11): p. 1135-7.
228. Gelegen, C., et al., *Staying awake--a genetic region that hinders alpha2 adrenergic receptor agonist-induced sleep.* Eur J Neurosci, 2014. **40**(1): p. 2311-9.
229. Vyssotski, A.L., et al., *EEG responses to visual landmarks in flying pigeons.* Curr Biol, 2009. **19**(14): p. 1159-66.
230. Tobler, I., T. Deboer, and M. Fischer, *Sleep and sleep regulation in normal and prion protein-deficient mice.* J Neurosci, 1997. **17**(5): p. 1869-79.
231. Taylor, S., et al., *A practical approach to RT-qPCR-Publishing data that conform to the MIQE guidelines.* Methods, 2010. **50**(4): p. S1-5.
232. Livak, K.J. and T.D. Schmittgen, *Analysis of relative gene expression data using real-time quantitative PCR and the 2(-Delta Delta C(T)) Method.* Methods, 2001. **25**(4): p. 402-8.
233. Stegmeier, F., et al., *A lentiviral microRNA-based system for single-copy polymerase II-regulated RNA interference in mammalian cells.* Proc Natl Acad Sci U S A, 2005. **102**(37): p. 13212-7.
234. Kehoe, L.A., Y. Bernardinelli, and D. Muller, *GluN3A: an NMDA receptor subunit with exquisite properties and functions.* Neural Plast, 2013. **2013**: p. 145387.
235. Das, S., et al., *Increased NMDA current and spine density in mice lacking the NMDA receptor subunit NR3A.* Nature, 1998. **393**(6683): p. 377-81.
236. Tong, G., et al., *Modulation of NMDA receptor properties and synaptic transmission by the NR3A subunit in mouse hippocampal and cerebrocortical neurons.* J Neurophysiol, 2008. **99**(1): p. 122-32.
237. Roberts, A.C., et al., *Downregulation of NR3A-containing NMDARs is required for synapse maturation and memory consolidation.* Neuron, 2009. **63**(3): p. 342-56.
238. Yuan, T. and C. Bellone, *Glutamatergic receptors at developing synapses: the role of GluN3A-containing NMDA receptors and GluA2-lacking AMPA receptors.* Eur J Pharmacol, 2013. **719**(1-3): p. 107-111.
239. Adesnik, H., et al., *NMDA receptors inhibit synapse unsilencing during brain development.* Proc Natl Acad Sci U S A, 2008. **105**(14): p. 5597-602.
240. Prut, L. and C. Belzung, *The open field as a paradigm to measure the effects of drugs on anxiety-like behaviors: a review.* Eur J Pharmacol, 2003. **463**(1-3): p. 3-33.

241. Tartar, J.L., et al., *Hippocampal synaptic plasticity and spatial learning are impaired in a rat model of sleep fragmentation.* Eur J Neurosci, 2006. **23**(10): p. 2739-48.
242. Stepanski, E.J., *The effect of sleep fragmentation on daytime function.* Sleep, 2002. **25**(3): p. 268-76.
243. Huber, R., T. Deboer, and I. Tobler, *Effects of sleep deprivation on sleep and sleep EEG in three mouse strains: empirical data and simulations.* Brain Res, 2000. **857**(1-2): p. 8-19.
244. Vyazovskiy, V.V., et al., *Local sleep in awake rats.* Nature, 2011. **472**(7344): p. 443-7.
245. Risold, P.Y., N.S. Canteras, and L.W. Swanson, *Organization of projections from the anterior hypothalamic nucleus: a Phaseolus vulgaris-leucoagglutinin study in the rat.* J Comp Neurol, 1994. **348**(1): p. 1-40.
246. Anthony, T.E., et al., *Control of stress-induced persistent anxiety by an extra-amygdala septohypothalamic circuit.* Cell, 2014. **156**(3): p. 522-36.
247. Mitra, A., G. Guevremont, and E. Timofeeva, *Stress and Sucrose Intake Modulate Neuronal Activity in the Anterior Hypothalamic Area in Rats.* PLoS One, 2016. **11**(5): p. e0156563.
248. Moffitt, J.R., et al., *Molecular, spatial, and functional single-cell profiling of the hypothalamic preoptic region.* Science, 2018. **362**(6416).
249. Lein, E.S., et al., *Genome-wide atlas of gene expression in the adult mouse brain.* Nature, 2007. **445**(7124): p. 168-76.
250. Tobler, I. and A.A. Borbely, *The effect of 3-h and 6-h sleep deprivation on sleep and EEG spectra of the rat.* Behav Brain Res, 1990. **36**(1-2): p. 73-8.
251. Zhang, Z., et al., *Neuronal ensembles sufficient for recovery sleep and the sedative actions of alpha2 adrenergic agonists.* Nat Neurosci, 2015. **18**(4): p. 553-61.
252. Feldman, D.E., *Synaptic mechanisms for plasticity in neocortex.* Annu Rev Neurosci, 2009. **32**: p. 33-55.
253. Reichert S., A.O.P., Rihel J., *Neuronal activity drives homeostatic sleep through engagement of the hypothalamic neuropeptide galanin.* bioRxiv, 2019.
254. Kroeger, D., et al., *Galanin neurons in the ventrolateral preoptic area promote sleep and heat loss in mice.* Nat Commun, 2018. **9**(1): p. 4129.
255. Mahmoud, S., et al., *Astrocytes Maintain Glutamate Homeostasis in the CNS by Controlling the Balance between Glutamate Uptake and Release.* Cells, 2019. **8**(2).

256. Papouin, T., et al., *Septal Cholinergic Neuromodulation Tunes the Astrocyte-Dependent Gating of Hippocampal NMDA Receptors to Wakefulness.* Neuron, 2017. **94**(4): p. 840-854 e7.

257. Haydon, P.G., *Astrocytes and the modulation of sleep.* Curr Opin Neurobiol, 2017. **44**: p. 28-33.

258. Clasadonte, J., et al., *Connexin 43-Mediated Astroglial Metabolic Networks Contribute to the Regulation of the Sleep-Wake Cycle.* Neuron, 2017. **95**(6): p. 1365-1380 e5.

259. Frey, M.C., R. Sprengel, and T. Nevian, *Activity pattern-dependent long-term potentiation in neocortex and hippocampus of GluA1 (GluR-A) subunit-deficient mice.* J Neurosci, 2009. **29**(17): p. 5587-96.

260. Kohl, J., et al., *Functional circuit architecture underlying parental behaviour.* Nature, 2018. **556**(7701): p. 326-331.

261. Boulant, J.A., *Role of the preoptic-anterior hypothalamus in thermoregulation and fever.* Clin Infect Dis, 2000. **31 Suppl 5**: p. S157-61.

262. Albert, D.J., et al., *Intermale social aggression: suppression by medial preoptic area lesions.* Physiol Behav, 1986. **38**(2): p. 169-73.

263. Suntsova, N., et al., *Sleep-waking discharge patterns of median preoptic nucleus neurons in rats.* J Physiol, 2002. **543**(Pt 2): p. 665-77.

264. Nakai, J., M. Ohkura, and K. Imoto, *A high signal-to-noise Ca(2+) probe composed of a single green fluorescent protein.* Nat Biotechnol, 2001. **19**(2): p. 137-41.

265. Gunaydin, L.A., et al., *Natural neural projection dynamics underlying social behavior.* Cell, 2014. **157**(7): p. 1535-51.

266. Yasuda, R., et al., *Imaging calcium concentration dynamics in small neuronal compartments.* Sci STKE, 2004. **2004**(219): p. pl5.

267. Chung, S., et al., *Identification of preoptic sleep neurons using retrograde labelling and gene profiling.* Nature, 2017. **545**(7655): p. 477-481.

268. Akeju, O., et al., *Dexmedetomidine promotes biomimetic non-rapid eye movement stage 3 sleep in humans: A pilot study.* Clin Neurophysiol, 2018. **129**(1): p. 69-78.

269. Seidel, W.F., et al., *Alpha-2 adrenergic modulation of sleep: time-of-day-dependent pharmacodynamic profiles of dexmedetomidine and clonidine in the rat.* J Pharmacol Exp Ther, 1995. **275**(1): p. 263-73.

270. Harris, N.A., et al., *Dorsal BNST alpha2A-Adrenergic Receptors Produce HCN-Dependent Excitatory Actions That Initiate Anxiogenic Behaviors.* J Neurosci, 2018. **38**(42): p. 8922-8942.
271. Morrison, S.F., *Central control of body temperature.* F1000Res, 2016. **5**.
272. Park, S.G., et al., *Medial preoptic circuit induces hunting-like actions to target objects and prey.* Nat Neurosci, 2018. **21**(3): p. 364-372.
273. Vertes, R.P. and B. Kocsis, *Brainstem-diencephalo-septohippocampal systems controlling the theta rhythm of the hippocampus.* Neuroscience, 1997. **81**(4): p. 893-926.
274. Hikosaka, O., *The habenula: from stress evasion to value-based decision-making.* Nat Rev Neurosci, 2010. **11**(7): p. 503-13.
275. Schiavo, G., et al., *Tetanus and botulinum-B neurotoxins block neurotransmitter release by proteolytic cleavage of synaptobrevin.* Nature, 1992. **359**(6398): p. 832-5.
276. Valjakka, A., et al., *The fasciculus retroflexus controls the integrity of REM sleep by supporting the generation of hippocampal theta rhythm and rapid eye movements in rats.* Brain Res Bull, 1998. **47**(2): p. 171-84.
277. Haun, F., T.C. Eckenrode, and M. Murray, *Habenula and thalamus cell transplants restore normal sleep behaviors disrupted by denervation of the interpeduncular nucleus.* J Neurosci, 1992. **12**(8): p. 3282-90.
278. Nagel, G., et al., *Channelrhodopsin-2, a directly light-gated cation-selective membrane channel.* Proc Natl Acad Sci U S A, 2003. **100**(24): p. 13940-5.
279. Lee, E.H. and S.L. Huang, *Role of lateral habenula in the regulation of exploratory behavior and its relationship to stress in rats.* Behav Brain Res, 1988. **30**(3): p. 265-71.
280. Han, X., et al., *A high-light sensitivity optical neural silencer: development and application to optogenetic control of non-human primate cortex.* Front Syst Neurosci, 2011. **5**: p. 18.

Publications

Published prior to PhD:

Latremoliere A., Latini A., Andrews N., Cronin S.J., Fujita M., Gorska K., Hovius R., Romero C., Chuaiphichai S., Painter M., **Miracca G.**, et al. (2015) *Reduction of neuropathic and inflammatory pain through inhibition of the Tetrahydrobiopterin pathway*. Neuron, 86(6), 1393 – 1406.

Alexandre C., Latremoliere A., Ferreira A., **Miracca G.**, et al. (2017) *Decreased alertness due to sleep loss increases pain sensitivity in mice*. Nature Medicine, *23*(6), 768-774.

Published during PhD:

Gelegen C.*, **Miracca G.***, et al. (2018). *Excitatory pathways from the lateral habenula enable propofol-induced sedation*. Current Biology, *28*(4), 580-587. *These authors contributed equally to the work.

Harding E.C., Yu X., Miao A., Andrews N., M, Y., Ye Z., Lignos L., **Miracca G.**, et al. (2018). *A neuronal hub binding sleep initiation and body cooling in response to a warm external stimulus*. Current Biology, *28*(14), 2263-2273.

Yu X., Li W., Ma Y., Tossell K., Harris J.J., Harding E.C., Ba W., **Miracca G.**, et al. (2019) *GABA and glutamate neurons in the VTA regulate sleep and wakefulness*. Nature Neuroscience, *22*(1), p.106.

Ma Y., **Miracca G.**, Yu X., Harding E.C., Miao A., Yustos R., et al. (2019) *Galanin neurons unite sleep homeostasis and α2 adrenergic sedation*. Current Biology, *29*, 1-8.